Development of a Novel Aerogel-Based Modified Bituminous Materials

by

Carlos Javier Obando Gamboa

A Dissertation Presented in Partial Fulfillment
of the Requirements for the Degree
Doctor of Philosophy

Approved March 2022 by the
Graduate Supervisory Committee:

Kamil E. Kaloush, Chair
Michael Mamlouk
Hasan Ozer
Elham Fini
Claudia Zapata

ARIZONA STATE UNIVERSITY

May 2022

ABSTRACT

Thermal susceptibility is one of the biggest challenges that asphalt pavements must overcome. Asphalt mixture's thermal susceptibility can increase problems related to permanent deformation, and the expansion-contraction phenomenon triggers thermal cracking. Furthermore, there is a common worldwide interest in environmental impacts and pavements. Saving energy and mitigating the urban heat island (UHI) effect have been drawing the attention of researchers, governments, and industrial organizations. Pavements have been shown to play an important role in the UHI effect. Globally, about 90% of roadways are made of asphalt mixtures. The main objective of this research study involves the development and testing of an innovative aerogel-based product in the modification of asphalt mixtures to function as a material with unique thermal resistance properties, and potentially providing an urban cooling mechanism for the UHI. Other accomplishments included the development of test procedures to estimate the thermal conductivity of asphalt binders, the expansion-contraction of asphalt mixtures, and a computational tool to better understand the pavement's thermal profile and stresses.

Barriers related to the manufacturing and field implementation of the aerogel-based product were overcome. Unmodified and modified asphalt mixtures were manufactured at an asphalt plant to build pavement slabs. Thermocouples installed at top and bottom collected data daily. This data was valuable in understanding the temperature fluctuation of the pavement. Also, the mechanical properties of asphalt binders and mixtures with and without the novel product were evaluated in the laboratory. Fourier transform infrared

(FTIR) and scanning electron microscope (SEM) analyses were also used to understand the interaction of the developed product with bituminous materials.

The modified pavements showed desirable results in reducing overall pavement temperatures and suppressing the temperature gradient, a key to minimize thermal cracking. The comprehensive laboratory tests showed favorable outcomes for pavement performance. The use of a pavement design software, and life cycle/cost assessment studies supported the use of this newly developed technology. Modified pavements would perform better than control in distresses related to permanent deformation and thermal cracking; they reduce tire/pavement noise, require less raw material usage during their life cycle, and have lower life cycle cost compared to conventional pavements.

DEDICATION

To my deeply loved ones:

Natalia, my beautiful, brave, and beloved wife

Samuel and Rafael, my brave, cute, and adorable children

Carlos and Soquito, my selfless, amorous, and encouraging parents

Jaime, my strong, noble, and supportive brother

ACKNOWLEDGMENTS

Deeply thanks to my incredible wife. She has been with me in good and bad, and helped me to make our dreams come true. No achievement may be possible without her help. She has always encouraged my soul, and her presence is the food of my life. She deserves this achievement more than anyone. Thanks to my brave kids, Samuel and Rafael, who have given me too much of their time to get this achievement. They are the light of my life. My sincere gratitude to my amazing parents, Carlos and Soquito. They have taught me how to keep stand and be constant, all my strengths are because of them. I deeply admire them. Thanks to my best friend and little brother, Jaime. His noble heart always has been a model to me.

I remember as if it was yesterday when I met my advisor, Professor Kamil Kaloush. The words that I used at that time were, “this is a miracle, Professor”. Just when I had written him, he replied to me to coordinate a meeting the next day, he was in Bogota, Colombia, for an IRF conference. Since that day, Professor Kamil has supported me, and I have learned to admire his mentorship, knowledge, and positivism. I am deeply grateful to him, for all his guidance that inspired me to take my career to a higher level. Thank you, Dr. Kamil for your patience, for having trusted me, allowed me to develop my creativity, and follow my passion.

I really wish to thank my committee members. Dr. Michael Mamlouk, Dr. Hasan Ozer, Dr. Claudia Zapata, and Dr. Elham Fini. Either through their fantastic classes, or writing articles, they have taught me the best practices in my field and have helped me to shape my doctoral research with their constructive criticism.

My sincere appreciation to Jolina Karam for having helped me from the beginning until the end of this journey. I received tremendous assistance from Jolina, without her support, many of my goals would not have been accomplished. Special thanks to Samuel Castro, who has unselfishly helped in many activities in all my journey, Dr. Jose Medina for his on-time support, Dr. Benjamin Mailhé for having helped me to develop the ACTScalc software, and Dr. Daniel Oldham for having taught me a lot about laboratory testing in asphalt binders. Thanks to all members and colleagues of the Advanced Pavements Research Group, Saed Aker, Seng Hkawn, Xiao Zhang, Ashraf Alrajhi, Nafiur Rahman, Sand Aldagari, Hasna Elmagri, Ali Zalghout, Dr. Ramadan Salim, and Dr. Hossein Noorvand. I want to also extend my thanks to Mr. Jeff Long and Mr. Peter Goguen. They always helped me in the laboratory with good recommendations and/or solving technical issues.

I want to acknowledge the invaluable support of the Fulbright Scholarship, and the Program Colombia Cientifica. Based on the Program Colombia Cientifica focuses/challenges related to Sustainable Energy, this work serves as a tool for Sustainable Construction and a Cleaner Transportation development. I would like to thank the The Kaiteki Institute, The Global Kaiteki Center at ASU, and Mitsubishi Chemical Holdings for the partial funding support. Especial thanks are also extended to The National Center of Excellence for SMART Innovations and the Advanced Pavement Laboratory at ASU. Also, thanks to my friends Michael Garrison and John Lopez for the invaluable support and their unselfish friendship along this journey. Finally, I want to say thanks to Dr. Peter Fox for much appreciated help in providing me the additional funding based on my status as Fulbright Scholar at Arizona State University.

TABLE OF CONTENTS

Page

CHAPTER Page

CHAPTER Page

CHAPTER Page

CHAPTER Page

CHAPTER Page

LIST OF TABLES

Table Page

Table Page

Table Page

Table Page

LIST OF FIGURES

Figure Page

Figure Page

Figure Page

CHAPTER 1

INTRODUCTION

1.1 Background

Nowadays, close to 95% of the paved roads in the world are made with asphalt (bitumen). Currently, it is estimated that about 100 million tons of bitumen are consumed globally in one year, and between 85% to 95% is utilized in road construction. Economies and societies in the world have become very dependent on the accessibility and reliability of the road infrastructure. In most countries, between 70% to over 80% of inland freight transport (in ton kilometers) corresponds to road transport, which is similar for the movement of people (in km-passenger) (Corté, 2020).

Pavements also play an important role in environmental impacts, such as boosting the urban heat island effect. Beyond conventional efforts on reflecting solar energy, pavement materials properties, such as thermal conductivity and heat capacity, can play an equally important role in minimizing heat transfer.

Despite of the broad use of asphalt material in pavements with a relative satisfactory performance, asphalt pavement requires maintenance involving surface treatments every three to five years to prevent thermal cracks and other surface defects. Effectiveness and the maintenance frequency will vary depending on many variables including, traffic, quality of the material, pavement condition, and proper time of the application.

It is necessary to evaluate and look for alternatives that meet the of new traffic loads and address the current and future environmental needs. Improving the asphalt material's

properties is needed to address better performance in terms of development, environment, and economic benefits (Hinislioglu, 2011). Asphalt pavements face problems related to their physical and mechanical characteristics.

The usage of modifiers in asphalt binders has been one of the most common methodologies to overcome performance challenges and thus improve the performance of bitumen mixes (Gordon , 2002). The mechanical properties are boosted to withstand the accumulated stresses within the pavement structure caused by both traffic and environment. These modifiers have one common goal which is reducing the major pavement distresses. This could be done by focusing on the elasticity of the binder, leading to a greater fatigue resistance, and a reduction in the crack propagation as well as permanent deformation.

One modifier of interest to this study is the use of aerogel in the modification of asphalt binders and mixtures. In 1953, the Standard Oil company introduced the use of aerogel in asphalt, but there were no further development or implementation of such use. This process consisted of blending different percentages by weight of aerogel particles within the asphalt mixtures (U.S, Lyndhurst, Ohio Patent No. 2,759,842, 1956). Aerogel is a synthetic porous ultralight material originated from a gel, where the liquid component of the gel has been substituted with a gas without a substantial collapse of the gel's structure. The result is a material with a unique geometrical structure and extremely low thermal conductivity (Thomas, 2012). There are different types of aerogels, but the most common is the silica based (Aerogel Technologies, 2004).

1.2. Problem Statement

One of the biggest challenges that asphalt pavement must overcome is its thermal susceptibility. Thermal susceptibility of the asphalt can boost problems related to permanent deformation at high environmental temperatures, and the expansion-contraction phenomenon triggers the appearance of thermal cracking.

The usage of aerogel may be an option to enhance the properties of the existing bitumen material. However, the direct use of aerogel in asphalt production possesses challenges; the mixing procedure needs to be further investigated since aerogel is susceptible of creating dust clouds due to its low density. Mixing aerogel with asphalt binder and within asphalt mixtures is a great challenge in terms of safety and practicality.

However, the novel product developed at Arizona State University through this study consists of pre-treated composite, aerogel Modified Bituminous material (aMBx), annuls all safety concerns brought by the use of direct aerogel particles and facilitate the blending with other bituminous materials. The pre-treated composite is attained due to the presence of an encapsulator around the aerogel particles creating the aMBx. This process facilitates that the aerogel particles are weighed down and do not cause the formation of dust clouds while performing any type of mixing and handling. Therefore, all safety protocols and operation procedures concerns can be dismissed. The thermal insulative properties of the aerogel are incorporated into the bituminous materials and are distributed within the mastic. By introducing this product into bituminous compounds, thermal and mechanistic benefits are achieved.

Beyond conventional efforts on reflecting solar energy, pavement materials properties, such as thermal conductivity and heat capacity, can now play an equally

important role in minimizing heat transfer and storage benefiting pavement performance and provide an urban cooling mechanism.

1.3 Objective

The main objective of this research study involves the development and testing of an innovative Aerogel-based product in the modification of asphalt mixtures to function as a material with unique thermal resistance properties for better durability and urban cooling. The scope of work included the following milestones:

- Investigate different aerogel products and perform a technical-economical assessment to define a suitable aerogel source.
- Develop suitable test procedures to estimate the thermal conductivity of asphalt binders, the expansion-contraction of asphalt mixtures, and computational tools to better understand the pavement's thermal profile and stresses.
- Address mixing methods for the aerogel composite, like the dry method (DM) when aMBx is added to hot aggregates, or wet method (WM) when added to hot binder, to manufacture asphalt mixtures modified with aMBx.
- Use the developed technology in real asphalt plant production operation; this necessitated designing and building of pavement test slabs, and monitoring temperature fluctuation of the pavements with and without aMBx.
- Evaluate the mechanical properties of different asphalt binders and mixtures with and without the novel composite, aMBx.

- Carry out essential analysis such as the Fourier Transform Infrared (FTIR) spectroscopy and scanning electron microscope (SEM) to further understand the interaction of the aMBx with the bituminous materials.
- Perform Life Cycle Assessment and Life Cycle Cost Analysis to quantify the environmental impact and the economic feasibility of the new technology implementation.

1.4 Dissertation Outline

This dissertation consists of 12 chapters as follows:

Chapter 1: Introduction

This chapter introduced the framework and the objectives of this research.

Chapter 2: Literature Review

This section defines Aerogel, presents the different types of Aerogels, the different characteristics and applications of some commercial Aerogels available in the market, and introduces the original study involving Aerogel in the modification of asphalt binders.

Chapter 3: Estimating Thermal Conductivity of Asphalt Binders

Because the limited availability of suitable test methods to calculate the thermal conductivity of asphalt binders (k), in this section, a new method is introduced to estimate this physical property.

Chapter 4: Characterization and Assessment of Aerogel-Modified Asphalt Binders

This chapter describes the procedures to add Aerogel in asphalt binders and the inherent limitations. It also presents the performance of three different asphalt binders when blended with diverse doses of Aerogel. Performance analysis is done based on tests such as Softening Point, Rotational Viscosity, Penetration, Dynamic Shear Rheology (DSR), Multiple Stress Creep Recovery (MSCR), the Bitumen Bond Strength (BBS), the Bending Beam Rheometer (BBR), and Thermal Conductivity.

Chapter 5: A Novel Porous Silica-Based Modifier, Aerogel Modified Bituminous Materials (aMBx)

In this section, the development of a novel Aerogel-Based modifier called aMBx is described. Different tests such are conducted to evaluate the performance of binders with and without aMBx.

Chapter 6: Asphalt Mixture Design Considerations

In this Chapter specifications, material properties and procedures to produce asphalt mixtures modified with aMBx are described. Two different methods are described: dry method (DM) when aMBx added to the hot aggregates, and wet method (WM) when aMBx is added to the hot binder.

Chapter 7: Field Production and Thermal Properties of aMBx Modified Asphalt Mixtures

Logistics, preparation, and construction of 6 in-field slabs and test sections are described. Thermal properties of control and aMBx modified mixtures are estimated, and temperature profile / behavior analysis based on the in-field temperature recording is done.

Chapter 8: Extending the Thermal Stresses Evaluation and Analysis in Asphalt Pavements

This section includes the estimation of the linear coefficient of expansion-contraction for control and aMBx modified mixtures using a new test setup developed in this study. A computational tool is proposed to calculate the pavement's temperature profile and thermal stresses. The thermal profile is estimated using a 1-dimensional model of heat transfer, and the thermal stresses are estimated using concepts of linear viscoelastic behavior.

Chapter 9: *Durability Assessment of the Novel Silica-Based Modified Asphalt Pavements*

In this chapter control and aMBx modified mixtures are measured in terms of durability. Mixtures tests include Dynamic Modulus, Uniaxial Fatigue, Flow Number, the Tensile Strength Ratio (TSR), Semicircular Bending Test (SCB), and the Hamburg (Immersion) wheel tracking test. The AASHTOWare Pavement Design software is used for the performance and durability analysis.

Chapter 10: Understanding the aMBx-interaction with Bituminous Materials

To understand the interaction between aMBx and the asphalt binders and mixtures, the Fourier Transform-Infrared Spectroscopy (FTIR) and Scanning Electron Microscopy (SEM) analysis are performed.

Chapter 11: Life Cycle Assessment Including Traffic Noise and Life Cycle Cost Analysis: Conventional vs. Silica-based Modified Pavements

This chapter includes a Life Cycle Cost Analysis (LCCA) and a Life Cycle Assessment (LCA) of a 20%aMBx modified mixture to help in the decision-making process and supporting future implementation of this new technology.

Chapter 12: Conclusions and Future Work

In this chapter, summary, conclusions, and recommendations for future work are presented.

A flow chart of the research plan executed is shown in Figure 1-1.

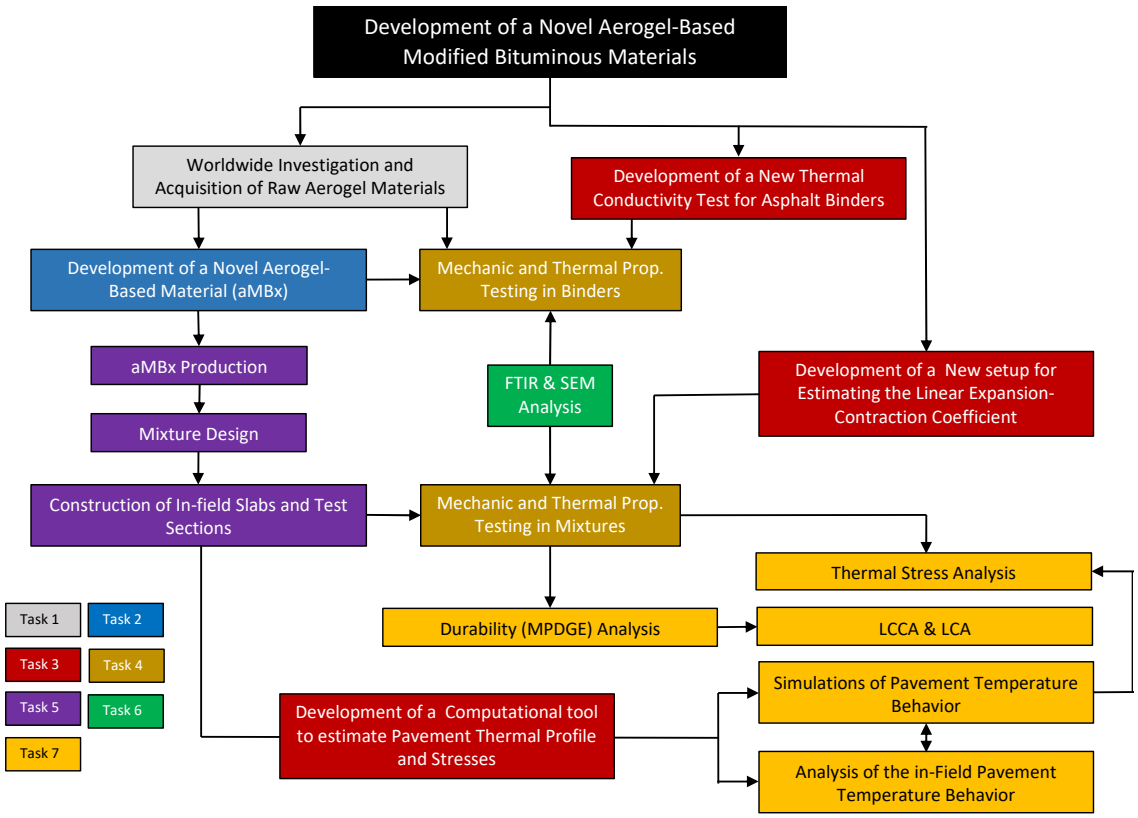

Figure 1-1. Overview Summary of Research Plan

CHAPTER 2

LITERATURE REVIEW

2.1 Brief History

Asphalt has been part of the human civilization for thousands of years. The ancient Mesopotamians and Phoenicians used it to waterproof temple baths, and ships. Egyptians used it as mortar to prevent erosion in the Nile River. The word asphalt comes from the Greek “asphaltos” which means “secure”, however, the first use of asphalt as a road-building material was registered in Babylon back in 625 B.C. In the early 1800s, Thomas Telford built about 900 miles of roads in Scotland, and John Loudon McAdam built a Scottish turnpike using broken stones. To reduce maintenance and dust, hot tar was used to bond the broken stones together, making “tarmacadam” pavements. In 1870, Belgian chemist Edmund J. DeSmedt built the first asphalt pavement in the U.S. in Newark, N.J. In 1876, Pennsylvania Avenue in Washington, D.C. was paved by DeSmedt using 54,000 square yards of sheet asphalt from Trinidad Lake. The Cummer Company opened the first central hot mix production facilities in the U.S. During World War II, asphalt technology was significantly improved because the need of military aircraft for surfaces that could support heavier loads (Virginia Asphalt Association, 2020). The growth of the automobile industry has boosted the increase of the usage of bitumen.

Nowadays, asphalt binder is broadly used for different purposes, however, one of the most common utilities is in road infrastructure. Pavements also play an important role in increasing the urban heat island effect. Globally, about 90% of roadways are made of asphalt mixtures. In the USA, 500 million tons of asphalt mixtures are produced annually

at a cost of 40 billion US dollars (FHWA, 2011). On the other hand, despite the relatively good performance and high resistance of conventional asphalt materials in pavements, it has been necessary to look for new ways to improve the asphalt performance because of increased temperature susceptibility requirements and the new highway traffic volume and load needs.

Some of the most known modifications has been the usage of polymers, (Styrene-butadiene-styrene block-copolymer, also known as SBS) and crumb rubber. They have demonstrated a great deal in changing the binder properties. However, the low ageing resistance, poor storage stability of some polymer modified bitumen (PMB), and high cost are some obstacles that limit the progress of bitumen polymer modification (Zhu, Birgisson, & Kringos, 2014). The SBS polymers predominantly have improved the temperature susceptibility of bitumen by increasing stiffness at high temperatures and reducing the probability of cracking at low temperatures (Collins, Bouldin, Gelles, & Berker, 1991).

With regards to the rubber modified mixtures, they have been incorporated into bituminous materials in the early 1930s - 1950 creating an elastic material used in the pavement maintenance and roofing industry (Bruton, 2020). However, the modern use of rubber in asphalt pavements started in the early 1960's by Charles McDonald in Phoenix, Arizona. There are two methodologies to introduce the rubber in the asphalt mixture. One, known as the dry process implement the rubber directly in the aggregates of the mix. The second, known as wet process, incorporates the rubber directly into the binder at high temperatures creating a new material with higher viscosity. This integration improved the mechanical behavior of asphalt mixtures. Additionally, advantages such as environmental

aspects because the recycling of used tires, and road friction benefits have been documented. Similar to the effect of SBS, this material is known to increase the flexibility of the binder resulting in more stability for longer periods comparing to conventional binders (FHWA, 2014). However, the implementation of rubber in asphalt mixtures has some downsides such as recyclability, binder storage stability, the fumes that it releases through the paving process, and workability. Asphalt rubber pavements are more expensive than conventional pavements materials and can be difficult for some contractors to get used to it because the stickiness, and the specific procedures for placing and compacting within a relatively narrow temperature frame (Kuennen, 2004).

2.1 Aerogel in Asphalt Binders

What material may change the world in terms of materials behavior and better susceptibility to temperatures? this is a question that could be drawing the attention of researchers, industries, innovators, and common people. Currently, a couple of new materials are taking the humanity's development one step ahead. Examples of these materials are: phosphorene nanoribbons, a nanomaterial which has a corrugated structure that could improve the charging ions in electric vehicles, aircraft, and solar batteries 1000 times faster; black gold, a new material that can absorb the entire visible and near-infrared region of solar light and carbon dioxide with potential applications such as seawater desalination, artificial photosynthesis (taking carbon dioxide and transforming it into fuel), and solar energy collecting; and Aerogel, a solid material even though 99.98% of it is air. Aerogels are extremely porous and very low in density. Mars's enthusiasts consider silica

aerogel could be employed to build domes near the red planet's polar ice caps (Thomas, 2019). Figure 2 presents the thermal conductivity of selected materials including aerogel (Happold, 2020) (Engineering ToolBox, 2003)

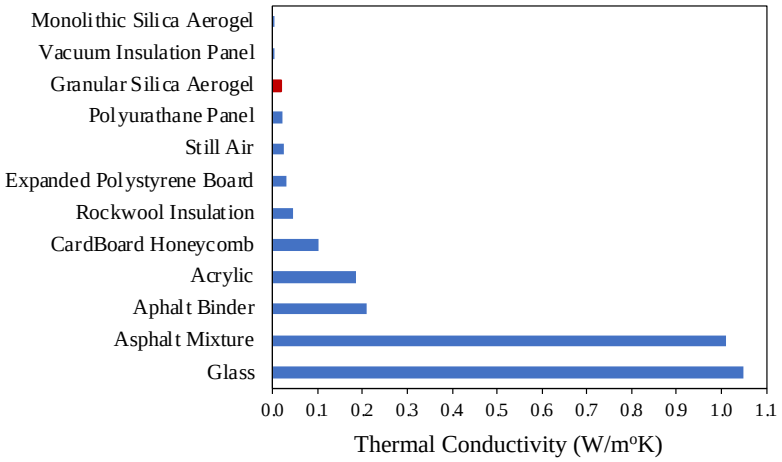

Figure 2-1. Thermal Conductivity of Different Materials (W/mK)

The use of aerogel in asphalt was attempted back in 1953 by the Standard Oil Company, Ohio. Blending aerogel particles within asphalt mixtures from 1% to 20% by weight showed that the resistance to flow increased with a higher percentage of aerogel. Samples with Aerogel do flow at room temperature, but slower than the ones without it (U.S, Lyndhurst, Ohio Patent No. 2,759,842, 1956). In this framework, aerogel, a material with a specific geometrical structure and extremely low thermal conductivity is an alternative to enhance the properties of the existing bitumen material. However, there was no further development or implementation of such use. It is presumed that the process was not successful because it presented safety concerns as the aerogel particles by themselves, having a very low density, need careful handling procedures. They are considered

hazardous; in the laboratory they need a fume hood, blast shield, non-flammable lab coat and specific gloves need to be worn by the user. These issues are magnified in field production at asphalt plants as the light-weight particles can cause dust clouds and ignite with the presence of the tiniest spark.

2.2 Aerogel's Characteristics

Steven Kistler invented Aerogel in 1931, and nowadays it is calling the interest of scientists due to its light weight and thermal properties (Acharya, Joshi, & Gokhale, 2013). Aerogels are a varied class of solid, highly porous materials with a collection of extreme material properties. Common aerogels are known for the extreme low density ranging between ~0.0011 and ~0.5 g/cm^3. In fact, aerogel could be made only three times heavier than air, then, it is the lowest density solid material that have ever been made (Aerogel.org, 2008).

Aerogels are made by the combination of a polymer with a solvent to form a gel, and then subtracting the liquid from the gel and interchanging it with air. Aerogels have been mainly a silica-based material merged with a solvent to produce a gel. The gel is exposed to a supercritical fluid extraction which involves the introduction of liquid carbon dioxide into the gel. The carbon dioxide exceeds its super critical point, and then is vented out multiple times to ensure that all liquids are removed from the gel (Aerogel.org, 2008). Instead of the expensive supercritical drying process, ambient pressure drying (APD) is of most interest to lower the costs compared to the expensive drying processes (Baetens, Jelle, & Gustavsen, 2011). The resulting product is a material called aerogel (NASA, 2017).

Therefore, the word aerogel refers to the fact that aerogels are derived from gels which were vacuumed to get only air instead of any liquid (Aerogel.org, 2008).

The expression aerogel does not denote any particular element, but rather to a geometry which a substance can take on–the same way a sculpture can be made out of plastic, clay, or of other materials. Aerogels can be created of a variety of substances, comprising: most of the transition metal oxides (e.g. iron oxide), several main group metal oxides (e.g. tin oxide), most of the lanthanide and actinide metal oxides (e.g. praseodymium oxide), organic polymers (e.g. resorcinol-formaldehyde, phenol-formaldehyde, polyacrylates, polystyrenes, polyurethanes, and epoxies), biological polymers (e.g. gelatin, etc.), semiconductor nanostructures (e.g. cadmium selenide quantum dots), carbon, carbon nanotubes, metals (such as copper and gold), and the most common, silica. Some of the properties of Aerogels include lowest optical index of refraction (1.002), lowest dielectric constant from 3-40 GHz (1.008), lowest density solid (0.0011 g/cm^3), lowest thermal conductivity (0.016 W/m^oK), and lowest speed of sound through a material (70 m/s) (Aerogel.org, 2008).

Worldwide there are different sources and types of aerogels, including quality and cost, thus, the identification and definition of which ones are the best alternatives to use in this study was a very important factor. Table 1 shows the collection of different Aerogel types and their characteristics. More common available Aerogels are those silica-based, and their principal usages are related with thermal insulation for industrial purposes including construction.

Table 2-1. Characteristics of Different Available Aerogels

Product ID.	Grains Availability	Maximum Particle's diameter (um)	Average Bulk Density (g/cm3)	Surface Chemistry	Average Thermal Conductivity (W/mK)	Average Surface Area (m2/g)	Average Pore Diameter (nm)	Average Porosity (> %)	Applications/Availability	Chemical Features	Price per Kilogram [based on AP8b)
AP1	Particles	700	0.13	Hydrophobic	0.012	800	20	90	* Coatings * Isulating Panels (Lumira) * Isulating Blankets	Silica Based Aerogel	26
AP2	Powder	20	0.065	Hydrophobic	0.020	700	20	90	* Isulating Tape * Isulating Coating * Isulating Blankets * Plaster * Cement and perlite composites	Silica Based Aerogel	4
AP3p	Powder	60	0.085	Hydrophobic	0.033	**			* Isulating Paneles * Mortars, cements, plasters and paints	Silica Based Aerogel	11
AP3b	Beads	20000	0.16		0.025						11
AP4	Granulates	3500	0.075	Hydrophobic	0.020	850	8.5	95	* Isulating Coating * Isulating Panels * Insulation to Pressure Atmospheric for the building	Silica Based Aerogel	5
AP5	Powder or Particles	5000	0.085	Hydrophobic/No Hydrophobic	0.020	550	60	90	* Isulating Panels * Isulating Blankets	Silica Based Aerogel	6
AP6	Powder	20	0.06	Hydrophobic	0.020	600	35	95	* Silica Aerogel Flexible Thermal Insulation Felts * Aerogel Thermal Insulation Cylinder and Special-shaped Parts * Aerogel Translucent Thermal Insulation Panel * Isulating panelsSilica Aerogel Flexible Thermal Insulation Felts	Silica Based Aerogel	**
AP7	Powder, Granulates and Beads	3000	0.20	Hydrophobic	0.024	800	70	95	* Food Packages * Pharm Packages * Laboratory Packages	Silica Based Aerogel	**
AP8p	Powder	0.01 - 0.2	0.15	Hydrophobic	0.019	300 - 350	20 - 50	95	* Blankets * Thermal Isulation Coatings	Silica Based Aerogel	1
AP8b	Beads	1000 - 6000	0.20		0.017						
AP9o	Granulates	0.01 - 0.2	0.15	Hydrophobic	0.019	300 - 350	20 - 50	95	* Blankets * Thermal Isulation Coatings	Silica Based Aerogel	6
AP9i		1000 - 6000	0.17	Hydrophilic	0.019						6

2.3 Other Applications of Aerogel

The uncommon properties of aerogels have opened the door to a variety of o applications in buildings. Their main benefits include energy and cost savings due to the low thermal conductivity, the acoustic properties for noise insulation, the fire retardation

capabilities, and the indoor air purification properties. The unusual optical transparency and low thermal insulation of aerogels allow its usage in solar collector covers and window panels (Acharya, et al., 2013).

Additionally, aerogel can be used to create a lightweight concrete by replacing the normal aggregates of Portland concrete. The incorporation of silica aerogel particles into the concrete matrix allows to prepare a lightweight and thermal insulating concrete material. Some properties of this lightweight concrete are low density (1.0 g/cm3), a low thermal conductivity (0.26 W/m^{o}K), and a good compressive strength (8.3 MPa) at an aerogel content of 60 vol.%. The density, thermal conductivity, and the mechanical properties of this concrete can be controlled by varying the aerogel content. Scanning electron microscopy (SEM) observations have revealed that the aerogel particles are stable during the hydration of cementitious materials, suggesting possibilities of combining aerogel and concrete materials for construction (Acharya, et al., 2013).

CHAPTER 3

ESTIMATING THE THERMAL CONDUCTIVITY OF ASPHALT BINDERS

3.1 Introduction

There is a common worldwide interest in environmental issues and pavements. One aspect is the mitigation of the urban heat island (UHI) effect. In road infrastructure, one of the important material properties in addressing the UHI of pavements is the determination of the thermal conductivity. The thermal conductivity is a physical property that is also related to the performance of the materials, which implies the energy transfer rate or heat transfer rate (Q) that occur when bodies in contact have different temperatures (Vimmrová & Výborný, 2002).

Heat can be transferred from one point to another by three different processes: conduction, convection, and radiation (Lienhard IV & Lienhard V., 2003). Conduction can occur in solids, and in liquids when there is no macroscopic movement. Convection occurs when liquids are in movement, and radiation occurs in the vacuum or air. These modes of heat transfer are governed by different laws, Fourier, Newton, and Stefan-Boltzmann, respectively. Table 3-1 shows a summary of these heat transfer modes.

Table 3-1. Modes of Heat Flow (Q).

Material	Conduction	Convection	Radiation
Solids	X		
Liquids/Gases	x	X	x
Vacuum/Air			X
Law	Fourier's	Newton's	Stefan–Boltzmann

x = no macroscopic movement of the liquid/gas, limited

This document addresses the conduction phenomenon of bitumen. In conduction, heat is transmitted through a material medium and there is no transport of matter. The rate at which heat is transferred through the material (dQ/dt) is represented by the letter Q and is called the heat flow rate. Empirically, the heat flow rate is proportional to the cross-sectional area (A) to the direction of the flow, to the temperature difference on both sides of the material (ΔT), and inversely proportional to the distance traveled from the place at the highest temperature (Δx) (Welty, Wilson, & Wicks, 1997). That is:

$$Q \approx \mathrm{A}\frac{\Delta \mathrm{T}}{\Delta \mathrm{x}} \tag{3-1}$$

To achieve the equality of the previous expression, a constant k is added, which is the thermal conductivity, the intrinsic ability of a material to transfer or conduct heat (Welty, Wilson, & Wicks, 1997) (Speight, 2017).

$$\mathrm{Q} = \frac{\mathrm{dQ}}{\mathrm{dt}} = \mathrm{k}\,\mathrm{A}\frac{\Delta \mathrm{T}}{\Delta \mathrm{x}} \tag{3-2}$$

The conduction into a cylindrical geometry, introduces the Equation (3-3) (Mills, 1999) (Holman, 2010).

$$Q = 2\pi hk\frac{\Delta T}{ln\frac{r2}{r1}} \tag{3-3}$$

Where:

Q: heat flow rate (W=joule/s)

A: the cross-sectional area (m^2)

ΔT: the temperature gradient (^oC)

Δx: the thickness (m)

k: the thermal conductivity (W/m^oK)

t: time (s)

h: length/height of the sample (m)

r1: inner radius (m)

r2: outer radius (m)

Thermal conductivity is inherent to each material and expresses the ability of a given material to conduct heat (Welty, Wilson, & Wicks, 1997). Thermal conductivity can be affected by moisture, ambient temperature, and the density of the material. If moisture, temperature, and density are increased, the thermal conductivity rises too, so thermal conductivity is not constant (Vimmrová & Výborný, 2002).

The exactitude of different methods for calculating thermal conductivity is extensively debated in several fields. In addition, the wide range of thermal characteristics of different materials generated several methods for the estimation of thermal conductivity (Yuksel, 2010).

Along the last two decades, the accuracy and the understanding of the principles of heat transfer have been improved for several materials. These techniques present different ranges of thermal conductivity even for the same material, different accuracy, temperature ranges, and specimen type (Yuksel N., 2016).

Although there are many methods to estimate thermal conductivity, there are few for specific materials like bitumen, or asphalt binder. There are two basic methods. The first one is a group of steady-state methods, and the second one is called the transient or a group of non-steady-state methods (Yuksel, 2010) (Yuksel, Avci, Kilic, 2012). The implementation of each method depends on the characteristic of the materials. All methods are based on electrical analogy and on the essential laws of heat conduction. Steady-state methods are mathematically simpler (Yuksel, 2010), while transient heat transfer methods are efficient to determine thermal diffusivity. However, steady-state methods are known as the most accurate for testing dry materials (Mohesnin, 1980).

The steady-state technique is related to an equilibrium state, then, these methods consider the data to do the calculations when a material reaches a constant temperature. As a disadvantage, to reach a steady temperature takes a long time (Vimmrová & Výborný, 2002). In addition, these methods involve expensive equipment and difficult experimental set-up installation. Nonetheless, steady-state methods are the most accurate and the main measurement methods. The non-steady-state or transient methods take measurements during the heating progression. These techniques estimate thermal conductivity using transient sensors. The time needed in these methods is relatively quick, which is the most important advantage over the steady-state systems (Czichos , Saito, & Smith, 2006). Table 3-2 shows a summary of the principal characteristics of the various methods (Yuksel, 2010).

In the Civil Engineering field, asphalt concrete represents the third most widely used material in the world, with asphalt-paved roads being its principal usage. One of the most important components of asphalt concrete is bitumen, a residue of oil distillation

processes. Bitumen is a highly susceptible viscoelastic material to temperature changes. This can be brittle as glass at low temperature and flow like oil at high temperatures (DeDene, Gorman, Marasteanu, & Sparrow, 2016). From this conception, the determination of thermal conductivity of the bitumen becomes very important to understand and improve its thermal performance.

Analytical models in different studies have been used to calculate the thermal conductivity. However, the accuracy of each model and technique is constricted by the physical properties and other factors of each material to test. Therefore, quantity and modeling of thermal conductivity are complex and need high precision. The approaches and the models used to study thermal behavior of materials must be clearly defined (Yuksel, 2010).

Based on the unique characteristics of bituminous materials, and the need to know their thermal properties for better understanding the potential improvement when using various modification techniques, this document presents an alternative method for determining the thermal conductivity of bitumen, while addressing issues like cost and accuracy.

Table 3-2. Summary of methods used for the determination of the thermal conductivity

Method		Usage	Uncertainly Estimation	Range of Temperature	Advantages	Disadvantages
Steady- state methods	Guarded hot plate	Solids, insulator materials	2% –5%	−93°C – 127°C	High level of accuracy	Long measurement time, low conductivity materials, large specimen size
	Heat-flow meter	Rocks, polymers, insulations, plastics, glasses, ceramics, some metals	3% –10% (normal), 0.5% –2% (axial) and 3% –15% (radial)	−100°C–200°C (normal), -183°C–126°C (axial heat flow), and 25°C – 2326°C (radial heat flow)	Easy operation and construction	Relative measurement, uncertainly
	Cylinder	Metals	2%	-269°C – 727°C	Simultaneous estimation of electrical conductivity, and temperature range	Long measurement time
	Pipe method	Calcium, silicates, solids, refractory fiber blankets and minerals	3% –20%	20°C – 2500°C	Good temperature range	Long measurement time, specimen set up
	Comparative	Plastics, metals, ceramics	10% –20%	20°C – 1300°C	Simple construction and operation	Relative measurement, uncertainly
	Direct heating	Tubes of electrical conductors, metals, wires, rods	2% –10%	127°C – 2727°C	Easy and fast measurements, simultaneous estimation of electrical conductivity	Limited to electrically conducting materials
Transient Methods	Hot disk (TPS technique)	Solids, powders, liquids, pastes	--	247°C – 927°C	Diverse thermal properties simultaneously, and accuracy	Conducting or insulating material
	Hot wire Hot strip	Hot wire: Solids, liquids, glasses, plastics, granules, powders Hot strip: Ceramics, glasses, foods	1% –10 % hot wire 5% –15% hot strip	20°C –2 000°C, −40–1600°C for hot wire and −50°C to 500°C for hot strip, 25°C – 1527°C for hot wire	Fast, accuracy, and, good temperature range	Only for low conductivity materials
	Photothermal (PT) Photoacoustic	Thin films, solids, liquids, gases	1%–10 % for PT	−50°C – 1500°C, and -73°C – 527°C for PT	Operational for liquids, gases, and thin films	Unknown accuracy, Nonstandard
	Laser flash	Polymer, ceramics, solids, liquids, powders, metals	1.5% –5 %	−373°C – 3027°C	Good temperature range, accuracy at high temperature, small specimens, fast	Expensive, not for insulation materials

3.2 Experimental Approach

3.2.1 Calibration

The determination of the thermal conductivity of bitumen samples using the method described in this document was first used on material of known characteristics and thermal conductivity. The calibration sample used was acrylic glass (Plexiglas V045i), which has

a known thermal conductivity range between 0.17W/m^{o}K and 0.20W/m^{o}K (Goodfellow, 2019) (Engineering ToolBox, 2011); in confirmation, and following the method developed at The National Center of Excellence for SMART Innovations at ASU (Carlson, Bhardwaj, Phelan, Kaloush, & Golden, 2010), the thermal conductivity of this material was estimated as 0.1852W/m^{o}K.

As it was explained above, thermal conductivity is related to the heat transfer rate, which is central in the estimation of thermal conductivity in this method. Due to the unique characteristics of the bitumen/asphaltic binder, the medium to transfer the heat was chosen as distilled water in no macroscopic movement. Then, the temperature transfer from the outside to the sample is realized using non-turbulent, distilled water. At the liquid-solid interface, the main mechanisms contributing to heat transfer are convection and conduction. However, the present work restricts the domain study to the sole solid sample. This assumption is sustained by the fact that the bitumen is considered as a solid. Therefore, it is possible to restrict the heat transfer rate (Q) calculation to a conduction-driven mechanism only, using Equation (3).

The heat flow rate is independent of radial location but varies depending on the temperature of the water; therefore, it was necessary to calibrate the model measuring the heat flow rate at several temperature points. This calibration method compares different water temperatures and the resulting heat flow rate, knowing the thermal conductivity, and the acrylic-sample's geometrical features.

To determine the heat flow rate, we need to measure the two final steady temperatures in the system. In this approach, the outer temperature is the water temperature being controlled by the water bath, and the inner temperature is the one in the center of the

acrylic sample. Note that the "system" includes all instrumentation features like water bath, thermocouple types and accuracy, and thermometers, which are described next.

3.2.2 Instrumentation

To avoid the interference of air currents that could alter the temperature readings and make it more difficult reaching the steady state temperatures, the experimental setup was employed inside a chamber conditioned at 25^{o}C. To control the water temperature, a water bath (Thermo Scientific, 180 Series, Model: Precision) was used. For temperature measurements, J type thermal couples (-40 to 510 ^{o}C) were used, and a software LabVIEW 8.6 with a DAQ system were used to record the temperature changes along with time. To check the accuracy of the temperature readings, a high precision thermometer (Precision RTD Handheld Data Logger Thermometer) was used.

The acrylic samples used to calibrate the model were cylindrical shaped. The samples are 40mm in diameter ($r_{2,}$ the outer radius is then 19mm), and 25mm in height (h), with a hole of 2mm diameter (r_1=1mm, which is the inner radius) in the center of the top circular face, extending to the middle of the sample. Figure 3-1 shows the cylinder's geometry.

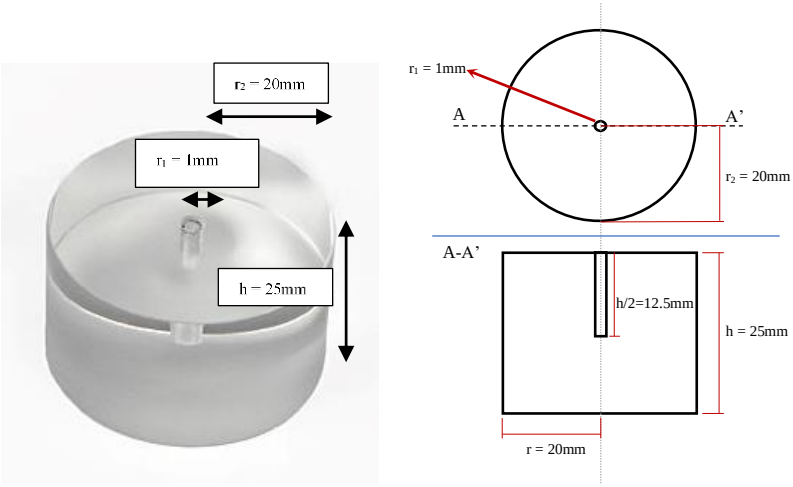

Figure 3-1. Acrylic sample characteristics

To measure the thermal conductivity in steady state using a conduction method, it is necessary to ensure that the heat flow goes only in one direction. A balsa wooden platform was used to place the samples inside the water bath. This setup is needed to avoid the water outer temperature affecting the inner temperature in the center of the acrylic cylinder. An insulator foam was used on the top of the acrylic sample, and a high vacuum grease silicone on the bottom. This grease has sealing ability and at the same time excellent resistance to water. Additionally, because the relative high specific heat capacity, 2900 J/kgK (Engineering ToolBox, 2003), a very low thermal conductivity, 0.045W/m^{o}K (Kotlarewski, Ozarska, & Gusamo, 2014), of the balsa wood, the very low power in the system (e.g. 0.09W at 47^{o}C), and the short time of the test (2 hours), it is considered that no significant heat enters from the bottom of the sample. The samples were submerged into the water bath taking care that the level of water goes just below the edge of the top circular face. For temperatures above 50^{o}C, it is recommended to cover partially the water bath to avoid water evaporation. Figure 3-2 shows the complete setup.

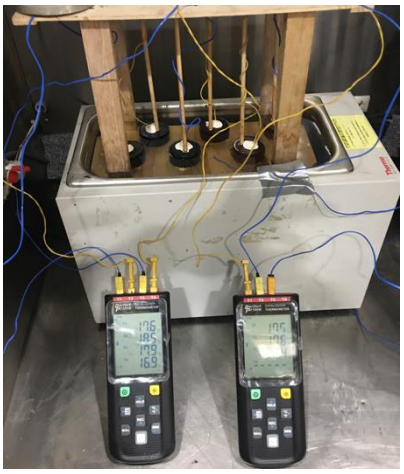

Figure 3-2. Complete set-up of the calibration test

The final data needed to calculate Q are the steady-state temperatures. Figure 3-3 shows examples of the temperature change recorded for various samples versus time. The steady-state temperatures are those when the inner (center of the sample) and outer (water) temperatures reach an unchanging condition.

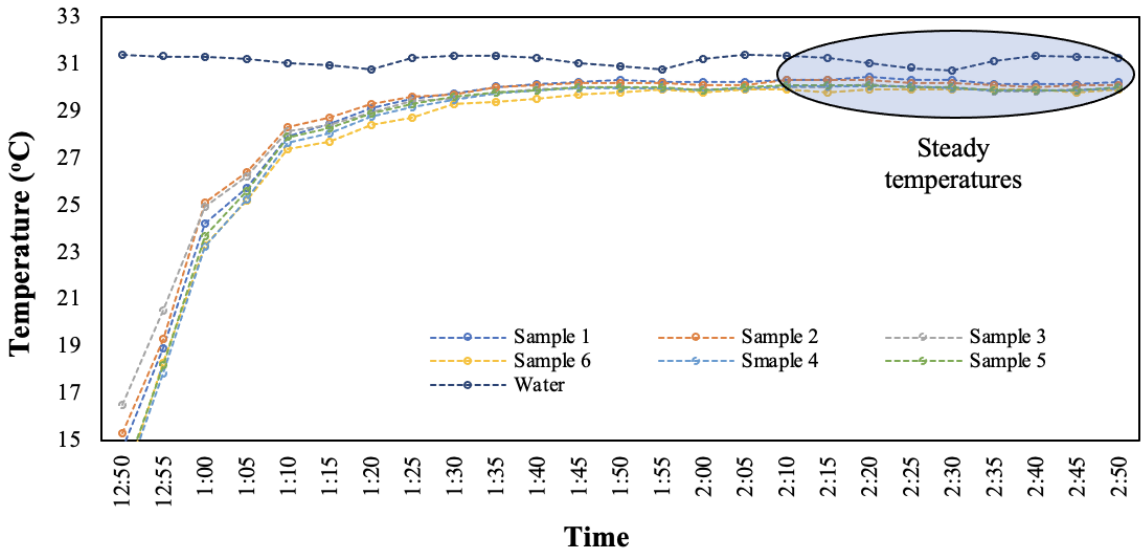

Figure 3-3. Temperature change recorded versus time

After certain period, the temperatures get to the steady state. Note that the time needed to get to the steady state may vary; however, for this setup the usual time was 1.5 hours. Once the steady-state temperatures are reached, it is recommended to continue recording readings for at least 30 minutes and calculate the average value.

From Equation (3-3), knowing the geometrical characteristics of the specimen (refer Figure 1), the thermal conductivity of the acrylic material (k), and the difference between inner and outer temperatures (ΔT), it is possible to calculate the heat flow rate for each temperature. Figure 3-4 shows Q for different water temperatures ranging between 31°C and 82°C.

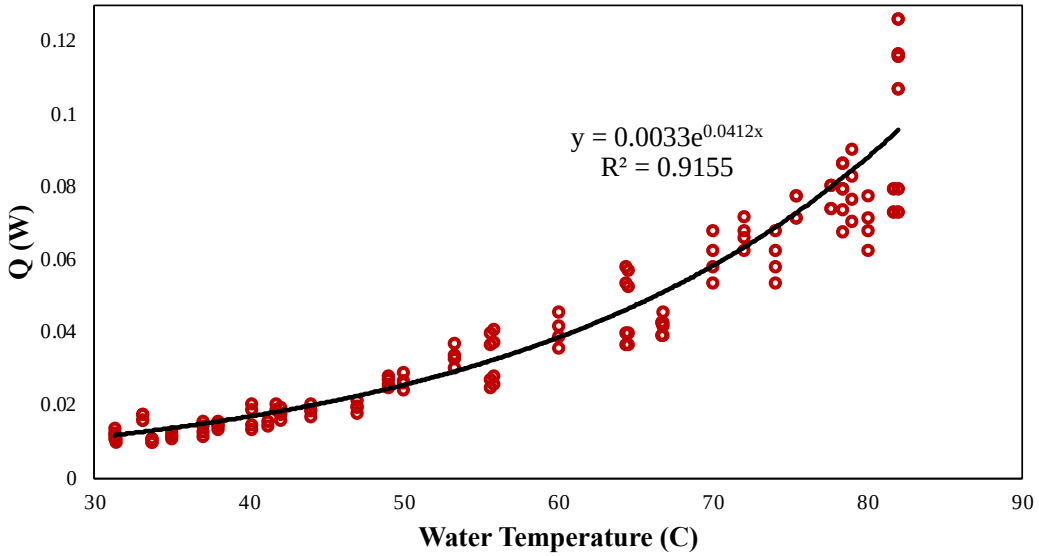

Figure 3-4. Heat flow rate (Q) as a function of temperature (°C)

Note that the acrylic material was used to estimate the heat flow rate of the system, which has a thermal conductivity of 0.185W/m°K. Equation (3-4) represents the results of

the calibration process to find Q as a function of water temperature; it can be used subsequently to calculate the thermal conductivity (k).

$$Q\ (W) = 0.0033e^{0.0412T1} \quad (3\text{-}4)$$

Where:

Q: heat flow rate (W=joule/s)

T1: the outer temperature (water temperature) (^{o}C)

The estimation of ¨Q¨ is an important step to determine the thermal conductivity of any test samples of interest using Equation (3-3). It depends on the thermal conductivity of the acrylic calibration sample being used. Therefore, the constant number 0.0033 in the exponential Equation (3-4) may change. In addition, the exponent part constant 0.0412 in the equation would remain the same if the system components being used are kept unchanged. This is because the exponent constant in the equation is dependent on the system configuration (e.g., water bath characteristics).

3.3 Thermal Conductivity of Bitumen/Asphalt Binder

To employ the above test procedure, it is needed to produce asphalt binder samples with similar dimensions to the acrylic cylinders. Therefore, special molds are needed to be made and used to pour in them the hot asphalt binder. The material used to create the mold was a commercial product that consists of two liquid substances. These substances need to be mixed in a specific proportion to get the raw silicone material. This silicone material

can support temperatures above 300°C. Figure 3-5 shows the silicone container / mold used to produce the asphalt binder samples for testing.

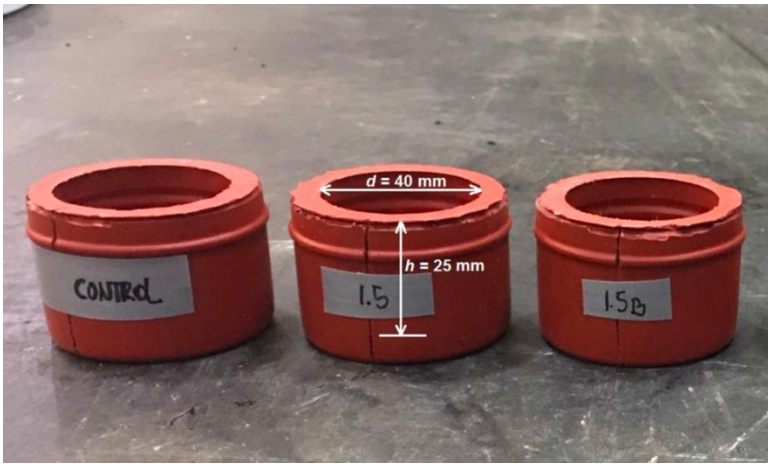

Figure 3-5. Silicon mold used for asphalt binder samples production and testing ("h" corresponds to the inner depth of the mold).

The use of silicone molds is very convenient due to their flexibility. Once the hot binder is poured in the mold and cooled down, a 2mm diameter hole is drilled in the center from the top to the middle of the cylinder height, like the acrylic cylinder test procedure described earlier. The hole in the center is made using a heated metallic rod or a screwdriver, both with appropriate diameters. As the air inside the samples can affect thermal conductivity, it is important to pour the material in the mold as hot as possible and leave it to cool down slowly undisturbed at room temperature. Before drilling or removing the samples from the mold, it is recommended to place the asphalt binder samples inside a freezer for 20 minutes at -10 °C. Figure 3-6 shows how the binder samples look like inside the silicone mold, and Figure 3-7 shows how those binder samples look like when removed from the containers.

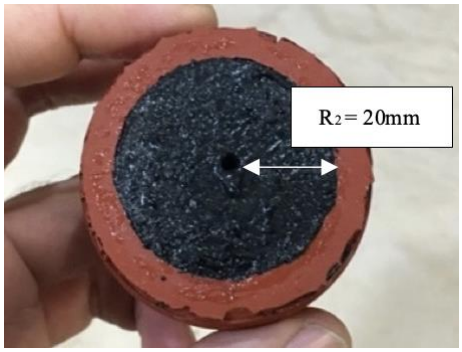

Figure 3-6. Asphalt binder sample inside the silicone mold.

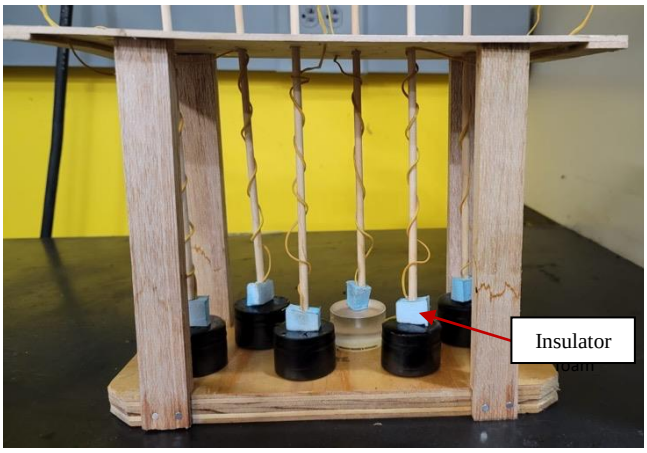

Figure 3-7. Asphalt binder samples ready to test.

Thermocouples are placed in the center hole, and the samples are placed on wooden platform. The insulator foam is placed on top, and high vacuum grease silicone on the bottom of the circular face of each sample. The grease helps the samples get locked on the wooden platform, insulating water at the bottom, and avoiding samples getting stuck. Figure 3-8 shows the final setup of the test before adding the foam on top. Note that the level of the water is just at the edge of the samples.

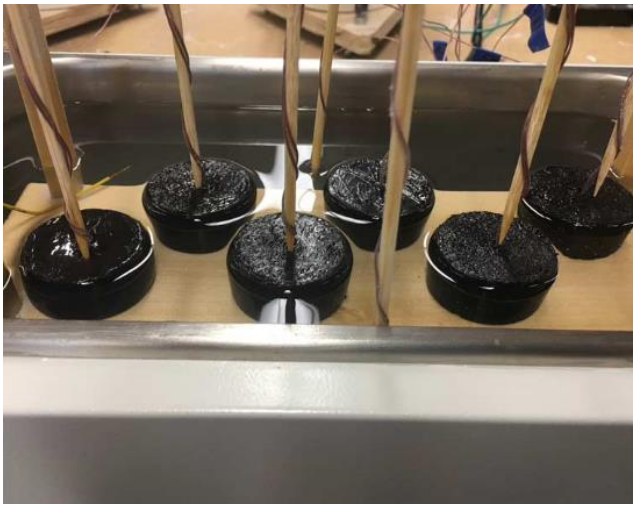

Figure 3-8. Setup of the thermal conductivity test for asphalt binders

Based on known thermal susceptibility of the asphalt binders, it is recommended to perform the test between 28°C and 40°C to avoid the softening of the samples. The temperature of the water would vary depending on the type of binder being evaluated. For softer binders such us PG58-22, and PG64-16, the recommended maximum test temperature is 28°C, which is about 15°C below their softening point measured with the ring and ball method (ASTM E28 – 67). For stiffer binders such as PG76-22, the recommended maximum test temperature is 33°C. Binders modified with polymers can be tested up to 40°C.

This method could be implemented using any type of water-bath following the calibration step described earlier in this document. In earlier experiments, the authors had also good success using type K thermocouples with an automatic USB output thermometer, and/or manually registering temperatures with time. Care in selecting, manipulating, and calibrating the thermocouples and water-bath will provide repeatable and accurate results.

This method can be used to calculate the thermal conductivity of any material with impermeable properties, so the water in the system, which controls the outer temperature, cannot get to the center of the sample where the inner temperature is taken.

3.4 Results of the Implementation

Eighteen samples of different virgin binders (PG58-22, PG64-16, and PG76-22), provided by HollyFrontier in Arizona, were tested using this developed method. Binders PG58-22 and PG64-16 are unmodified bitumen used for hot mix asphalt, emulsion production or further modification for higher temperature paving grades; whereas binder PG76-22 is a modified asphalt cement used for hot mix asphalt. The softest of these asphalt binders is PG58-22 and the stiffest is PG76-22 (Marathon Petroleum, 2018). Soft binders are more susceptible to temperatures changes and flow more at high temperature than stiff binders. It is also noted that lower ability of the binders to conduct heat (lower k) means better thermal resistance.

To get the heat flow rate (Q) for the three asphalt binders, Equation (3-4) of the base calibration model were used. Once Q is found, thermal conductivity is calculated based on Equation (3-3) by solving for Thermal Conductivity (k). As it was mentioned before, the whole system is employed inside a chamber setup at 25^{o}C, and the resulting thermal conductivity is estimated under this condition. Table 3-3 shows all the test results. The average test results for each binder grade produced repeatable outcomes that are like known thermal conductivity values; the coefficient of variation was also under 10% for

each binder. While the average thermal conductivity between the binder grades is statistically the same, there seem to be a trend of having slightly lower thermal conductivity for stiffer binders. This result is rational as one would expect a PG76-22 binder with a polymer modification should have lower thermal conductivity compared to a conventional / softer binder.

Table 3-3. Thermal conductivity of different binders

Binder Type	Sample No.	Sample's Height h (m)	Sample's radius r_2 (m)	Radius of the whole r_1 (m)	Outer Temp. (water) T1 (C)	Flow Rate Q (W) From Eq 3-4.	Sample's Inner Temp. T2 (C)	k (W/m°K) From Eq 3-3.	Av. k (W/m°K)	COV
Binder PG58-22	1	0.0250	0.020	0.001	31.37	0.01202	30.23	0.201	0.210	0.08
	2	0.0250	0.020	0.001	31.15	0.01191	30.16	0.229		
	3	0.0250	0.020	0.001	31.15	0.01191	29.89	0.180		
	4	0.0250	0.020	0.001	31.20	0.01193	30.18	0.223		
	5	0.0250	0.020	0.001	31.00	0.01184	29.95	0.215		
	6	0.0250	0.020	0.001	31.40	0.01203	30.32	0.212		
Binder PG64-16	7	0.0250	0.020	0.001	31.37	0.01202	30.16	0.189	0.206	0.07
	8	0.0250	0.020	0.001	31.15	0.01191	30.1	0.212		
	9	0.0250	0.020	0.001	31.15	0.01191	29.9	0.184		
	10	0.0250	0.020	0.001	31.20	0.01193	30.15	0.217		
	11	0.0250	0.020	0.001	31.00	0.01184	29.98	0.221		
	12	0.0250	0.020	0.001	31.40	0.01203	30.31	0.211		
Binder PG76-22	13	0.0250	0.020	0.001	31.37	0.01202	30.25	0.205	0.199	0.08
	14	0.0250	0.020	0.001	31.15	0.01191	29.9	0.178		
	15	0.0250	0.020	0.001	31.15	0.01191	29.9	0.179		
	16	0.0250	0.020	0.001	31.20	0.01193	30.10	0.207		
	17	0.0250	0.020	0.001	31.00	0.01184	29.95	0.215		
	18	0.0250	0.020	0.001	31.40	0.01203	30.31	0.211		

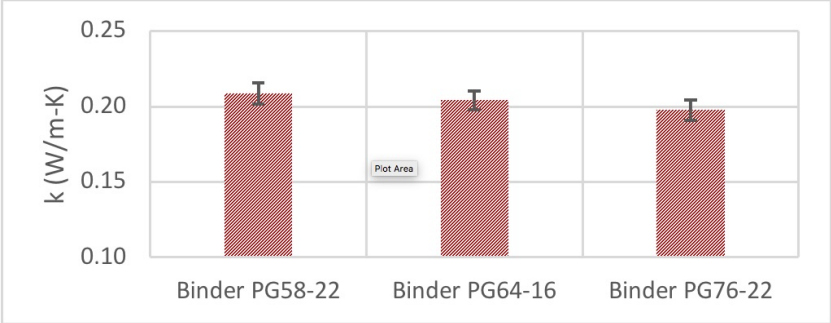

Figure 3-9. Average thermal conductivity of binder with the standard error

Thermal conductivity of asphalt binders in the literature range between 0.17W/m^{o}K and 0.28W/m^{o}K (Engineering ToolBox, 2003) (Côté, Grosjean, & Konrad, 2013). From Table 3-3, k varied between 0.23W/m^{o}K and 0.18W/m^{o}K (note that in the calculation, Celsius degrees are transformed to Kelvin).

To better demonstrate the capability of the developed test method in capturing a different thermal conductivity value for modified binders, the PG76-22 binder was modified with 5% AP1 Aerogel (refer Table 2-1). Aerogel is a material with extremely low thermal conductivity of about 0.012 (W/m^{o}K) (Pekala, 1989) (Cabot Corporation, 2013). The effect of the Aerogel's low thermal conductivity when added to binder was studied using the proposed method. For sample preparation, once the PG76-22 binder reached 165^{o}C in the oven, 5% of AP1 Aerogel by weight of binder was added and blended manually using a wooden stick for about 1 minute. The Aerogel modified binder along with a control were tested using the proposed method and the thermal conductivity results obtained are shown in Table 3-4.

Table 3-4. Thermal conductivity of unaged binder PG76-22 with different methods

Binder Type	Sample No.	Sample's Height h (m)	Sample's radius r_2 (m)	Sample's radius r_1 (m)	Outer Temp. (water) T1 (C)	Flow Rate Q (W) From Eq 4.	Sample's Inner Temp. T2 (C)	k (W/m°K) From Eq 3.	Average k (W/m°K)	COV
Control	1	0.0250	0.019	0.001	33.91	0.06185	32.71	0.211	0.199	0.06
	2	0.0250	0.019	0.001	33.91	0.06185	32.63	0.198		
	3	0.0250	0.019	0.001	33.91	0.06185	32.56	0.188		
5% Aerogel	1	0.0250	0.019	0.001	33.91	0.06185	32.25	0.153	0.166	0.08
	2	0.0250	0.019	0.001	33.91	0.06185	32.49	0.179		
	3	0.0250	0.019	0.001	33.91	0.06185	32.38	0.166		

The results supported the capability of the proposed test method in capturing lower thermal conductivity values, as expected, for the Aerogel modified binder. The precision was slightly higher, most likely due to the difficulty in uniformly distributing the Aerogel particles in the binder samples.

3.5 Concluding Remarks

The determination of thermal conductivity of the asphalt binders is very important in the understanding and improvement of its thermal performance. There are very few test methods and equipment to measure thermal conductivity of asphalt binders. Some of those are expensive and require special equipment and instrumentation. This study developed and validated a simplified alternative testing technique to measure thermal conductivity of asphalt binders. The determination of the thermal conductivity of bitumen samples using the method described was validated on material of known thermal conductivity. In addition, eighteen samples of different binder grades were tested using the developed method. The average test results were repeatable and within known thermal conductivity

values reported in the literature; the coefficient of variation between the various samples were in the 7 to 8% range. Additionally, the sensitivity and capability of the proposed method to capture lower thermal conductivity values were proven by using an Aerogel modified binder. This method to estimate thermal conductivity of bitumen samples was found to provide an affordable alternative test procedure with good accuracy and precision.

CHAPTER 4

CHARACTERIZATION AND ASSESSMENT OF AEROGEL-MODIFIED ASPHALT BINDERS

4.1 Introduction

Despite conventional asphalt binders have been used over decades with a relative satisfactory performance, nowadays it is necessary to re-evaluate their adequacy in meeting the demand for much extreme environmental impacts, higher traffic loads, and larger traffic volume. In addition, to tackle problematics associated with sustainable development, the improvement of the asphalt's resistance properties is needed (Hinislioglu, 2011).

The usage of modifiers in asphalt binders has been one of the most common methodologies to overcome actual necessities and thus improve the durability of bitumen mixes (Gordon, 2002). Some of the most known modifications has been the usage of polymers and crumb rubber, which predominantly have improved the temperature susceptibility of bitumen by increasing stiffness at high temperatures and reducing the probability of cracking at low temperatures (Collins, Bouldin, Gelles, & Berker, 1991) (Bruton, 2020), however, the low ageing resistance, poor storage stability of polymer modified bitumen (PMB), and high cost are some obstacles that limit the progress of bitumen polymer modification (Zhu, Birgisson, & Kringos, 2014), whereas the implementation of conventional use of crumb rubber in asphalt mixtures has some downsides such as binder storage stability, production complexities, the fumes that it releases through the paving process, and in some cases workability (Kuennen, 2004).

Although these technologies have been developed to make longer lasting asphalt pavements, they have not shown remarkable responses to overcome cost and production problems in their implementation.

As mentioned earlier, there are different innovative material that could make a different change in terms of material behavior. Examples of these materials are: phosphorene nanoribbons, a nanomaterial which has a corrugated structure that could improve the charging ions in electric vehicles, aircraft, and solar batteries 1000 times faster; black gold, a new material that can absorb the entire visible and near-infrared region of solar light and carbon dioxide with potential applications such as seawater desalination, artificial photosynthesis (taking carbon dioxide and transforming it into fuel), and solar energy collecting; and Aerogel, a solid material even though 99.98% of it is air. Aerogels are extremely porous and very low in density. Mars's enthusiasts consider silica aerogel could be employed to build domes near the red planet's polar ice caps (Thomas, 2019).

In this context, aerogel, a material with a unique geometrical structure and extremely low thermal conductivity (Tomas, 2012), would be an alternative technology to enhance the properties of the bitumen material, through the transference of its thermal properties to make a more stable asphalt material. Accordingly, this research effort is destined to provide insight on how the aerogel could effectively modify the asphalt binder in terms of thermal resistance. Moreover, not only the usage of the aerogel in asphalt binders due to the thermal conductivity benefits should be explored and assessed, but also the complexity in the implementation. Procedures related with safety concerns must be addressed.

4.2 Method and Materials

4.2.1 Asphalt Binder

The asphalt binders used in this study were Superpave Performance Grade, PG58-28, PG 64-16, and PG76-22, supplied by Holly Frontier, Glendale, AZ. The binder properties are shown in Table 4-1.

Table 4-1. Binders Properties

Type of Binder	Original Binder Properties				RTFO Binder Properties								PAV Binder Properties		
	G*/sin d, kPa	Abs Vis, P	SpG	Flash-point °C	G*/sin d, kPa	Mass Loss, %	Rec, 0.1 kPa, %	Rec, 3.2 kPa, %	Rec Diff, %	Jnr, 0.1 kPa, kPa^{-1}	Jnr, 3.2 kPa, kPa^{-1}	Jnr Diff, %	G*sin d, kPa	Stiff-ness Mpa	Rate
PG 58-28	1.26	1987	1.025	300	3.46	-0.21	1.27	0.00	100.%	3.80	5.60	47.4%	4.381	250	0.317
PG 64-16	1.58	2005	1.027	300	3.33	-0.21	3.77	0.61	83.8 %	2.75	3.05	10.9%	2.867	90.4	0.384
PG 76-22	1.60	2250	1.028	300	3.48	-0.22	89.03	80.06	10.1 %	0.11	0.20	86.5%	1.145	124	0.324

4.2.2 Aerogels Used

Different sources and types of aerogels were identified to determine which ones are the most promising to use in this study. One consideration was cost as each provider offered different price. It is very important to better understand the availability and characteristics of the various commercial products. Although more than eight different sources of Aerogel were found and characterized, in the beginning of this study only AP1 (refer Table 2-1) was used for the initial laboratory tests. AP1 was used in the three different binders with doses that ranged between 1% up to 10%. After, a weighting analysis considering variables such as cost per kilogram and laboratory results was done including five different types of Aerogels from four different sources to define the most suitable source to do all research plan of this dissertation. AP1 initial results were considered as the benchmark. Table 4-2

shows a summary of the aerogel products used in this research with their respective main characteristics.

Table 4-2. Characteristics of Aerogels used in this study

Aerogel Brand	Grains Availability	Maximum Particle's diameter (um)	Average Bulk Density (g/cm3)	Surface Chemistry	Average Thermal Conductivity (W/mK)	Price per Kilogram (US$)
AP1	Particles	700	0.13	Hydrophobic	0.012	$ 26.00
AP3b	Beads	20000	0.16	Hydrophobic	0.025	$ 11.00
AP8b	Beads	1000 - 6000	0.20	Hydrophobic	0.017	$ 1.00
AP9o	Granulates	0.01 - 0.2	0.15	Hydrophobic	0.019	$ 6.00
AP9i		1000 - 6000	0.20	Hydrophilic	0.019	$ 6.00

4.2.3 Implementation of Aerogel in Asphalt Binders

To be able to successfully blend in the two components, several safety measures should be considered. Aerogel, by nature, is volatile due to its low density and high specific surface. Procedure of mixing should be done inside a fume hood, with additional protection of a blast shield. The operator must wear flame-resistant lab coat and be grounded. These safety considerations are necessary to eliminate all kind of danger related to the formation of dust clouds and electrostatic discharges.

The period of mixing binder with aerogel was set to approximately 1 minute by manual mixing, while the binder is continuously maintained at the desired mixing temperature. Normally, a PG 76-22 requires a mixing temperature of 165°C.

Equipment needed to blend Aerogel with binder consider an oven, a heating plate, metallic containers, a spoon, a scale, and some wooden sticks. To blend Aerogel with binder, a specific procedure was established as follow:

- Preheat the virgin binder in the oven depending on the type of binder. For soft binders (PG50 to 60) 165^{o}C is enough, whereas for stiffer binders (PG70), 190^{o}C would provide the best conditions. Since Aerogel is a well-known insulator, mixing temperature is important to facilitate the blending and workability of the binder. As the mixing procedure has been carried on, the binder was cooling down much faster than usual.
- Preheat the heating plate. The heating plate is used in this case to provide additional heat and delay the cooling of the binder while mixing it with Aerogel (refer Figure 4-1.)
- Estimate the amount of binder needed to carry on the binder testing and calculate the needed amount of Aerogel as per the needed content. Add the needed amount of Aerogel with a metallic spoon to the binder. The metallic container where the binder is blended with Aerogel must be also grounded. As the amount of binder is determined, Aerogel is added using a scale.
- Mix the two materials using wooden sticks for 1 minutes using manual mixing. The binder and Aerogel are thoroughly mixed by means of a wooden stick, for 1 minute by hand to ensure dispersion of the particles
- Pour the samples according to the need for testing.

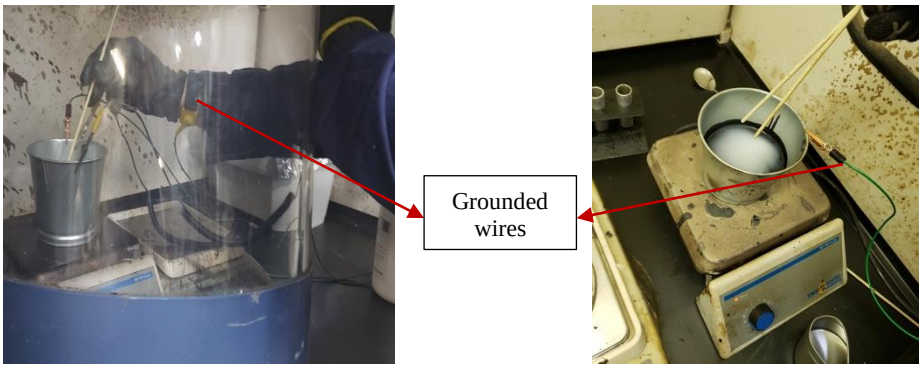

Figure 4-1. Mixing procedure – Aerogel plus Binder

4.2.4 Binder Testing Protocols

Main binder testing was done using AP1 in different percentages. As previously it was mentioned, the results of the testing using AP1 were considered as a benchmark. Binder study considered the following tests.

- Softening Point based on ASTM D36/D36M-14 (Standard Test Method for Softening Point of Bitumen, Ring-and-Ball Apparatus).
- Penetration test at 25°C based on ASTM D5- 97 (Standard Test Method for Penetration of Bituminous Materials).
- Rotational viscosity at 5 different temperatures (211, 250, 275, 300, 351°F) according to ASTM D4402-02 (Standard Test Method for Viscosity Determination of Asphalt at Elevated Temperatures Using a Rotational Viscometer).

Previous tests were performed for the three asphalt binders. Percentages of Aerogel by bitumen weight considered were Control (0% Aerogel) and 5% of Aerogel.

- Rheology of the binder using the Dynamic Shear Rheometer (DSR) as per ASTM D7175-08 (Standard Test Method for Determining the Rheological Properties of Asphalt Binder Using a Dynamic Shear Rheometer). Dynamic Shear Modulus was completed at 58^{o}C, 64^{o}C, 70^{o}C, 76^{o}C, 82^{o}C, 88^{o}C, and 96^{o}C. Ten frequencies ranging from 0.1 to 100 rad/s were considered in the test. This test was performed for the three binders using 0% (Control), 1.5%, 3.0%, 5.0%, 7.0% and 10.0% of Aerogel by bitumen weight.
- High temperature PG grading as per AASHTO M320. This test was conducted to evaluate the effect of different Aerogel contents into the binder at high temperatures. The PG grading was performed in short term aged (RTFO) binders, then $G^*/Sen\delta \geq 2.2kPa$.
- Stress Creep and Recovery (MSCR) based on AASHTO M-332-14 (Performance-Graded Asphalt Binder Using Multiple Stress Creep Recovery). This test was carried out for the three binders considering Control (0% Aerogel) and 5% of Aerogel by bitumen weight.
- Asphalt Binder Bond Strength (BBS) Test as per AASHTO Designation: TP-XX-11. The pull off tensile strength of asphalt binder from a siliceous surface was measured and determined via the bitumen bond strength test according to AASHTO TP 91. The substrate chosen was polished rock. The testing apparatus was the PATTI Quantum Gold Model which was calibrated before each testing set to a loading rate of 100 psi/second. This test was completed for the three binders considering 0%, 1.5%, 3%, 5%, 7.5% and 10% of Aerogel by bitumen weight.

- Thermal Conductivity of Asphalt Binders. This test was developed in The National Center of Excellence for SMART Innovations at ASU and described detailly in Chapter 3 of this Dissertation. Currently with a patent application in the United States Patent and Trademark Office: serial number 63/146,987 filed on February 8, 2021. Contents of Aerogel by bitumen weight used in this test were 0% (control), 5% and 15%. This test only was performed using an unaged binder PG76-22. To perform the test, samples were poured into a cylindrical silicon mold with a height of 25 mm, a half-height indent of 2 mm in the center, and a total radius of 20 mm. After being demolded, thermocouples were placed on the sample to track the temperature change between the sample's inner and outer layers. Equation (3-3) and (3-4) were used to calculate the heat passing through the sample (Q), and the thermal conductivity (k) respectively (Obando & Kaloush, 2021).
- Flexural Creep Stiffness of Asphalt Binder Using the Bending Beam Rheometer (BBR) as per AASHTO T 313-19. In terms of properties at sub-zero temperature, bending beam rheometer test was used to measure stiffness and stress relaxation capacity. The test is a three-point bending test of a bitumen beam with fixed length, width, and height performed under a cold bath of ethanol. The test measures flexural creep stiffness (S) and stress relaxation capacity (m-value) by applying a load of 980 ± 50 mN for the duration of 240s at the midpoint of the beam. The beam deflection (d) is measured at the center of the beam during the loading time and used to calculate the stiffness. This test was performed only for binder PG64-16 with 0%, 5%, 7.5% and 15% of Aerogel by asphalt binder weight.

4.2.5 Assessment of Different Aerogel Types by a Weighting Process

The weighting analysis was done to define the suitable Aerogel source to carry out all the research tasks considered in this Dissertation. Four Aerogel sources chosen to be used in the research for the weighting process. However, the fourth product considered hydrophobic and hydrophilic Aerogel. According to Tabla 2-1, these Aerogel materials are AP1, AP3b, AP8b, AP9o (hydrophobic), and AP9i (hydrophilic). Figure 4-2 shows the five different Aerogel acquired for laboratory testing.

Parameters such as penetration, softening point, the viscosity-temperature susceptibility parameters Ai and VTSi, %Recovery, bonding, thermal conductivity, and cost per kilogram were considered. The weighting process starts with a normalization process. Normalization factors were designed depending on each criterium to make possible the comparisons. Once all criterium are normalized, weighting process initiates considering scores depending on the target characteristics that are considered the proper for the research objectives (e.g., low thermal conductivity, low cost, high stability). Most important parameters that describe the thermal resistance of asphalt binders are %Recovery and thermal conductivity, so then these aspects were weighted with 10% and 25% respectively. Other important aspects are the once related with the mechanic properties such bonding, weighted with 10%, and with feasibility, such as cost. The last one weighted with 35%.

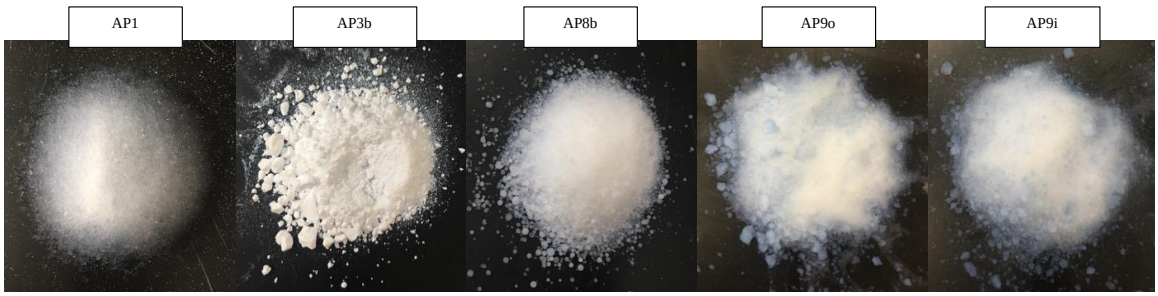

Figure 4-2. Different Aerogels acquired for laboratory testing.

4.3 Results and Discussion

4.3.1 Softening Point (SP) Test and Penetration (Pen)

The softening point (SP) is a distinctive property of the asphalt binder. It is defined as the temperature at which the binder has flowed under defined test conditions. One of the most important indicators towards the improvement in terms of thermal susceptibility of asphalt binders is the "softening point". According to the laboratory results, this aspect increases with the increase of aerogel content. Higher temperature reached in the test means better response of the asphalt binder. The penetration test measures the consistency of the asphalt binder. The higher the penetration value, the softer the binder. Penetration was measured for all the binder specimens and decreased with the increase of aerogel content. Adding 5% of aerogel, softening point increased and penetration decreased in about 25% and 55% respectively in all binder types. Therefore, all binders with aerogel increase the temperature of flow and the consistency. The results of softening point and penetration are summarized in Table 4-3.

Table 4-3. Aerogel content vs. Softening point and Penetration

Specimen Type	Softening Point (ºC)		Penetration (0.1 mm) @ 25ºC	
	Average	COV	Average	COV
Control PG58-28	41.5	0.017	92.75	0.052
PG58-28 + 5% aerogel	52.5	0.013	45.25	0.021
Control PG64-16	45.9	0.003	55.50	0.010
PG64-16 + 5% aerogel	57.0	0.025	18.80	0.190
Control PG76-22	60.5	0.012	51.75	0.053
PG76-22 + 5% aerogel	76.0	0.019	19.50	0.148

4.3.2 Rotational Viscosity (RV)

This test is performed to study the thermal susceptibility to change in temperature based on the measured viscosity at different temperatures. Outcomes of this test showed that the viscosity of the binder increases drastically when aerogel is added. It is also noted that with the increase of aerogel the workability of the binder decreases, aspect that should be addressed and further studied by increasing the binder's working temperature. The results of this test are shown in Table 4-4.

Table 4-4. Rotational viscosity.

Temp. °C	Binder PG58-28				Binder PG64-16				Binder PG76-22			
	Control		5% aerogel		Control		5% aerogel		Control		5% aerogel	
	Viscosity (cP)	COV	Viscosity (cP)	COV	Viscosity (cP)	COV	Viscosity (cP)	COV	Viscosity (cP)	COV	Viscosity (cP)	COV
98.9	2827.67	0.0016	149000.00	0.0841	3557.67	0.0028			20199.00	0.0814		
121.1	667.53	0.0033	17866.67	0.0963	807.67	0.0432	18941.33	0.1181	3384.00	0.0088	80210.00	0.0611
148.9	176.13	0.0056	2427.67	0.7599	208.93	0.0218	3732.00	0.0459	784.03	0.0136	16880.00	0.0211
176.7	63.33	0.0241	1300.33	0.0288	74.30	0.0088	1878.33	0.0448	275.60	0.0215	3616.33	0.0957

Temperature susceptibility analysis, involved penetration, viscosity, and softening data. The 5% aerogel content showed the lowest slope with respect to control (unmodified

binder). This indicated that binders modified with aerogel have lower susceptibility to temperature changes. Figure 4-3 shows the results for a binder PG76-22 modified with aerogel with a tabular inset into them for presenting the viscosity-temperature susceptibility parameters Ai and VTSi.

VTSi and Ai parameters represent the slope and the y-intercept respectively. The lower the slope (VTSi) the more stable behavior at different temperatures. So then, the flatter the curves the better thermal response (i.e., less deformation). Additionally, the parameter Ai, which represents the viscosity of the binder at low temperature, is lower for all binders modified with aerogel. This aspect denotes that the modified binders have lower viscosity at lower temperatures, which is translated into less cracking potential by stiffening at low temperatures. Figure 4-3 shows that binders modified with 5% aerogel have less thermal susceptibility.

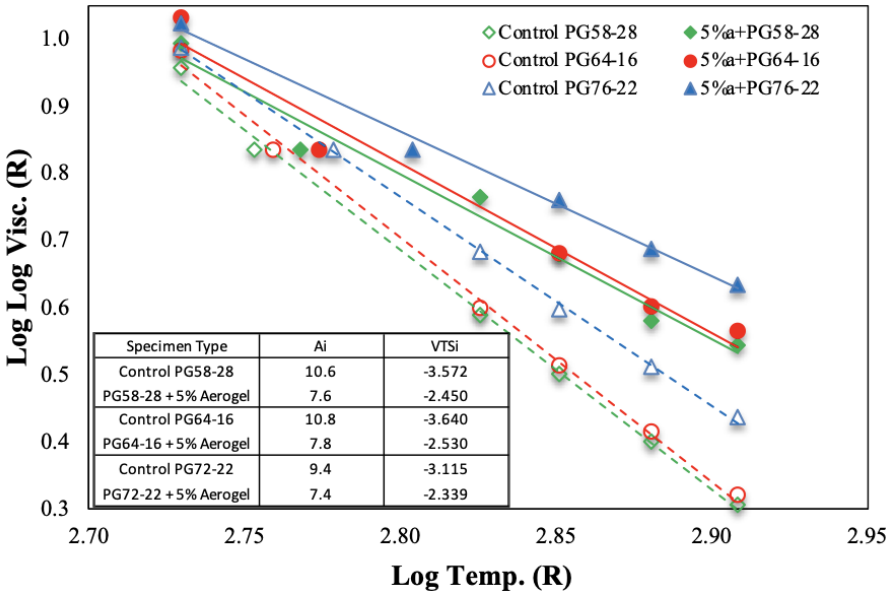

Specimen Type	Ai	VTSi
Control PG58-28	10.6	-3.572
PG58-28 +5% Aerogel	7.6	-2.450
Control PG64-16	10.8	-3.640
PG64-16 +5% Aerogel	7.8	-2.530
Control PG72-22	9.4	-3.115
PG72-22 +5% Aerogel	7.4	-2.339

Figure 4-3. Viscosity – Temperature Susceptibility of the Aerogel-Modified Asphalt Binders

4.3.3 Dynamic Shear Modulus |G|*

The most common way to present dynamic shear modulus is the Master Curve function. In The analysis of |G*| for binder PG64-16 is presented in Figure 4-4, where it increases with the increase of aerogel content, showing a good behavior of the binder at high temperatures. Concerning the phase angle, it decreases with the increase of aerogel content. In general, having aerogel mixed with the binder will increase the binder response at high temperatures. This means that the pavement would behave well in terms of rutting. As for the lower phase angle, it reflects that the binder with aerogel tends to behave more flexible. Table 4-5 presents a summary of the results at 82ºC, 10rad/sec for the three binders.

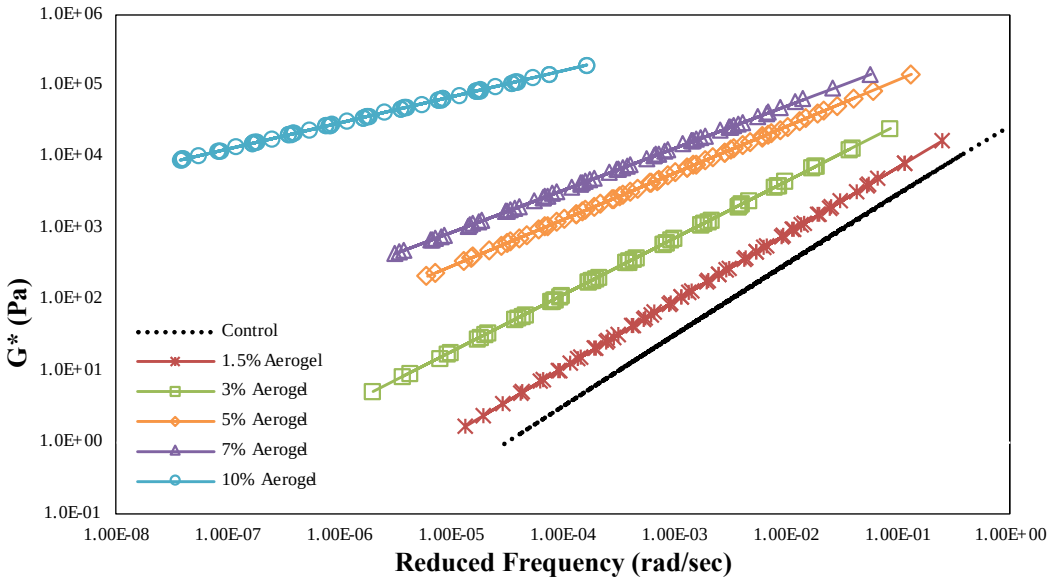

Figure 4-4. Dynamic Modulus G* Master Curves for binder PG64-16.

Table 4-5. │G*│ and Phase Angle values for the three binders

Specimen	PG58-28				PG64-16				PG76-22			
	Dynamic Shear Modulus │G*│ (Pa)	COV	Phase Angle (º)	COV	Dynamic Shear Modulus │G*│ (Pa)	COV	Phase Angle (º)	COV	Dynamic Shear Modulus │G*│ (Pa)	COV	Phase Angle (º)	COV
Control	105.8	0.33	89.9	0.11	161.3	0.22	89.5	0.11	957.0	0.04	72.0	0.14
1.5% aerogel	250.3	0.14	87.9	0.12	342.1	0.10	84.9	0.12	2364.5	0.01	68.0	0.15
3.0% aerogel	358.2	0.10	84.5	0.12	614.8	0.06	77.4	0.13	2700.3	0.01	57.2	0.18
5.0% aerogel	1158.0	0.03	82.0	0.12	4444.7	0.01	63.1	0.16	6965.1	0.01	52.6	0.19
7.0% aerogel	7250.3	0.00	48.6	0.21	6421.4	0.01	63.3	0.16	20887.0	0.00	44.5	0.23
10.0% aerogel	22350.2	0.00	38.3	0.27	41241.0	0.00	35.0	0.29	64253.0	0.00	33.2	0.31

4.3.4 High Temperature PG Grading

The classification of an asphalt binder using the asphalt pavement relative performance at different temperatures is known as the performance grade (PG). It was initially developed through the Strategic Highway Research Program (SHRP) in the 1990's (SuperPaveTM). This methodology is based on the concept that asphalt binder properties should be related to the conditions under which the binder is used (air and pavement temperatures). Short term aging PG asphalt binders are classified and selected to meet performance criteria, in this case high temperature considering the relation between G* and phase angle, which must be equal or grader than 2.2kPa (Minnesota Asphalt Pavement Association, 2008).

Table 4-6. High Temperature PG for Binders modified with Aerogel.

Aerogel Content	PG58-28	PG64-16	PG76-22
Control	58	64	76
1.5% aerogel	58	64	76
3.0% aerogel	58	64	82
5.0% aerogel	64	70	82
7.0% aerogel	64	70	82
10.0% aerogel	70	76	88

Table 4-6 presents the results of the high temperature PG grading for RTFO aerogel modified binders PG58-28, PG64-16 and PG76-22 evaluated at ≥ 2.2 kPa, 10rad/sec. Results show that all binders increase the high temperature grading as the aerogel content increases. This means that all modified binders keep meeting the performance criteria at higher temperatures demonstrating that the aerogel modified binders have much better response than conventional bitumen.

4.3.5 Multiple Stress Creep Recovery Test (MSCR)

This test is mainly performed to understand the rutting behavior of the pavement structures. It studies the accumulated permanent strain (which is represented by the rutting depth) and the percent of strain recovery under a cyclic load of 0.1s loading and 0.9s resting period. This test was performed at 58ºC, 64ºC, and 76ºC, for binders PG58-28, PG64-16, and PG76-22 respectively. Testing for aerogel modified binders was done accordingly their high temperature PG grading. Results are summarized in Table 4-7.

As for the MSCR test, the recovery values for the specimen having aerogel are considerably high for both loading of 0.1 and 3.2 kPa. It can be clearly seen that a big

portion of the strain is recovered, whereas for the control binder the percent recovery is relatively low.

Considering the non-recoverable creep compliance (Jnr), it is decreasing with the increase of aerogel content. This reflects that aerogel specimens are very good in terms of rutting distresses and behave very well for these cases. As the Jnr is lower and %Recovery is higher in more than %100 in both aspects for all type of binders, the response of these specimens shows a good overall behavior for the pavement structure.

Table 4-7. Recovery and Jnr results.

Aerogel Content	Recovery 0.1kPa	COV	Recovery 3.2kPa	COV	Jnr 3.2kPa (1/kPa)	COV
Control PG58-28	0.00	0.00	0.00	0.00	7.14	0.10
5.0% aerogel PG58-28	66.35	0.11	10.72	0.70	0.41	0.34
Control PG64-16	0.00	0.00	0.00	0.00	8.75	0.16
5.0% aerogel PG64-16	85.98	0.09	6.18	1.21	0.61	1.16
Control PG76-16	36.93	0.20	3.20	1.14	6.30	1.19
5.0% aerogel PG76-16	92.41	0.08	56.35	0.13	0.07	1.01

4.3.6 Asphalt Binder Bond Strength by Means of the Binder Bond Strength (BBS)

The asphalt binder bond strength (BBS) was determined for the three binders, however, the temperature of application (i.e., the temperature at which the binder is applied to the substrate) to ensure he appropriate bonding. Therefore, the higher the aerogel content, the temperature of application increases. This concept should be further considered in the process of mixing when making asphalt mixtures.

The results showed that the bonding mechanism varied depending on the type of binder and the percentages of aerogel. Failure in the pull-off test must be by cohesion (i.e.,

failure in the binder) not by adhesion, where it is observed a total separation between binder and substrate. In this context, it is possible to conclude that the best response for binders PG58-28 and PG64-16 in terms of bond strength could be found around 7% of aerogel content, whereas in binder PG76-22, the best response could be between 5% and 7% of aerogel content.

Besides to the workability evaluated by the viscosity, this is the first technical approach to determine the desirable range of aerogel content in asphalt binders. Table 4-8 shows a summary of the results.

Table 4-8. Binder Bond Strength test results for the three binder types.

Binder PG58-28						
Conditions	Tensile Strength (kPa)					
Aerogel Content	Control	1.5%	3.0%	5.0%	7.0%	10.0%
App. Temp 75ºC	1586.3	773.2	773.9	1604.5	1609.1	653.1
COV	0.0399	0.0477	0.1126	0.0097	0.1392	0.0890
Type of Failure	COHESION					
Binder PG64-16						
Conditions	Tensile Strength (kPa)					
Aerogel Content	Control	1.5%	3.0%	5.0%	7.0%	10.0%
App. Temp 75ºC	1801.7	994.5	943.9	1824.9	1887.4	963.4
COV	0.0706	0.0495	0.0088	0.0335	0.1392	0.0804
Type of Failure	COHESION					
Binder PG76-22						
Conditions	Tensile Strength (kPa)					
Aerogel Content	Control	1.5%	3.0%	5.0%	7.0%	10.0%
App. Temp 105ºC	1901.3	1581.6	1888.8	1862.2	1855.9	1905.2
COV	0.0502	0.0149	0.0377	0.0190	0.0194	0.0342
Type of Failure	COHESION				ADHESION	

4.3.7 Thermal Conductivity of Asphalt Binders

Results of thermal conductivity are encouraging. Thermal conductivity decreases while the aerogel content increases (binder with aerogel content is less thermal susceptible). It is known that asphalt binders are highly susceptible facing temperature changes and at high temperatures, consequently, getting a lower thermal conductivity would provide insulating properties to the binder, it is that the lower the thermal conductivity the heat transfer decreases improving the response of asphalt pavements. Table 4-9 presents a summary of thermal conductivity for binder PG76-22 with different aerogel contents.

Table 4-9. Thermal conductivity of binder PG76-22.

Binder Type	Sample No.	k (W/m^{o}K) From Eq 3.	Average k (W/m^{o}K)	COV
Control	1	0.201	0.195	0.04
	2	0.198		
	3	0.186		
5% aerogel	1	0.153	0.170	0.09
	2	0.179		
	3	0.177		
15% aerogel	1	0.132	0.132	0.06
	2	0.140		
	3	0.125		

Figure 4-5 shows two samples of unaged binder PG76-22. At the right-hand side is Control (0% aerogel), and at the right-hand side a binder with 10% of aerogel content by weight of bitumen. Those two samples were put into a convection oven at 70^{o}C for 40mins. It can be seen the extraordinary response of the aerogel modified with aerogel; while the control binder sample ended totally collapsed, the one with 10% of aerogel did not suffer

easy notable deformations. This empirical test confirms the remarkable response of the modified binder with aerogel to suppress the heat effect. The lower thermal conductivity limits the heat transfer, so then it results into a less thermal susceptible and much more stable asphalt binder

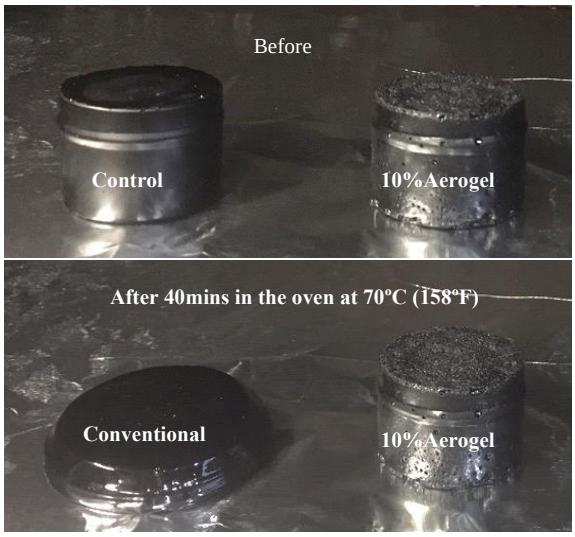

Figure 4-5. Empirical test of the aerogel binder thermal stability.

4.3.8 Flexural Creep Stiffness of Asphalt Binder Using the Bending Beam Rheometer (BBR)

In this test, only beams of binder PG64-16 were performed. Samples were placed in a bath of Ethanol at -6^{o}C and -22^{o}C. The maximum bending strain is calculated based on the dimensions of the specimen and the deflection for the respective loading times. Two parameters are of interests: the creep stiffness of the sample at the test temperature and the m-value. The creep stiffness of the sample is calculated by dividing the maximum bending stress by the maximum bending strain. It describes the low temperature stress-strain response of the sample. As for the m-value, it is the absolute value of the slope of the

logarithm of stiffness vs. time, then, the higher the m-value the more flexible binder's behavior at low temperatures. In general, it must be ensured that the binder is soft enough at low temperatures and that it can relax (deform) quickly enough to prevent cracking.

The results for control and the modified binders are summarized in Table 4-10 and Table 4-11. The results show a slightly increase in the creep stiffness but not in the m-value which decreases slightly respect to control when aerogel is added into the binder. In other words, one can say that the binder modified with aerogel becomes stiffer at subzero temperatures without losing the original flexible properties.

Table 4-10. BBR results for binder PG64-16 at -6°C.

Specimen	Stiffness (MPa)			m-Value		
	Average	Std. Error	COV	Average	Std. Error	COV
Control	76.2	5.6	0.1	0.411	0.0078	0.033
Aerogel 5%	90.4	1.3	0.0	0.389	0.0032	0.014
Aerogel 7.5%	105.2	6.5	0.1	0.375	0.0068	0.031
Aerogel 15%	93.4	1.4	0.1	0.381	0.0031	0.011

Table 4-11. BBR results for binder PG64-16 at -22°C.

Specimen	Stiffness (Mpa)			m-Value		
	Average	Std. Error	COV	Average	Std. Error	COV
Control	427.7	3.5	0.1	0.239	0.0081	0.041
Aerogel 5%	505.8	1.6	0.1	0.229	0.0042	0.018
Aerogel 7.5%	484.8	5.2	0.2	0.217	0.0072	0.038
Aerogel 15%	459.6	1.6	0.0	0.230	0.0028	0.020

Table 4-12 shows the results of the low temperature PG for the binder checking the stiffness and m-value. Taking the temperature vs. m-value and temperature vs. stiffness at

the two different temperatures, it was supposed a linear behavior to obtain the low PG grading considering the Superpave binder specification requirements. Based on the results, contrary to the high temperature PG grading, the low temperature PG grading of binders modified with aerogel is not improved, however, it is slightly decreased in about 1.5^{o}C.

The evaluation of binders at low temperature requires a high m-value because as the thermal stresses accumulate and the temperature decreases, the stiffness changes quite fast. A fast change in stiffness means that the binder tends to release stresses that would otherwise reach a level where low temperature cracking would occur. The Superpave binder specification requires a minimum m-value of 0.300 (FHWA, 2017). To prevent cracking, creep stiffness has a maximum limit of 300 MPa.

Table 4-12. Low temperature PG grading.

Specimen	Maximum Stiffness 300 MPa	Minimum m-value 0.300
	PG	PG
Control	-16.19	-16.33
Aerogel 5%	-14.07	-14.94
Aerogel 7.5%	-14.21	-14.62
Aerogel 15%	-15.03	-14.57

4.3.9 Assessment of Different Aerogel Types by a Weighting Process

The evaluation and feasibility of different aerogel alternatives were completed using an unaged binder PG76-22 based on a normalization and weighting process. In this assessment 3% of aerogels AP1, AP3b, AP8b, AP9o, and AP9i was used to modify the binder. Table 4-13 present the test results of all tests for each type of aerogel with the respective normalization factor to apply.

Table 4-13. Test results and Normalization factors.

Test	Normalization Factor	Test Results					
		Control	AP1	AP3b	AP8b	AP9o	AP9i
Penetration 0.1mm (pen)	1-(pen/100)	51.75	38	27.5	26.0	21.25	22
Softening Point (ºC) (Sof)	Sof/100ºC	60.5	74.5	74	74.5	74.5	74.5
Ai	2-(Ai/5)	9.44	7.96	8.76	9.03	8.24	8.97
VTSi	1+(VTSi/10)	-3.12	-2.57	-2.85	-2.95	-2.66	-2.93
High Temp. PG	PG/150	76	82	82	82	82	82
* Dynamic Shear Modulus |G*| (Pa)	G*/5000 Pa	956.97	2700.3	1526.7	1419.3	3021	2193.6
* Phase Angle (δ)	1-(δ/100)	72	57.22	60.81	61.2	55	58.73
% Recovery 0.1kPa (R0.1)	R0.1/100 Kpa	36.93	88.38	89.26	82.1	88.29	89.31
% Recovery 3.2kPa (R3.2)	R3.2/100 Kpa	3.2	41.78	36.27	37.23	39.13	39.95
BBS - Tensile Strength (PSI)	BBS/200 kPa	1166.14	1164.93	1164.13	1162.67	1143.86	1156.85
Thermal Conductivity W/mK (k)	1-k (W/mK)	0.195	0.187	0.189	0.188	0.187	0.188
Cost per Kilogram (US$)	1-(cost/540)	N/A	26.0	11.0	1.0	6.0	6.0

* Evaluated at ≥ 1.0 kPa, 10rad/sec

Table 4-14 shows a summary of the different tests results. Although, it is noted that the technical tests response of all different aerogels is similar, “cost” is the aspect that stands out in the feasibility analysis.

Table 4-14. Weighting factors and Results of the assessment.

TEST	Weighting Factor	Control	AP1	AP3b	AP8b	AP9o	AP9i
Penetration 0.1mm (pen)	1	0.48	0.62	0.725	0.74	0.7875	0.78
Softening Point (ºC) (Sof)	6	3.63	4.47	4.44	4.47	4.47	4.47
Ai	2	0.22	0.81	0.50	0.39	0.70	0.41
VTSi	2	1.37	1.49	1.43	1.41	1.47	1.41
High Temp. PG	2	0.96	1.01	1.01	1.01	1.01	1.01
* Dynamic Shear Modulus |G*| (Pa)	2	0.38	1.08	0.61	0.57	1.21	0.88
* Phase Angle (δ)	2	0.56	0.86	0.78	0.78	0.90	0.83
% Recovery 0.1kPa (R0.1)	3	1.10	2.65	2.98	2.61	2.95	2.98
% Recovery 3.2kPa (R3.2)	10	0.32	4.18	3.63	3.72	3.91	4.00
BBS - Tensile Strength (PSI)	10	8.45	8.45	8.44	8.43	8.30	8.39
Thermal Conductivity W/mK (k)	25	20.11	20.33	20.28	20.3	20.33	20.30
Cost per Kilogram (cost)	35	N/A	1.10	23.66	33.7	29.23	29.23
Result	100		47.04	68.48	**78.14**	75.26	74.68

In Table 4-14 is shown each weighting factor according to the weighting process explain in section 4.2.5. Although these factors can be of arbitrary nature, scoring changes depending on the application. In this case, the weighting score for each test result was estimated considering the problem statement of this study, decrease the asphalt materials' thermal susceptibility to tackle thermal cracking. Contemplating the eventual economic feasibility for the real implementation, the cost of the aerogel, was highly weighted. Test results are operated by the normalization and then by the weighting factor giving a score for each aspect evaluated. The higher value of the summation of the all the scores for each type of aerogel defines the best aerogel source. Thermal resistance properties and cost per kilogram of each product ended up determining the suitable aerogel product to continue further testing and future development of this research work. AP8b resulted as the most

proper alternative to continue with further analysis considered in the next Chapters of this dissertation.

4.4 Conclusions

One of the most important indicators towards the improvement in terms of thermal susceptibility of asphalt binders is the “softening point”. Penetration was measured for all the binder specimens and decreased with the increase of aerogel content. Adding 5% of aerogel, softening point increased and penetration decreased in about 25% and 55% respectively in all binder types. Therefore, all binders with aerogel increase the temperature of flow and the consistency. The outcomes of Rotational Viscosity showed that the viscosity of the binder increases drastically when aerogel is added. Based on the parameters VTSi and Ai, the modified binders have lower viscosity at lower temperatures, which is translated into less cracking potential by stiffening at low temperatures.

The value of $|G^*|$ increases with the increase of aerogel content, showing a good behavior of the binder at high temperatures. Concerning the phase angle, it decreases with the increase of aerogel content. As for the lower phase angle, it reflects that the binder with aerogel tends to be far from the pure viscous behavior. Results of the high temperature PG grading for RTFO aerogel modified binders showed that all binders increase the high temperature grading as the aerogel content increases. This means that all modified binders keep meeting the performance criteria at higher temperatures, so then, the aerogel modified binders have much better response than conventional bitumen. As the Jnr is lower and %Recovery is higher in more than %100 in both aspects for all type of binders, aerogel specimens are very good in terms of rutting distresses and behave very well for these cases.

The best BBS response for binders PG58-28 and PG64-16 could be found around 7% of aerogel content, whereas in binder PG76-22, the best response could be between 5% and 7% of aerogel content.

Results of thermal conductivity are encouraging. The aerogel modified binders have remarkable response suppressing the heat effect. The lower thermal conductivity limits the heat transfer, so then it results into a less thermal susceptible and much more stable asphalt binder.

Results of BBR showed that aerogel makes increase the creep stiffness of the bitumen but not in the m-value which decreases slightly respect to control. One can say that the binder modified with aerogel becomes stiffer at subzero temperatures without losing the original flexible properties. Based on the results, contrary to the high temperature PG grading, the low temperature PG grading of binders modified with aerogel is not improved, however, it is slightly decreased in about 1.5^{o}C.

It was concluded that the technical response of the five different aerogels considered in this study is very similar, then "cost" is the aspect that stands out in the feasibility analysis. Thermal resistance properties and cost per kilogram of each product could determine the suitable aerogel product for further utilization.

The outcomes of this investigation are encouraging. The usage of Aerogel made possible to improve the thermal susceptibility of bitumen, which would be advantageous in terms of permanent deformation and thermal cracking, however, the mixing/working temperature of binders with aerogel may be increased to have better workability/fluidity. On the other hand, further investigation needs to be directed to meet the successfully implementation of aerogel in bituminous materials and other possible applications. Mixing

procedures need further refining and research to be optimized and standardized. The procedures need to meet all the safety requirements and eliminate the dust formation and electrostatic discharges. In addition, the homogeneity and right dispersion of the aerogel particles inside the binder must be evaluated and addressed.

CHAPTER 5

A NOVEL POROUS SILICA-BASED MODIFIER, AEROGEL MODIFIED BITUMINOUS MATERIALS (aMBx)

5.1 Introduction

Aerogel is a low density, highly porous, and effective insulating material. Albeit the usage of aerogel in asphalt binders have shown that the thermal susceptibility of these materials decreases substantially making stronger and then likely longer-lasting bituminous materials, the use of aerogel particles directly into the asphalt binders or mixtures associates some complexities such as the difficulty to blend aerogel with binders, and safety concerns as it was presented in Chapter 4. These considerations drastically limit the implementation of aerogel. Safety glasses, special gloves, blast shield, grounding to avoid electrostatic discharges due to the fine aerogel particles friction, and the development of a Safety Operation Procedure (SOP) is necessary to conceive as a possibility the implementation of aerogel. Therefore, it is necessary to develop an alternative approach to using the aerogel in the asphalt materials. A new methodology to facilitate, make doable and feasible, the implementation of aerogel in the asphalt industry was developed and improved upon throughout this research work as one of the main accomplishments of this study. The new product can be used directly into an asphalt mixture and is referred to as aMBx (Aerogel Modified Bituminous Materials). aMBx is a synthetic porous silica-based material developed in the Advanced Pavement Laboratory at Arizona State University currently with a patent application in the United States Patent and Trademark Office: serial

number 63/210,891 filed on June 15, 2021, of which the author of this Ph.D. Dissertation is co-inventor.

5.2 Development of aMBx

This new product is processed through a special treatment of aerogel particles with asphalt binder and/or other products. The concept of using aerogel in asphalt binders and mixtures safely is one of most important focus of this research. It fits the general idea that asphalt binders and mixtures can be modified to reduce thermal cycling in pavements and other materials and increase their durability. The use of pre-treated aerogel composites would solve the safety and handling concerns. This invention involved the design, development and testing of an innovative porous product (aMBx) as a modifier in bituminous constituents to function as a material with unique thermal resistance properties and provide urban cooling benefits. The versatility of this product is such that it is possible to use aMBx in different infrastructure applications.

This chapter presents the development of novel aerogel modified bituminous binders and mixtures (aMBx) to minimize pavements' thermal susceptibility and role in urban heat through lower temperature conductivity. aMBx is an aerogel composite, comprising aerogel in the form of granular or powder, with the presence of a co-product of the petroleum-refinery system (e.g., heavy oil products, asphalt binders) or compatible material (e.g., synthetic polymers, organic polymers, lignin) as an encapsulator. These elements are blended at different percentages by weight, and the result is a composite.

The conception of the composite, aMBx, as a determining factor to transfer all the aerogel benefits studied in Chapter 4 into the asphalt industry ensuring the implementation and removing the safety concerns, marked a milestone. Different particle size of the aerogel was tried, as also different temperature and amount of kinetic energy were improved along the process. The engineering process of manufacturing aMBx was repeated multiple times considering equipment, raw material characteristics and ratios, and time to get the desirable product. Figure 5-1 present some of the initial versions of aMBx until deciding on the current final product.

Figure 5-1. Different version of the aMBx composite.

The novel modified paving material can provide performance benefits solving common shortcomings of asphalt pavements, namely, high temperature deformation and thermal cracking. The aMBx will increase resistance to temperature susceptibility, provide a more durable roadway (refer to Chapter 8 and 9), and reduce heat conduction contributing to the night-time urban cooling (refer to Chapter 7). Figure 5-2 shows various aMBx products manufactured using different sources of aerogel as they were described in Chapter 4.

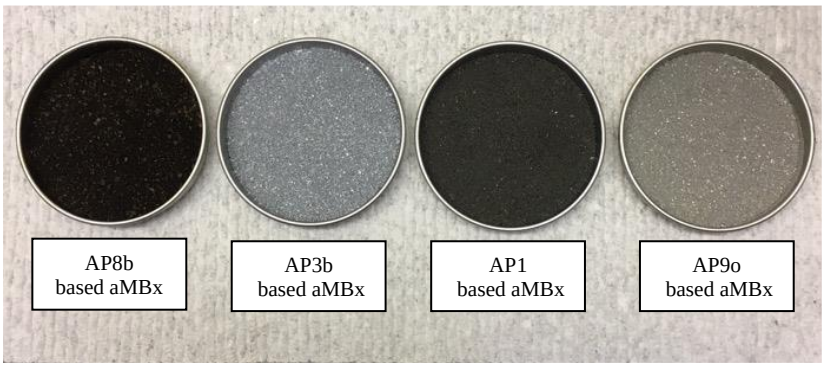

Figure 5-2. aMBx products based on different aerogel sources.

5.3 aMBx Specifications

The invention presented herein annuls all safety concerns brought by the aerogel particles and facilitate the blending with other bituminous materials such as asphalt emulsions used in different road surface treatments, asphalt mixtures (hot, warm, and cold), asphalt roofing shingles, and asphalt sealants (crack repairs and joint protection). As these particles are weighed down by the presence of the encapsulator. The term composite is used to denote a composite of matter of the invention with at least two components (i.e., asphalt binder, aerogel particles and other additives). Therefore, the invention provides an asphalt-based composite (aMBx), in which aerogel particles are ground and blended as part of the treatment.

The process of the invention involves creating a product with a unique combination of high kinetic energy mixing steps at high temperatures with unique equipment designed for these purposes. This process allows the obtention of a relatively quick coating of the

aerogel particles and a homogeneous blend leading to granular ending product (aMBx). The steps of mixing are conducted under conditions of high sheer rate, meaning the mixing is performed under such conditions that high kinetic energy is produced into the mixture while mixing. Figure 5-3 shows some of the equipment used to produce aMBx.

Figure 5-3. Manufacturing of aMBx.

The thermal insulative properties of aerogel are therefore incorporated into the bituminous materials and are distributed within the mastic by the addition of aMBx in different contents depending on the needs. By introducing this product into bituminous compounds, thermal and mechanistic benefits are achieved.

Because its components, this composite presents hydrophobic properties. This material has relatively low thermal conductivity and density. The density ranges from 0.32

to 0.38 g/cm^3 and thermal conductivity from 0.08 to 0.12 W/m^{o}K, properties related to the fact that this material is around 50% air. The total size of the coated particle could range from 0.1 to 3mm. Table 5-1 shows the gradation of the material.

Table 5-1. Granulometric Distribution of aMBx.

Sieve (US – mm)	% Passing
#16 - 1.18	94.77%
#30 - 0.6	59.64%
#50 - 0.3	22.89%
#100 - 0.15	3.85%
#200 - 0.075	0.55%
PAN	0.00%

One important feature of aMBx is the relatively low thermal conductivity and light-weight density. Consequently, this low thermal conductivity will provide thermal benefits and decreased thermal susceptibility to bituminous materials. Other benefits were realized by the addition of this modifier and will be discussed in the following paragraphs.

5.4 aMBx Modified Binders' Laboratory Tests Analysis

In Chapter 4, it was demonstrated that the usage of aerogel in asphalt binders improve their thermal/stability response. In this Chapter, aMBx-modified asphalt binders' properties are compared with unmodified and aerogel-modified binders to confirm that the properties of the aerogel are transferred to the asphalt binder by adding aMBx.

To add aMBx to the asphalt binders, the binder is heated at its maximum operational temperature given by the viscosity analysis. The process requires normal stirring until the

modifier (aMBx) is totally blended with the binder. Test such us softening point, penetration, rotational viscosity, dynamic shear modulus, high temperature performance grading (PG) by means of the dynamic shear rheometer (DSR), multiple stress creep recovery (MSCR), asphalt binder bond strength (BBS), thermal Conductivity, and Flexural Creep Stiffness of Asphalt Binder Using the Bending Beam Rheometer (BBR) to obtain the low temperature PG grading, are performed to confirm the benefits of aMBx in asphalt binders. Characterization and evaluation of the benefits of aMBx in asphalt mixtures are presented in Chapters 7 to 11.

For the following tests, a binder PG64-16 was used using Control (unmodified binder), 10% aMBx, and 5% of aerogel which would correspond to 10% aMBx. Percentages of aMBx and aerogel are calculated based on the weight of the binder. Protocols and materials used to perform all laboratory analysis are the same followed in Chapter 4. Results of the test are presented below:

5.4.1 Softening Point (SF) and Penetration (Pen)

SF test based on ASTM D36/D36M-14 (Standard Test Method for Softening Point of Bitumen, Ring-and-Ball Apparatus), and Pen test at 25°C based on ASTM D5- 97 (Standard Test Method for Penetration of Bituminous Materials). Table 5-2 presents the results of softening point and penetration.

Table 5-2. Softening point and Penetration.

Specimen Type	Softening Point (ºC)		Penetration (0.1 mm) @ 25ºC	
	Average	COV	Average	COV
Control	45.9	0.003	55.50	0.010
5% aerogel	57.0	0.025	18.80	0.190
10% aMBx	53.0	0.022	25.50	0.185

One of the important indicators towards the improvement of the asphalt binder performance is “softening point”. This value increased with the increase of aMBx content. Higher temperatures were reached in the test meaning better performance of the asphalt binder. On the other hand, penetration values decrease as the aMBx content increases, which indicates that the binder get stiffer with the addition of aMBx.

5.4.2 Rotational Viscosity (RV)

This test was performed at 5 different temperatures (98.9ºC, 121.1ºC, 148.9ºC, and 176.7ºC) according to ASTM D4402-02 (Standard Test Method for Viscosity Determination of Asphalt at Elevated Temperatures Using a Rotational Viscometer). Table 5-3 shows the results of RV.

Table 5-3. Rotational viscosity.

	Control		5% aerogel		10% aMBx	
	Viscosity (cP)	COV	Viscosity (cP)	COV	Viscosity (cP)	COV
98.9	3557.67	0.0028				
121.1	807.67	0.0432	18941.33	0.1181	13256.23	0.0632
148.9	208.93	0.0218	3732.00	0.0459	2088.58	0.0312
176.7	74.30	0.0088	1878.33	0.0448	748.30	0.0128

Outcomes of this test showed that the viscosity of the binder increases drastically when aerogel is added. It is also noted that with the increase of aerogel the workability of the binder decreases, aspect that should be addressed and further studied by increasing the binder's working temperature.

5.4.3 Rheology of the Binder Using the Dynamic Shear Rheometer (DSR)

This test as per ASTM D7175-08 (Standard Test Method for Determining the Rheological Properties of Asphalt Binder Using a Dynamic Shear Rheometer). Dynamic Shear Modulus was completed at 58ºC, 64ºC, 70ºC, 76ºC, 82ºC, 88ºC, and 96ºC. Ten frequencies ranging from 0.1 to 100 rad/s were considered in the test. Figure 5-4 display the plots of the master curves functions.

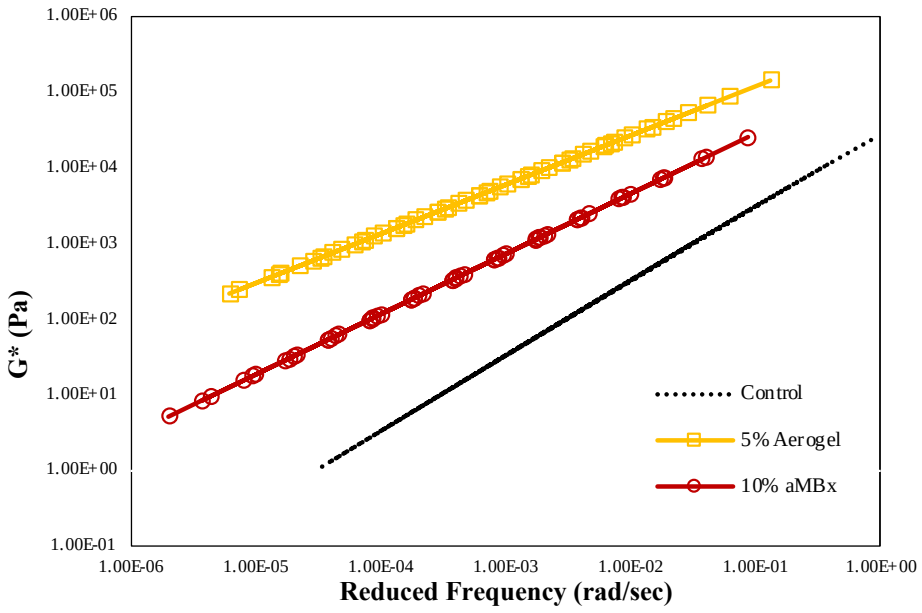

Figure 5-4. Dynamic Modulus G* Master Curves.

Figure 5-4 show the results of complex shear modulus G* when adding 10% aMBx, 5% aerogel and Control. As asphalt binders are viscoelastic, and depending on temperature and loading frequency, they behave partly like elastic solids and viscous liquids. As elastic solids, the deformation induced by the loads is partly recoverable. The DSR can detect both properties. The complex shear modulus represents the total resistance to deformation when repeatedly subjected under shear stress. The higher the G*, the stiffer is the binder. The stiffer the binder, the higher the resistance to rutting, as the asphalt binder will not deform as much. When the binder is modified with aMBx the response is like the one modified with aerogel, in both cases, G* shows better response than Control binder.

5.4.4 High Temperature PG Grading

As per AASHTO M320. The PG grading was performed in short term aged (RTFO) binders, then $G^*/Sen\delta \geq 2.2kPa$. In this case the gap (separation between the DSR plates) was set at 1.5mm to avoid any friction effect due to the aerogel or aMBx particles that could affect the real behavior of the binder itself. Table 5-4 present the results of the PG grading.

Table 5-4. High Temperature PG for Binders modified with Aerogel/aMBx.

Aerogel Content	PG64-16
Control	64
5.0% aerogel	70
10% aMBx	70

Results show that all binders increase the high temperature grading as the aerogel content increases. This means that all modified binders keep meeting the performance criteria at higher temperatures demonstrating that the aerogel/aMBx modified binders have much better response than conventional bitumen.

5.4.5 Stress Creep and Recovery (MSCR)

Based on AASHTO M-332-14 (Performance-Graded Asphalt Binder Using Multiple Stress Creep Recovery). Also, in this case the gap was set at 1.5mm. Table 5-5 shows the recovery and Jnr values for each specimen

Table 5-5. Recovery and Jnr results.

Aerogel Content	Recovery 0.1kPa (%)	COV	Recovery 3.2kPa (%)	COV	Jnr 3.2kPa (1/kPa)	COV
Control	0.00	0.00	0.00	0.00	10.75	0.16
5.0% aerogel	25.18	0.08	9.1	1.21	1.61	1.16
10% aMBx	20.93	0.20	7.8	1.14	2.10	1.19

The response of the MSCR test is different than the response from the previous test. In the previous procedure, the parameter $G^*/\sin(\delta)$ is measured by applying an oscillating load at low shear strain. In the MSCR test, two different parameters are measured: the Jnr, the non-recoverable creep compliance and the Recovery, the percent recovery during each loading cycle. The lower the Jnr value, the better, while the Recovery should be higher. Relating this to the results obtained, it is noted that the Jnr value diminishes, and the percent

recovery increases with the increase of aMBx. Note that the recovery here decreases compared with the recovery gotten in the Chapter 4 because in this case the gap was increased to 1.5mm (instead of 1.0mm). This was done to dismiss any possible effect of friction, so then to compare the response of the different specimens in a more objective way. This behavior is like the binder modified with aerogel, and in both cases, the response is much better than Control binder.

5.4.6 Asphalt Binder Bond Strength (BBS)

Test as per AASHTO Designation: TP-XX-11. The pull off tensile strength of asphalt binder from a siliceous surface was measured and determined via the bitumen bond strength test according to AASHTO TP 91. The substrate chosen was polished rock with a temperature of application of 75ºC (i.e., the binder's temperature at which the stub is pushed against it to get bonded with the substrate). Table 5-6 presents the results of the test.

Table 5-6. Binder Bond Strength test results.

Conditions	Tensile Strength (kPa)		
Specimen	Control	5.0% aerogel	10% aMBx
App. Temp 75ºC	1801.7	1824.9	1855.25
COV	0.070	0.033	0.055
Type of Failure	Cohesion		

This test method measures the tensile force needed to pullout a stub adhered to a solid substrate with asphalt binder. The evaluation of the pullout tensile strength on

aggregate substrate provides a measure of the asphalt-aggregate compatibility. As per the test results, the bonding strength for the binders with the aMBx are comparatively the same as the conventional binders. Therefore, the addition of the aMBx did not affect the bond between the aggregate and the binder, however, based on the results of BBS using different percentages and binder types in Chapter 4, it is suggested that the maximum amount of aMBx should be around 20% (i.e., aMBx content about 45% of aerogel) to avoid a decrease in the bonding mechanism between aggregates and binder.

5.4.7 Thermal Conductivity (TC) of Asphalt Binders

This test was developed in The National Center of Excellence for SMART Innovations at ASU and described in Chapter 3 of this Dissertation. Currently with a patent application in the United States Patent and Trademark Office: serial number 63/146,987 filed on February 8, 2021, of which the author of this Ph.D. Dissertation is co-inventor. Table 5-7 shows the results of the TC for the specimens considered.

Table 5-7. Thermal conductivity of the specimens.

Binder Type	Average k (W/m^oK)	COV
Control	0.206	0.07
5% aerogel	0.181	0.09
10% aMBx	0.188	0.06

In Table 5-7, the aMBx samples exhibited lower thermal conductivity values. The lower the thermal conductivity, the less heat the sample is conducting. These results can be translated in a better performance of the asphalt in the road.

The significance of the lower thermal conductivity in an asphalt binder can be shown in a simple temperature-stability-response test. In this test, unmodified samples and aMBx-modified specimens are subjected to high temperature in a convection oven for 1 hour. To maximize the response, in this test, binder PG70-10, the most common binder in the Phoenix, Arizona area, was modified with 20% of aMBx. Thermal conductivity of this material was estimated as 0.162W/m^{o}K. The oven was set at 70^{o}C, and pictures were taken each 10 minutes. Figure 5-5 shows the deformation of the specimens after 1 hour.

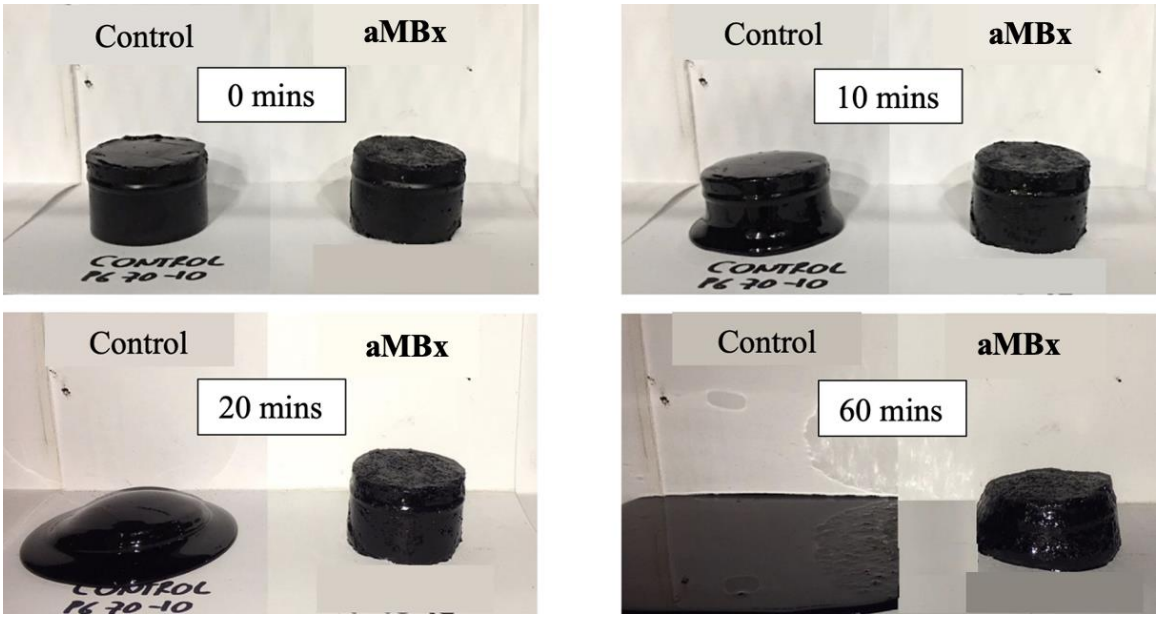

Figure 5-5. Deformation of the samples during the Temperature-Stability test.

As it can be seen, the stability of the samples modified with 20% of aMBx are much better that control. Control sample collapsed only 10 minutes after starting the test, while

the aMBx-modified sample, kept standing even after the hour. These results are very encouraging. Bituminous materials modified with aMBx would be much longer lasting against high temperatures.

5.4.8 Flexural Creep Stiffness of Asphalt Binder (BBR)

Test as per AASHTO T 313-19. This test was performed at -6^{o}C and -22^{o}C, so based on these temperatures, the low temperature PG grading was obtained. Based on the results, contrary to the high temperature PG grading, the low temperature PG grading of binders modified with aMBx is not improved but also it is not jeopardized. A high m-value is required because as the thermal stresses accumulate and the temperature decreases, the stiffness changes quite fast. A fast change in stiffness means that the binder tends to release stresses that would otherwise reach a level where low temperature cracking would occur. The Superpave binder specification requires a minimum m-value of 0.300 (FHWA, 2017). Table 5-8 show results of the m-value at different temperatures and the result of the low PG grading. To prevent cracking, creep stiffness has a maximum limit of 300 MPa. Table 5-9 presents the results of stiffness, where it is seemed that the addition of aMBx to the binders does not negatively affect the response at low temperatures. Binders modified with aerogel in equivalent aMBx amount, presents slightly lower response than control and the aMBx-modified binders in both, m-value, and stiffness.

Table 5-8. m-value results and low temperature PG grading.

m-Value	Temperature in ^{o}C		Minimum m-value 0.300
	-6	-22	Low Temp. PG in ^{o}C
Control	0.411	0.239	-16.33
Aerogel 5%	0.389	0.229	-14.94
aMBx 10%	0.410	0.236	-16.12

Table 5-9. Stiffness results and low temperature PG grading.

Stiffness (MPa)	Temperature in ^{o}C		Maximum Stiffness 300 MPa
	-6	-22	Low Temp. PG in ^{o}C
Control	76.17	427.74	-16.19
Aerogel 5%	90.40	505.75	-14.07
aMBx 10%	78.17	414.88	-16.54

5.5 Assessment of Aerogel and aMBx Binders by a Normalization Process

The evaluation of the response of aMBx with respect of aerogel to modify binders was completed using a normalization process. In this assessment all the test results of control, aerogel and aMBx binders were considered. Table 5-10 present the test results of each type of sample with the respective normalization factor to apply.

Table 5-10. Test results and Normalization factors.

Test	Normalization Factor	Test Results			Normalized 5% aerogel	Normalized 10% aBMx	Normalized Control
		5% aerogel	10% aMBx	Control			
Softening Point	100ºC	57.0	53.0	45.9	57.0%	53.0%	45.9%
Rotational Viscosity at 176.7ºF	2500 (cP)	1,878.3	748.3	74.3	75.1%	29.9%	3.0%
Hight Temp. Performance Grade	82 (ºC)	70.0	70.0	64.0	85.4%	85.4%	78.0%
Low Temp. Performance Grade	16	14.0	16.0	16.0	93.8%	100.0%	100.0%
MSCR - Recovery 0.1kPa	10 (%)	7.2	5.9	0.0	71.8%	59.3%	0.0%
Jnr 3.2kPa (1/kPa)	(20 - Jnr)/20	1.610	2.100	10.750	92.0%	89.5%	46.3%
BBS	2000 (kPa)	1,824.9	1,855.3	1,801.7	91.2%	92.8%	90.1%
Thermal Conductivity	1 - k (W/mK)	0.170	0.173	0.195	83.0%	82.7%	80.5%

Figure 5-6 presents the results graphically. In this plot, aMBx-modified binders response very close to the aerogel modified ones.

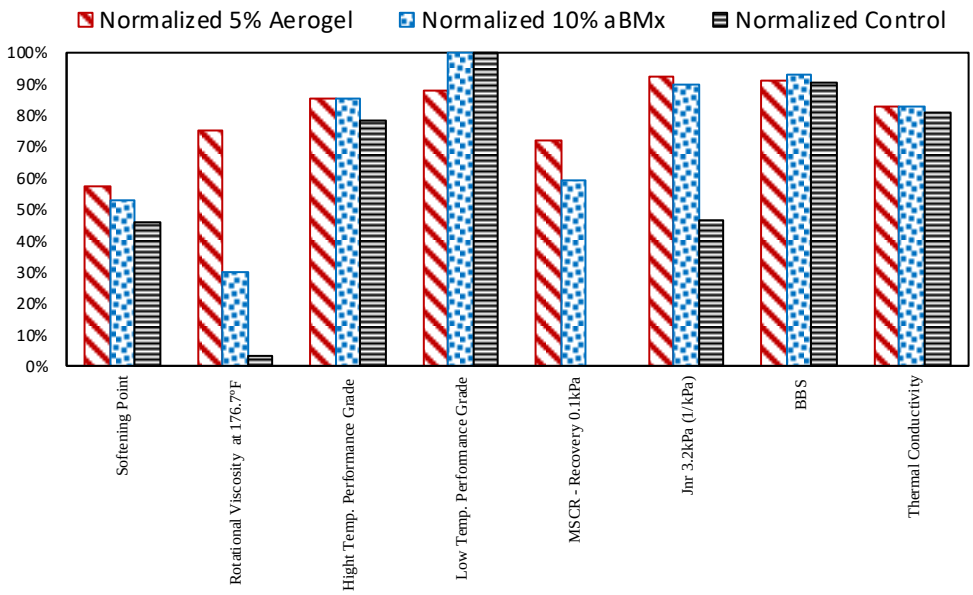

Figure 5-6. Comparison between aerogel and aMBx modified binders.

5.6 Conclusions

Tests results showed that the benefits of using aerogel in asphalt binders (refer Chapter 4) are similar when the aerogel-based composite, aMBx, is utilized. Important aspects to consider are that the aMBx binders has lower viscosity at high temperatures than the aerogel ones, it could help during the mixing process when working with asphalt mixtures and/or to make more workable modified binders with these modifiers. Low temperature PG grading is not affected with respect to control when binders are modified with aMBx, which represents an advantage of the aerogel modification. The usage of aMBx is replicating the aerogel effect in binders and can facilitate the blending with other bituminous materials such as asphalt emulsions used in different road surface treatments, asphalt mixtures (hot, warm, and cold), asphalt roofing shingles, and asphalt sealants (crack repairs and joint protection). Based on the test results, both, aMBx and aerogel present better response than control.

All concerns related to health, security, and workability to make doable the implementation of the aerogel technology in bituminous materials is solved by the implementation of the aMBx composite, which constitutes the most important improvement of aMBx over the aerogel implementation. In other words, the aMBx technology brings the possibility of creating a new generation of bituminous materials with remarkable low thermal susceptibility to build longer lasting road applications.

CHAPTER 6

ASPHALT MIXTURE DESIGN CONSIDERATIONS

6.1 Introduction

Hot Mixture Asphalt (HMA) mixture design is a procedure to determine the aggregates and asphalt binder to use, and the optimum combination of these two ingredients. This process is important to any agency and industry because it addresses performance indicators such as deformation, fatigue, and low temperature crack resistance. Additionally, the designed asphalt mixture must be durable, moisture damage resistant, skid resistant and workable. The asphalt mix design has limitations; however, it is a cost-effective method to offer essential information to articulate a high-performance pavement (Roberts, et al., 1996).

6.2 Materials and Methods

The materials used in this project were the most widely used aggregates and binders in Phoenix. The Superpave mix design method was used to design the asphalt mixtures and the City of Phoenix (CoP) specifications were followed during the mix design (FHWA, 2001) (FHWA, 2017). In the mixture design, mixtures were modified with aMBx, a new modifier developed at Arizona State University. aMBx considered in this study are 0%aMBx (Control), 10%aMBx, 20%aMBx, and 30%aMBx. All percentages are based on

the asphalt binder weight. Characteristics of the materials used in the mix designs are presented below.

6.2.1 Modifying Material (composite)

The new proposed material, named "aMBx", is a synthetic porous silica-based material developed in the Advanced Pavement Laboratory at Arizona State University currently with a patent application in the United States Patent and Trademark Office: serial number 63/210,891 filed on June 15, 2021 (refer Figure 6-1). This material is used to modify the HMA pavements in three different contents: 10%, 20%, and 30% by weight of the asphalt binder.

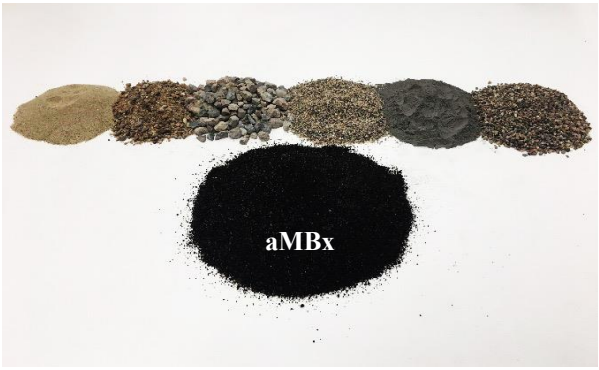

Figure 6-1. Appearance of aMBx composite.

Because its components, this composite presents hydrophobic properties. This material has relatively low thermal conductivity and light-weight density. The density ranges from 0.32 to 0.38 g/cm^3 and thermal conductivity from 0.08 to 0.12 W/m^{o}K, properties related to the fact that this material is around 57% air. The total size of the coated particle could range from 0.1 to 3mm. Table 6-1 shows the gradation of the material.

Table 6-1. Granulometric Distribution of aMBx.

Sieve (US – mm)	% Passing
#16 - 1.18	94.77%
#30 - 0.6	59.64%
#50 - 0.3	22.89%
#100 - 0.15	3.85%
#200 - 0.075	0.55%
PAN	0.00%

6.2.2 Asphalt Binder

The asphalt binder used in this study was a Superpave Performance Grade Binder, PG 64-16 supplied by Holly Frontier, Glendale, AZ. Specific gravity (SpG) of the binder is 1.027. The binder properties are shown in Table 6-2.

Table 6-2. PG 64-16 Binder Properties.

Samples	Test	Test Temperatures	Results	Specification
Original Binder	Flash Point, T48		300 ºC	Min. 230 ºC
	Apparent Viscosity, T316	135 °C	0.428 Pa-s	Max. 3 Pa-s
		175 °C	0.082 Pa-s	
	Dynamic Shear, T315, G*/sin δ	70 °C	1.58 kPa	Min. 1.00 kPa
Residue from RTFO	Mass Change		-0.210%	Max 1.0
	Dynamic Shear, T315, G*/sin δ	64°C	3.33 kPa	Min. 2.20 kPa
Residue from PAV	PAV Aging Temperature	100°C		
	Dynamic Shear, T315, G*sin δ	28°C	2.87 kPa	Max. 5.0 kPa
	Creep Stiffness, T313	-6°C	90.4 MPa	Max. 300 MPa
	m-value, T313	-6°C	0.384	Min. 0.300

6.2.3 Aggregates

The aggregates used in the asphalt layer have a nominal maximum aggregate size (NMAS) of 19mm (¾ inches), provided by M.R. Tanner El Mirage Pit. The gradation is shown in Table 6-3 and the aggregates properties are shown in Table 6-4 below.

Table 6-3. Aggregate Gradation.

US -- mm	w/o Admix % Passing	w/ Admix % Passing	Specification Limits			Production Limits		
11/2 " -- 37.5	100.00	100						
1 " -- 25	100.00	100						
3/4 " -- 19	100.00	100		100				
1/2 " -- 12.5	91.00	91	85	--	100	84	--	98
3/8 " -- 9.5	85.00	85	62	--	85	79	--	91
1/4" -- 4.75	68.00	68						
#4 -- 4.75	59.00	59						
#8 -- 2.36	43.00	43	40	--	50	37	--	49
#10 -- 2.36	39.00	40						
#16 -- 1.18	31.00	31						
#30 -- 0.6	20.00	21						
#40 -- 0.425	15.00	16	10	--	20	12	--	20
#50 -- 0.3	11.000	12						
#100 -- 0.15	7	8						
#200 -- 0.075	5.3	6.2	2	--	10	4.2	--	8.2

Table 6-4. Aggregates properties.

Aggregate Property	Coarse Agg.	Fine Agg.	Comb. without Admix.	Comb. with Admix.	Specification
Bulk oven dry (OD) Specific Gravity	2.648	2.607	2.629	2.624	2.35 - 2.85
Saturated surface dry (SSD) Specific Gravity	2.687	2.657	2.674	2.668	
Apparent specific gravity	2.755	2.745	2.751	2.744	
Absorption (%)	1.471	1.927	1.675	1.655	0.00 - 2.50
Effective specific gravity (Gse)				2.683	
Sand equivalent					50 Min
Plasticity index		NP			NP
% 1 or more fracturated face	95				85 Min
% 2 or more fracrurated face	90				80 Min
Uncompacted voids		46.7			45 Min
Los Angeles abrasion					
% Loss @ 100 Rev. - Grading B	3				9 Max
% Loss @ 500 Rev. - Grading B	17				40 Max
% Flat & elongated (5:1 ratio)	1.6				10 Max
% Soundness loss (NaSO4)	1				
% Clay lumps & Friable Particles	0.2	0.1			

6.2.4. Mixture Design Results (Dry Method – Wet Method)

As aMBx is a new material, it is needed to find the proper way to introduce it into the mixture. In this study, two different approaches were considered for the asphalt mixture designs. Dry Method (DM) and Wet Method (WM).

- *Dry Method (DM)*

In this method, the composite, aMBx, is added to the raw aggregates before the addition of the binder to make the asphalt mixture. Mixing and Compaction Temperatures in the laboratory, 160^{o}C and 150^{o}C respectively. The implementation of aMBx, make safer the process of mixing. When the aMBx is added to the aggregates while this are rotating,

no aerogel fume is detected. Figure 6-2 shows the process to include the aMBx's properties in the mixture by DM in the laboratory.

Figure 6-2. Initial process for adding the benefits of aMBx in Asphalt mixtures.

- *Wet Method (WM)*

In this process, the composite is blended with the asphalt binder, so then, the binder plus aMBx (aMBx-binder) is added to the raw aggregates. Figure 6-3 presents the mixing sequence for each method. Mixing and Compaction Temperature in the laboratory, 175°C and 160°C respectively.

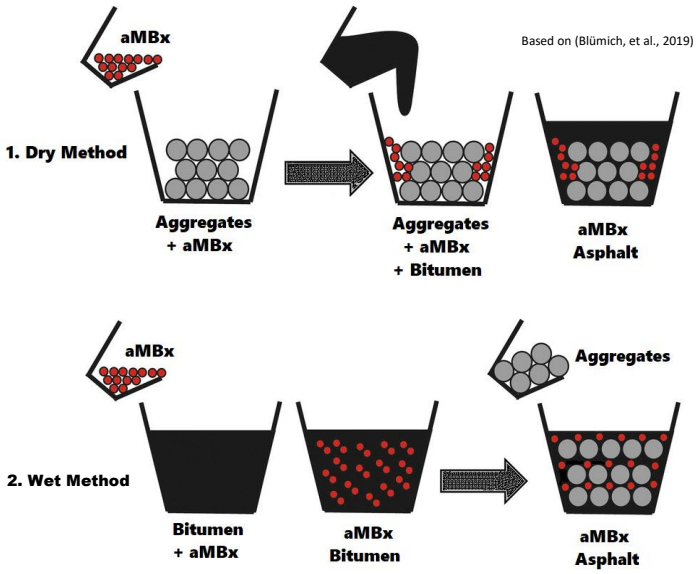

Figure 6-3. Sequence for the two methods of mixing.

In this study, design ESALs ≥ 30 million, then the number of gyrations for the Superpave Gyratory Compactor (SGC) specimens is 125, and the voids filled with asphalt (VFA) should be between 65%-75%. As the Nominal Maximum Aggregate Size (NMA) is 19mm, the minimum voids in the mineral aggregate (VMA) should be 13% (FHWA, 2017).

Content of aMBx by bitumen weight and the respective mixing methods are: 0% (Control), 10%DM, 10%DM, 10%WD, 20%WM, and 30%DM. The variety of mixtures is to consider different material's properties and then responses. Viscosity of binders increases using 30%aMBx making the mixing process difficult, then, instead of 30%WM, 20%WM was implemented.

Tables 6-5 shows the mixture characteristics of Control (0%), 10%aMBx (DM), 10%aMBx (WM), 20%aMBx (WM), and 30%aMBx (DM) modified asphalt mixtures. The optimum binder content is based on the weight of the raw aggregates weight. The composite gradation of the aggregates for each type of mixture (modified and unmodified) varies with the introduction of aMBx into the mix.

Table 6-5. Properties of the Five Mixtures.

Properties	0% aMBx (Control)	10%aMBx (DM)	10%aMBx (WM)	20%aMBx (WM)	30%aMBx (DM)	Specification
% Total Binder Content*	5.27	5.29	5.29	5.32	5.35	
Number of Gyrations	125	125	125	125	125	
% Air Voids	4.00	4.00	4.00	4.00	4.00	
% VMA	13.48	14.36	15.53	15.30	15.49	Min. 13%
% Air Voids Filled	70.33	72.14	74.25	73.85	74.17	65% - 75%
% Eff Asphalt Total Mix	4.53	4.63	4.51	4.50	4.85	
Film Thickness (μ)	8.00	8.00	8.00	8.00	8.20	Min. 8μ – 14μ
Max. Theoretical Specific Gravity	2.4636	2.4513	2.4526	2.4509	2.4403	

6.3 Conclusions

According to Table 6-5, the binder content slightly increases with an increase of aMBx content. This is expected as there is a need to adhere the additional aMBx particles into the mastic or mixture.

Although the target air voids percentage of (4%) and gradations are the same for all the mixtures evaluated in this Chapter, the percent Voids in the Mineral Aggregates (VMA) differs. The increase of VMA with the increase content of aMBx is attributed to the fact that the mixture with higher aMBx content has lower bulk specific gravity of compacted mixture (G_{mb}). In this situation, the intergranular void space between the aggregate particles of the compacted mixtures increase as well (Chadbourn, Skok, Newcomb, Crow, & Spindler, 1999). This statement is supported by Chapter 10 findings, where it was clearly shown that an aMBx mixture is more porous than a conventional one. VMA data shows that the portion of space in a compacted asphalt pavement that is not occupied by aggregates is higher when aMBx increases. Although the durability of the mixtures may be questioned when the voids content is high, tests such as Tensile Strength Ratio (TSR) performed in Chapter 9, showed that the aMBx mixtures responses were even better than the conventional mixture. Some of these outcomes may be accredited to the hydrophobic characteristics of aMBx, as some of the aerogel particles may not be completely coated with the asphalt cement.

The effective asphalt and the portion of the voids in the mineral aggregate (VFA) that contain the asphalt binder increases as the aMBx increases; this is also due to the increase of optimum binder and possibly the presence of binder as the encapsulator agent

in the aMBx itself (refer to Chapter 5). This phenomenon also supports the proper asphalt film thickness needed to ensure a good aggregate coating.

The specific gravity excluding air voids is the theoretical maximum specific gravity (G_{mm}) of an HMA mixture. Therefore, hypothetically, if all the air voids were removed from an HMA specimen, the combination of the specific gravities of the remaining aggregate and the asphalt binder may be G_{mm} (Pavement Interactive, 2021). In this case, the presence of the aMBx particles either in the asphalt binder (using the WM) or in the raw aggregates (using the DM) would mean a change in the aggregates and/or asphalt binder specific gravities with a decreasing effect; this result in a decrease in G_{mm} values when aMBx is present in the mixture.

Finally, the two methods used to introduce the aMBx in the asphalt mixtures (DM and WM) have an impact in the distribution of the aMBx particles in the mixture. Chapters 7, 8 and 9 will show that the response of the modified asphalt mixture with aMBx is best when the WM is used. These outcomes simply suggest that when the aMBx is added to the hot binder, the distribution of the aMBx particles is better than the DM, therefore the performance of the mixtures is enhanced.

CHAPTER 7

FIELD PRODUCTION AND THERMAL PROPERTIES OF aMBx MODIFIED ASPHALT MIXTURES

7.1 Introduction

In this part of the study, field production of aMBx modified asphalt mixtures were produced and three test sections were paved to study the effect of the modifier on the asphalt pavements' temperature profile. Field temperatures were monitored and recorded. In addition, temperature modeling was also implemented to better understand the pavement's surface temperature behavior and the gradient of temperature for the three scenarios. The temperature analyses of both modeling and recorded temperature included winter and summer seasons, allowing for a better understanding of the thermal behavior of the pavement throughout the year. This chapter / analysis includes the thermal properties measurements of the field produced mixtures but does not include a durability assessment as it is addressed later.

Temperature differences or thermal gradients along the pavement profile are associated to thermal cracking (Ling, et al., 2019) and (Obando, et al., 2021). The thermal profile of an asphalt pavement depends on different properties such as specific heat capacity (SHC), thermal conductivity (TC), density (δ), and geometrical characteristics like thicknesses of the layers (h). Furthermore, by varying these parameters, the thermal profile will ultimately change. One can say that the lower the variation of temperature along the

depth of the pavement's structure (thermal profile), the less thermal susceptibility or more thermal resistant a pavement structure is. In this framework, it is needed to find the proper pavement's set of thermal properties to design longer lasting roads in terms of thermal cracking potential.

On the other hand, a previous study stated that the top of the pavement thermal profile (i.e., pavement's surface temperature) can't be addressed by solely adjusting the thermal properties of the pavement because it primarily relies on the pavement's surface color (Sen, 2015). However, other studies have evaluated the effects of thermal modification on the pavement properties by varying the thermal conductivity in addition to an increasing albedo. It was also found that higher albedo could decrease pavement temperature at various depths. As for increasing the thermal conductivity of asphalt mixtures, the maximum and minimum pavement temperatures were reduced. Such pavements also generate less heat output in the daytime, but higher in the nighttime (Chen, et al., 2017). Thermal conductivity can be increased by the addition of certain modifiers such as mineral powers of fillers, graphite power and aluminum oxide powder. Powders with higher thermal conductivity can improve the efficiency of heat capture and transfer more heat from the asphalt layer into the structure (ShengYue, et al., 2013).

There are different approaches to mitigate the Urban Heat Island (UHI) effect. Some of those by using materials containing higher solar radiation and leading the lower heat storage capacity. The Asphalt Pavement Alliance (APA) and ASU showed that a porous Hot Mix Asphalt (HMA) layer with low albedo can potentially have a lower nighttime surface temperature compared to a conventional HMA layer with higher albedo (Stempihar, et al., 2012). Just as many researchers believe that surface reflectivity is the

most important parameter to mitigate the UHI effects, others suggest that the pavement's porosity affects the speed at which solar energy is absorbed (Haselbach, 2009). In other words, the voids will allow the infiltrated water to evaporate, which lead to cooler temperatures.

In this document, the behavior of the pavement temperature profile is analyzed when the asphalt pavement is modified with a novel silica-based material. This adjustment triggers a change in the pavement thermal properties, which will alter the pavement thermal profile and behavior.

7.2 Materials and Methods

Description and/or information of the modifying Material (aMBx composite), asphalt binder type, and aggregates, and mixture design are described in Chapter 6. Composite material was used to modify the HMA pavements in two different contents: 10% and 30% by weight of the asphalt binder, by the dry method (DM).

In this case, manufacture of the three different mixture was done in an asphalt plant. During the mixing procedure in the plant, aMBx was added while mixing the aggregates in the drum, following a dry method (DM) of mixing. The process is like the conventional asphalt mixing procedures according to City of Phoenix standards.

7.2.1 Test Sections and Slabs Construction

Three different mixtures (Control, 10% and 30% aMBx) were produced with the cooperation of Southwest Asphalt, a division of Fisher Industries. Three test sections and

three test slabs were built within their asphalt plant located in Litchfield Park, Arizona. A total of 33tons of asphalt were produced corresponding to 15m^3 of HMA mixtures. Table 7-1 shows a summary of the materials quantities used in the construction process.

Table 7-1. Summary of Materials for the Construction of the Slabs and Sections.

Mixture Type	Raw Aggregates (kg)	Binder (kg)	aMBx (kg)	Total (kg)
Control	10661.6	579.6	0	11241.2
10% aMBx	10451.8	569.9	75*	11096.4
30% aMBx	10013.9	553.2	182*	10762.2

*Note that the aMBx weight was increased in about 3.0% based on the binder weight assuming losses during the mixing process.

The slabs were constructed following the City of Phoenix specifications. In addition, loose asphalt mixtures were sampled from the plant corresponding to the three different mixtures to obtain the thermal properties in the laboratory at ASU. In total, 6 slabs (3.6m by 3.6m) with two thickness (7.5cm and 15cm) were built for the control, 10% and 30% aMBx dosages. The asphalt layers are directly compacted on top of a well compacted subgrade granular material. Figure 7-1 presents pictures of the construction process.

Figure 7-1. Construction Process.

7.2.2 In-situ Temperature Recordings

Wireless thermocouples (thermistor iButton DS1922E) were placed at the near-surface depth (1.27cm below the surface) of the slabs. It is important to note that the collection of surface temperatures with thermocouples could lead to possible erroneous recordings since they have a different color from the pavement. Besides, the fact that these sensors are exposed to the environment could be challenging. To avoid the possible irregularities of the subgrade and ensure the data collection at the same depth, wireless sensors were placed at 5cm below the surface for the 7.5cm thick slabs (thin scenario), and

at 10cm deep for the 15cm thick slabs (thick scenario). To do this, a coring machine was used to extract cores and then place the wireless thermocouples at the desired depth. This activity was repeated every 25 days to extract the data and to reset the sensors to ensure proper data collection. These sensors were set to collect data daily, every 30 minutes.

7.2.3 Thermal Model Tool

The thermal profile of the pavement was simulated in full using The Asphalt Concrete Thermal Stress Calculation (ACTS Calc) software. This tool was developed at The National Center of Excellence for SMART Innovations at ASU, of which the writer of this Dissertation is co-author. It involves and enhances previous research studies on the calculation of the thermal pavement profile using a 1-D semi-infinite thermal model. The principle behind this model relies on a transient energy balance of the pavement, which involves solar radiation. The incoming solar energy and outcoming infrared radiation (albedo) are defined by convection: heat exchanges with air, considering wind velocity and the occurrence of turbulence (if needed), and conduction: heat transfer into the ground (semi-infinite solid) (Gui, et al., 2007). The development and application of the mathematical model is presented in Chapter 8, and the manual of the ACTS Calc software appear as Appendix A.

The model was validated showing simulations that reflects field measurements accurately. It provides close estimates of the pavement temperature profile (1.5^{o}C as a standard deviation, and R^2 equal to 0.99, as it is validated in Chapter 8) (Gui, et al., 2007) (Obando, et al., 2021). This tool was done on Jupyter Notebook with a Python kernel into

a Graphical User Interface (GUI) developed based on the DearPyGui library (Obando, et al., 2021).

The climatic parameters needed are obtained from the Arizona Meteorological Network (AZMET), as the weather stations are updated daily. As for the materials' parameters, they were obtained experimentally and referenced. Whether information used is presented in Table 8-5 of Chapter 8.

7.2.4 Thermal Properties Testing

Samples of each type of mixture were collected in the plant for further laboratory testing in the Advanced Pavement Laboratory at ASU. Three different bags of the same material were placed in the oven for 1.5 hours at 160ºC to reach compaction temperature and were then mixed. The mixed samples were compacted as per the SUPERPAVE method to reach a 18cm height for a target of 6% of air void content. Cores of 7.5cm and 10cm diameter were extracted from the compacted samples to proceed with the estimation of the thermal properties. These procedures are described in the sections below.

7.2.4.1 <u>Thermal Conductivity (TC)</u>

The thermal conductivity of the samples was determined in a closed and conditioned chamber to minimize the effect of the ambient air on the samples. This test was also developed at The National Center of Excellence for SMART Innovations at ASU. A cylindrical heating probe is inserted inside each compacted cylinder having a diameter of 10cm and length of 18cm length. Eight thermocouples were then used to measure the temperatures: four on the inside of the specimen, and four on the outside. The experiment

ended when the steady state temperature was reached. Figure 7-2 shows the setup for this experiment. The thermal conductivity is calculated according to Equation (7-1) (Carlson J. , Bhardwaj, Phelan, Kaloush, & Golden, 2010):

$$k = \frac{Q_{Heater} * \ln\left(\frac{r_2}{r_1}\right)}{2 * \pi * L * (T_1 - T_2)} \quad (7\text{-}1)$$

Where:

k = Thermal Conductivity (W/m^{o}K),

Q_{Heater} = Power into the heating probe (W); $(V * A)$, where V is the Voltage and A is the current

r_2 = outer radius (m)

r_1 = inner radius (m)

T_1 = Average of the outer temperatures (^{o}C)

T_2 = Average of the inner temperatures (^{o}C)

Figure 7-2. Thermal Conductivity Setup.

7.2.4.2 Specific Heat Capacity (SHC)

The method used in this study was developed at The National Center of Excellence for SMART Innovations at ASU, which gave the most consistent results for multiple trials. It consists of heating the specimens in the oven for 8 hours and then submerging them into water at room temperature. The system is placed in a completely insulated container, minimizing the energy exchange with the exterior environment. The cylinder size used for this experiment has a 7.5cm diameter and a 18cm height. The change in temperature between the sample and water is recorded until the water temperature reaches a constant value (around 20 mins). The calculation of the specific heat capacity is done using Equation (7-2) (Ohanian & Markert, 2007). Figure 7-3 shows the setup used for this procedure.

$$SHC = \frac{(m_w C_w \Delta T_w) + (m_f C_f \Delta T_f)}{m_s \Delta T_s} \quad (7\text{-}2)$$

Where:

m = mass (Kg),

T = temperature (^oC),

SHC = Specific Heat Capacity ($J/^oC/Kg$)

"w" is for water; "f" is for flask and "s" is for specimen.

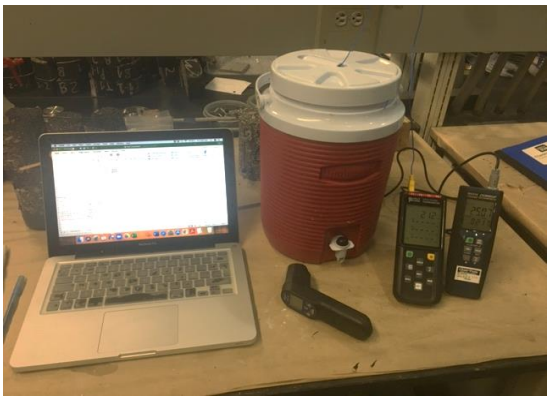

Figure 7-3. Specific Heat Capacity Setup.

7.3 Results and Analysis

7.3.1 Thermal Conductivity and Specific Heat Capacity

In addition to the thermal properties for the field produced mixtures, densities for each type of mix were obtained. Densities and thermal properties are summarized in Tables 7-2, 7-3 and 7-4 below.

Table 7-2. Density for the three different mixtures.

Pavement Type	Density (K/m^3)	Standard Deviation	Standard Error	COV
Control	2175.82	35.2	20.32	0.016
10%aMBx_DM	2109.82	30.1	17.38	0.014
30%aMBx_DM	2084.97	34.3	19.80	0.016

Table 7-3. Specific Heat Capacity (SHC) results for the three different mixtures.

Pavement Type	SHC (J/kg^oC)	Standard Deviation	Standard Error	COV
Control	939.68	32.709	0.135	0.035
10%aMBx_DM	1016.16	83.640	0.082	0.082
30%aMBx_DM	1298.03	96.890	0.399	0.075

Table 7-4. Thermal Conductivity (TC) results for the three different mixtures.

Pavement Type	k (W/m^{o}K)	Standard Deviation	Standard Error	COV
Control	1.001	0.008	0.004	0.008
10%aMBx_DM	0.885	0.064	0.032	0.073
30%aMBx_DM	0.741	0.047	0.023	0.063

Mixtures with aMBx have lower density than control. The higher amount of aMBx the lower the mixture's density. Based on the results, lower thermal conductivity and higher specific heat capacity values are observed with an increase in aMBx contents. It can be translated in a lower heat transfer and higher heat storage for the modified mixtures.

7.3.2 Temperature Profile and Gradient of Temperature

Collected field readings and model results for winter (January 2021) and Summer (June 2021), showed that 30%aMBx slabs tend to have the lowest temperatures during the day and the highest temperatures during the night at 1.27cm ("Up") below the surface for both scenarios, thin and thick. The Control and 10%aMBx slabs presented similar behavior.

At 5cm and 10cm below the surface for thin and thick scenarios respectively ("Down"), the 30% aMBx slabs present the lowest temperatures during the day for both thin and thick scenarios. However, during the night, these slabs have the highest temperatures for thin and thick scenarios. In addition, the Control and 10% aMBx slabs showed similar behavior at these locations. Table 7-5 presents a summary of the pavement's temperature behavior from the field and the model results for both seasons winter and summer.

Table 7-5. Winter and Summer Field vs. Model Temperature Readings.

Considerations			Max (day) Temperature (°C)				Min (night) Temperature (°C)				Gradients (°C)			
			Up		Down		Up		Down		Up		Down	
			Field	Model	Field	Model	Field	Model	Field	Model	Field	Model	Field	Model
Winter	Thin	Control	28.50	27.81	25.50	23.65	3.50	3.32	5.50	5.56	25.00	24.49	20.00	18.09
		10% aMBx	28.50	27.90	24.00	23.58	3.00	3.03	5.50	5.38	25.50	24.87	18.50	18.20
		30% aMBx	26.00	27.03	20.50	22.59	3.50	3.19	6.00	5.72	22.50	23.84	14.00	16.86
	Thick	Control	28.50	27.42	19.00	19.34	4.00	3.73	8.50	8.46	24.50	23.70	10.50	10.88
		10% aMBx	28.50	27.47	19.00	18.84	3.50	3.59	9.00	8.63	25.00	23.88	10.00	10.20
		30% aMBx	26.00	26.82	18.00	17.45	4.00	3.90	9.50	9.49	22.00	22.92	8.50	7.96
Summer	Thin	Control	70.50	68.43	65.50	62.44	24.00	29.31	26.50	32.74	46.50	39.12	39.00	29.70
		10% aMBx	70.50	68.76	65.50	62.52	24.00	28.99	26.50	32.60	46.50	39.77	39.00	29.92
		30% aMBx	66.50	67.98	55.50	61.46	26.00	29.50	28.50	33.45	40.50	38.48	27.00	28.01
	Thick	Control	69.00	67.74	54.50	55.58	24.50	30.07	31.50	37.14	44.50	37.67	23.00	18.44
		10% aMBx	69.00	67.90	54.50	55.01	24.50	30.01	31.50	37.61	44.50	37.89	23.00	17.41
		30% aMBx	66.00	67.22	51.00	53.20	26.50	30.81	32.50	39.29	39.50	36.41	18.50	13.90

Notes: For both, thin and thick scenarios "Up" sensor location corresponds to 1.27cm below the surface of the pavement
For thin scenario, "Down" sensor location corresponds to 5cm below the surface of the pavement
For thick scenario, "Down" sensor location corresponds to 10cm below the surface of the pavement

Figure 7-4 present a plot of the data gathered from the field in June 2021 for the thick scenario where both locations are shown, “Up” and “Down”.

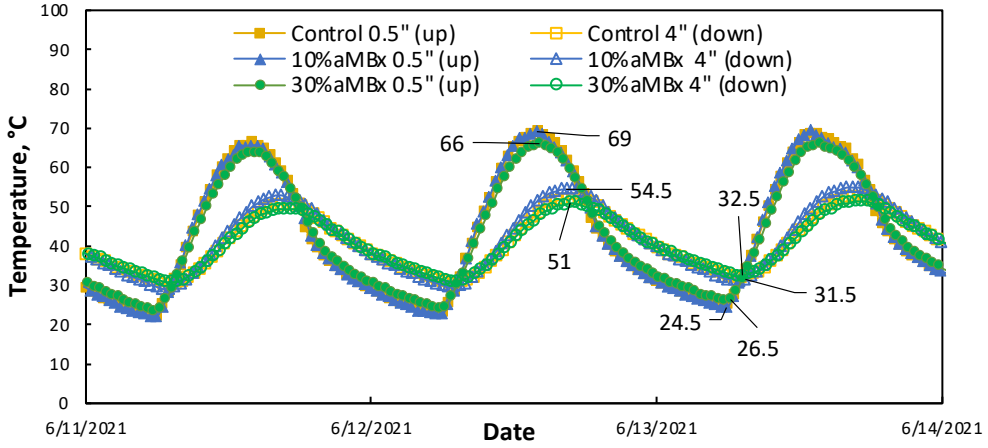

Figure 7-4. Field Temperature behavior for a thick scenario (slab of 15cm thick).

Since the collection of temperatures from the field was not carried out for the top (surface) and the bottom of the slabs, the ACTScalc software was used to forecast and analyze this data given proved high accuracy of this tool (Gui, et al., 2007) (Obando, et al., 2021).

In addition to the dew point, atmospheric temperature, wind speed, and solar radiation, weather information obtained from the Arizona Meteorological Network (AZMET) for January and June 2021. This software needs the climatic data to configure the environment and the thermal properties of each pavement layer. Figure 7-5 shows the input needed to run the software.

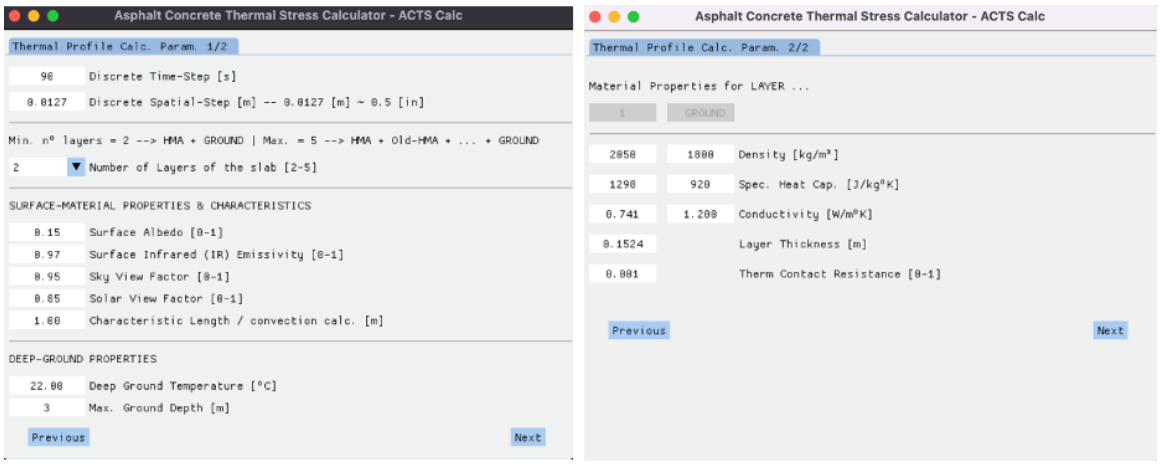

Figure 7-5. Inputs about environment and pavement information.

Results of the model are presented every 1.27cm from the surface of the pavement. Figure 7-6 shows a graphical representation of the outcomes.

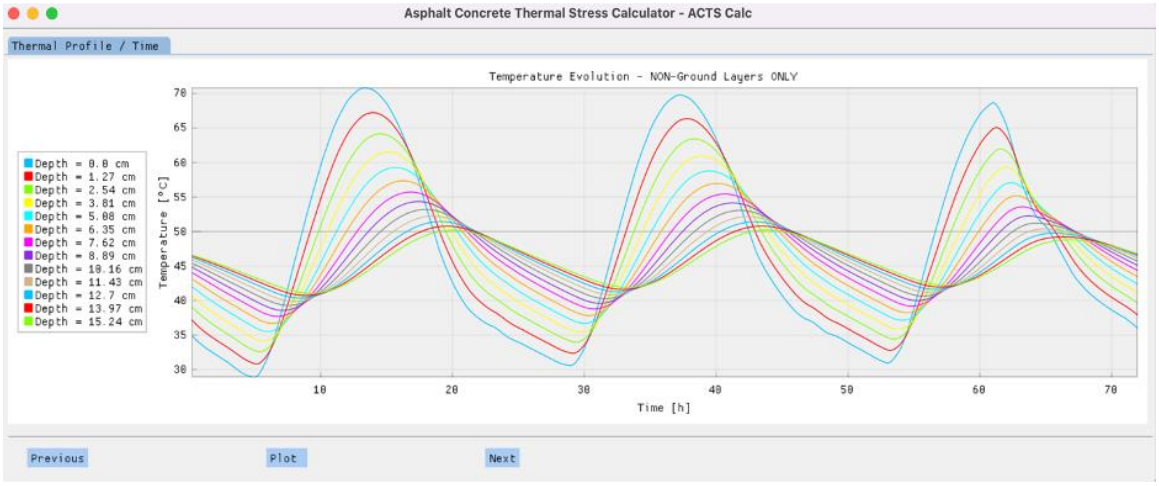

Figure 7-6. Outcomes of the model: Temperature measured at different depths.

In Winter, the modeling results show that the 30% aMBx surface temperatures are lower by ~0.3°C compared to Control during the day and night for the thin scenarios and are like Control for the thick scenarios. Bottom temperatures are the lowest during the day, but the highest during the night. The 10% aMBx slabs presented the highest surface temperature during the day, approximately 0.3°C higher than Control. During the night, the10% aMBx surface temperature tends to be the lowest.

In Summer, the results show in contrast that 30% aMBx surface temperatures are higher by approximately 0.26°C compared to Control during the day for both thin and thick scenarios. During the night, surface temperature is lower than Control for thin structures by ~0.2°C, but higher by ~0.2°C for thick structures. Bottom temperatures are the lowest during the day, but the highest during the night for thin and thick structures. The 10%aMBx slabs presented the highest surface temperature during the day, about 0.5°C higher than Control. During the night, the 10%aMBx surface temperature tends to be the lowest. Table 7-6 presents a summary of all the outcomes.

Table 7-6. Temperature Prediction Results for Winter and Summer.

Considerations			Max (day) Temperature (ºC)		Min (night) Temperature (ºC)		Gradients (ºC)	
			Top	Bottom	Top	Bottom	Top	Bottom
Winter	**Thin**	Control	29.73	21.79	2.42	6.77	27.31	15.02
		10% aMBx	30.01	21.71	2.42	6.61	27.59	15.10
		30% aMBx	29.55	20.85	2.08	6.93	27.47	13.92
	Thick	Control	29.44	17.36	2.79	10.12	26.65	7.24
		10% aMBx	29.72	16.97	2.56	10.26	27.16	6.71
		30% aMBx	29.49	16.01	2.67	10.96	26.82	5.06
Summer	**Thin**	Control	70.98	59.42	27.90	34.51	43.08	24.91
		10% aMBx	71.52	59.49	27.44	34.41	44.08	25.08
		30% aMBx	71.18	58.62	27.69	35.19	43.50	23.43
	Thick	Control	70.46	51.98	28.59	39.25	41.86	12.73
		10% aMBx	70.92	51.54	28.37	39.65	42.55	11.89
		30% aMBx	70.79	50.20	28.81	41.04	41.98	9.16

Notes: For both, thin and thick scenarios "Top" sensor location corresponds to the surface of the pavement
For thin scenario, "Bottom" sensor location corresponds to 7.5cm below the surface of the pavement
For thick scenario, "Bottom" sensor location corresponds to 15cm below the surface of the pavement

Based on the temperature behavior for all considered cases, lower values of thermal conductivity (TC) create an insulating (non-conducting) effect, which refers to higher surface temperatures for thin and thick pavement structures. This means that the heat transfer from the outside to the inner pavement structure is limited and the surface temperature is higher (heat is kept on the surface). On the other hand, this will refer to lower temperatures deeper within the pavement structure.

The specific heat capacity is another very important aspect to consider. Higher specific heat capacity means a greater heat storage. Thus, once the heat is inside the pavement structure, the release of the heat could take more time depending on the thermal mass.

Overall, managing pavement surface temperature can be addressed not only by changing the color of the surface (i.e., changing the Albedo), but also by varying the thermal properties of the pavement material and thickness. Working on the mitigation of the Urban Heat Island effect groups different initiatives and strategics that also depends on the surroundings' characteristics.

Finally, the temperature gradient is defined as the change in temperature of a specific point or location in the pavement structure when the weather conditions change. In this case, the change of temperature was evaluated between the maximum (day) and minimum (night) temperatures at different depths. The effect of the temperature change in a specific point is defined as the thermal stress. Therefore, the higher the gradient, the more likely is the occurrence of thermal cracking. Values in Tables 9 and 10 show that the gradient of temperature is lower for the aMBx modified pavements along most of the pavement structure. For this reason, it is concluded that the aMBx modified asphalt pavements with lower TC have lower thermal susceptibility. Thermal susceptibility in asphalt pavements is associated to different distresses, where one of those is the thermal cracking. The results of this study show that having materials with lower TC can make pavements less susceptible to temperature change, which could be translated into pavements less prone to thermal cracking.

7.4 Conclusions

Many barriers were overcome since the inception of the study in transforming what started as a laboratory task to a successful field implementation of a product to potentially be used in one of the largest industries in the world.

Manufacturing of 270 kg of aMBx in the laboratory was a triumph. The implementation of the mixtures design method was successful at the plant production level. More than 33 tons of asphalt mixtures were produced and paved successfully. Six test slabs with two different thicknesses and three different mixtures designs were constructed.

The results showed that the modified mixtures have lower heat transfer and higher heat storage. In Winter, pavement materials with lower TC and higher SHC than conventional (control) result with lower surface temperatures by approximately 0.3^{o}C during the day and night for thin scenarios, and similar values for thick scenarios. In Summer, results showed in contrast that surface temperatures of materials with lower TC and higher SHC are higher by 0.26^{o}C compared to Control during the day for both, thin and thick scenarios. During the night, surface temperatures are lower than Control for thin structures by ~0.2^{o}C, and higher by 0.2^{o}C for thick structures.

Based on the temperature profile behavior, lower values of TC create an insulating (non-conducting) effect, which determines higher surface temperature for thin and thick pavement structures. This refers to limited heat transfer from the outside to the inner depths of the pavement structure reflecting higher surface temperatures but lower inner temperatures. In addition, higher specific heat capacity refers to a larger heat storage. Thus, once the heat is inside the pavement structure, its release could take more time depending on the thermal mass of the structure.

Overall, managing pavement surface temperature is concluded to be addressed not only by changing the color of the surface (i.e., changing the Albedo), but also by varying the thermal properties of the pavement materials and overall thickness.

Finally, the gradient of temperature is deemed to be an important parameter. It has been found to be lower for the aMBx modified pavements along mostly the entire structure. This concludes that the aMBx modified asphalt pavements with lower TC have lower thermal susceptibility and therefore are less prone to thermal cracking.

CHAPTER 8

EXTENDING THE THERMAL STRESSES EVALUATION AND ANALYSIS IN ASPHALT PAVEMENTS

8.1 Introduction

The day-to-day or recurrent seasonal temperature cycling incites the tensile stress to surpass the tensile asphalt pavement's strength resulting in thermal cracking on the pavement's surface. Even, when the stress level is lower than the tensile strength of the pavement, the repetitive temperature cycle eventually induces a fatigue associated to thermal cracking in the material (Vinson & Janoo, 1989). Thermal cracking distress is related to the environment or climate influences instead of a loading issue.

Low temperature thermal cracking has been widely studied. Asphalt pavements under low temperature tends to "shrink", accumulates strain energy at the bottom of the surface layer making the transverse and longitudinal cracks appear on the surface. Cracking of flexible pavements due to thermal effects is related to the occurrence of low temperatures which induces tensile stresses in the pavement materials, so in turn it results in fractures (Yoder & Witczak, 1975).

Because high-temperature cracking is not documented and moreover it is assumed that high temperature cracking is like low-temperature, thermal cracking remains to be an essential asphalt pavement distress mechanism in hot climate places that needs to be further studied. The propagation of cracks due to thermal cracking produces significant

damage to the integrity of the pavement and generates pathways for the intrusion of water into the granular layers and even in the subgrade (Dave & Hoplin, 2015).

The use of modifiers such as crumb rubber, styrene-butadiene-styrene (SBS), polyphosphoric acid (PPA), and sulfur, has been the most common methodologies to overcome actual necessities and thus improve the performance of asphalt mixtures (Gordon, Rheolgical evaluation of ethylene vinyl acetate polymer modified bitumens., 2002). All these modifications predominantly have improved the temperature susceptibility of bitumen by increasing stiffness at high temperatures and reducing the probability of cracking at low temperatures (Collins, Bouldin, Gelles, & Berker, 1991). However, the low ageing resistance, poor storage stability of polymer modified bitumen (PMB), and high cost are some obstacles that limit the progress of bitumen polymer modification (Zhu, Birgisson, & Kringos, 2014), whereas the implementation of rubber in asphalt mixtures has some downsides such as recyclability, binder storage stability, the fumes that it releases through the paving process, and workability (Kuennen, 2004). Therefore, the study on the implementation of new materials is still needed (Hinislioglu, 2011).

Since the thermal stresses are associated to how the temperature in a specific point of the asphalt structure fluctuates, the estimation of the pavement's thermal profile along the time is required. Thermal profile estimation can be obtained by measuring in the field or simulated knowing some thermal properties of the material such as thermal conductivity (TC), and specific heat capacity (SHC). Another thermal property considered is the coefficient of thermal expansion (α_e) and thermal contraction (α_c). These coefficients can provide a better insight about the pavement's thermal cracking potential. These

coefficients are reported by several researchers to be temperature dependent variables (Islam & Tarefder, 2015).

Thermal cracking can make shorter the lasting of the pavement, cause safety issues, and increase the maintenance costs. Therefore, better understanding, and estimation of thermal cracking are still needed to improve the performance of roads.

In this Chapter, information collected from Long-Term Pavement Program (LTPP) serves to identify how the environmental conditions affect thermal cracking. A new set-up to measure the thermal expansion and contraction of the asphalt mixtures is proposed to better understand this phenomenon and feed further analysis. A thermal model is proposed to determine temperature and thermal stresses along the thicknesses of the asphalt pavement layer, and field measurement serve as the based to estimate the accuracy of the model. The new modifier, aMBx, is used to produce five different mixtures to analyze the thermal stresses for different asphalt mixtures and identify the key thermal characteristic to mitigate thermal cracking. Based on the simulations' outcomes, a better understanding of how the thermal cracking work is obtained. Thermal cracking behaves differently depending on the seasons of the year, and it is expected that in zones where the gradient of temperature is considerable, the development of thermal cracking is most likely.

8.2 Materials and Method

Description and/or information of the modifying Material (aMBx composite), asphalt binder type, and aggregates, and mixture design are described in Chapter 6. Composite material was used to modify the HMA pavements in different contents: 10%, 20% and 30% by weight of the asphalt binder.

In this Chapter, the two different approaches to include aMBx into the mixture were considered, dry method and wet method. Control (0%), 10%aMBx (DM), 10%aMBx (WM), 20%aMBx (WM), and 30%aMBx (DM) modified asphalt mixtures were included. The variety of mixtures is to consider different material's properties and then responses. Viscosity of binders increases when using 30%aMBx making the mixing process difficult, then, instead of 30%WM, 20%WM was implemented. The optimum binder content is based on the weight of the raw aggregates weight.

8.2.1 In-situ Temperature Recordings and Thermal Properties

Collecting of the data is the same as Chapter 7. Data corresponds to Winter (January 2021) and Summer (June 2021) gathered from 6 different slab pavements located at Litchfield Park, Arizona. The slabs were constructed following the City of Phoenix specifications. The configuration of the slabs is 3.6m by 3.6m, with two thickness (7.5cm and 15cm). Pavements slabs have different material characteristics and are named as Control, 10%aMBx_DM and 30%aMBx_DM. The asphalt layers were directly compacted on top of a well compacted subgrade granular material. Wireless thermocouples (thermistor iButton DS1922E) were placed at the near-surface depth (1.27cm below the surface, "Up") of all the slabs. Wireless sensors were also placed at 5cm below the surface for the 7.5cm

thick slabs (thin scenario, “Down”), and at 10cm deep for the 15cm thick slabs (thick scenario, “Down”). Table 8-1 present the respective information.

Table 8-1. Winter and Summer Field Temperature Readings (January 2021, and June 2021)

Considerations			Max (day) Temperature (ºC)		Min (night) Temperature (ºC)		Gradients (ºC)	
			Up	Down	Up	Down	Up	Down
Winter	**Thin**	Control	28.50	25.50	3.50	5.50	25.00	20.00
		10% aMBx	28.50	24.00	3.00	5.50	25.50	18.50
		30% aMBx	26.00	20.50	3.50	6.50	22.50	14.00
	Thick	Control	28.50	19.00	4.00	8.50	24.50	10.50
		10% aMBx	28.50	19.00	3.50	9.00	25.00	10.00
		30% aMBx	26.00	18.00	4.00	9.50	22.00	8.50
Summer	**Thin**	Control	70.50	65.50	24.00	26.50	46.50	39.00
		10% aMBx	70.50	65.50	24.00	26.50	46.50	39.00
		30% aMBx	66.50	55.50	26.00	28.50	40.50	27.00
	Thick	Control	69.00	54.50	24.50	31.50	44.50	23.00
		10% aMBx	69.00	54.50	24.50	31.50	44.50	23.00
		30% aMBx	66.00	51.00	26.50	32.50	39.50	18.50

* For both, thin and thick scenarios "Up" sensor location corresponds to 1.27cm below the surface of the pavement
* For thin scenario, "Down" sensor location corresponds to 5cm below the surface of the pavement
* For thick scenario, "Down" sensor location corresponds to 10cm below the surface of the pavement

Also, information of thermal conductivity (TC) and specific heat capacity (SHC) of all type of mixtures corresponds to the previous Chapter 7. However, in this case 2 additional materials were included (10%aMBx_WM and 20%aMBx_WM) following the same methodology explained in Chapter 7. Table 8-2 present the density of each material given in kg/m^3. This information is needed to feed the proposed thermal stresses model. Table 8-3 and 8-4 show the mentioned thermal properties

Table 8-2. Densities for all different mixtures.

Pavement Type	Density (K/m^3)	Standard Deviation	Standard Error	COV
Control	2175.82	35.2	20.32	0.016
10%aMBx_DM	2109.82	30.1	17.38	0.014
10%aMBx_WM	2160.00	29.5	17.03	0.014
20%aMBx_WM	2155.00	33.8	19.51	0.016
30%aMBx_DM	2084.97	34.3	19.80	0.016

Table 8-3. Thermal Conductivity (TC) results for all different mixtures.

Pavement Type	k (W/m^oK)	Standard Deviation	Standard Error	COV
Control	1.001	0.008	0.004	0.008
10%aMBx_DM	0.885	0.064	0.032	0.073
10%aMBx_WM	0.831	0.017	0.010	0.021
20%aMBx_WM	0.775	0.042	0.024	0.054
30%aMBx_DM	0.741	0.047	0.023	0.063

Table 8-4. Specific Heat Capacity (SHC) results for all different mixtures.

Pavement Type	SHC (J/kg^oC)	Standard Deviation	Standard Error	COV
Control	939.68	32.709	0.135	0.035
10%aMBx_DM	1016.16	83.640	0.082	0.082
10%aMBx_WM	1011.70	48.551	0.0474	0.048
20%aMBx_WM	1120.23	15.00	0.0617	0.013
30%aMBx_DM	1298.03	96.890	0.399	0.075

8.2.2 Weather Information

To properly run the physical thermal model, explained below, various inputs are needed. Meteorological measurements between 1 to 3 days are needed. The climatic parameters needed are obtained from the Arizona Meteorological Network (AZMET). In this case, weather information was consulted for winter (January 3-5, 2021) and Summer (June 26-28, 2021). The required data is the measured time stamp [h], the atmospheric

temperature [ºC], the dew point temperature [ºF], the solar irradiance [W/m²], and the wind velocity [mph]. Table 8-5 presents an example of the weather information needed.

Table 8-5. Weather information for 1 day (Winter and Summer, 2021).

Time [h]	Winter (January 3, 2021)				Summer (June 26, 2021)			
	T.atm (ºC)	DewPoint (ºF)	SolarRad (W/m²)	Wind Speed (mph)	T.atm (ºC)	DewPoint (ºF)	SolarRad (W/m²)	Wind Speed (mph)
0	5.56	33.00	0.00	0.00	22.00	44.80	0.00	0.00
1	5.83	33.00	0.00	0.00	20.50	49.10	0.00	0.00
2	5.00	33.00	0.00	0.00	20.89	44.80	0.00	0.00
3	4.57	33.00	0.00	0.00	19.61	43.90	0.00	0.00
4	5.00	33.00	0.00	0.00	18.61	44.20	0.00	0.00
5	1.67	31.00	0.00	0.00	18.39	42.10	27.89	0.00
6	1.11	31.00	0.00	2.00	22.61	44.10	185.95	0.20
7	1.11	31.00	0.00	3.00	28.11	36.70	393.97	0.20
8	0.56	32.00	0.00	3.00	31.28	32.20	593.87	0.90
9	0.56	30.00	0.00	3.00	33.28	28.00	771.68	2.70
10	0.00	32.00	80.00	0.15	35.39	27.00	911.14	2.20
11	0.00	35.00	225.00	3.00	37.50	24.40	999.46	0.40
12	8.89	35.00	300.00	4.00	38.50	25.00	1,025.03	1.10
13	8.89	35.00	525.00	4.00	39.61	25.50	989.00	3.40
14	13.33	35.00	600.00	1.00	40.72	21.70	893.71	4.00
15	13.33	35.00	590.00	5.00	41.22	21.00	757.73	2.70
16	16.67	34.00	525.00	1.00	41.61	19.20	583.41	3.60
17	16.67	34.00	400.00	0.15	41.39	17.80	383.52	3.80
18	16.67	40.00	290.00	3.00	40.78	14.90	169.68	2.70
19	13.33	40.00	80.00	4.00	37.72	23.20	22.08	1.10
20	13.33	40.00	0.00	2.00	31.11	38.30	0.00	0.00
21	13.33	40.00	0.00	3.00	26.61	44.60	0.00	0.00
22	8.89	38.00	0.00	0.00	26.61	45.00	0.00	0.00
23	7.22	38.00	0.00	2.00	25.72	46.40	0.00	0.20
24	6.11	39.00	0.00	0.00	22.00	46.40	0.00	0.00

8.2.3 Dynamic Complex Modulus |E|, (AASHTO T 342-11)*

This test provides valuable information about the viscoelastic properties of asphalt mixtures. The proposed model to estimate the thermal stresses needs the Dynamic Modulus results. Cylindrical specimens of 100mm in diameter and 150mm in height were used. Before the test, samples were instrumented with three linear variable displacement transducers (LVDTs) spaced at 120° intervals on the specimen's surface. Temperatures of

-10, 4.4, 21.1, 37.8, and 54.4°C, with frequencies of 25, 10, 5, 1, 0.5, and 0.1 Hz were utilized. Before testing, lubricated membranes were placed between the loading platens and the sample to reduce any end effects.

8.2.4 LTPP data analysis

This analysis looks for an insight on how the external conditions, mostly related with temperature, affects thermal cracking. Information about thermal cracking and temperature gradient, mainly of Arizona where the temperature gradients are large, was downloaded from LTPP. To make all data comparative, it was selected the same Construction Number (CN) and top asphalt layer information of the sections from Arizona, and Illinois.

To analyze thermal cracking, MEPDG AC Cracking Length (m/km) was selected. According to LTPP, this information corresponds to the length of transverse cracking per unit length using AASHTO MEPDG designations. It incorporated only transverse cracks at least 1.8m long.

Based on the date of the survey (cracking collection data date), it was calculated the average amount of cracking (m/km) for each section per year. This data was compared with the freeze-thaw number of days per month (Days/Month experienced), which means the number of days in the period (monthly) when the air temperature goes from less than 0^{o}C to greater than 0^{o}C; it assumes minimum daily temperature occurs before maximum daily temperature.

8.3 Thermal Expansion-Contraction New Test Set-up

This proposed laboratory test set-up intends to capture the strains that occurs due to the temperature variation along time, and then estimate the linear coefficients of expansion and contraction of asphalt mixture samples. The advantages of this procedure rely on the frictionless test set-up, on the sensibility of the features to accurately capture the data, and on the broad range of temperature to make a proper analysis. For this test, samples are made in the laboratory following AASHTO R 30 using a Superpave Gyratory Compactor (SGC) until to reach 180mm high. From the SGC specimens, samples of 75mm diameter and 150mm length are prepared. Since the heat transfer into the chamber happens by convection, the size of the sample is the adequate to ensure that a conditioning period of 2 hours is good enough to obtain a homogeneous heat distribution in the whole sample. The air voids content must be the same (±0.5%) in all type of mixtures.

This set-up consists in a LabVIEW 8.6 software with a data acquisition system (DAQ) to manage the recording of the displacements and temperature changes. An ESPEC chamber model BTZ-475 linked to a WinTest 7 software to control the temperature change along time is used to condition the samples. Two core linear variable differential transformers (LVDTs) type MHR010 are used. The sets of LVDTs are assembled with 1-72 threaded rods made of 18-8 Stainless Steel, whose coefficient of thermal expansion is 17.3E10-6°C-1, therefore, this material is thermal resistant enough to ensure the accuracy on the measuring of the specimen's thermal displacement. Rods and LVDTs are held by mounting buttons which are attached to the mix sample with acrylic paste. The two sets of LVDTs are placed on the samples with an angle of 90^{o}. The buttons' axes are 100mm spaced out. One end of the rod is displacement allowed (i.e., it ends in the core LVDT,

which capture the displacement), while the other end is fixed (i.e., it is fixed in the mounting button). Configuration of the two rods is the same but the displacing ends are in opposites sides of the mixture. In the end, the final displacements are obtained by the average of both LVTDs readings. Figure 8-1 shows the mounting buttons, LVDTs, and rods set-up.

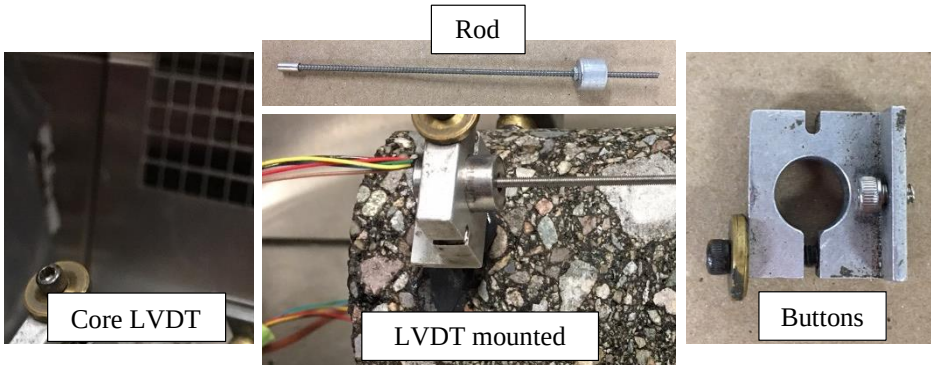

Figure 8-1. MHR10 core LVDT and rods.

The automated temperature wave has a range of -15ºC to 55ºC and the sequence is designed to provide a broad spectrum of strains to analyze the mixture's response. The temperature wave follows 25ºC, 35ºC, 45ºC, 55ºC, 35ºC, 25ºC, 15ºC, 5ºC, -5ºC, -15ºC, 25ºC, 55ºC, -15ºC, and 25ºC. Once each temperature is reached, it remains for 2 hours (the time need to homogenize the sample temperature) while the displacements in the sample are induced and captured. The change of the temperature occurs at a ratio of 0.0167ºC/sec. A thin metal rack, big and strong enough to support the sample holds the sample in 3 thin points avoiding friction an allowing the heat penetrates the specimen from everywhere. With this configuration the heat reaches the sample homogenously from everywhere. Thermal couples type K are used to take the air temperature (chamber temperature wave)

and the mixture sample's temperature. Two identical samples are place into the chamber. One is instrumented with the LVDTs to measure the strains, and the other with an insulated sensor to measure the change of the inner sample's temperature. Figure 8-2 presents the set-up of the test.

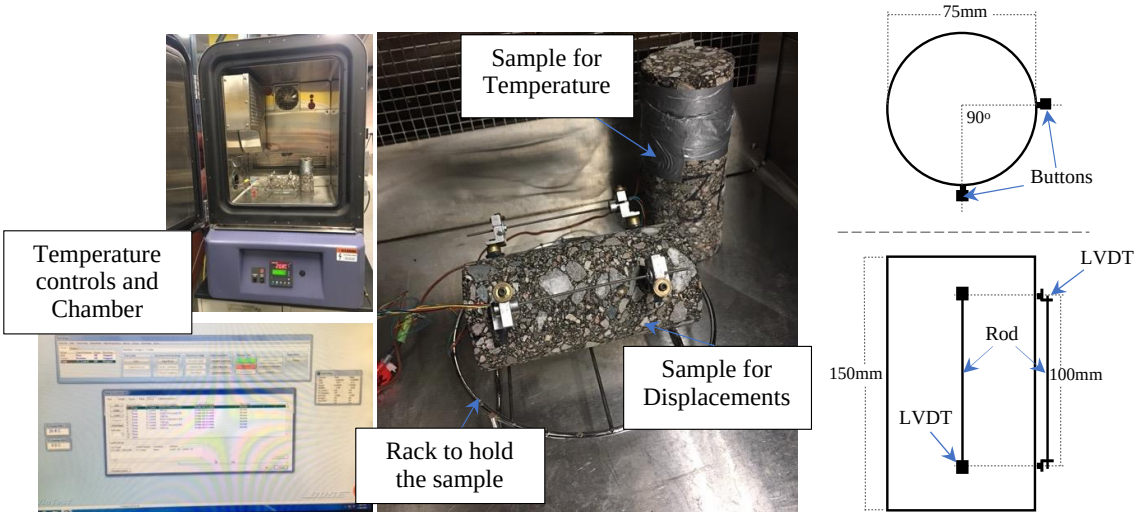

Figure 8-2. Set-up of the Expansion-Contraction test.

All type of mixtures were tested. Displacement's data captured is given in millimeters. To convert the displacements in strains, all displacements are divided by the separation of the mounting buttons, which is 100mm. Having the displacements and the respective temperature, calculation of the coefficients of thermal expansion (α_e) and contraction (α_c) is carried out. To calculate α_c and α_e it was used the Equation (8-1), below presented (Osterkamp & Baker, 1986) (Islam & Tarefder, 2014):

$$\alpha_c = \frac{\Delta L}{L * \Delta T} \qquad (8\text{-}1)$$

Where:

ΔL = change in length due to temperature [mm]

L = initial length of sample [mm]

ΔT = change in temperature [^{o}C]

8.4 Pavement's Thermal Profile and Stresses Model

The model is divided in two different procedures. The first one is a method to estimate the Temperature Profile of the asphalt layer at different times, and the second one is a model to estimate Stresses by Temperature for different depths and temperatures.

8.4.1 Temperature Profile Model

Phenomena in technology, nature and science like wave propagation and heat distribution can be descripted in a physical domain determining the boundaries of the domain. In this framework, temperature changing along the depth of the asphalt can be modeled using an initial boundary condition (BC).

A Forward-Time Central-Space (FTCS) Finite Difference scheme, also known as "explicit scheme", is used to solve the general 1-D diffusion equation. The system of equation resulting from the FTCS scheme implementation induces recurring terms, as shown in the next paragraphs of this document. This is due to some equations relying on temperature results calculated at the same time-step, that themselves depend on these equations.

This way, the thermal profile slowly converges at each step until reaching the definitive solution, in an iterative process A matrixial "Frobenius" norm of the difference between thermal profile at iteration $i-1$ and iteration i is used to evaluate the convergence of the recurring algorithm and define a suitable stopping criterion as Equations (8R-1) and (8R-2) show.

$$X = [\text{ThProfile}]^{i-1} - [\text{ThProfile}]^{i} \quad (8R\text{-}1)$$

$$||X||_F = \sqrt{\sum_i \sum_j |x_{ij}|^2} \quad (8R\text{-}2)$$

The implied model allows the obtention of an accurate thermal profile thanks to the implementation of the different physical phenomena accounting for heat exchanges between the asphalt and its surroundings. Radiation: incoming solar energy and outcoming infrared radiation (albedo); convection: heat exchanges with air, considering wind velocity and the occurrence of turbulence (if needed); and conduction: heat transfer into the ground (semi-infinite solid). This can be schematically seen in the Figure 8-3 (Gui, et al., 2007).

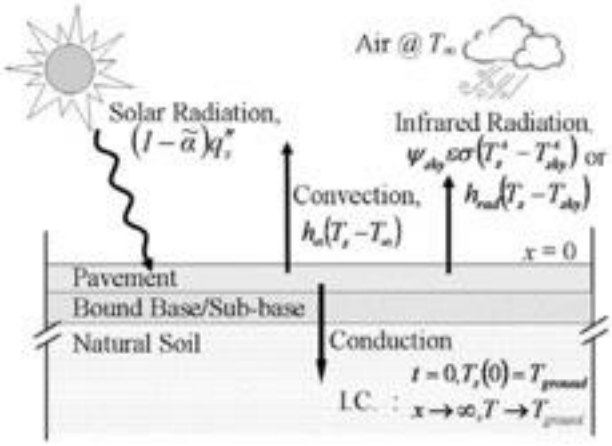

Figure 8-3. Heat exchange between the pavement and its surroundings.

To run the physical thermal model, various inputs are needed. The model needs meteorological measurements between 1 to 3 days (refer Table 8-5). The required data is:

- The measured time stamp [h]
- The atmospheric temperature [ºC]
- The dew point temperature [ºF]
- The solar irradiance [W/m²]
- The wind velocity [mph]

Additionally, it is needed to consider some calculation parameters to perform the thermal profile estimation. These are:

- The discrete time-step [s]
- The discrete spatial step [m]
- The number of layers in the model [2-5]: There are at least two layers, the Hot Mix Asphalt (HMA) layer and the ground layer. However, it is possible to include 3 more layers in-between those two (these could be old-HMA layers or other relevant soil information).
- The surface material and characteristic properties, including:
    - Surface albedo (0-1)
    - Surface emissivity (0-1)
    - Sky view-factor (0-1)
    - Solar view-factor (0-1)
    - Characteristic length (for convection modelling) [m]
- The deep-ground properties, namely:

- Deep-ground temperature [ºC]
- Maximum ground depth [m]

For each input layer, the following properties are needed: Density [kg/m³], specific heat capacity [J/kgºK], thermal conductivity [W/mºK] (refer Tables 8-2, 8-3 and 8-4). For non-ground layers, two more properties are need: the layer thickness [m], and the thermal contact resistance between this layer and the adjacent one (0-1). The thermal contact resistance corresponds to the resistance between asphalt layers.

Initially it is needed to model the exchange of heat from the pavement's surroundings and the pavement. The mathematical and physical description is explained below.

8.4.1.1 Outgoing Radiation Properties

To calculate the outgoing radiation from the surface to the horizon, a sky temperature needs to be estimated. This is realized through Equation (8-2).

$$T_{sky} = T_{atm}(0.004T_{dew} + 0.8)^{0.25} \quad (8\text{-}2)$$

Where:

T_{sky} the sky temperature [ºK]

T_{atm} the atmospheric dry-bulb temperature [ºK]

T_{dew} the dew-point temperature [ºC]

8.4.1.2 Expressions Used within the Recurring Scheme

The following equations show recurrent terms. These depend on the surface temperature, which is calculated using the results of Equation (8-3). These equations are integrated within the recurring scheme and solved iteratively until the defined convergence criterion is reached.

- **Outgoing Radiation Coefficient Calculation:**

$$h_{rad} = \Psi_{sky}\varepsilon\sigma\left(T_S^2 + T_{sky}^2\right)\left(T_S + T_{sky}\right) \quad (8\text{-}3)$$

Where:

h_{rad} the abbreviated parameter for outgoing radiative heat transfer coefficient []

ψ_{sky} the sky view-factor []

ε the infrared emissivity of the surface []

$\sigma = 5.67e^{-8}$ the Stefan-Boltzmann constant [W/m²/ºK^4]

T_S the pavement surface temperature [ºK]

- **Convection Heat Transfer Calculation:**

The air film temperature depends on the asphalt surface temperature and the atmospheric temperature. It represents the temperature of the air film at the air-asphalt interface.

$$T_{film} = \frac{T_{surface}+T_{atm}}{2} \quad (8\text{-}4)$$

T_{film} isused together with "Reference air film properties" to interpolate or extrapolate the "actual" air film properties:

- $\nu_{film}(T_{film})$ the kinematic viscosity [m²/s]
- $\kappa_{film}(T_{film})$ the conductivity [W/m°K]
- $\alpha_{film}(T_{film})$ the diffusivity [m²/s]
- $Pr(T_{film})$ the Prandtl number []

- **Reynolds Number of Air Film:**

To properly consider, the convective heat exchange between the air and the asphalt surface, it is necessary to know if the conditions at the interface are representative of a laminar or turbulent air flow. The Reynolds number of the air film is thus calculated.

$$Re = \frac{U_{film} L}{\nu_{film}} \tag{8-5}$$

Where:

Re the Reynolds number of air []

U_{film} the wind velocity [m/s]

L the characteristic length of the pavement [m]

ν_{film} the kinematic viscosity of air [m²/s]

If $Re \leq 5^5$, then the flow is laminar. Else it is turbulent. The Nusselt number of the air film is thus calculated accordingly Equations (8-6x), and the convective heat transfer coefficient estimated from it, Equations (8-7x).

- **Nusselt Number of Air Film in Function of Laminar/Turbulent Flow:**

For laminar flow:

$$Nu_{laminar} = 0.664 \left[Pr^{1/3} Re^{0.5}\right] \quad (8\text{-}6.1)$$

For turbulent flow:

$$Nu_{turbulent} = 0.037 \left[Pr^{1/3} Re^{0.8}\right] \quad (8\text{-}6.2)$$

Where:

Nu_{xxx} the Nusselt number of air []

Pr the Prandtl number of air []

- **Convective Heat Transfer Coefficient of Air (h_∞):**

For laminar flow:

$$h_{laminar} = 0.664\left[k_{film} Pr^{1/3} \nu_{film}^{-0.5} L^{-0.5} U_{film}^{0.5}\right] \quad (8\text{-}7.1)$$

$$h_{laminar} = Nu_{laminar} \frac{k_{film}}{L} \quad (8\text{-}7.2)$$

For turbulent flow:

$$h_{turbulent} = 0.037\left[k_{film} Pr^{1/3} \nu_{film}^{-0.8} L^{-0.2} U_{film}^{0.8}\right] \quad (8\text{-}7.1b)$$

$$h_{turbulent} = Nu_{turbulent} \frac{k_{film}}{L} \quad (8\text{-}7.2b)$$

Where:

$h_{xxx} = h_\infty$ the convective heat transfer coefficient of air []

k_{film} the thermal conductivity of air [W/m°K]

8.4.1.3 Stability Verification: Courant-Friedrichs-Lewy (CFL) Criterion

The FTCS Finite Difference scheme is not intrinsically stable, due to its explicit nature. To ensure the algorithm convergence and the precision of the model, a stability check is thus necessary. This is realized through the calculation of the Courant-Friedrichs-Lewy - CFL criterion at each iteration since it depends on the convective heat transfer coefficient (and then on the surface temperature).

$$\Delta t \leq \frac{\rho_S \cdot c_S \cdot \Delta x^2}{2(h_{rad}\Delta x + h_\infty \Delta x + k_S)} \quad (8\text{-}8)$$

With:

ρ_S the density of the surface layer [kg/m³]

c_S the specific heat capacity of the surface layer [J/kg°K]

k_S the thermal conductivity of the surface layer [W/m°K]

Δt the temporal discretization step [s]

Δx the spatial discretization step [m]

At each iteration, the algorithm verifies that the temporal discretization step initially defined by the user is lower that the CFL criterion and advise the user to adapt if necessary.

8.4.1.4 Heat Equations Development Using Finite Differences (FD)

Equation (9) represents the governing form of the BC which describes transient heat conduction in a plane wall (SimScale, 2017). A Forward-Time Central-Space (FTCS) FD scheme, also known as "explicit scheme", is used to solve the general 1-D diffusion equation:

$$\frac{\partial u}{\partial t} = \alpha \frac{\partial^2 u}{\partial x^2} \quad (8\text{-}9)$$

Where:

α is the diffusivity of AC [m²/s]

u is the value of interest (here: the temperature) [°C]

t elapsed time (h)

x measured depth from the surface of the pavement (m)

As the true initial thermal profile of the pavement is unknown, the "Initial Boundary Condition" (BC) $T(t = 0, all\ depth) = T_{ground}$ is used. Additionally, the following BC is considered: $T(all\ time, \infty) = T_{ground}$.

Finally, it is worth noting that, due to the lack of initial thermal profile, an iterative recurring scheme is needed to compute the solution. This recurrence is realized applying $T(t = 0, all\ depth) = T(t_{final}, all\ depth)$ at each iteration (except the first one, where the initial BC applies).

Using the FTCS Finite Difference scheme, Equation (8-9) translates into the following:

$$\frac{u_m^{t+1}-u_m^t}{\Delta t} = \frac{u_{m-1}^t-2u_m^t+u_{m+1}^t}{\Delta x^2} \quad (8\text{-}10)$$

Where:

m represents the spatial position of the value of interest u

t represents the temporal position of the value of interest u

u_m^{t+1} is the sole unknown of the equation

The pattern associated to the FD-FTCS scheme (also known as stencil) is shown in the Figure 8-4:

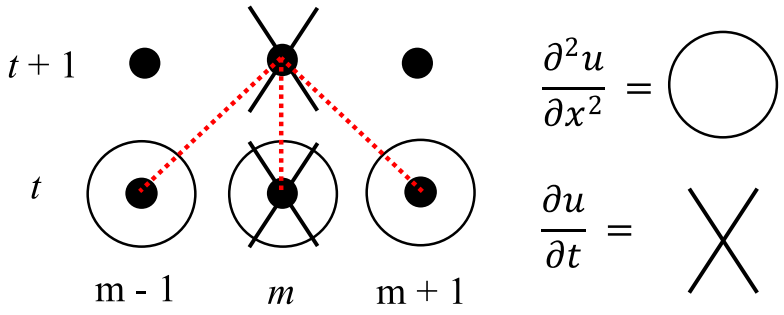

Figure 8-4. FD-FTCS scheme stencil.

To consider the different phenomena involved in the heat exchange between the pavement and its surroundings (i.e., environment, old asphalt layers, ground) (refer Figure 8-3), the general 1-D diffusion equation is solved in a different way in function of the calculation depth of interest (Gui, et al., 2007).

In this way, at the surface (depth = 0m), the Equation (8-10) is modified to consider the input solar radiation, the output infrared radiation of the pavement, the thermal convection as well as the thermal conduction. The resulting "Equation A" can be seen below.

On the other hand, for interior-nodes (depth > 0m), only thermal conduction must be considered. Thus, a simpler "Equation B" is developed and used at those points.

A special case of this equation can be encountered when there is a thermal contact resistance R_{ij}, Equation (11.2) between two different layers. Such specificity is considered thanks to "Equation C" that allows considering the phenomenon while ensuring heat flux continuity between the i and j layers, as shown in Equation (8-11.1):

$$k_i \frac{\mathrm{d}T_i}{\mathrm{d}x} = k_j \frac{\mathrm{d}T_j}{\mathrm{d}x} \tag{8-11.1}$$

and

$$R_{ij} = \frac{T_{i,interface} - T_{j,interface}}{q"_{interface}} \tag{8-11.2}$$

Where:

$T_{i,\text{interface}}$ and $T_{j,\text{interface}}$ the interface temperatures at the i^{th} and j^{th} layers, respectively

$q"_{interface}$ the heat flux flowing through the interface

Equation (A): Heat equation for surface-node S

$$T_s^{t+1} = \frac{2\Delta_t}{\rho_s c_s \Delta_x}\left[h_\infty^{t+1}(T_{atm}^{t+1} - T_S^t) + h_{rad}^{t+1}\left(T_{sky}^{t+1} - T_S^t\right) + \Psi_{solar}(1-\overline{\alpha})q''^{t+1}_s + k_s\frac{T_1^t - T_s^t}{\Delta_x}\right] + T_S^t$$

Where:

T_S^{t+1} the surface temperature at time $t+1$ [^{o}K]

Ψ_{solar} the solar view factor []

$\overline{\alpha}$ the surface albedo []

q''^{t+1}_s the input solar radiation flux [W/m^2]

T_1^t the temperature at the first discretized depth at time t [^{o}K]

`T_S^t the surface temperature at time t [^{o}K]

Equation (B): Interior-node at depth $\boldsymbol{m}$

$$T_m^{t+1} = \frac{k_i \Delta t}{\rho_i c_i \Delta x^2}[T_{m-1}^t - 2T_m^t + T_{m+1}^t] + T_m^t$$

With:

T_m^{t+1} the temperature at depth m and time $t+1$ [^{o}K]

ρ_i the density of layer i [kg/m^3]

c_i the specific heat capacity of layer i [J/kg^{o}K]

k_i the thermal conductivity of layer i [W/m^{o}K]

T_{m-1}^t the temperature at depth $m-1$ and time t [^{o}K]

T_m^t the temperature at depth m and time t [^{o}K]

T_{m+1}^t the temperature at depth $m+1$ and time t [^{o}K]

Equation (C): Interface-node at depth $\boldsymbol{m = n}$

$$T_n^{t+1} = \frac{1}{2}\left(T_{i,\text{interface}} + T_{j,\text{interface}}\right)$$

$$T_n^{t+1} = \frac{1}{2}\left[\frac{2\Delta x k_i + k_i k_j R_{ij}}{k_i k_j R_{ij} + \Delta x k_i + \Delta x k_j}\left(T_{n-1}^t\right) + \frac{2\Delta x k_j + k_i k_j R_{ij}}{k_i k_j R_{ij} + \Delta x k_i + \Delta x k_j}\left(T_{n+1}^t\right)\right]$$

Where:

T_n^{t+1} the temperature at depth n and time $t + 1$ [^{o}K]

k_i and k_j the thermal conductivity of layer i and j, respectively [W/m^{o}K]

R_{ij} the thermal contact resistance between layers i and j (0-1)

T_{n-1}^t the temperature at depth $n - 1$ and time t [^{o}K]

T_{n+1}^t the temperature at depth $n + 1$ and time t [^{o}K]

- **Coefficient Calculations for Non-surface Depths:**

For each i^{th} layer, some parameters are defined. These are directly related to the heat equations that govern the heat energy in- and out-take, as well as their diffusion within the pavement.

Some parameters can be computed outside of the iterated recurring scheme as they are fixed. This is the case for the parameters $\delta_i, A_i \; and \; B_i,$ associated with the interior-node heat Equation B.

$$T_m^{t+1} = A_i T_m^t + B_i(T_{m-1}^t + T_{m+1}^t) \qquad (8\text{-}12)$$

Where:

$\delta_i = \frac{2\Delta t}{\rho_i c_i \Delta x}$

$$A_i = 1 - \left[\delta_i \frac{k_i}{\Delta x}\right]$$
$$B_i = \frac{\delta_i k_i}{2\Delta x}$$

Identically, parameters $C_{ij}\ and\ D_{ij}$, related to the interface-node Equation C applied on the i^{th} and j^{th} layers, are computed in advance.

$$T_n^{t+1} = C_{ij} T_{n-1}^t + D_{ij} T_{n+1}^t \quad (8\text{-}13)$$

Where:

- $C_{ij} = \frac{1}{2}\left[\frac{2\Delta x k_i + k_i k_j R_{ij}}{k_i k_j R_{ij} + \Delta x k_i + \Delta x k_j}\right]$
- $D_{ij} = \frac{1}{2}\left[\frac{2\Delta x k_j + k_i k_j R_{ij}}{k_i k_j R_{ij} + \Delta x k_i + \Delta x k_j}\right]$

- **Coefficient Calculations for Surface:**

In the case of the surface-node, in Equation A, only 2 of the 4 parameters can be calculated outside the iterative loop: $\delta_S\ and\ B_S$.

$$T_S^{t+1} = A_S^{t+1} T_S^t + B_S T_1^t + C_S^{t+1} \quad (8\text{-}14)$$

Where:

$$\delta_S = \frac{2\Delta t}{\rho_S c_S \Delta x}$$

$$A_S^{t+1} = 1 - \delta_S \left[h_\infty^{t+1} + h_{rad}^{t+1} + \frac{k_S}{\Delta x}\right]$$

$$B_S = \delta_S \frac{k_S}{\Delta x}$$

$$C_s^{t+1} = \delta_s \left[h_\infty^{t+1} T_{atm}^{t+1} + h_{rad}^{t+1} T_{sky}^{t+1} + \Psi_{solar}(1 - \bar{\alpha}) q''^{t+1}_s\right]$$

However, parameters A_S^{t+1} and C_S^{t+1} need to be included into the recurring scheme as they depends on the convective (h_∞) and outgoin gradiative (h_{rad}) coefficients, which themselves depend on the surface temperature T_S^t.

8.4.2 Thermal Stresses Model

The stress calculation is realized only on the 1st pavement layer. Thus, only this part of the thermal profile previously calculated is considered in the following. This approach was chosen since the thermal cracking phenomenon mostly affect the top part of the pavement structure.

The stress profile within the surface layer is enough to estimate the pavement's cracking potential. Reducing the calculation to this sole portion of the pavement allows to decrease the computational burden of the calculation. Also, focusing the calculation of stresses in the first layer avoids the stress-discontinuity at the layers' interface due to the different thermal contraction coefficients.

To assess a thermal stress analysis, a Generalized Maxwell Model (GMM) also known as Wiechert Model is used. The associated mechanistic scheme is shown in Figure 8-5 (Adamczak & Bochnia, 2016).

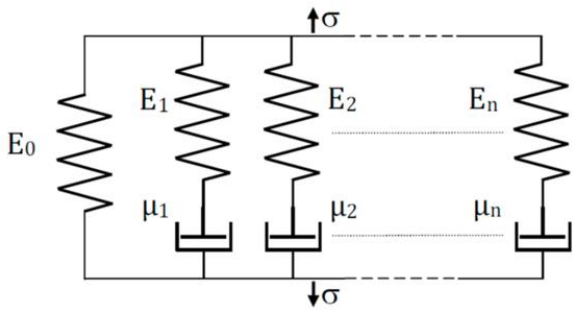

Figure 8-5. Generalized Maxwell Model for Relaxation Modulus.

The associated equations, known as Prony series, are presented below:

$$Erel(\xi) = E_0 + \sum_{i=1}^{N} E_i\left(e^{-\xi/10^{\rho_i}}\right) \quad (8\text{-}15)$$

$$Erel(\xi) = E_0 + \sum_{i=1}^{N} E_i + \sum_{i=1}^{N} E_i\left(e^{-\xi/10^{\rho_i}} - 1\right) \quad (8\text{-}16)$$

$$Erel(\xi) = E_{glassy} - \sum_{i=1}^{N} E_i\left(1 - e^{-\xi/10^{\rho_i}}\right) \quad (8\text{-}17)$$

Where:

$Erel(\xi)$ the relaxation modulus at reduced time ξ [GPa];

E_0 the equilibrium relaxation modulus [GPa] - at $\xi \to +\infty$

E_i local relaxation modulus values [GPa]

$\rho_i = \log(\tau_i)$ the log of the relaxation time [s]

E_{glassy} the glassy relaxation modulus [GPa] - at $\xi \to 0^+$

The Relaxation Master Curve is obtained applying the Time-Temperature Superposition Principle (TTSP) that stands for thermorheologically simple materials (Olidid & Hein, 2004). Its construction is realized through the automatic horizontal shifting technique of the non-reference curves (Witczak, Roque, Hiltunen, & Buttlar, 2000). To obtain a continuous evolution of the shift-factor with the temperature, a rheological *Arrhenius law* is fitted to those discrete experimental data points, as shown in Equation (8-18).

$$\log(a_T)\left(T, T_{ref}\right) = \frac{E_a}{\ln(10)R}\left(\frac{1}{T} - \frac{1}{T_{ref}}\right) \quad (8\text{-}18)$$

Where:

T the working temperature [ºC]

T_{ref} the reference temperature [ºC]

a_T the shift-factor at temperature T with reference temperature T_{ref}

E_a the material activation energy [J/mol]

R the ideal gas constant with $R \approx 8.314$ [J/(K.mol)].

The Prony series, Equation (8-15) to (8-17) is then optimized on the Relaxation Master Curve to obtain a continuous evolution of the Relaxation Modulus in function of the reduced time. However, the series cannot be used directly on experimental data, due to the data noise content and the high number of degrees of freedom (D^{o}F) that such equation allows. An additional pre-smoothing process is thus realized using a sigmoid function according to Equation (19). The simulated results obtained with the optimized sigmoid curve are the one used to obtain the Prony Coefficients.

$$\log|Erel(\xi)| = \delta + \frac{\alpha}{1+e^{\beta+\gamma\log\xi}} \quad (8\text{-}19)$$

Where:

$Erel(\xi)$ the relaxation modulus at reduced time ξ [GPa]

$\alpha, \beta, \gamma \; and \; \delta$ the parameters of the sigmoid law here employed

Equation (8-20) is the one-dimensional linear viscoelastic constitutive relationship, which represents the ordinary differential equation (ODE) to solve the thermal stresses (Alavi, Hajj, & Sebaaly, 2017)

$$\sigma(t) = \sum_{i=1}^{m}[e^{-\frac{\Delta\xi}{\tau_n}}\sigma_n(t-\Delta t) + G_n(\Delta\varepsilon)\frac{\tau_n}{\Delta\xi}\left(1-e^{\frac{-\Delta\xi}{\tau_n}}\right)] \quad (8\text{-}20)$$

Where:

$\Delta\xi$: change of the reduced time over time t−Δt to t

$\Delta\varepsilon$: change in thermal strain over time t−Δt to t

G_n and τ_n: Prony coefficients of asphalt mixture relaxation modulus

m: numbers of Maxwell arms in Prony series of relaxation modulus

However, the thermal stress is here calculated using the *Boltzman Superposition Integral*, which allow to transform the ODE into an integral equation. Indeed, integrals consist in continuously summing operations, and it is thus possible to express the material viscoelasticity at a given time as the continuous sum (integral) of the responses to excitations imposed at all previous times. Therefore, such type of integral is also known as "hereditary integral", since the resolution of it at time t receives from past "experience". In the present case, integral Equation (8-21) is obtained (Roylance, 2001).

$$\sigma(t) = \int_{0^+}^{t} Erel(t-\xi)\mathrm{d}\varepsilon = \int_{0^+}^{t} Erel(t-\xi)\frac{\mathrm{d}\varepsilon(\xi)}{\mathrm{d}\xi}\mathrm{d}\xi \quad (8\text{-}21)$$

Where:

ξ: reduced time over time

ε: thermal strain over time

Erel: relaxation modulus (Gpa)

t: time

Strains (ε) in Equation (8-22) corresponds to the strain at reduce time ξ which can be represented as showed in Equation (8-23) (Mallick & El-Korchi, 2018).

$$\varepsilon = \alpha_c(T(\xi') - T_o) \quad (8\text{-}22)$$

Where:

α_c is the linear coefficient of thermal contraction

$T(\xi')$ is the pavement temperature at reduced time ξ'

T_o is the pavement temperature when $\sigma = 0$

When facing complex excitation, as in the present case, finding a solution to this hereditary integral can be challenging, even using Fourier or Laplace integral transforms. A way to solve it is to use correspondence principles, that allow converting the stress-strain integral relationship into a simple elastic-like (i.e., linear) stress-strain relation (Schapery, 1984) (Schapery, 1999). To tackle viscoelastic problems, Schapery proposed the use of known as "pseudo-variables" (Schapery, 1975) (Schapery, 1975).

In short, the pseudo-variables method states that stresses in an elastic and viscoelastic body are the same, and thus, that it is possible to solve a viscoelastic problem

using the set of Equations (8-23) and (8-24) considering a Generalized Maxwell Model as stated in Equation (17).

$$\sigma = E^R \varepsilon^R \tag{8-23}$$

$$\varepsilon^R = \frac{1}{E^R} \int_{0^+}^{t} \left[E_{glassy} - \sum_{i=1}^{N} E_i \left(1 - e^{\frac{(t-\xi)}{\tau_i}} \right) \right] \frac{d\varepsilon(\xi)}{d\xi} d\xi \tag{8-24}$$

Where:

ξ: reduced time over time

ε: thermal strain over time

E: relaxation modulus (Gpa)

σ: stress (kPa)

τ_i: Prony coefficients of asphalt mixture's relaxation modulus

E_{glassy} the glassy relaxation modulus [GPa] - at $\xi \rightarrow 0^+$

A numerical implementation for isotropic material proposed by Hinterhoelzl and Schapery has been employed to integrate the equation discreetly in time, through the calculation of pseudo-variables increments (Hinterhoelzl & Schapery, 2004) (Ozer, 2020) (Ozer, 2014) (Ozer, 2020). This method showed better stability regardless of the time increment, as much as a high reliability. This technique is thus the one employed to compute all thermal stress calculations presented below.

8.5 Results and Discussion

8.5.1 Dynamic Complex Modulus |E|*

The stiffness changes from high values (low temperatures) to lower values (high temperatures). Results of the Dynamic Modulus tests suggest that all modified mixtures with aMBx present better rutting resistance (high temperature response), and similar fatigue resistance (low temperature response) than control. However, the behavior of the 20%aMBx_WM mixture samples is remarkably better than the other considered mixtures. Table 8-6 presents the results of the five different asphalt mixtures considered.

Table 8-6. Dynamic Modulus – Relaxation Modulus Results.

Temperature (ºC)	Frequency (Hz)	Control		10%aMBx_DM		10%aMBx_WM		20%aMBx_WM		30%aMBx_WM	
		Average (Gpa)	COV	Average (Gpa)	COV	Average (Gpa)	COV	Average (Gpa)	COV	Average (Gpa)	COV
-10	25	28.7	0.119	29.4	0.161	30.4	0.136	34.99	0.296	30.4	0.036
	10	28.1	0.118	29.1	0.172	29.7	0.130	34.17	0.242	29.9	0.083
	5	27.3	0.120	28.3	0.166	28.9	0.123	33.24	0.246	29.0	0.198
	1	25.1	0.129	25.9	0.165	26.9	0.101	30.89	0.312	26.7	0.113
	0.5	24.2	0.136	25.0	0.164	25.8	0.094	29.68	0.266	25.8	0.624
	0.1	22.1	0.144	22.9	0.171	23.4	0.061	26.86	0.453	23.6	0.415
4.4	25	18.3	0.103	21.4	0.034	23.2	0.263	25.57	0.312	20.3	0.136
	10	17.3	0.104	19.7	0.052	21.8	0.269	24.00	0.126	19.1	0.130
	5	16.4	0.094	18.8	0.043	20.0	0.290	22.05	0.094	17.9	0.123
	1	13.9	0.087	16.3	0.038	16.5	0.318	18.17	0.087	15.1	0.100
	0.5	13.0	0.086	15.1	0.040	14.9	0.313	16.40	0.126	13.9	0.094
	0.1	11.0	0.082	12.5	0.027	12.0	0.285	13.25	0.082	11.1	0.080
21.1	25	10.8	0.153	9.9	0.042	10.9	0.269	12.00	0.336	10.9	0.147
	10	9.2	0.133	9.0	0.083	9.6	0.221	10.51	0.257	9.4	0.155
	5	8.1	0.133	7.9	0.101	8.6	0.276	9.49	0.276	8.2	0.139
	1	5.6	0.153	5.5	0.098	6.2	0.279	6.77	0.211	5.6	0.113
	0.5	4.7	0.151	4.7	0.109	5.4	0.256	5.90	0.291	4.7	0.120
	0.1	3.0	0.167	3.0	0.141	3.5	0.185	3.88	0.185	2.9	0.144
37.8	25	3.6	0.263	3.7	0.238	4.2	0.173	7.19	0.042	3.4	0.004
	10	2.6	0.269	2.7	0.242	3.2	0.155	5.43	0.083	2.4	0.022
	5	2.1	0.290	2.1	0.246	2.5	0.139	4.25	0.198	1.9	0.031
	1	1.1	0.317	1.2	0.264	1.4	0.259	2.31	0.113	1.0	0.042
	0.5	0.9	0.313	0.9	0.266	1.0	0.181	1.77	0.109	0.8	0.024
	0.1	0.5	0.285	0.5	0.265	0.6	0.099	0.99	0.141	0.4	0.042
54.4	25	0.6	0.173	0.7	0.360	1.1	0.136	3.06	0.215	0.7	0.274
	10	0.4	0.156	0.5	0.377	0.8	0.130	2.23	0.172	0.6	0.257
	5	0.3	0.139	0.4	0.398	0.6	0.234	1.75	0.166	0.4	0.276
	1	0.2	0.180	0.2	0.371	0.4	0.112	1.01	0.165	0.3	0.279
	0.5	0.2	0.178	0.2	0.339	0.3	0.094	0.80	0.116	0.2	0.291
	0.1	0.1	0.099	0.2	0.192	0.2	0.076	0.64	0.191	0.2	0.185

8.5.2 LTPP Thermal Cracking Analysis

Based on the LTPP data analysis, in which it was analyzed more than 75 data points in Arizona, and more than 10 in Illinois, it was found a clear relationship between the monthly number of freeze-thaw days and the length of the thermal cracks that could appear yearly (note the less amount of the data in Illinois because the number of freeze-thaw data days is much lower than Arizona). The higher number of freeze-thaw days the higher meters per kilometer of thermal cracks. This suggest that the higher cumulative gradient of temperature in the day along the time can promote the flourishing of thermal cracks. Figure 8-6 show the relationship before announced for Arizona and Illinois respectively.

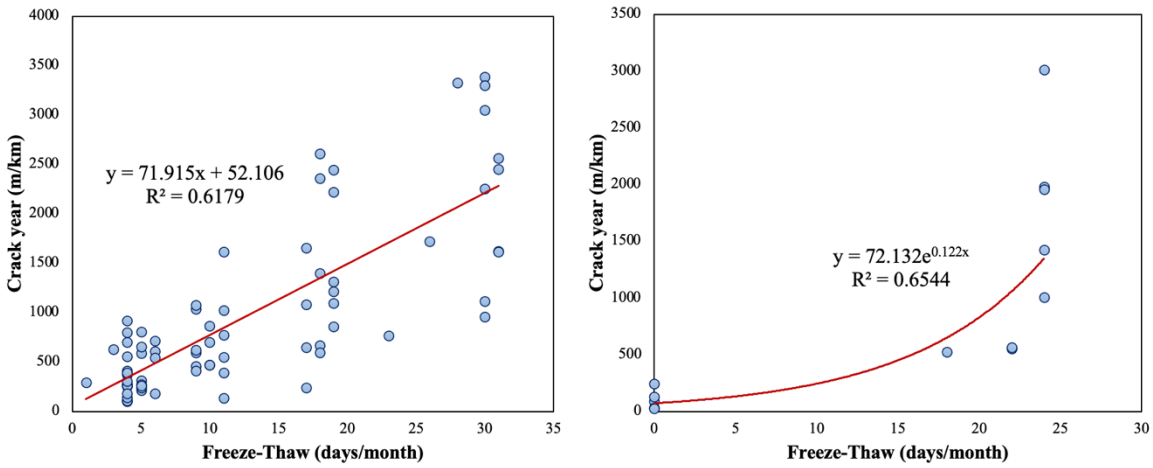

Figure 8-6. Relationship between Freeze-Thaw days and yearly cracks m/km. Left Arizona, right Illinois.

Since the thermal cracking can be promoted by the high daily gradient of temperature, a possible solution to mitigate the proliferation of thermal cracking is to consider more resilient mixtures to the temperature change.

8.5.3 Expansion-Contraction Test (EC)

From the expansion-contraction test it was possible to note that the level of strains for the modified mixtures is lower than control, which foretells lower thermal stress so then lower thermal cracking. Figure 8-7 present the development of the strains along the time when the temperature changes. Temperature fluctuation has two cycles, starting at 25ºC, going up to 55ºC, going down to -15ºC and coming back to 25ºC.

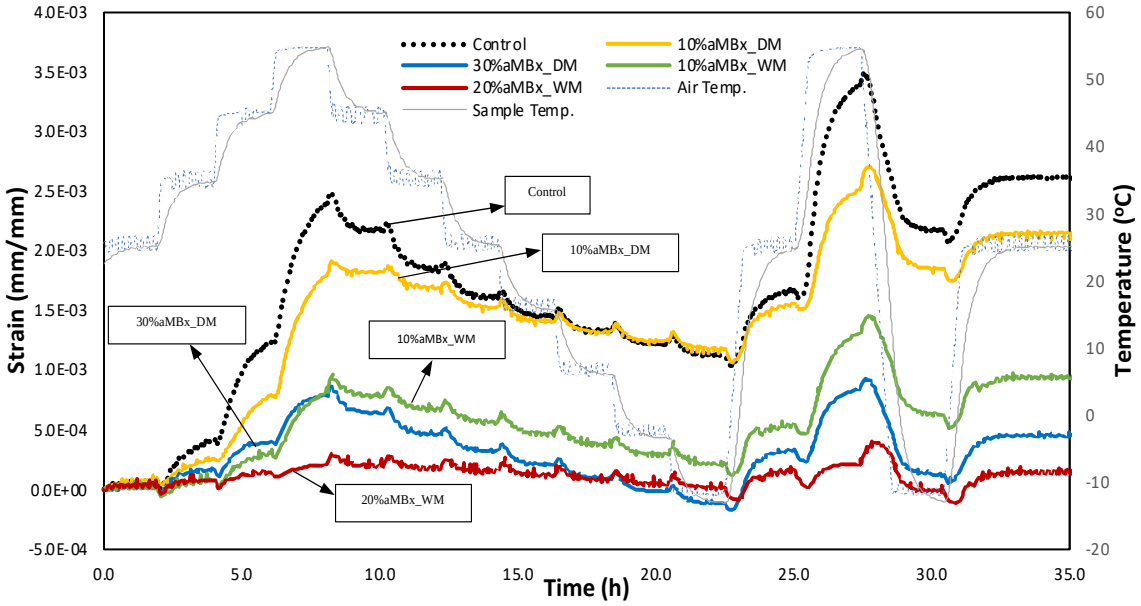

Figure 8-7. Development of thermal strains for the different mixtures.

After the inducing of expansion and contraction in the asphalt mixtures, it was observed that certain deformation remains, which is the permanent thermal induced deformation (PTID). The lower the PTID at the end of temperature cycle the more thermal resilient/less thermal susceptible the material. Table 8-7 shows the PTID for all the evaluated mixtures.

Table 8-7. PTID for all the evaluated mixtures.

Sample	PTID (mm)	COV
Control	0.238	0.137
10%aMBx_Dry	0.195	0.146
10%aMBx_Wet	0.094	0.017
20%aMBx_Wet	0.015	0.076
30%aMBx_Dry	0.055	0.242

Previous authors have reported the coefficients of expansion and contraction of asphalt mixtures. The configuration of the tests was different from one to another; however, the results are quite similar. Some studies considered samples of 100mm diameter and 50mm height. Results of α_e and α_c in a temperature range of 25ºC and 40ºC are 3.11E^{-5}/°C and 2.56E^{-5}/°C respectively (Islam & Tarefder, 2015). Other studies used beams (50mm x 50mm x 390mm) and cylinders (100mm in diameter x 150mm in height) in a temperature range of 0–60ºC. These studies reported α_e and α_c in a range of 2.064-6.321E^{-5}/°C and 2.046-6.121E^{-5}/°C respectively (Mamlouk, Witczak, Kaloush, & Hasan, 2005).

Table 8-8. Average coefficients of thermal expansion-contraction for 30%aMBx_DM mixture.

Temp C	Strain*10^{-5} (mm/mm)	Heating/Cooling	30%aMBx_DM		
	ΔL/L		△T (ºC)	△L/L (mm/mm) *10^{-5}	α 10^{-5}/°C
24.90	1.55	Heating			
34.68	15.73		9.78	14.18	1.449803
44.49	38.36		9.81	22.63	2.305695
54.60	77.96		10.11	39.60	3.916488
45.18	63.95	Cooling	-9.42	-14.01	1.487239
35.27	46.47		-9.91	-17.48	1.763078
25.31	32.60		-9.96	-13.87	1.393027
15.44	24.15		-9.87	-8.45	0.855896
5.65	13.08		-9.79	-11.07	1.130999
-4.67	2.89		-10.32	-10.19	0.987574
-13.05	-11.67		-8.38	-14.56	1.738447

Outcomes showed that α_e and α_c vary depending on the temperature of the evaluation. Table 8-8 present the results of α_e and α_c for 30%aMBx_DM mixture considering different ranges of temperature. Coefficient of thermal expansion has higher values as the temperate range of evaluation increases. Coefficient of thermal contraction tends to be higher as lower the temperature of evaluation is. Table 8-9 shows α_e and α_c for temperatures between 25°C and 35°C following the proposed method. Results at this range of temperature are like previous reports (Mamlouk, Witczak, Kaloush, & Hasan, 2005) (Islam & Tarefder, 2014), then in consistency, thermal coefficient in this study were taken in the temperature range 25°C – 35°C.

Table 8-9. Coefficients of thermal expansion-contraction for the mixtures.

Mixture Type	Coefficient of Thermal Expansion $\alpha_e 10^{-5}$/°C	Standard Deviation	Standard Error	COV	Coefficient of Thermal Contraction α_c 10^{-5}/°C	Standard Deviation	Standard Error	COV	Coefficient of Thermal Expansion-Contraction α_{ec} 10^{-5}/°C
Control	3.486	0.355	0.205	0.102	2.449	0.228	0.132	0.093	2.967
10%aMBx_DM	1.831	0.198	0.114	0.108	1.640	0.228	0.132	0.139	1.735
10%aMBx_WM	1.455	0.191	0.110	0.131	1.105	0.138	0.080	0.125	1.280
20%aMBx_WM	0.403	0.229	0.132	0.569	0.226	0.056	0.032	0.248	0.314
30%aMBx_DM	1.450	0.388	0.224	0.267	1.393	0.238	0.138	0.171	1.421

Tables 8-7 and 8-9 shows that all mixtures modified with aMBx have lower PTID and α_e and α_c. However, the thermal resilience of the 20%aMBx_WM is remarkable better than the others. The effect of aMBx in the asphalt mixtures is less thermally susceptible asphalt materials.

8.5.4 Pavement's Thermal Profile and Stresses Model

First: the temperatures profile was calculated as per the procedure previously explained in this study. Table 8-10 shows the results of the modeling and the in-field temperature readings for Winter and Summer seasons at the specified depths.

Table 8-10. Winter and Summer Field vs. Model Temperature Readings.

Considerations			Max (day) Temperature (°C)				Min (night) Temperature (°C)				Gradients (°C)			
			Up		Down		Up		Down		Up		Down	
			Field	Model	Field	Model	Field	Model	Field	Model	Field	Model	Field	Model
Winter	**Thin**	Control	28.50	27.81	25.50	23.65	3.50	3.32	5.50	5.56	25.00	24.49	20.00	18.09
		10% aMBx	28.50	27.90	24.00	23.58	3.00	3.03	5.50	5.38	25.50	24.87	18.50	18.20
		30% aMBx	26.00	27.03	20.50	22.59	3.50	3.19	6.00	5.72	22.50	23.84	14.00	16.86
	Thick	Control	28.50	27.42	19.00	19.34	4.00	3.73	8.50	8.46	24.50	23.70	10.50	10.88
		10% aMBx	28.50	27.47	19.00	18.84	3.50	3.59	9.00	8.63	25.00	23.88	10.00	10.20
		30% aMBx	26.00	26.82	18.00	17.45	4.00	3.90	9.50	9.49	22.00	22.92	8.50	7.96
Summer	**Thin**	Control	70.50	68.43	65.50	62.44	24.00	29.31	26.50	32.74	46.50	39.12	39.00	29.70
		10% aMBx	70.50	68.76	65.50	62.52	24.00	28.99	26.50	32.60	46.50	39.77	39.00	29.92
		30% aMBx	66.50	67.98	55.50	61.46	26.00	29.50	28.50	33.45	40.50	38.48	27.00	28.01
	Thick	Control	69.00	67.74	54.50	55.58	24.50	30.07	31.50	37.14	44.50	37.67	23.00	18.44
		10% aMBx	69.00	67.90	54.50	55.01	24.50	30.01	31.50	37.61	44.50	37.89	23.00	17.41
		30% aMBx	66.00	67.22	51.00	53.20	26.50	30.81	32.50	39.29	39.50	36.41	18.50	13.90

Notes: For both, thin and thick scenarios "Up" sensor location corresponds to 1.27cm below the surface of the pavement
For thin scenario, "Down" sensor location corresponds to 5cm below the surface of the pavement
For thick scenario, "Down" sensor location corresponds to 10cm below the surface of the pavement

To determine the accuracy of the model, it was used an ANOVA single factor analysis using Microsoft Excel. The adopted level of significance (α) was 0.05, and the P-value obtained from the statistical analysis was 0.77. This result shows that the difference between the measured and the predicted pavement temperatures are not statistically significant. Figure 8-8 presents a comparison between the actual and the predicted

pavement temperatures. The average standard error and standard deviation between the actual values and the predicted ones using the model is 1.05°C and 1.5°C respectively. The R^2 of the linear regression is 0.98 denotating the high accuracy of the proposed thermal model.

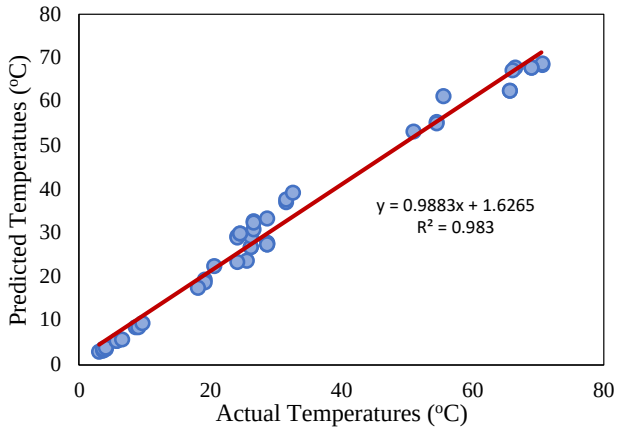

Figure 8-8. Actual vs. Predicted Pavement Temperatures.

Second: Once the temperature profile has been obtained. The thermal profile can be estimated following the process before explained. In this case the coefficient of thermal contraction and the results of the Dynamic Modulus are inputted in the model. Stresses were estimated for Winter and Summer in Phoenix, AZ. Figures 8-9, 8-10, 8-11 and 8-12 show the results of the thermal stresses profiles for day-time and night-time each 1.27cm starting from the pavement's surface, for both, thin (7.5cm) and thick (15cm) pavement structures considered.

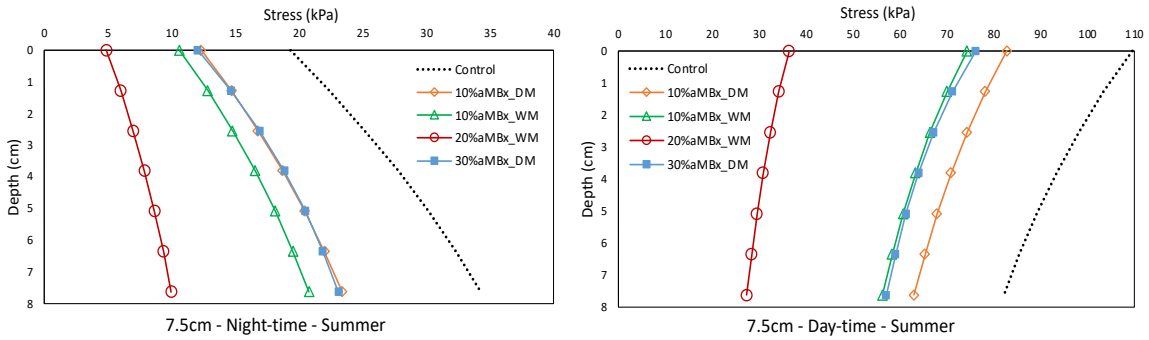

Figure 8-9. Evolution of Thermal Stresses for thin (7.5cm) Pavements – Summer.

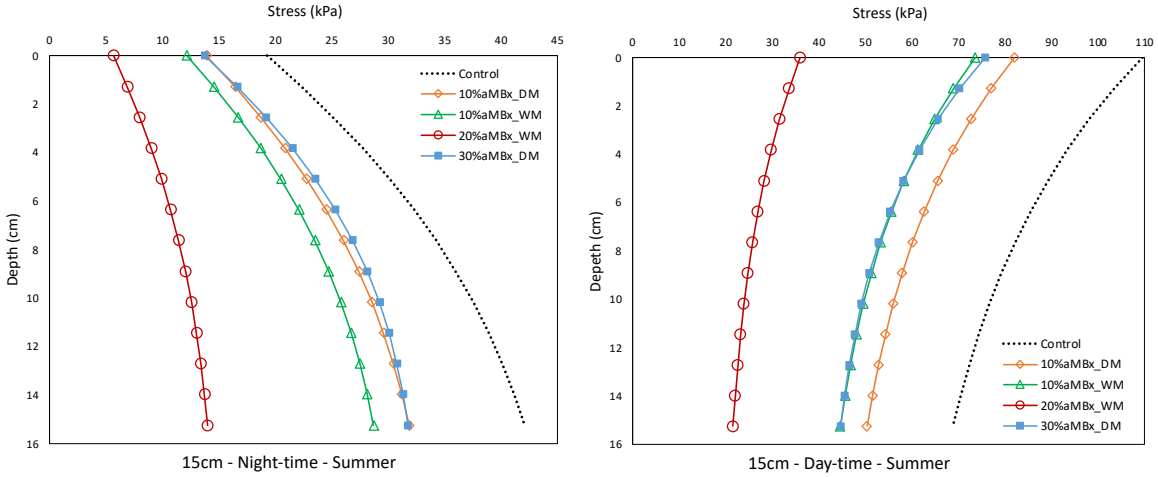

Figure 8-10. Evolution of Thermal Stresses for thick (15cm) Pavements – Summer.

Based on Figures 8-9 and 8-10, model's results in Summer of all considered thin (7.5cm) and thick pavements (15cm) show that during day-time, the maximum thermal stress occurs at the surface of the pavement and decreases as it goes deeper into the pavement structure. In the night-time, it is the opposite. The maximum thermal stress is found in the bottom and decreases as it goes up in the pavements structure. These differences are associated to the heating and cooling processes. During the day, the heating process starts at the top of the structure where the ambient temperature directly interacts

with the pavement, then the eventual temperature is the maximum at the top of the pavement.

In the night-time, the heat is released. The heat in the bottom of the structure needs more time to be freed because the distance to reach the exterior is longer from the bottom of the structure, so then, the bottom is warm for more time, therefore, the stresses are due to tension forces (i.e., hot asphalt mixtures expanse).

It is noted slightly higher stresses in thick pavement structures which could be associated to the bigger mass. Remarkably, day-time and night-time thermal stresses are the lowest for 20%aMBx_WM mixtures, and the highest for control. The other three mixtures, with very similar responses, present stresses between control and 20%aMBx_WM.

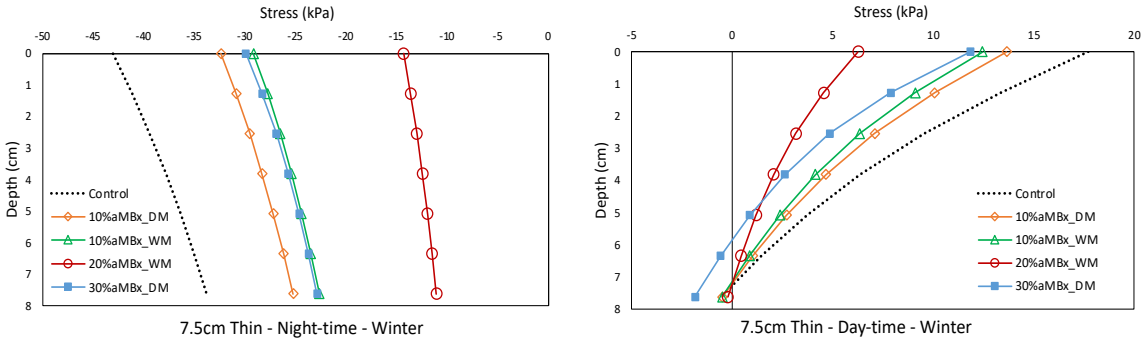

Figure 8-11. Evolution of Thermal Stresses for thin (7.5cm) Pavements – Winter.

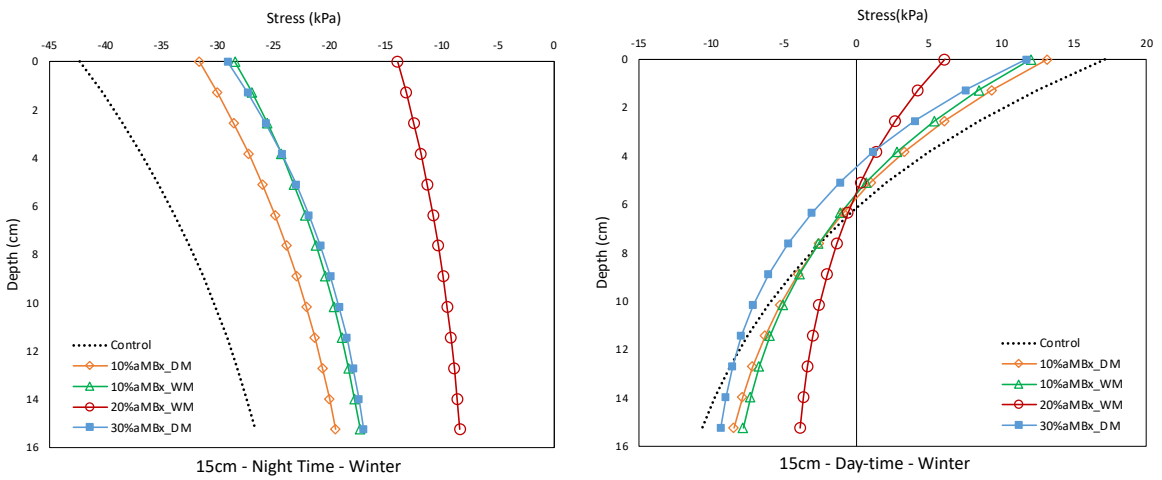

Figure 8-12. Evolution of Thermal Stresses for thin (15cm) Pavements - Winter.

In Winter, thermal stresses work in different way. Not only tension forces appear but also compression. According to Figures 8-11 and 8-12, in the night-time the entire pavement structure, for both, thin and thick pavement, suffers compression thermal stresses because of the absence of external heat. Stresses are higher at the surface of the pavement and decrease as it goes deeper in the structure.

In the day-time, thermal stresses are also higher at the surface of thin an thick pavements, but at this case the force in the surface is tension and decreases as it gets deeper. Indeed, in the day-time, the upper portion of the pavement tends to experience tension forces, however, there is a certain depth at which the forces remain in compression. For thin pavements, the amount of heat provided in day-time is almost enough to heat up the whole structure. Just a little portion in the bottom of the pavement is not warm enough, therefore, compression forces are experienced by the structure. In thick pavements, the bottom half of the structure remain cold, so only the top half part of the structure experiences tension (during the day) and compression (during the night) forces. According

to the analysis, in both structures' configuration, thin and thick, the top 7cm of the pavement is critical to consider thermal stresses. It is in this top zone, where the higher stresses, tension and compression are found, and where tension and compression forces happen in one day.

Tension and compression thermal stresses are the highest for control and the lowest for 20%aMBx_WM. The other three type of mixes, with very similar responses, show stresses between control and 20%aMBx_WM. Materials with lower SHC capacity (control) will store less heat, then will cool down faster. But when the structure gets cold in the bottom (experiencing compression forces), the upper surface has gotten warm again (facing tension forces). It is why control mixtures experiences higher changes in tension and compression forces than the other mixtures considered in this study. In mixtures with higher SHC (aMBx modified), it takes more time to release heat because they have higher heat storage, so then, the bottom is warmer, and the compression forces in the bottom are lower. This explains, why mixtures with aMBx, experience lower compression effects during day-time than control.

The stresses are associated to the presence of heat. When the asphalt mixture is warm tends to expand generating tension forces, otherwise, when the mixture is cold tends to contract, generating compression forces. It is to consider also, that in this case, mixtures with higher SHC have lower TC. This means that the heat transfer, from hot to cold and vice versa, happens at lower pace. The aMBx modified mixtures are less thermally susceptible than control. The change from cold to hot and vice versa happens in a smoother way, therefore, trauma associated with temperature changes is lower.

In this context, the analysis of thermal stresses could be classified as a good thermal potential indicator. Thermal stresses analysis matches with the previous one about the number of freeze-thaw days per month (i.e., air temperature goes from less than 0°C, contraction, to greater than 0°C, tension, in the same day). The region where the freeze-thaw day per month is high, is the region where the thermal cracking could flourish in particular if the mixture is not wisely chosen.

As the highest thermal stresses are found at the surface of the pavement, Figures 8-13 and 8-14 shows the evolution of thermal stresses along 1.5 days at the top of pavement's structure. In these graphs also is presented the change of temperature, which is very similar for all the mixtures considered in this study. Based on the plots, one can see that Control mixture is very temperature susceptible. Control's thermal stresses narrowly follows the change of the pavement surface temperature, which responds directly to the air-temperature change. While 20%aMBx_WM mixture is far from it. According to the expansion-contraction experiment, 20%aMBx_WM is the lowest thermal susceptible mixture, so then, it is facing the lowest thermal stresses.

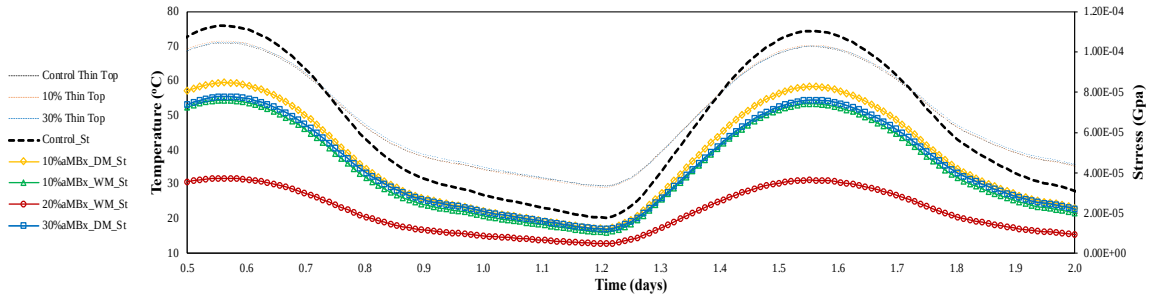

Figure 8-13. Surface thermal stresses evolution for thin (7.5cm) Pavements – Summer.

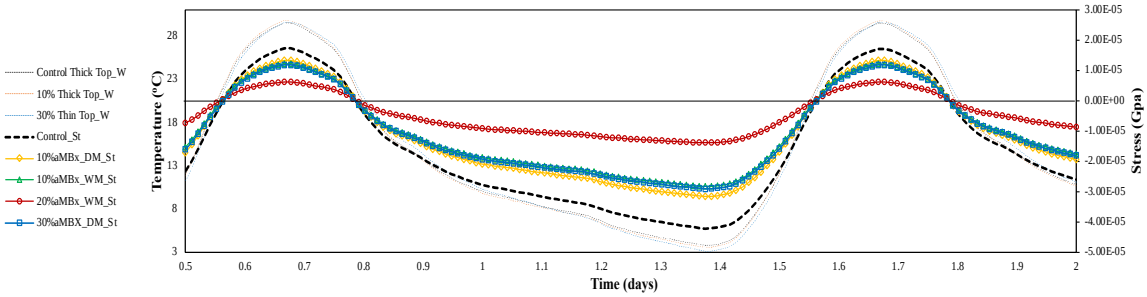

Figure 8-14. Surface thermal stresses evolution for thick (15cm) Pavements – Winter.

8.6 Conclusions

The expansion-contraction test showed that the level of strains for mixtures with lower thermal conductivity is also lower. This foretells lower thermal stresses so then lower thermal cracking. All mixtures modified with aMBx have lower α_e and α_c and vary depending on the temperature of the evaluation. Also, after inducing the thermal deformation of an asphalt mixture, it was observed that certain deformation remains, this is the permanent thermal induced deformation (PTID). The lower the PTID at the end of temperature cycle, the more thermal resilient/less thermal susceptible the material. The thermal resilience of the 20%aMBx_WM mixture is remarkably better than the others.

From the comparison between the in-field pavement's temperature data and the proposed thermal model's outcomes, a high accuracy in the model was found, then, the thermal stresses calculation is reliable.

Thermal stresses can be understood as tension and compression phenomena and are associated to the presence of heat. Thermal stresses are the highest for control and the lowest for 20%aMBx_WM mixture. The other three type of mixes, with very similar responses, show stresses between control and 20%aMBx_WM. Materials with lower SHC

capacity (control) will store less heat, then would cool down faster. But when the structure gets cold in the bottom (experiencing compression forces), the upper surface has gotten warm again (facing tension forces). It is why control mixtures experiences higher changes in tension and compression forces than the other mixtures considered in this study. In mixtures with higher SHC (aMBx modified), it takes more time to release heat because they have higher heat storage, so then, the bottom stays warmer, and the compression forces in the bottom are lower. This explains, why mixtures with aMBx experience lower compression effects during day-time than control.

In this study, mixtures with higher SHC have lower TC. This means that the heat transfer, from hot to cold and vice versa, happens at lower pace, making the aMBx modified mixtures less thermal susceptible than control. The change from cold to hot and vice versa happens in a smoother way, therefore, trauma associated with temperature changes is less.

The highest thermal stresses are found at the surface of the pavement, however, there is a critical thermal stress zone up to 7 cm below the pavement's surface. In this zone, the pavement is prone to suffer tension and contraction forces in the same day. Results are supported by the LTPP data analysis. Thermal stresses results match with the analysis of the number of freeze-thaw days per month (i.e., air temperature goes from less than 0^{o}C, contraction, to greater than 0^{o}C, tension, in the same day). Then, a clear relationship between the monthly number of freeze-thaw days and the length of the thermal cracks was found in this study. The higher number of freeze-thaw days the higher meters per kilometer of thermal cracks. The estimation and analysis of thermal stresses can be catalogued as a good thermal cracking potential indicator.

A comparison between the evolution of thermal stresses along 1.5 days at the top of pavement's structure and the change of temperature, showed that mixtures with higher TC and expansion and contraction coefficient is very temperature susceptible. Thermal stresses of this mixtures narrowly follow the change of the pavement surface temperature, which responses directly to the air-temperature change. Mixtures with lower thermal coefficient and TC, experience well far stresses from the air-temperature, then, these mixtures are less thermal susceptible.

Since the thermal cracking can be promoted by the high daily gradient of temperature, a solution to mitigate the proliferation of thermal cracking is to consider mixtures more resilient to temperature change. The geographical regions where the freeze-thaw days per month is high, are the ones where the thermal cracking could flourish mostly if the proper mixture is not chosen. Therefore, the process of a mixture design not only has to consider mechanical aspects, but also the thermal properties of the mixture. To overcome or mitigate the proliferation of thermal cracking and then make longer lasting pavements, it must be considered in the mixture design, properties such as low thermal conductivity, high specific heat capacity and low thermal expansion and contraction coefficients.

CHAPTER 9

PORTRAYAL AND DURABILITY ASSESSMENT OF NOVEL SILICA-BASED MODIFIED ASPHALT PAVEMENTS

9.1 Introduction

Although pavements are robust structures capable of supporting large traffic loading and the inclement weather, high temperature differences and traffic during the year extensively affect paved roads. As a result of the external solicitations, different pavement distresses like cracking and permanent deformation appear. The propagation of cracks produces significant damage to the integrity of the pavement and generates pathways for the intrusion of water into the granular layers and subgrade as well, whereas permanent deformation causes safety issues. Cracking and deformation can make shorter the lasting of the pavement and increase the maintenance costs. Therefore, one of the biggest problems that asphalt pavement must overcome is its thermal susceptibility.

The usage of modifiers in asphalt binders has been one of the most common methodologies to overcome actual necessities and thus improve the performance of asphalt mixtures (Gordon, Rheolgical evaluation of ethylene vinyl acetate polymer modified bitumens., 2002). Some of the most known modifications has been the usage of polymers and crumb rubber, which predominantly have improved the temperature susceptibility of bitumen by increasing stiffness at high temperatures and reducing the probability of cracking at low temperatures (Collins, et al., 1991) (Bruton, 2020), however, the low

ageing resistance, poor storage stability of polymer modified bitumen (PMB), and high cost are some obstacles that limit the progress of bitumen polymer modification (Zhu, et al., 2014), whereas the implementation of rubber in asphalt mixtures has some downsides such as recyclability, binder storage stability, the fumes that it releases through the paving process, and workability (Kuennen, 2004). Although these technologies have been developed to make longer lasting asphalt pavements, have not shown remarkable responses to overcome cost problems in their implementation. Therefore, new research on the implementation of new materials is still needed to address, better understand, and improve the durability of asphalt pavement (Hinislioglu, 2011).

Thermal cracking in asphalt pavement can be promoted by the high daily gradient of temperature, and the permanent deformation is boost by the exposition at high temperatures. As a possible solution to mitigate the proliferation of thermal cracking and rutting, the implementation of more resilient mixtures to temperature changes is very important. In this study, an innovative composite called aMBx is introduce. Three different percentages (10%, 20%, and 30%) by bitumen weight, and two different methods to include the composite in the mixture, wet and dry, were implemented. aMBx is a synthetic porous light silica-based material developed in the Advanced Pavement Laboratory at Arizona State University currently with a patent application in the United States Patent and Trademark Office: serial number 63/210,891 filed on June 15, 2021.

Characterization of the aMBx-modified mixtures was done through tests such as dynamic modulus (E*), semicircular bending (SCB), moisture susceptibility (TSR), Hamburg wheel (HW), cyclic uniaxial fatigue (CUF). Thermal conductivity (TC), specific heat capacity (SHC), and the coefficient of thermal contraction (α_c) data taken from Tables

8-3, 8-4, and 8-9 respectively, plus a shear dynamic modulus test results in asphalt binders (G*) were used to do a pavement performance prediction using the AASHTOWare Pavement ME analysis. Performance assessment considered cold and hot climates for thin (75mm) and thick (150mm) pavements.

The AASHTOWare Pavement Design Guide is a pavement design methodology based on engineering mechanics and has been validated with extensive road test performance data. It is based on both mechanistic and empirical designs and represents a major change from the typical pavement design methods used nowadays. As it has been developed in the NCHRP Project 1-37A, it is able to predict the major distresses such as permanent deformation, fatigue, thermal cracking, and roughness in terms of International Roughness Index (IRI). For a given traffic, climate, pavement structure and pavement design life, the results of the AASHTOWare Pavement ME give valuable insight on the pavement performance over the lifespan of the pavement. The outputs will help in assessing the quality of the modification introduced into the mixture, and if the pavement performance will be improved over time. The software has 3 levels of analysis, Level 1 (requiring lab testing and has the best accuracy), Level 2 (requires some lab tests and is accurate) and Level 3 (uses default values and is the least accurate). The results gave an indication of how well the modified asphalt mixture respond to thermal cracking and rutting down different conditions.

9.2 Methods and Materials

Description and/or information of the modifying Material (aMBx composite), asphalt binder type, and aggregates, and mixture design are described in Chapter 6. Composite material was used to modify the HMA pavements in three different contents: 10%, 20% and 30% by weight of the asphalt binder.

In this Chapter, the two different approaches to include aMBx into the mixture were considered, dry method (DM) and wet method (WM). Control (0%), 10%aMBx (DM), 10%aMBx (WM), 20%aMBx (WM), and 30%aMBx (DM) modified asphalt mixtures were included. The variety of mixtures is to consider different material's properties and then responses. Viscosity of binders increases using 30%aMBx making the mixing process difficult, then, instead of 30%WM, 20%WM was implemented. The optimum binder content is based on the aggregates weight.

9.2.1 Laboratory Characterization and Testing

Samples of each type of mixture were made in the laboratory following AASHTO R 30 using a Superpave Gyratory Compactor (SGC) until to reach 180mm (7") high. All experiments were carried out at the Advance Pavement Laboratory and at The National Center of Excellence for SMART Innovations at Arizona State University (ASU).

9.2.1.1 Semi-Circular Bend Test (SCB) with Crack Mouth Opening Displacement (CMOD)

This test evaluates the Asphalt Mixture Cracking Resistance. The SCB test procedure developed at the University of Illinois (IL-SCB) was implemented in this study. To ensure a constant strain rate on specimens, a closed-loop computer-controlled fracture test setting was implemented. The asphalt mixtures were tested at -10°C and 10°C using an UTM system, endowed with an environmental chamber to carry out experiments at specific temperatures. The experiment was conducted based on a controlled displacement using a crack month opening displacement (CMOD) signal to provide a constant displacement rate on samples, in this case 0.7mm/min. An extensometer attached on the bottom of the SCB specimen by means of two metal buttons glued on the specimen was used to attach the CMOD. The two extensometers have a range of -1mm and 1mm. Specimens are 50mm thick and 150mm diameter cut in semicircular halves. These samples were obtained from the center part of a Superpave gyratory compacted (SGC) specimens. Each of the two middles slices has a vertical edge notch of 15mm and about 2mm width. The specimen is loaded at the top and supported symmetrically at the bottom. Two rollers support the SCB specimen to minimize the friction in the contact area at the bottom of specimen. The spacing between the two supports is 120mm. Figure 9-1 shows the set-up of the experiment.

Figure 9-1. IL-SCB with CMOD Test Setup.

Additional tests were done according to the corresponding standards, as follow:

9.2.1.2 Dynamic Complex Modulus |E*|, (AASHTO T 342-11)

This test provides valuable information about the viscoelastic properties of asphalt mixtures. Cylindrical specimens of 100mm in diameter and 150mm in height were used. Previous the test, samples were instrumented with three linear variable displacement transducers (LVDTs) spaced at 120° intervals on the specimen's surface. Temperatures of -10, 4.4, 21.1, 37.8, and 54.4°C, with frequencies of 25, 10, 5, 1, 0.5, and 0.1 Hz were utilized. Before testing, lubricated membranes were placed between the loading platens and the sample to reduce any end effects.

9.2.1.3 Flow Number (FN), Repeated Load Permanent Deformation, (AASHTO T 378)

Test was executed using cylindrical specimens of 100mm in diameter and 150mm in height. The test was performed under an axial stress level of 160kPa, at 50°C and at atmospheric conditions. The deformations were measured using the average of three linear variable displacement transducers (LVDTs) spaced at 120° intervals on the specimen's surface. Before the test, thin membranes were placed between the sample and the loading platens to avoid friction and prevent end effects.

9.2.1.4 Moisture Susceptibility (TSR), (ASTM D4867/D4867M)

Evaluation of the effects of saturation and accelerated water conditioning, with a freeze-thaw cycle, of compacted asphalt mixtures. Two sets of HMA samples are subjected to a split tensile test (often called an indirect tensile" test) at 25°C. Prior, one set (3 samples for each type of mixture) is conditioned by partial vacuum saturation with water, with the freeze-thaw cycle at -18°C for 16 hours and soaking in water at 60°C for 24 hours. The other set is used as a control with no conditioning. The ratio of the average split tensile strength of the conditioned samples over the average split tensile strength of the unconditioned (control) samples is reported as the tensile strength ratio (TSR).

9.2.1.5 Hamburg Wheel-Track Testing (HW), (AASHTO T 324-11)

This test evaluates the rutting and moisture-susceptibility of hot mix asphalt (HMA) pavement samples using a Hamburg Wheel-Tracking Machine. The wheel shall make

approximately 50 passes across the specimen per minute. The maximum speed of the wheel shall be approximately 0.305 m/s (1 ft/sec) and will be reached at the midpoint of the specimen. Size of the HMA samples compacted by a SGC is 150mm diameter and 60mm thick. The specimens were submerged in a temperature-controlled water bath at 50ºC (122ºF). The deformation of the specimen, caused by the wheel loading, is measured along 20,000 passes (wheel-tracking device shall shut off).

9.2.1.6 Cycling Uniaxial Fatigue (CUF), (AASHTO TP 107)

This test determines the damage characteristic curve via direct tension cyclic fatigue tests. The results of the test help to predict the fatigue life of asphalt concrete. Differing from the test protocol, size of the samples was 75mm in diameter and 100mm in height. Axial fatigue tests were performed in controlled actuator displacement mode at a temperature of 10°C and at a 10Hz frequency. A repeating sinusoidal deformation occurs along the axis of a cylindrical test specimen until it failed.

9.2.1.7 Complex Shear Modulus |G*|, (AASHTO T 315-12)

This test was used for the determination of the rheological properties of asphalt binder using a Dynamic Shear Rheometer (DSR). Neat binder PG-64-16 tested in 10 different frequencies from 0.1 to 100 rad/sec, and 6 temperatures from 64ºC to 96ºC were used. The specimen size and plate diameter were 2mm (0.08 inches) thick and 25 mm (1 inch) in diameter respectively. Normally, the sample for this test is 1mm thick, however, because the presence of aMBx particles it was decided to increase the thickness up to 2mm

to avoid bias results due to friction. Particles of aMBx were selected to be lower than 2mm in diameter. Control (0% aMBx), 10%aMBx, 20%aMBx, and 30%aMBx were included in the test.

9.2.1.8 AASHTOWare Pavement ME Analysis

The AASHTOWare Pavement ME is a mechanistic-empirical approach that has been recently improved in the pavement industry. It uses various input parameters, such as the dynamic modulus of the asphalt binder and mixture, as well as multiple mix design parameters. The generated results of this software are the distresses prediction over time. Such predictions can help designers and pavement engineers to have a knowledge of how their designed pavements would perform over years.

In this study, Level 1 was used for permanent deformation and fatigue, where the dynamic modulus of the binder (G*), mixture (E*), target air void and effective binder content parameters are needed. For the thermal behavior, level 2 analysis was used as the thermal parameters (coefficient of thermal contraction, specific heat capacity and thermal conductivity), are determined throughout the study.

To run the AASHTOWare Pavement ME and compare the results obtained, a typical scenario was set having a common subgrade and traffic level for all designs, with different asphalt layer thicknesses and climatic conditions. The different parameters used are found in Table 9-1. Two different climatic regions were analyzed: Phoenix and Chicago. These regions are different in climate throughout the years and will help in

depicting the effect of aMBx on the distresses for both hot and cold climates. The pavement structure considered consists of the asphalt layer on top of subgrade.

Table 9-1. AASHTOWare Pavement ME Input Parameters.

Asphalt Layer Thickness (mm - inches)	Traffic (AADTT)	Subgrade Type
75mm - 3” (thin)	2000	A-1-a
150mm - 6” (thick)	2000	A-1-a

Those input parameters were used for the different mix designs (with and without aMBx) according to the wet and dry mixing methods.

9.3 Results and Discussion

9.3.1 Semi-Circular Bend Test (SCB) with Crack Mouth Opening Displacement (CMOD)

SCB test showed that mixtures modified with aMBx using the wet method (WM) would have similar performance at low temperatures (-10^{o}C) and moderate low temperatures (10^{o}C) than control. Although, the peak load of the WM modified mixtures is almost the same as control in both scenarios, -10^{o}C and 10^{o}C, the fracture energy of control mixture is slightly higher at -10^{o}C but is lower than the WM modified mixtures at 10^{o}C. Indeed, results expose that the higher the aMBx content in the mixture it behaves stiffer and should perform better than control as the temperature increase.

On the other hand, aMBx mixtures made by the dry method (DM) present lower resistance at low temperatures than the WM ones and control. It means that the WM is a

better alternative to incorporate the aMBx into the mixture. Figures 9-2 and 9-3 present the results of the SCB test with a tabular inset into them for -10°C and 10°C respectively.

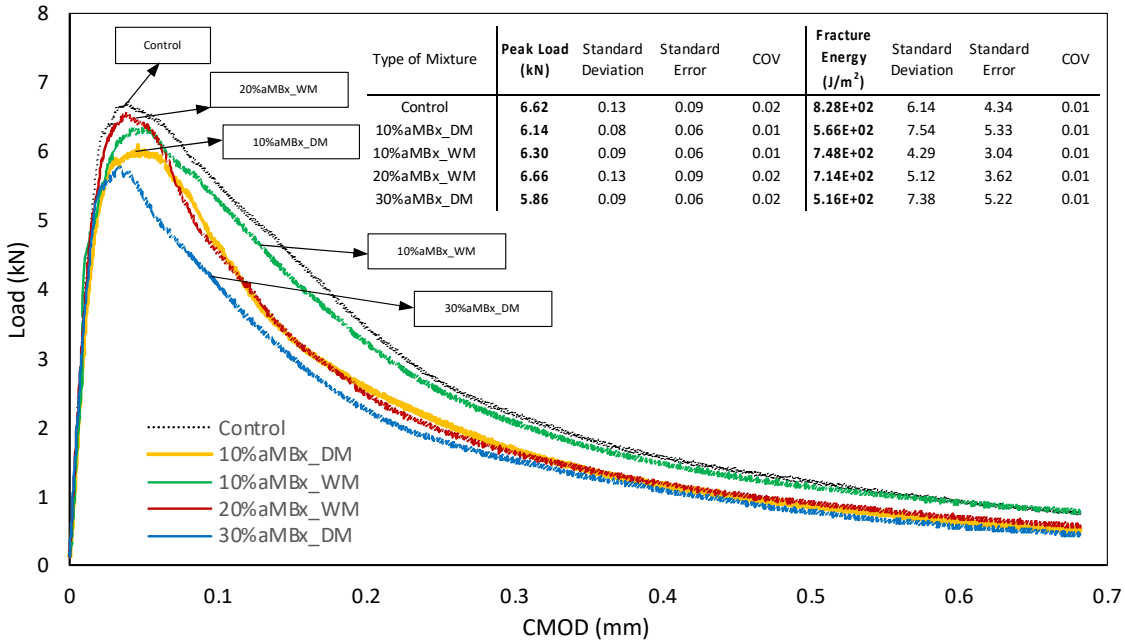

Type of Mixture	Peak Load (kN)	Standard Deviation	Standard Error	COV	Fracture Energy (J/m^2)	Standard Deviation	Standard Error	COV
Control	**6.62**	0.13	0.09	0.02	**8.28E+02**	6.14	4.34	0.01
10%aMBx_DM	**6.14**	0.08	0.06	0.01	**5.66E+02**	7.54	5.33	0.01
10%aMBx_WM	**6.30**	0.09	0.06	0.01	**7.48E+02**	4.29	3.04	0.01
20%aMBx_WM	**6.66**	0.13	0.09	0.02	**7.14E+02**	5.12	3.62	0.01
30%aMBx_DM	**5.86**	0.09	0.06	0.02	**5.16E+02**	7.38	5.22	0.01

Figure 9-2. SCB with CMOD test results at -10°C for all the mixtures.

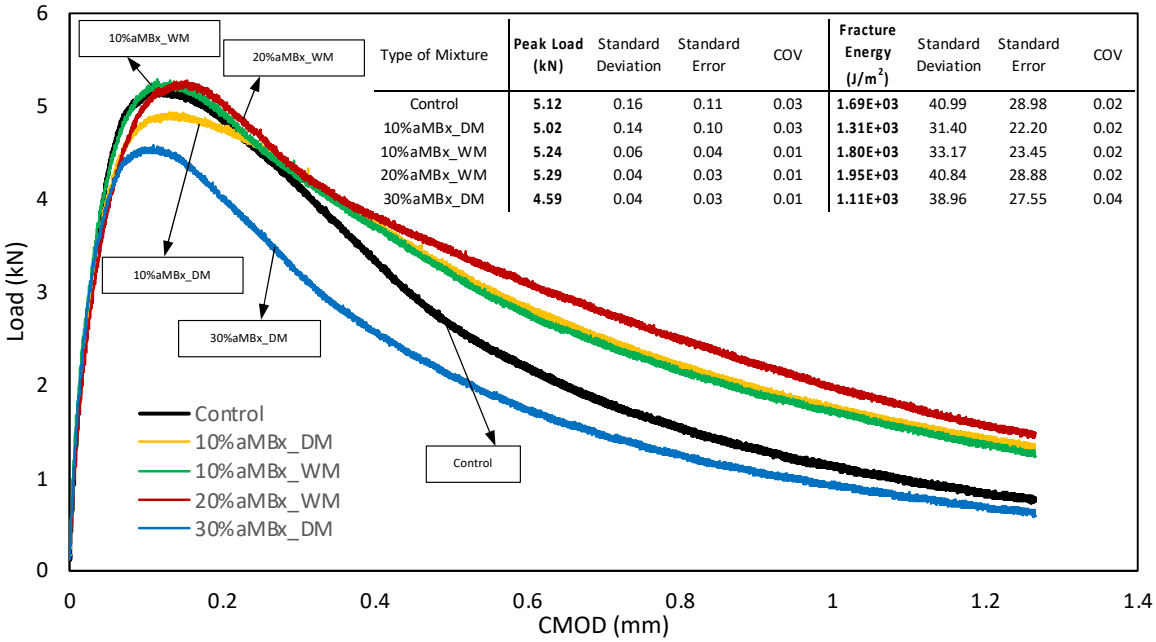

Type of Mixture	Peak Load (kN)	Standard Deviation	Standard Error	COV	Fracture Energy (J/m^2)	Standard Deviation	Standard Error	COV
Control	**5.12**	0.16	0.11	0.03	**1.69E+03**	40.99	28.98	0.02
10%aMBx_DM	**5.02**	0.14	0.10	0.03	**1.31E+03**	31.40	22.20	0.02
10%aMBx_WM	**5.24**	0.06	0.04	0.01	**1.80E+03**	33.17	23.45	0.02
20%aMBx_WM	**5.29**	0.04	0.03	0.01	**1.95E+03**	40.84	28.88	0.02
30%aMBx_DM	**4.59**	0.04	0.03	0.01	**1.11E+03**	38.96	27.55	0.04

Figure 9-3. SCB with CMOD test results at 10oC for all the mixtures.

9.3.2 Dynamic Complex Modulus |E|, (AASHTO T 342-11)*

The usual method to article dynamic modulus information is the master curve function. The procedure used in this study was develop in Arizona State University by Witczak. In this method a principle of time-temperature superposition is used for the construction of master curves. A factor or constant of change is applied with respect to the logarithm of the time to obtain a smoothed curve. In general, the stiffness master curve can be mathematically modeled by a sinusoidal function (Witczak, 2004). Shifting was done considering 21°C as a reference temperature. Figure 9-4 shows the master curves for each type of mixture.

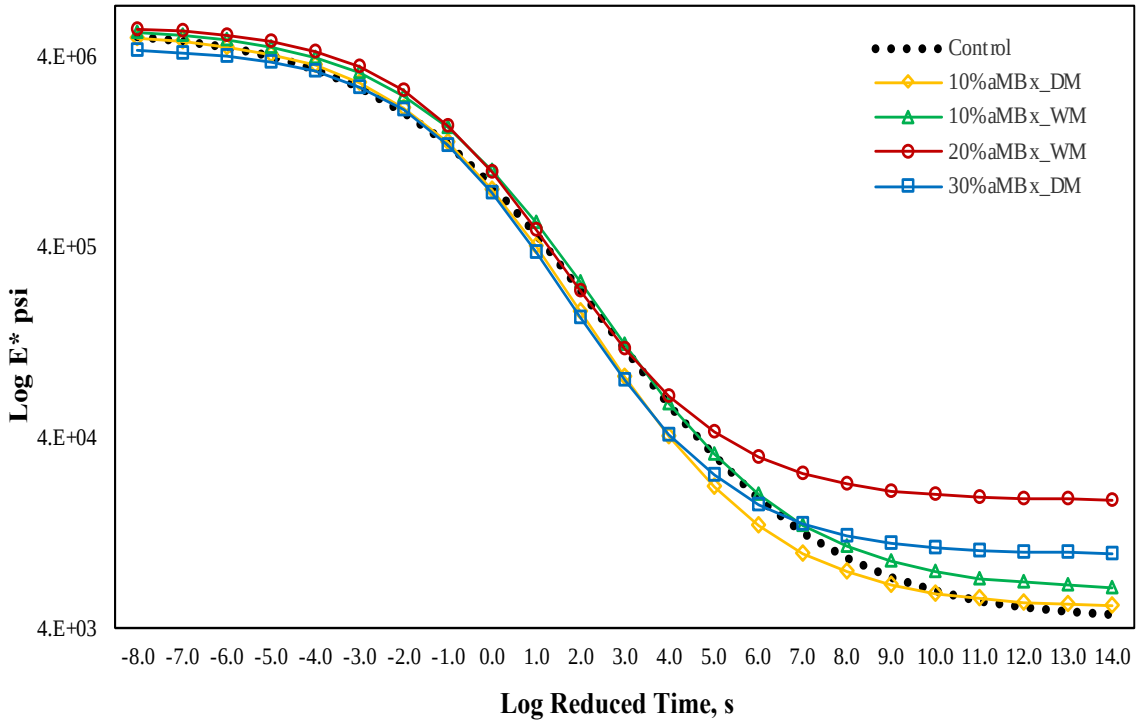

Figure 9-4. Dynamic Modulus Master Curve for the five asphalt mixtures considered.

The master curve provides a relationship between the mixture stiffness as a function of reduced frequency (or temperature). The stiffness changes from high values (low temperatures, left side) to lower values (high temperatures, right side). Accordingly, the master curve makes it possible to predict viscoelastic properties over a wide frequency range and to predict viscoelastic properties at any temperature. Analysis based on the master curves suggest that all modified mixtures with aMBx present better rutting resistance (high temperature performance), and similar fatigue resistance (low temperature performance) than control. aMBx modified mixtures present higher modulus at high temperatures and low frequency than control, this shows that the modified mixtures present a more stable behavior when facing high temperatures, which is related with lower deformation. However, the behavior of the 20%aMBx_WM mixture samples is remarkable better than the other considered mixtures confirming the WM would be the best mechanism to implement the aMBx in the mixtures. This analysis goes perfectly in tune with the FN analysis (below) and the previous SCB results.

Additionally, according to previous studies, an elastic behavior in the mix occurs when phases angles are below 5º, viscoelastic behavior with phase angles between 5º and 45º, and predominant viscous behavior with phase angles above 45º (Biligiri & Kaloush, 2008). In this framework, aMBx mixtures would have the most elastic behavior at low temperatures. Table 9-2 presents phase angle values for all types of mixtures at low (-10ºC) and high temperatures (54.4ºC).

Table 9-2. Phase angle values for all types of mixtures.

Temp. ºC	Frequency Hz	Phase Angle (δ)				
		Control	10%aMBx _DM	10%aMBx_ WM	20%aMBx _WM	30%aMBx _DM
-10.0	25	6.6700	6.3100	2.9700	3.4000	4.6100
	10	8.6900	9.2800	4.4700	4.1300	7.8700
	5	9.0100	10.4200	6.0300	5.1000	8.0900
	1	10.0600	11.7300	7.1400	5.3900	9.7300
	0.5	10.5500	11.1000	7.1200	6.4300	10.0300
	0.1	11.4900	11.9100	8.2500	8.0000	10.4200
54.4	25	36.8300	38.1100	36.2800	39.8300	36.4400
	10	37.3800	38.5300	36.0900	40.2600	37.7100
	5	37.5300	36.0700	38.0400	41.8300	36.8900
	1	33.8400	33.7800	36.7500	33.5100	36.5500
	0.5	30.8200	29.4900	34.3100	34.4800	33.3300
	0.1	25.1300	24.2300	29.5000	29.1300	25.6700

9.3.3 Flow Number (FN) Also Known as Repeated Load Permanent Deformation, (AASHTO T 378)

Flow number test values are shown in Figure 9-5 and presented as a tabular inset into it. A mixture accumulates strain at a slower rate and experiences more repetitions before reaching the onset of flow. All modified mixtures with aMBx exhibit better permanent strain response than control under the repeated loading, being the WM-aMBx mixtures the ones with better results. 10%aMBx-WM exhibits an increase in average flow number of 166% compared to control mixtures. 10%aMBx and 30%aMBx DM mixtures presented 40% and 67% increase in FN respect to control respectively. Extraordinarily, 20%aMBx-WM sample did not reach the FN under the conditions of the test (50ºC), which mean that this asphalt sample is thermal unsusceptible with a rigid behavior at 50ºC.

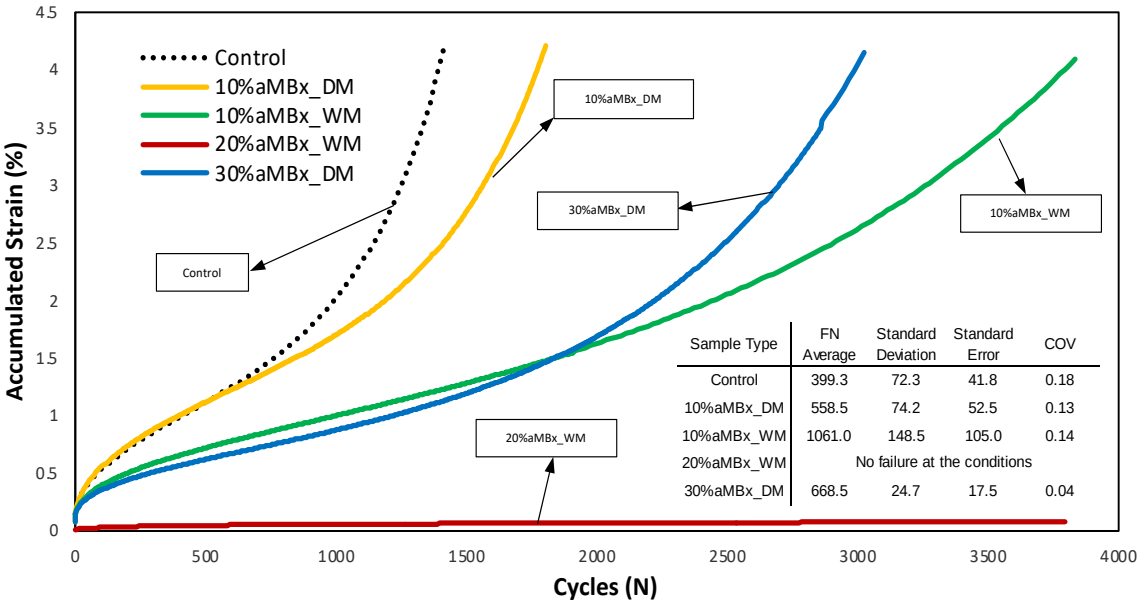

Figure 9-5. Flow Number (FN) of all asphalt mixtures considered.

9.3.4 Moisture Susceptibility (TSR), (ASTM D4867/D4867M)

The effect of water interaction between the asphalt binder-aggregate adhesion in the asphalt mixture is called moisture damage. This interaction can cause a reduction of adhesion between the asphalt binder and aggregate, called stripping, which can lead to various forms of asphalt pavement distress like fatigue cracking. Cracking potential estimation using the in indirect tensile strength test showed that the addition of aMBx up to 30% do not affect the mixture's response. Even, Table 9-3 presents a slightly increase in all aMBx-samples' response respect to control. This phenomenon is attributed to the fact that aMBx has hydrophobic properties.

Table 9-3. Effect of moisture in all asphalt concrete mixtures.

Type	ITS Dry (kN)	ITS Conditioned (kN)	TSR	St. Error	COV
Control	18.53	15.52	0.84	0.008	0.016
10%aMBx_DM	19.01	16.18	0.85	0.013	0.026
10%aMBx_WM	19.33	16.79	0.87	0.040	0.079
20%aMBx_WM	19.90	17.78	0.89	0.016	0.031
30%aMBx_DM	19.77	17.05	0.86	0.017	0.034

9.3.5 Hamburg Wheel-Track Testing (HW), (AASHTO T 324-11)

This empirical test is considered as a torture rutting test. It is used to evaluate the resistance to rutting and moisture susceptibility of asphalt mixtures. Metallic wheels are passed over asphalt mixture samples when these are submerged in water at 50^{o}C. The conditions simulate the effect of traffic (conditions of load, speed, and temperature) while the development of the rut profile is monitored at specified intervals during the test. Table 9-4 shows the results.

Table 9-4. Hamburg Wheel-Track Results.

Sample Type	Average (mm of rutting)	Standard Deviation	Standard Error	COV
Control	-4.815	0.035	0.025	-0.007
10%aMBx_DM	-3.745	0.276	0.195	-0.074
10%aMBx_WM	-3.395	0.021	0.015	-0.006
20%aMBx_WM	-0.575	0.262	0.185	-0.455
30%aMBx_DM	-3.405	0.064	0.045	-0.019

The results of HW test indicate that all samples with aMBx have better rutting behavior; again, remarkably, the 20% aMBx WM sample showed significantly better

rutting resistance than the other mixtures. These results agree very well with the stiffness test (E*) and Flow Number (FN) results.

However, despite of the 30%aMBx_DM samples presented a good permanent deformation response, after analyzing the state of the samples it was noted a higher affection in the binder-aggregates adhesion interaction than the rest of the mixtures. This phenomenon is not directly associated to a moisture effect or stripping, but to a deficiency in the bonding mechanism between binder and aggregates because the relatively high aMBx content. Then, aMBx contents above 20% would interfere in the binder-aggregates bonding mechanism. Note that these results agree with the SCB test results.

9.3.6 Cycling Uniaxial Fatigue (CUF), (AASHTO TP 107)

This test measures the durability of the pavement against cracking and in terms of load cycles. Samples were tested at 10°C. The results indicated that aMBx does not affect the fatigue cracking response of the pavement. Figure 9-6 summarizes the results.

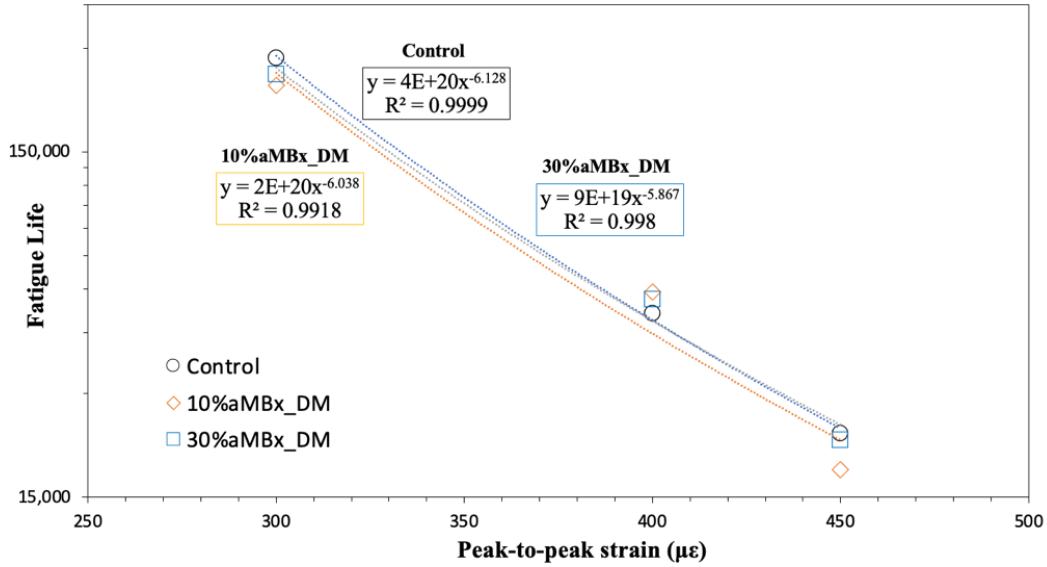

Figure 9-6. Fatigue life of all asphalt mixtures considered.

Uniaxial fatigue analysis is used to estimate the fatigue life of an element under cyclic loading when the crack is initiated due to a uniaxial state of stress.

This test does not characterize the propagation of macrocracks in asphalt mixtures, but it is important to note that aMBx does not harm the fatigue life of asphalt mixtures, but also does not enhance it at low temperatures. Then, it is not expected to improve the response of asphalt materials at low temperatures using aMBx, contrasting the response of aMBx modified mixtures and binders at medium and high temperatures, where the performance of these materials is improved. These results are consistent with the findings of the SCB test and with the Dynamic Modulus analysis presented earlier.

9.3.7 Complex Shear Modulus (G), (AASHTO T 315-12)*

The master curve for all the binders considered in this study is shown in Figure 9-7 below. Based on the results, the slopes of the master curves are noticeably differing. In other words, the aMBx-modified binders seem to be less susceptible to the change in temperature/frequency compared to control binder. As higher the increase of aMBx content the better temperature/frequency-change response. Modified binders with aMBx would have better response/stability than control at high temperatures, and relative similar behavior at low temperatures.

Additionally, the phase angle, δ, provides a relative indication of the elastic and viscous comportment of the asphalt binder. Binders with a phase angle of 0^{o}C are completely elastic, while materials with a phase angle of 90^{o}C are completely viscous (Asphalt Institute, 2022). Table 9-5 presents phase angle values for all types of binder at moderate high (64^{o}C) and high temperatures (96^{o}C) and some of the frequencies. Test was

performed with 2mm gap. The results suggest that all aMBx modified binders have less viscous, so then more elastic behavior than control with a trend in which the higher the aMBx content the more stable binder.

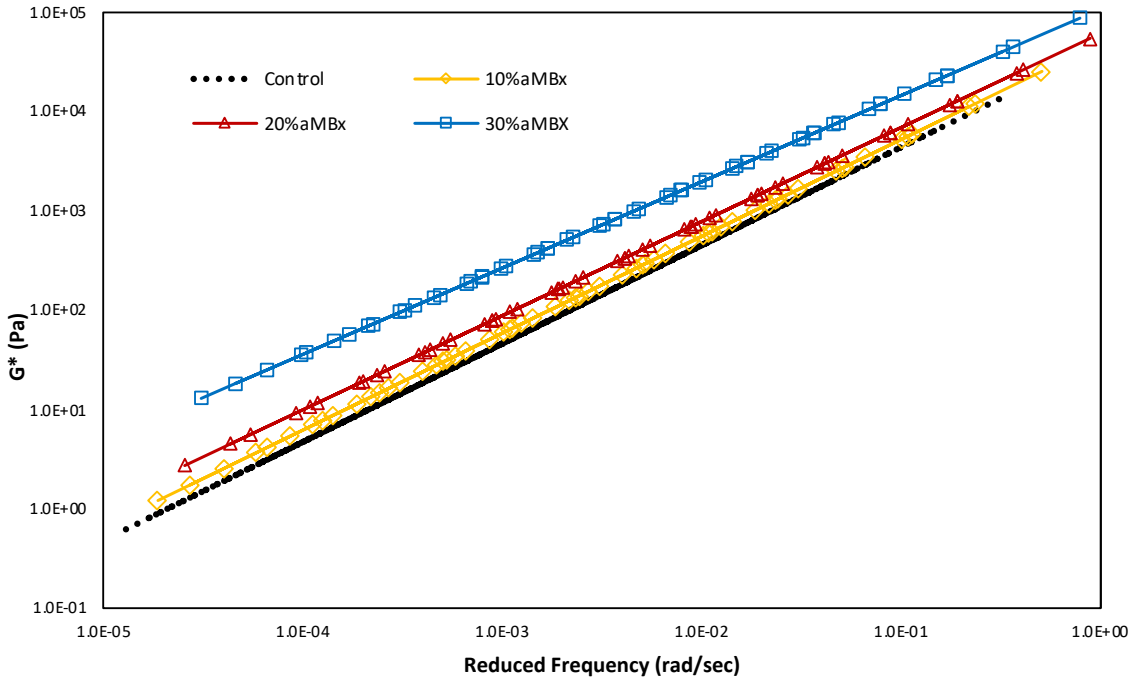

Figure 9-7. Shear Dynamic Modulus (G*) Master Curves.

Table 9-5. Phase angle values for all types of binder.

Temperature	Frequency	Control	10%aMBx	20%aMBx	30%aMBx
(°C)	(rad/sec)	Phase Angle	Phase Angle	Phase Angle	Phase Angle
64	100	83.8	82.4	78.4	76.6
64	46.4	84.9	84.0	80.2	78.6
64	0.464	89.1	88.5	86.2	82.5
64	0.215	89.3	88.7	86.5	81.1
64	0.1	88.8	88.9	85.5	79.8
96	100	90.0	87.7	89.2	85.3
96	46.4	90.0	86.6	87.3	84.2
96	0.464	86.9	82.6	86.9	72.9
96	0.215	85.0	90.0	87.5	73.0
96	0.1	90.0	84.8	82.3	68.6

9.3.8 AASHTOWare Pavement ME Results

Based on the different scenarios and input parameters discussed in the previous sections, the following results were generated in Table 9-6. The thin design refers to an asphalt layer of 75mm (3”), whereas the thick refers to the thickness of 150mm (6”).

Table 9-6. AASHTOWare Pavement ME Generated Results Summary.

Climate	Design Type	Mixture	IRI (m/Km)	Total Permanent Deformation (cm)	Fatigue (%Lane)	Thermal Cracking (m/Km)	Top-Down Fatigue (%Lane)	AC Permanent Deformation (cm)
Chicago	Thin	Control	2.77	1.37	28.18	588.92	17.23	0.28
		10%D	2.77	1.35	28.18	466.32	16.20	0.26
		10%W	2.73	1.32	28.19	385.32	15.14	0.25
		20%W	**2.30**	**1.14**	**16.31**	**59.88**	**4.69**	**0.15**
		30%D	2.60	1.35	27.12	342.26	12.12	0.24
	Thick	Control	2.61	0.89	1.66	588.92	14.19	0.15
		10%D	2.55	0.91	1.73	490.26	14.13	0.18
		10%W	2.52	0.86	1.57	412.36	14.07	0.13
		20%W	**2.21**	**0.74**	**1.46**	**47.35**	**14.28**	**0.05**
		30%D	2.37	0.91	1.72	289.47	13.88	0.16
Phoenix	Thin	Control	2.80	1.32	25.93	605.56	12.23	0.51
		10%D	2.80	1.30	26.23	578.56	12.00	0.48
		10%W	2.69	1.27	23.46	401.04	11.78	0.43
		20%W	**2.44**	**0.99**	**14.48**	**83.46**	**11.35**	**0.23**
		30%D	2.62	1.30	25.33	325.30	11.15	0.48
	Thick	Control	2.33	0.97	2.19	587.28	11.35	0.36
		10%D	2.25	1.00	2.55	424.51	11.29	0.35
		10%W	2.14	0.89	1.83	339.19	11.22	0.30
		20%W	**1.89**	**0.66**	**1.46**	**83.45**	**11.23**	**0.10**
		30%D	2.11	1.01	2.58	256.66	11.13	0.35

In terms of IRI (International Roughness Index), it is noticed that the IRI values decrease with an increase in aMBx content. However, when the wet method is implemented, the decrease is greater at 20% aMBx. The same trend appears when it comes to the other distresses. It is important to note the behavior of the aMBx modified mixtures with respect to the control one. The 30% aMBx mixture has very similar behavior to the

control in all the pavement distresses mentioned except for the thermal cracking. This trend highlights the thermal and physical benefits of adding aMBx to asphalt mixtures.

For the two different climates, a decrease in the expected permanent deformation (total and in the asphalt layer) is noted with increasing aMBx contents.

The main impact of aMBx lies on the predicted thermal cracking, where the decrease is drastic compared to control. Finally, it is important to note the effect of the method used to implement aMBx into the mixture. The dry method denotes some advancements when adding aMBx. However, the wet method (WM) has a greater improvement noted across all distresses as seen in Table 9-6 This could refer to a better distribution of aMBx within the mixture when added to the binder instead of the aggregates during the asphalt mixing process.

9.4 Conclusions

Regards to thermal properties, tests results showed that the modified mixtures with aMBx have higher value of SHC, this means that it is needed more energy to heat this type of material but also, more heat storage capacity. The capability to transfer heat is lower for the modified mixtures because the TC is lower when the aMBx is present. In this framework, temperature fluctuation in the mixture with this type of characteristics will be lower in the modified asphalt mixtures. Based on the EC test, the level of strains of the modified mixtures is lower than control, which foretells lower thermal stress so then lower thermal cracking. Cracking tests such as SCB and fatigue, showed that mixtures modified with aMBx using the wet method (WM) would have similar performance at low

temperatures (-10^{o}C) and moderate low temperatures (10^{o}C) than control. Results exposed that the higher the aMBx content in the mixture it behaves stiffer and should perform better than control as the temperature increase. Cracking potential estimation using the indirect tensile strength test considering the moisture effect and freeze-and-thaw process, showed that the addition of aMBx up to 30% do not affect the mixture's response. Even, it is notable a slightly increase in all aMBx-samples' response respect to control. This phenomenon is attributed to the fact that aMBx has hydrophobic properties. Analysis based on the E*, G*, and FN suggested that all modified mixtures with aMBx expose better rutting resistance (high temperature response) than control. Also, the viscoelastic analysis results indicated that all aMBx modified asphalt materials considered in this research have less viscous, so then a more elastic behavior than control. The higher the aMBx content the more stable bituminous material. All results indicated that the responses of the 20%aMBx_WM mixture is remarkable better than the other considered mixtures. This confirmed that the WM would be the best mechanism to incorporate the aMBx in the mixtures. However, based on the results of HW and SCB analysis, aMBx contents above 20% are not recommended because the possible aMBx's interference in the binder-aggregates bonding mechanism. Looking at the *AASHTOWare Pavement ME* analysis for the two different climates considered (cold and hot), pavements modified with aMBx would perform better than control in distresses related to IRI, permanent deformation, and thermal cracking. 20%aMBx_WM pavements may have 0.15, 0.9, and 8 times better performance than control in IRI, AC permanent deformation and thermal cracking respectively. Permanent deformation and thermal cracking are the highlighted responses in all aMBx pavements, being the main impact of aMBx the predicted thermal cracking. A comprehensive asphalt

pavement materials evaluation was carried out in this study. As a result of this research, it was found that the aMBx composite is an innovative product in the modification of asphalt mixtures to function as a material with unique thermal resistance properties for a better durability.

CHAPTER 10

UNDERSTANDING THE aMBx-INTERACTION WITH BITUMINOUS MATERIALS

10.1 Introduction

aMBx, is a synthetic porous silica-based composite material developed in the Advanced Pavement Laboratory at Arizona State University. Exhaustive analyses carried out using aMBx in asphalt binders and mixtures have shown that the inherent thermal susceptibility of bituminous materials is reduced as the content of aMBx increases. Because the nature of its components, this composite presents hydrophobic properties. This material has relatively low thermal conductivity and light-weight density. The density ranges from 0.32 to 0.38 g/cm3 and thermal conductivity from 0.08 to 0.12 W/m^{o}K, properties related to the fact that this material is around 50% air. As one of the components of aMBx is aerogel, aMBx is an open-porous material (i.e., the gas in the aerogel is not trapped inside solid pockets) and have pores in the range of 14.65nm and 22.65nm (billionths of a meter) (Liao, et al., 2018). The total size of the coated particle could range from 0.1 to 3mm. Figure 10-1 presents aMBx respect to other petrous materials.

Figure 10-1. Appearance of aMBx respect to other construction materials.

Preliminary microscopic imaging was performed. Below, Figure 10-2 shows some pictures taken for comparison. The images show with a naked eye that the mixtures with aMBx exhibit higher porosity.

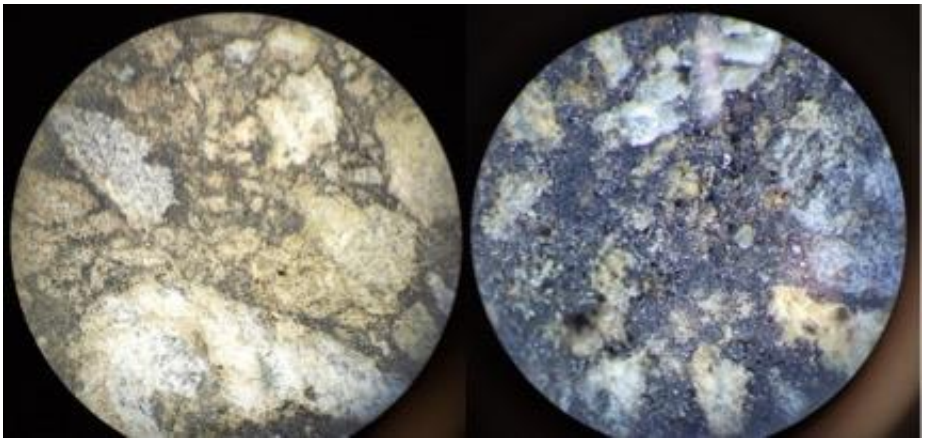

Figure 10-2. Closeup for Control Mixtures (left) and 30% aMBx Content (right) (2x magnified).

As more than a half of the aMBx's volume is air, modified materials with this composite may be provided with additional porosity creating new nano-porous materials.

To identify if a chemical change and/or a physical-mechanical effect occurs in the modified asphalt binder when aMBx is added, FTIR analysis were performed in a binder PG64-16. Also, SEM analysis were carried out on asphalt binders and mixtures modified with 30% by bitumen weight to observe the structure of the aMBx materials.

To add the composite, the binder was heated up to 155ºC in a convection oven. The incorporation of the aMBx in the binder occurs gradually by manual stirring for a period of 30 seconds. For mixtures, small samples were taken from an asphalt mixture modified with 30% using the dry method described in Chapter 6.

10.2 Fourier-Transform Infrared Spectroscopy (FTIR) Analysis

This test, known as the Fourier-Transform Infrared Spectroscopy, uses infrared light to study the chemical characteristics of a certain sample. The radiation sent by the testing machine can be either absorbed by the sample or passed through it. Furthermore, the absorbed radiation is converted into a rotational/vibrational energy by the sample molecules. Then, each sample will have a unique spectrum or "signature", reflecting its chemical structure based on the absorption levels for different wavelengths. Different molecular bonds (e.g., C=O, S=O, C=O…) show absorbance at well-defined wavelengths. By comparing an obtained spectrum (absorbance vs. wavenumber) of the modified samples to the unmodified ones, the new samples can be identified, and the chemical structure of the binder analyzed. Introducing additives to asphalt binder in general may alter the

binder's signature, leading to a possible chemical change in its structure. In this study, a Genesis II FTIR, PIKE Miracle. Figure 10-3 shows the FTIR equipment used in this study.

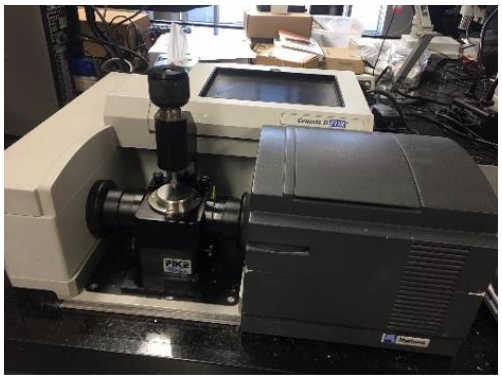

Figure 10-3. Genesis II, FTIR equipment used in this study.

The main purpose of this analysis is to observe the Carbonyl (C=O) and the Sulfoxide (S=O) bonds, which are denoted by the chemical fractioning of asphalt binder, more specifically referring to the oxygen uptake (ageing/stiffening) of the binder. In addition, other detected peaks that are not present in the original (control) binder's spectrum will indicate a chemical change in other bonds. For this reason, neat binder, and modified binder with 30% aMBx by weight of the binder were analyzed under the FTIR. The sulfoxides are the chemicals found at a wavelength of 1030 cm^{-1} whereas the carbonyls are found between 1900 to 1600 cm^{-1}. The results are shown in Figures 10-4 and 10-5 below.

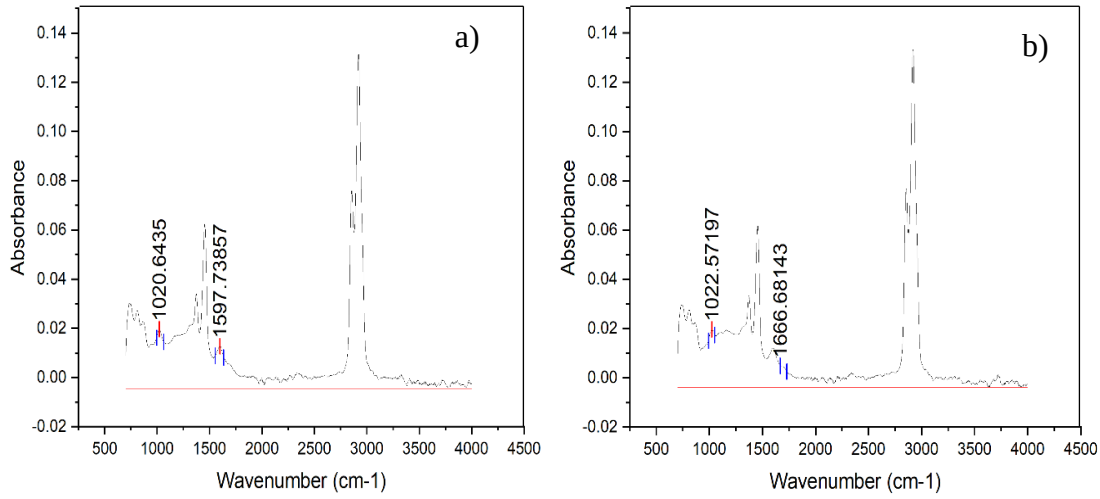

Figure 10-4. FTIR Analysis a) Control Binder b) 30% aMBx Modified Binder

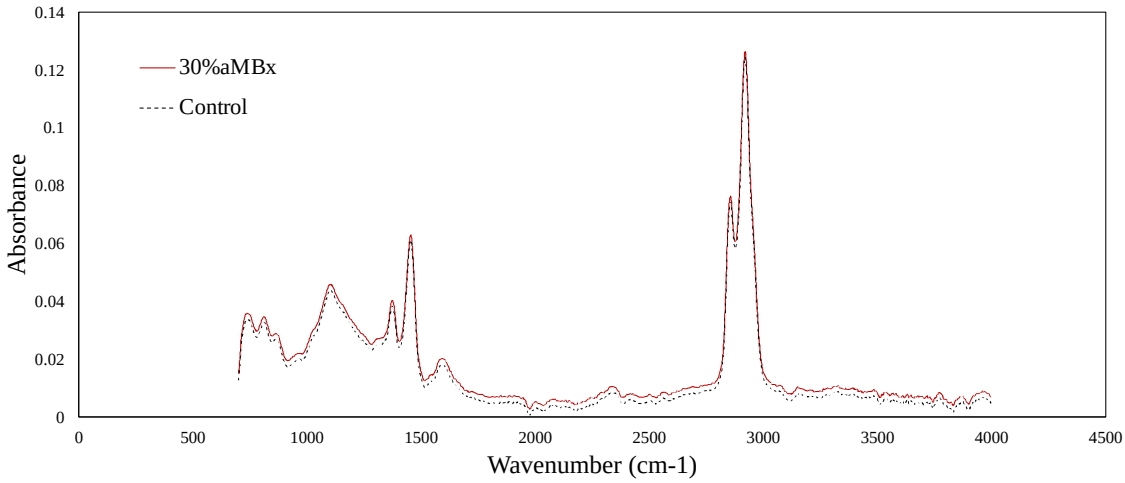

Figure 10-5. Comparison between control and 30% aMBx Modified Binder - FTIR results

None new peak was found in the 30%aMBx binder compared with the original (control) binder; this spectrum indicates that there is not a chemical change in the bonds when aMBx in added to the asphalt binder. Also, the quantity of sulfoxides and carbonyls

were found. These results are very similar for both binders, control and 30%aMBx. Results are presented in Table 10.1.

Table 10-1. Sulfoxides and Carbonyls from FTIR Analysis.

Chemical/Sample	Control	30% aMBx
Sulfoxides	1.60	1.51
Carbonyls	0.61	0.56

No chemical change has been detected between the two, which means that the addition of aMBx into the binder would be only mechanical and/or physical and that it acts as an additive to the binder.

10.4 SEM Analysis

The scanning electron microscope (SEM) uses electrons instead of light to form an image. To achieve this, the team has a device (filament) that generates a beam of electrons to illuminate the sample. The electrons generated from the interaction with the surface of the sample are later collected with different detectors to create an image that reflects the surface characteristics thereof. By mean this process, it is possible to provide information on the shapes, textures, and chemical composition of its constituents. When the electron beam falls on the sample, it interacts with it and various effects are produced to be captured and displayed depending on the equipment used. (Purdue University, 2019). Figure 10-6 shows the NOVA 200-SEM utilized in this study.

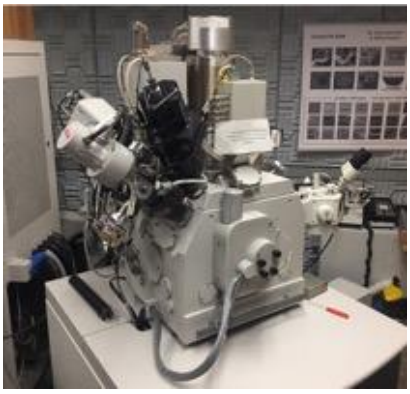

Figure 10-6. NOVA 200-SEM machine utilized in this study.

Special preparations must be done to the sample because the SEM operates down vacuum conditions and uses electrons to form an image, the samples intended for SEM must meet two conditions: they must be dry and conductive. The drying process must be carried out preserving the original structure of the sample as much as possible. The sample needs to be covered later with a material that makes it conductive and allows its observation under the microscope. All metals are conductive and require no preparation before being used. A process of covering with a thin layer of conductive material is needed for all non-metals to made them conductive. A device which uses an electric field and argon gas called "sputter coater", is used to do the covering. Sputter coating in scanning electron microscopy is a sputter deposition process to cover a sample with a thin layer of conductive material, typically a metal, such as a gold/palladium (Au/Pd) plating. A conductive coating is needed to prevent charging of a sample with an electron beam in the conventional SEM (high vacuum, high voltage) mode. (Purdue University, 2019). Figure 10-7 shows a DETON Vacuum Desk II sputter coater used in the study with some samples already coated.

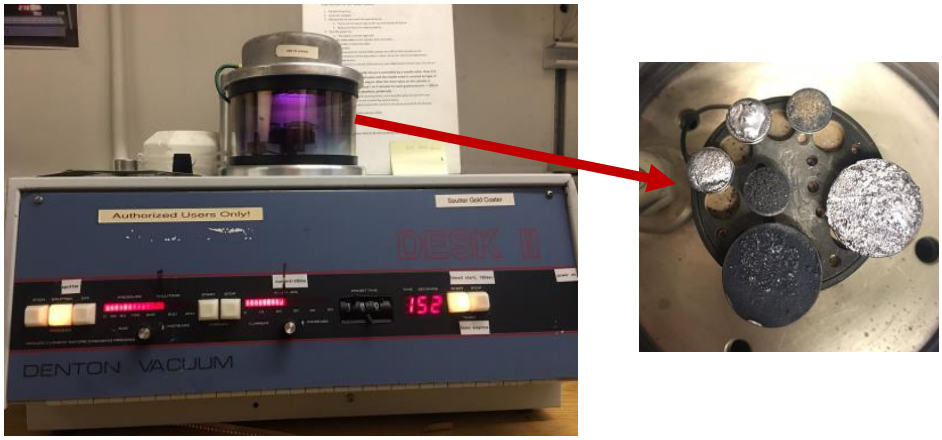

Figure 10-7. Sputter coater and coated samples for SEM.

The identification of unknown particles or contaminates, the cause of failure and interactions between materials is possible by performing a visual analysis of a surface using scanning electron microscopy (Element, 2022).

In this case, asphalt binders and mixtures were analyzed. The 30% aMBx by dry method (DM) was utilized for exam mixtures because the wed method (WM) contain the aMBx in the bitumen, and bitumen was analyzed separately. Also, asphalt binder, AP8b aerogel, and aMBx were analyzed with SEM to observe the shape and structure.

Figures 10-8 shows in the left-hand side AP8b aerogel with a magnification of 65x, and in the right-hand side with 750x. In the center-bottom, silica aerogel at 10000x is displayed. Particles of aerogel with heterogeneous shape and size are shown. A porous and/or reticulated structure is appreciated at high magnification.

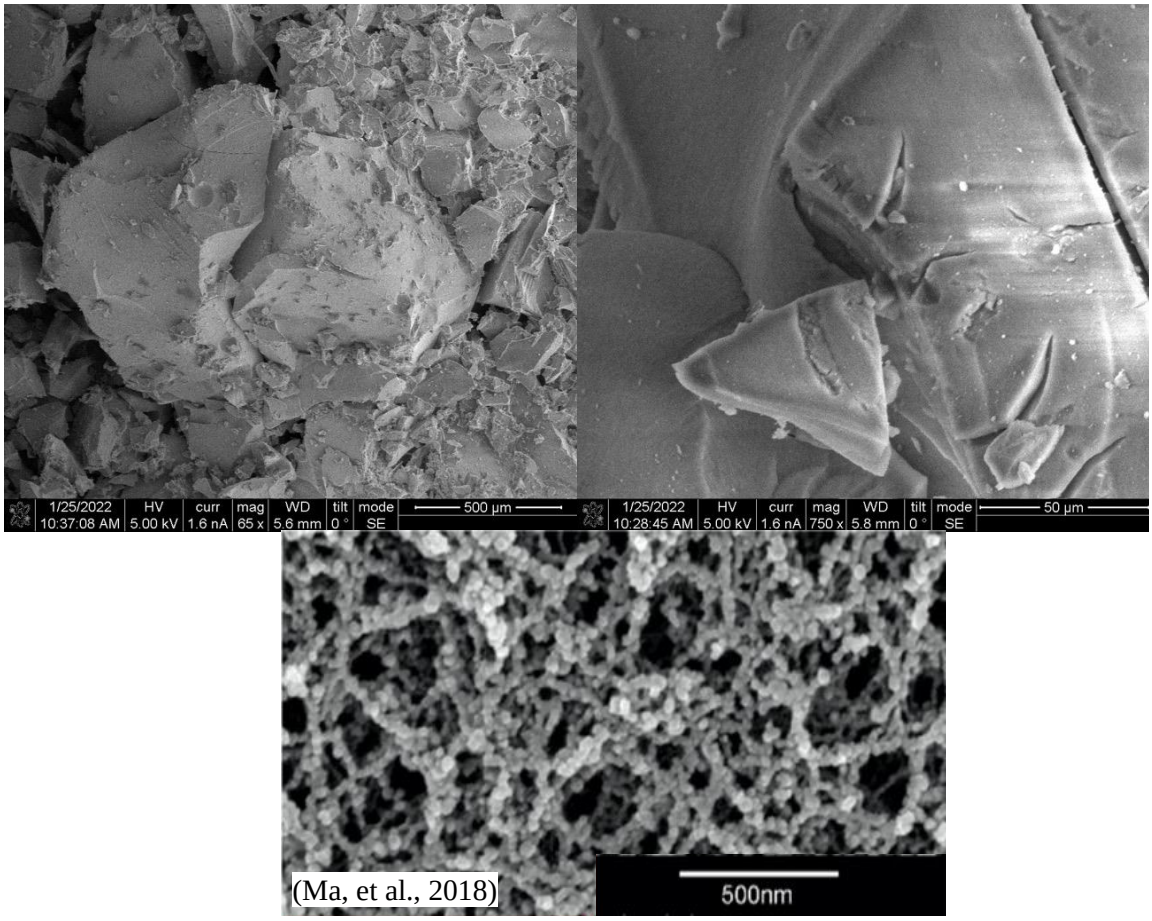

Figure 10-8. Aerogel at 65x, 750x and silica aerogel at 10000x.

Figure 10-9 present how the composite, aMBx, looks like at different magnifications. The size and the shape of the particles are heterogenous. It is possible to see amorphous particles as well as shaped particles such us spheres.

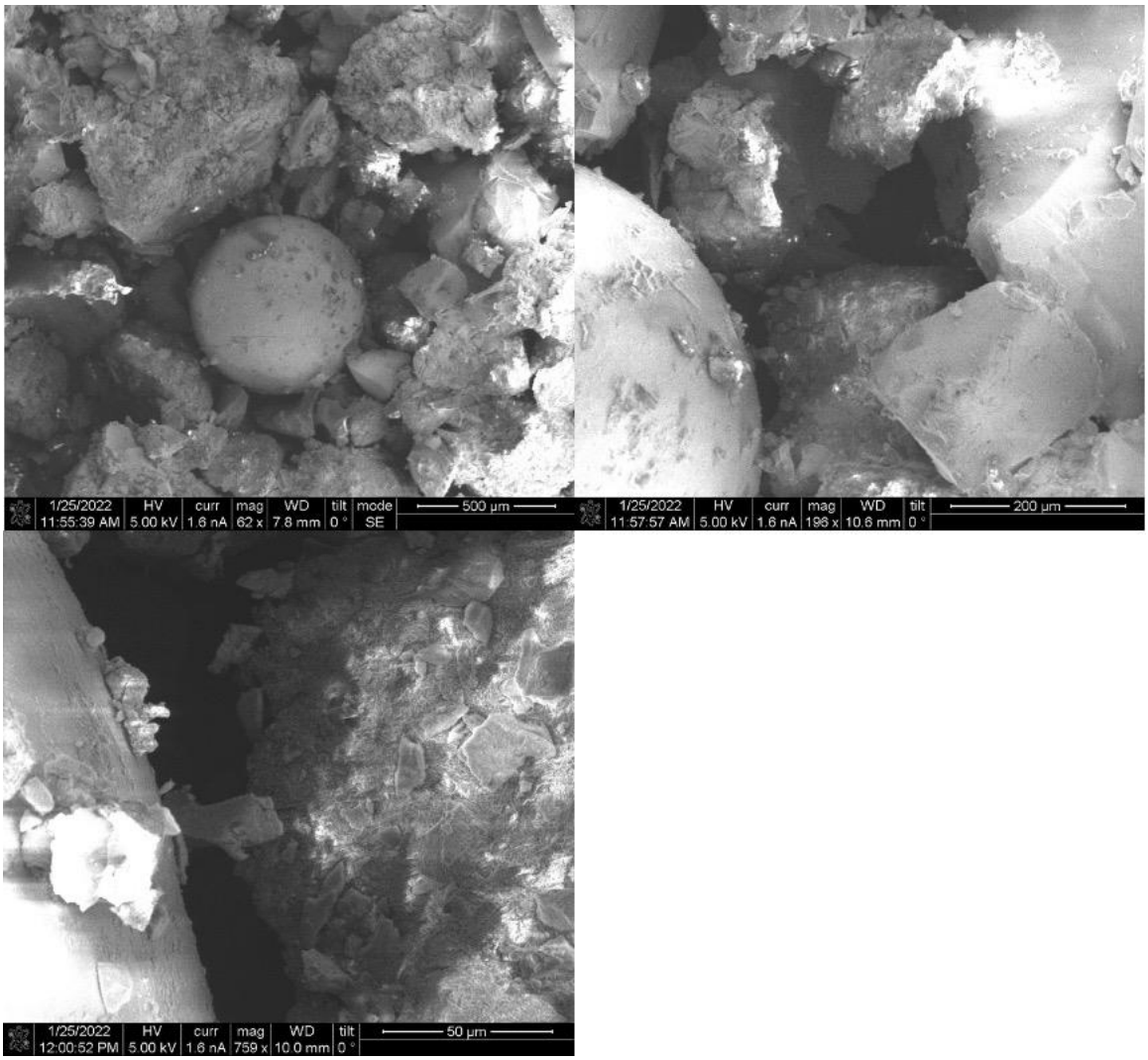

Figure 10-9. aMBx composite at different magnifications.

Figure 10-10 makes a comparison between neat asphalt binder and the aMBx-modified binder at different magnifications. In the left-hand side neat binder is presented while at the right-hand side the modified one. The control binder exposes a plane surface, while the aMBx one appears to be a foam-like structure with different asphalt-made frames.

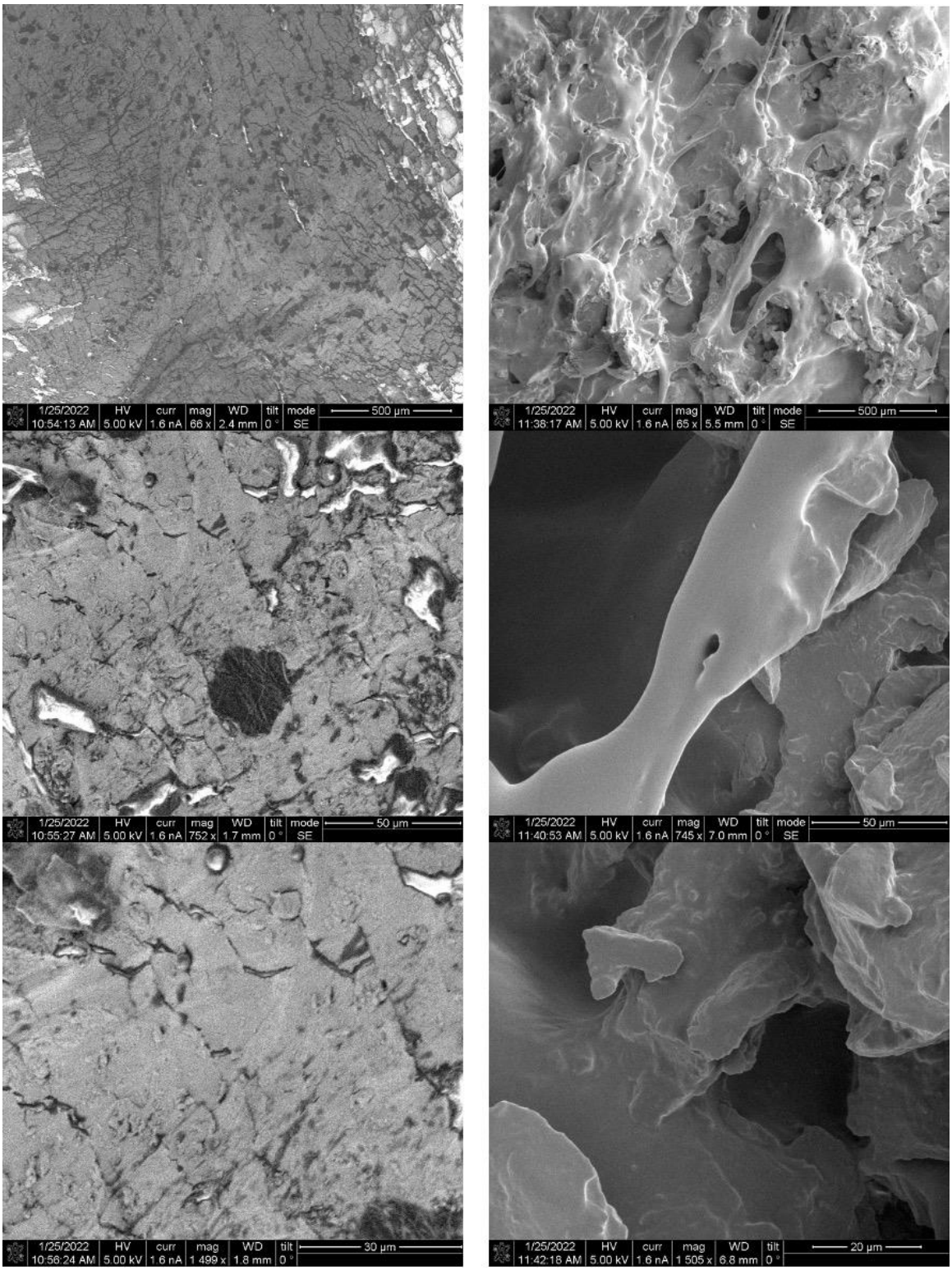

Figure 10-10. Control vs. aMBx-Binder at different magnifications.

Figure 10-11 makes a comparison between control asphalt mixture and the aMBx-modified mixture at different magnifications. In the left-hand side neat binder is presented while at the right-hand side the modified one. Also, the aMBx-modified sample appears as a porous assembly resembling the aerogel's reticulated structure.

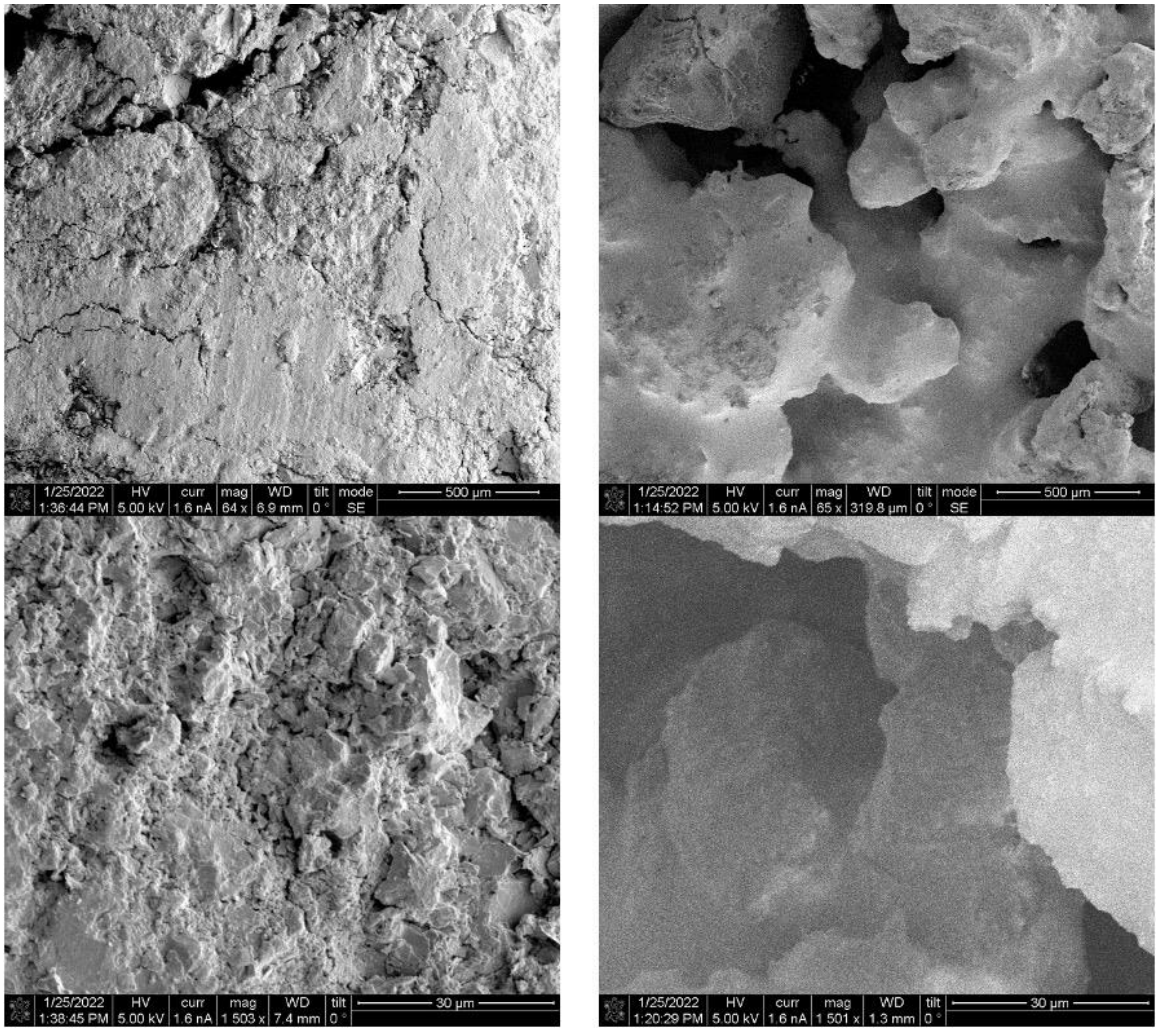

Figure 10-11. Control and aMBx-modified mixtures at different magnifications.

10.5 How It Works

Based on the FTIR analysis, the effect of the aMBx in asphalt material is not a chemical change. Thus, all the improvements and/or changes in the asphalt binders and mixtures may be a physical-mechanical phenomenon.

All test results of asphalt binders and mixtures along this study and the SEM analysis have shown that aMBx operates in two different ways when interacts with asphalt materials: the heat transfer, and the mechanical distribution of loads.

10.5.1 Heat Transfer Hypothesis

According to Chapter 4 of this study, thermal conductivity of materials modified with aMBx decrease as the amount of aMBx rises. The lower the thermal conductivity of the material the less thermal susceptible (i.e., the material has better ability to resist heat transfer, and lower deformation at high temperature), and consequently the more the insulation's efficiency.

Overall, the very low thermal conductivity of gases is the main base of the thermal insulation. Gases possess poor thermal conduction properties compared to liquids and solids. Gases and air are commonly good insulators. But the main benefit is in the deficiency of convection. Consequently, several insulating materials (e.g., aerogel) function simply by having many gas-filled pockets which prevent large-scale convection. Alternation of solid material and gas pocket causes that the heat must be transferred through numerous interfaces producing quick decrease in heat transfer phenomenon (Nuclear Power, 2022).

Indeed, the heat transfer in a material such as aMBx operates through convection in the pores, conduction through the solid and pores, and radiation, then, the total thermal conductivity depends on these three ways of heat transfer.

Pores within conventional insulation are typically over 1mm wide, allowing gas molecules free movement and transfer thermal energy by convection. Aerogel's pores, main component of aMBx, can be as small as 20-40nm or even smaller than the 'mean free path' of air at 60-100nm. This characteristic allows that the individual air molecules within the pores have no space to effectively transfer thermal energy by convection (Happold, 2020).

Because the nano-porosity of aMBx, there is little space for convection, so air molecules constantly collide with the walls of the pores, suppressing gas conduction. Therefore, conduction through the solid structure and air molecules within aMBx is also minimal. Moreover, because aerogel only contains 0.1-5% silica (the rest is air) and the thermal conductivity of air is very low, heat transfer is minimal (Aerogel.org, 2008).

The amount of radiative heat transfer through the principal component of aMBx, aerogel, is dependent on the intensity and wavelength of the thermal radiation, the size and shape of its pores and its overall thickness. At ambient temperature, the nano-pores structure provides effective reduction of infrared thermal radiation due to high levels of absorption and reflection (Dowson ,, et al., 2011).

Because the physical characteristics of the main constituent of aMBx, aerogel, the heat transfer phenomenon is well reduced. This implies a lower thermal conductivity, so then better good insulating properties that support the reduced thermal susceptibility. A

bituminous material with lower thermal susceptibility has better resistance to flow/warp so then more stability. This stability is translated in a better road performance.

10.5.2 Mechanical Distribution of Loads Hypothesis

One of the main composites of the aMBx, aerogel, has a reticulated or foam-like structure. As it can be appreciated in the SEM pictures, the aMBx reticulated structure is transferred to the bituminous aMBx-modified materials. This reticulated structure is hypothesized to provide better load distribution in the asphalt mixture, and better stability of the bituminous part of the material. Figure 10-12 shows a binder PG64-16 modified with aMBx with 480x of magnification.

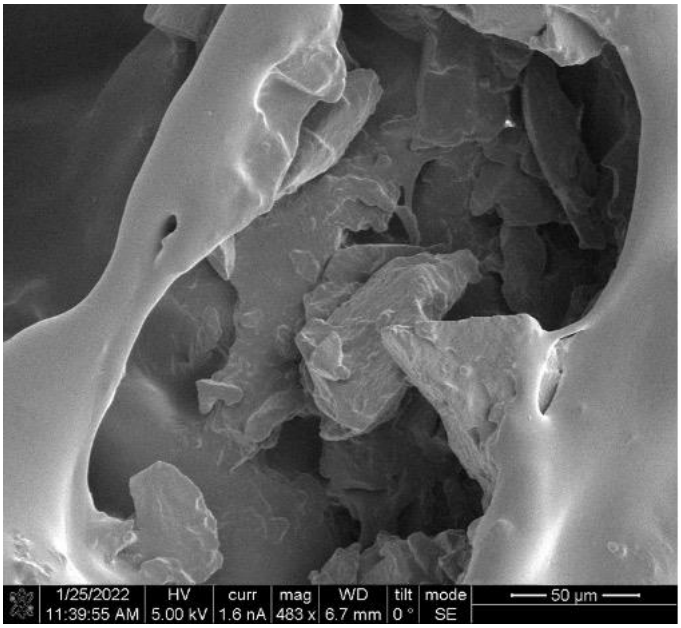

Figure 10-12. Binder PG64-16 modified with aMBx at 480x of magnification.

In structural engineering, reticulated structures are one of the main types of structure, which provide a practical, lightweight, and economical solution for the construction of bridges, buildings, towers to support power transmission lines, etc. These structural elements are composed of steel or wood bars that are interconnect with each other to form triangular structures that form a rigid framework, these structures are subject to tension and compression (Ye, et al., 2011).

In this case, the reticulated structure is made up of different frames without a specific shape interconnected with each other in multi-nodes, forming a rigid and resistant assembly. Then, the distribution of the stresses in this type of structure is divided by all the interconnected frames. The frames in this matrix would be composed then by bitumen and some particles of aMBx.

In conclusion, the high stability of bituminous materials (lower deformation and flow) modified with aMBx lies on the lower thermal susceptibly due to the porous/reticulated structure. This concept explains the high response at medium and high temperatures. Also, the aMBx-bitumen reticulated structure provides damping characteristics so then it absorbs better the loading providing higher recovery (less permanent deformation) as shown in Chapter 4. Finally, this porous structure allows a good load distribution when it exits externally (traffic).

CHAPTER 11

LIFE CYCLE ASSESSMENT INCLUDING TRAFFIC NOISE AND LIFE CYCLE COST ANALYSIS: CONVENTIONAL VS. aMBx MODIFIED PAVEMENTS

11.1 Introduction

The transportation sector is a significant contributor to contamination affecting the human quality of life and the nature (EPA, 2018). Transportation's pollution comes not only from the automobiles' pipes, but also from raw material production for road infrastructure, activities related to construction and maintenance of pavements (Stokstad, 2020). Additionally, mainly in urban and suburban zones near the main roads, noise is one of the central factors that affects people's quality of life. 80% of the noise in cities can come from the motor vehicles (Matthews K. , 2018). According to the World Health Organization, human health can be affected negatively by noise when the equivalent levels exceed 55 dB(A) at night and 65 dB(A) during the day (Garraín, Franco, Vidal, Moliner, & Casanva , 2008). Substantial work has been done to advance methods for the measurement of noise. One method that allows to estimate traffic noise without in-field measures consists in considering the viscoelastic properties of the asphalt mixture. The Dynamic Modulus test (E*) and the definition of phase angle have been broadly studied and proved to estimate the level of noise in decibels (dB) due to the interaction between the pavement and the traffic in the road (Biligiri, 2008).

Pavement construction and maintenance are an essential part of the transportation sector, and they demand plenty of resources while contributing to emissions. There is a

challenge in how we can manage the demand of resources using alternative engineering practices to reduce the environmental impacts (Santero, Masanet, & Horvath, 2010) (Matthews & Hendrickson, 2001). For almost two decades, Life Cycle Assessment (LCA) methodology has been used to describe the climate-change mitigation benefits associated with pavements and different alternatives. Based on the Pavement Type Selection Policy Statement of the Federal Highway Administration (FHWA), the practice of LCA methodology is stimulated as decision-support tool (Harvey, et al., 2016) (U.S Department of Transportation, 2016). In this context, also the analysis of the cost of road construction, which involves design expenses, material extraction, construction equipment, maintenance and rehabilitation strategies, and operations throughout the whole pavement's service life is a very important aspect to address. The usage of an economic analysis practice identified as Life-Cycle Cost Analysis (LCCA) to estimate the cost-efficiency of different pavements alternatives is a crucial methodology to evaluate cost aspects to get optimum pavement life-cycle costs (Babashamsi, Md Yusoff, Ceylan, & Md Nor, 2016).

Agencies are always looking for alternatives to improve the service life of pavements. Achieving pavements four to six years longer lasting is a reasonable expectancy. The New traffic loads and highway requirements make necessary to evaluate and look for new pavement technologies (Walker, 2021). The usage of modifiers in asphalt binders has been one of the most common methodologies to overcome actual necessities and thus improve the durability of bitumen mixes (Gordon, 2002). Some of the most known modifications has been the usage of polymers and crumb rubber, which predominantly have improved the temperature susceptibility of bitumen by increasing stiffness at high temperatures and reducing the probability of cracking at low temperatures (Collins,

Bouldin, Gelles, & Berker, 1991) (Bruton, 2020), however, the low ageing resistance, poor storage stability of polymer modified bitumen (PMB), and high cost are some obstacles that limit the progress of bitumen polymer modification (Zhu, Birgisson, & Kringos, 2014), whereas the implementation of rubber in asphalt mixtures has some downsides such as recyclability, binder storage stability, the fumes that it releases through the paving process, and workability (Kuennen, 2004). Although these technologies have been developed to make longer lasting asphalt pavements, have not shown remarkable responses to overcome cost problems in their implementation.

Along this study, it has been shown that the aMBx is a new and alternative technology capable to make longer lasting asphalt pavements. A comprehensive durability assessment done in previous Chapters has demonstrated that an asphalt pavement modified with 20% of aMBx by bitumen weight can at least doble up the service life of the asphalt pavements.

Different studies using an Attributional Life Cycle Assessment (ALCA) approach have shown that the implementation of alternative technologies such as rubberized asphalt mixtures provides beneficial environmental impacts when comparing with conventional technologies (Bartolozzi, Antunes, & Rizzi, 2013) (Altieb, Aziz, Bin Kassim, & Jibrin, 2016) (Farina, Zanetti, Santagata, & Blengini, 2017) (ADOT, 2017). There are studies to use the Consequential Life Cycle Assessment (CLCA) in pavements as a policymaking in the road pavement sector (AzariJafari, Yahia, & Amor, 2019), to evaluate pavement maintenance and rehabilitation strategies (DeCarlo, Mo, Dave, & Locore, 2017) (Haslett, Dave, & Mo, 2019), however, this study is unique in the aspect of comparing both pavements alternatives, conventional asphalt (CA) and aMBx-modified pavement

(aMBxA), also through a consequential method. On the other hand, despite the fact that noise assessment has been done for decades, the inclusion of noise impacts in LCA is not constantly taken into account for environmental impact assessments (Heijungs & Cucurachi, 2017) (Garraín, Franco, Vidal, Moliner, & Casanva , 2008).

Despite of noise evaluation has been done for decades, the inclusion of noise impacts in LCA is not constantly considered for environmental impact assessments in pavements. This study compares an aMBx modified asphalt road with a conventional one, with the inclusion of traffic noise as part of the LCA. Noise data is obtained based on proved methodologies that correlate the Phase angle of asphalt mixtures with the emission of noise. The Attributional LCA (ALCA) and Consequential LCA (CLCA) are implemented in this study as a decision tool and a guide for the assessment of both scenarios (aMBxA and CA) to evaluate the environmental responses and effects. Finally, a LCCA process is used to estimate the cost-efficiency of the two pavements alternatives using the equivalent uniform annual cost (EUAC), and the net present value (NPV) methods.

11.2 Method

This study evaluated the environmental impacts of conventional and aMBx asphalt concrete, from “cradle to grave”, which means from the collecting of raw materials needed to make the product to the instant when all materials return to the earth. The Life Cycle Assessment considered the rules of international standards ISO 14044 for the definition of

the system boundary, and ISO 14040 for the life cycle inventory. LCA in this study involves two methods: Attributional LCA (ALCA) and consequential LCA (CLCA).

For the Attributional Life Cycle Assessment (ALCA) it is assessed part of the global environmental burdens that belong to the study alternatives, while in the Consequential Life Cycle Assessment (CLCA) it is estimated how the environmental flows are affected by the product implemented. The CLCA includes marginal data on the total production volume, while the ALCA is based on average data on the production systems (Finnveden, et al., 2009).

As in other studies where a replacement scenario was considered to do a CLCA (Kua & Lu, 2016) (Ghose, Pizzol, & McLarenab, 2017), in this case, the emissions from the implementation of aMBx (production of raw materials, manufacturing of aMBx) is considered to conduct the CLCA. In general, the CLCA considers how the processes are affected by a change respect to the conventional asphalt. CLCA does not estimate the actual consequences but the projected ones within the analysis period (Ekvall, 2019).

In contrast, the ALCA approach does not include the environmental benefits or other indirect consequences that happen outside the life cycle when aMBx is implemented. Instead, the raw material emissions and use of a production process are divided between the products of each process (e.g., fuel consumption in the raw aggregates production by the average environmental burden of the fuel system per unit of fuel distributed).

In this study, the CLCA includes both the emissions from the CA and aMBxA pavements, and the reduction/increase in emissions because of the implementation of aMBx in the asphalt mixtures (refer Figure 11-1).

Based on Ekvall, 2019

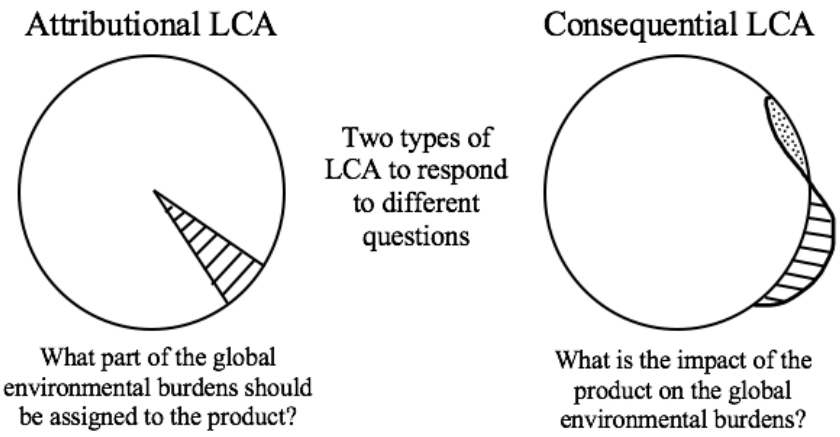

Figure 11-1. Illustration of attributional and consequential LCA.

To include the effects of traffic noise in the LCA, a methodology developed by the swiss author Gabor Doka (2003) was used. This methodology adapted the Müller-Wenk's concept (1999, 2002, 2004) in which it is possible to calculate the Disability Adjusted Life Year (DALY) from the traffic noise by different models. Logical approximations were adopted to come a simplified formula up to measure the damage, in DALY, per vehicle-kilometer based on the emission noise in decibels (dB) (Garraín, Franco, Vidal, Moliner, & Casanva , 2008). Equation (11-1) and Table 11-1 summarize the model (Doka, 2003).

$$EP_L = K.10^{(a.L_p+b)} \quad (11\text{-}1)$$

Where:

Lp: Measured Noise value (dB)

EPL: Environmental pollution from noise per vehicle kilometer (DALY)

a, b and K are regression parameters depending on the time of the journey

Table 11-1. Values of the regression parameters of Doka's formula.

	Slope "a" (1/dB)	Intersection "b" (dimensionless)	Factor K (DALY)
Average Journey (7% of vkm at night)	0.099962	-6.243371	1.23E-07
Daytime Journey	0.09998766	-6.3738654	7.61E-08
Night-time Journey	0.0999043	-5.5943622	2.30E-07

The noise levels were estimated based on a proved correlation between phase angle of the mixture and the noise level produced in the field. Phase angle data of the CA and aMBxA was obtained from previous characterization studies (refer Chapter 9). One test parameter of interest is the phase angle, which indicates the elastic and viscous properties of an asphalt mixture. It has been found that viscoelastic material with governing elastic component would dampen noise less than a material with dominant viscous component (Biligiri, 2008). The department of transportation of Arizona (ADOT) collected field noise measurements for many different pavement surface types. It was found that the average peak phase angle for each mix type associates well to the field sound intensity measurements. Figure 11-2 shows a plot comparing the average measured peak phase angles for different pavement types to the sound intensity noise measurements in the field. The plot displays a rational non-linear tendency, in which the higher the phase angle, the lower the sound intensity. According to Figure 11-2, typical test temperatures range from 38.8^{o}C (100^{o}F) and 54.4^{o}C (130^{o}F), and frequencies at which these peak phase angles occur correspond to low (low speed) to high (high speed) frequencies (Biligiri, 2008). Then,

based on the correlation shown in Figure 11-2 and based on the phase angle of CA and aMBxA mixtures, the level of noise for each of these pavements can be estimated.

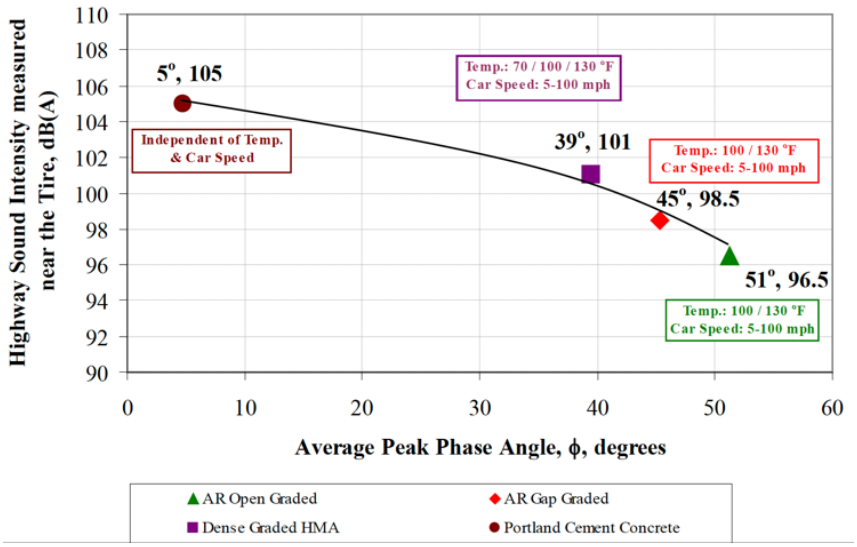

Figure 11-2. Relationship between highway sound intensity measured by the sound intensity method and the average peak Phase Angle of the mixture measured in the Dynamic Modulus Test (E*).

Estimation of material's quantities for the initial construction of both pavements, CA and aMBxA, was done based on the mixture designs information, the usual asphalt pavement data such as density, and adopted thickness. Not available information such as some environmental and performance indicators was obtained from Ecoinvent. Life cycle inventory analysis was done with SimaPro.

Based on the results of an AASHTOWare Pavement ME Analysis, a maintenance projection for both CA and aMBxA was carried out. From the maintenance projection, quantities of materials were calculated. Quantities of materials for the initial construction, maintenance & rehabilitation, and final disposed materials feed the LCA. The different activities consigned in the maintenance projection feed the LCCA. Cost of each activity

for the corresponding unitary unite of execution was obtained from the construction industry. Equivalent uniform annual cost (EUAC), and the net present value (NPV) methods were used to do the economic analysis. Figure 11-3 presents the process.

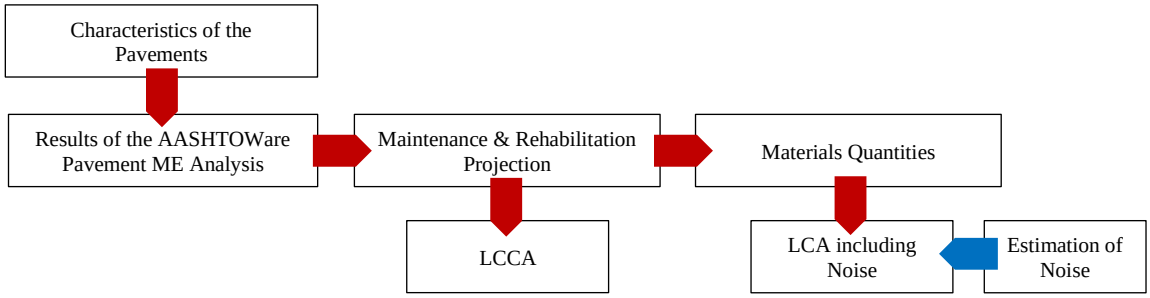

Figure 11-3. Logic Flow to do the LCA and LCCA.

The LCCA of projects could be done using different indices. The equivalent uniform annual cost (EUAC), the internal rate of return (IRR), benefit/cost ratio (B/C) and net present value (NPV) are the most common indicators. The selected analysis period needs to be compared in terms of performance, costs of each alternative and time. The equivalent uniform annual costs (EUAC) and/or the net present value (NPV) are used for this purpose (Walls & Smith, 1998). The estimated value in terms of the present value of money is utilized for the initial, maintenance and rehabilitation costs and salvage value. The discount rate factor is subsequently applied to compute the time value of money (Babashamsi, Md Yusoff, Ceylan, & Md Nor, 2016). Equation (11-2) can be applied for a pavement case using the concept of NPV (Prasada, Rangaraju, & Guven, 2008).

$$\text{NPV} = \text{Initial Const. Cost} + \sum_{k=1}^{N} \text{Future Cost}_k \left[\frac{1}{(1+i)^{n_k}}\right] - \text{Salvage Value}\left[\frac{1}{(1+i)^{n_e}}\right] \qquad (11\text{-}2)$$

Where:

N = Number of future costs incurred over the analysis period

i = Discount rate in percent

nk = Number of years from the initial construction to the expenditure

ne= Analysis period in years

When budgeting is carried out annually, EUAC is a preferred indicator. Present and future expenditures are converted to a uniform annual cost to present the equivalent uniform annual costs (EUAC). Equation (11-3) is the expression used for EUAC (Prasada, Rangaraju, & Guven, 2008):

$$\text{EUAC} = \text{NPV}\left[\frac{(1+\text{i})^{\text{n}}}{(1+\text{i})^{\text{n}}-1}\right] \quad (11\text{-}3)$$

Where:

i = Discount rate

n= Years of expenditure

In this study, the LCCA is evaluated in a period of 55 years. The current annual discount rate adopted was 0.25%. The LCCA is carried out down to different scenarios. The first one adopting the actual costs of the basic raw material, aerogel, and the second one, taking a minimum estimated cost per kilogram of aerogel.

11.3 Goal and Scope

This study assesses two different asphalt mixtures. Both mixtures follow the Superpave mix design method and the City of Phoenix (CoP) specifications. The asphalt binder used in this study was a Superpave Performance Grade Binder, PG 64-16 supplied by Holly Frontier, Glendale, AZ. The aggregates used in the asphalt layer have a nominal maximum aggregate size (NMAS) of 19mm (¾ inches), provided by M.R. Tanner El Mirage Pit. Optimal asphalt binder based on the raw aggregates weight for the CA and aMBxA are 5.27% and 5.24% respectively.

The composite, “aMBx”, is a synthetic porous silica-based material developed in the Advanced Pavement Laboratory at Arizona State University currently with a patent application in the United States Patent and Trademark Office: serial number 63/210,891 filed on June 15, 2021. This material is used to modify the HMA pavements in 20% based on the binder weight. aMBx and asphalt binder were blended through a wet process (WM). In this process, the composite is blended with the asphalt binder, so then, the aMBx-binder is added to the raw aggregates (refer Figure 11-4).

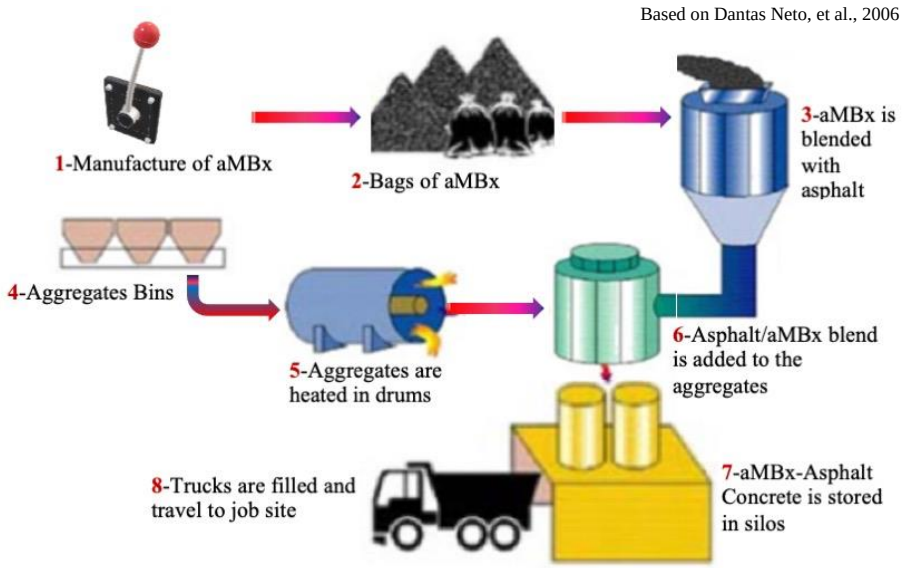

Figure 11-4. Manufacturing scheme of aMBx asphalt by wet way.

This study is focused on describing how the life cycle environmental impact change with the use of a dense graded hot mixture asphalt (HMA) modified with aMBx, and whether, conventional asphalt (CA) or aMBx asphalt (aMBxA) exhibits better environmental performance. The consumptions and emissions immediately related to the life cycle of both pavement technologies, CA and aMBxA, are presented through the ALCA, whereas the CLCA approach is used mostly to inform the effect of implementing aMBxA in the emissions and consumptions as a support for the decision-making process.

Emissions were quantified from the materials production, pavement design/production, use, maintenance & Rehabilitation, and end of life in both CA and aMBxA. Initial construction (laying of the asphalt layer) was not included because the costs and emissions are similar for most pavements, hence, in this study further analysis was not performed. The noise effect was considered in the LCA of use-phase.

Table 11-2 presents the results of an AASHTOWare Pavement ME Analysis calibrated for the Phoenix, AZ, climate zone. Based on these outcomes, a maintenance projection for both, CA and aMBxA was estimated. In this study, the thickness for both CA and aMBxA is 7.5cm.

Table 11-2. AASHTOWare Pavement ME Generated Results Summary.

Climate	Design Type	Mixture	IRI (m/Km)	Total Permanent Deformation (cm)	Fatigue (%Lane)	Thermal Cracking (m/Km)	Top-Down Fatigue (%Lane)	AC Permanent Deformation (cm)
Phoenix	Thin	CA	2.80	1.32	25.93	605.56	66.92	0.51
		aMBxA	2.44	0.99	14.48	83.46	77.22	0.23

The lifetime for a conventional asphalt pavement could vary depending on the materials used, construction process and maintenance, however, generally the life of the conventional materials is 10 years (U.S. Department of transportation, 2019). Based on the AASHTOWare Pavement ME results summary aMBxA showed to have more than twice the CA's service life. aMBxA can better resist thermal cracking and fatigue, has less IRI and permanent deformation. In a 25-years analysis period, maintenance cost for a CA is more than two times the one needed for aMBxA.

Projection of the maintenance and rehabilitation is presented in Table 11-3. In the process of manufacturing aMBxA (design/production phase, blending aMBx-binder and aggregates) a higher temperature of mixing is needed, therefore a greater energy consumption is required for production (Obando, Karam, Castro, Medina, & Kaloush, 2021). The functional unit is one-lane of 3.5m width per kilometer without shoulders over

a 25-years analysis period. Reference Flow is kilogram of materials for one-lane kilometer. The LCA results and interpretation will be presented for the functional unit.

Table 11-3. Proposed Maintenance & Rehabilitation Projection for CA and aMBxA Pavements.

Years	Conventional	aMBxA
0	Initial Construction	Initial Construction
3	Crack Sealing (m)	No Action
7	CS + Surface Treatment	Crack Sealing (m)
10	Crack Sealing (m)	No Action
14	2.5 cm mill and fill	Surface Treatment
20	Crack Sealing (m)	Crack Sealing (m)
25	Reconstruction	2.5 cm mill and fill
25	Salvage	

This study aims to presents the consumptions and emissions immediately related to the life cycle of a both pavement technologies (CA and aMBxA) through the ALCA, whereas the CLCA approach is used mostly to inform the effect of implementing aMBxA in the emissions and consumptions as a support for the decision-making process.

11.4 Life Cycle Assessment (LCA)

11.4.1 System Boundary

The system boundary diagram (Refer Figure 5) was adapted from the Federal Highway Administration framework (Harvey, et al., 2016) and the National Asphalt Pavement Association (Mukherjee, 2016). Figure 11-5 represents the system boundary flowchart and processes that will be included and excluded. Life Cycle Assessment (LCA)

is a "cradle-to-grave" study in which the system boundary includes the following phases: (P1) raw materials production, (P2) asphalt pavement mix design/production, (P4) Use, (P5) maintenance and rehabilitation (M&R), and (P6) end of life (EOL).

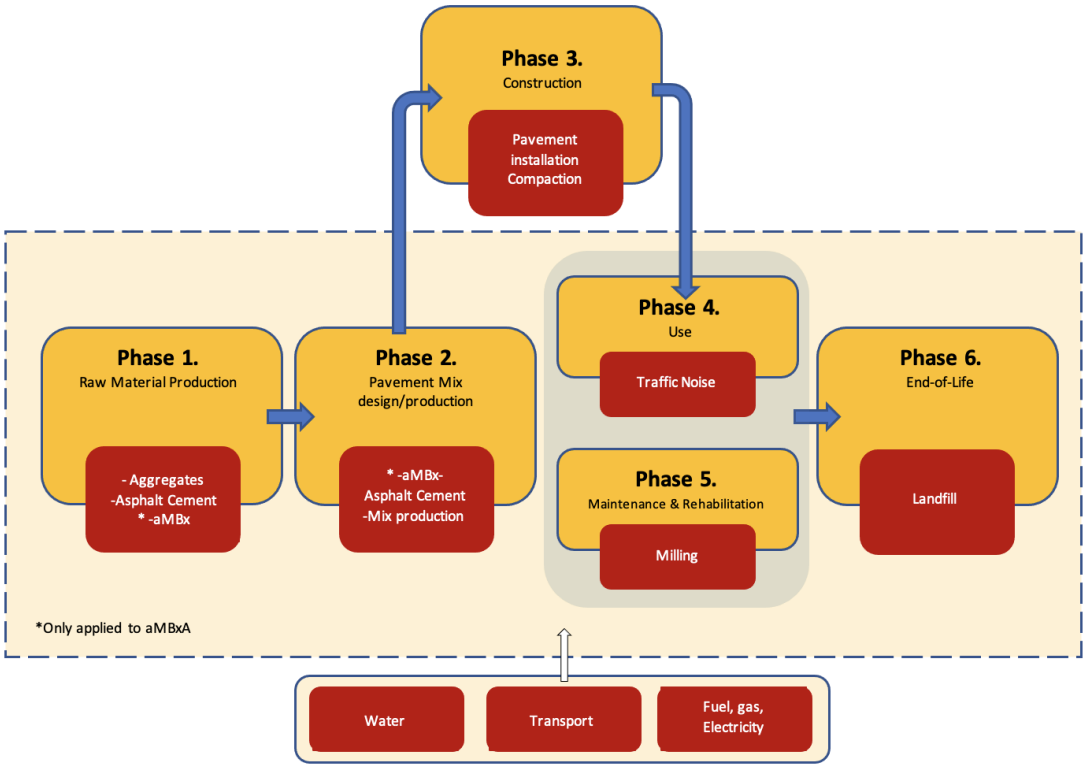

Figure 11-5. CA and aMBxA System Boundary Flowchart.

Initial construction phase was excluded as previously it was explained. Phase of Materials production includes all processes in the acquisition and processing of raw materials (e.g., mining, crude oil extraction, aMBx manufacturing). Phase of Asphalt pavement mix design/production involves the pavement structural composition and required materials (e.g., manufacturing of aMBx-asphalt cement and asphalt concrete). Phase of Use includes traffic noise. Phase of Maintenance and rehabilitation accounted for the overall road serviceability. Phase End of life includes the land fill disposal.

11.4.2 Life Cycle Inventory

This LCA study was focused on the effects of adding aMBx to the asphalt layer, while the granular layers keep the same structural composition for both aMBxA and CA, so these do not need calculations since have equal input data. According to the case of study, the top layer thickness for both aMBxA and CA is 7.5cm. Tables 11-4 and 11-7 detail the required materials for the construction and transportation for both aMBxA and CA top layer, all maintenance and rehabilitation interventions along the analysis period of 25 years (refer Table 11-3), and EOL phase. The bitumen and aggregates proportions of CA are 5.27% and 94.73% by weight for dense asphalt mixtures. In the case of aMBxA, 5.24% of bitumen and 94.76% of aggregates were implied considering a dense HMA. As previously it was mentioned, 20% by weight of the bitumen corresponds to aMBx. Milling procedure of 2.5cm of the surface accounts as a material to be disposed in the landfill usage as part of the end-of-life phase (refer Table 11-4). Table 11-8 presents a summary of the Life Cycle Inventory (LCI) data considered in the study and the respective sources.

Table 11-4. Material Input Data for aMBx and Conventional Asphalt Mix Design.

aMBx ASPHALT (aMBxA)			
aMBx-binder 5.27%	39,748.98	Kg/Km	Landfill
aMBx 20% from 5.27% of aMBx-binder	7,949.80	Kg/Km	188,562.50 Kg/km
Bitumen 80% from 5.27% of aMBx binder	31,799.18	Kg/Km	87.50 m3/km
Aggregates 94.73%	714,501.03	Kg/Km	
Crack Sealing	2,800.00	m2	
Surface Treatment	3,500.00	m2	
CONVENTIONAL ASPHALT (CA)			
Bitumen 5.24%	97,019.81	Kg/Km	Landfill
Aggregates 94.76%	1,806,822.69	Kg/Km	475,960.63 Kg/km
Crack Sealing	14,000.00	m2	218.75 m3/km
Surface Treatment	3,500.00	m2	

11.4.2.1 Aggregates and Bitumen Production

Production of 1 kg of aggregates needs 0.01 kWh/kg (diesel plus electricity) (Stripple, 2001). Production of 1 kg of bitumen requires 1.36 kWh/kg using gas (Chehovits & Galehouse, 2010).

11.4.2.2 Production of aMBx

Manufacturing of aMBx involves 11.9 kWh/kg in the production of aerogel (Wagle, 2020), 1.36 kWh/kg in the production of asphalt binder (Chehovits & Galehouse, 2010), 0.73 kWh/kg in the machinery used in the process (heat, kinetic energy) (The Engineering ToolBox, 2003). However, based on the specific requirements from each of these aspects, the energy consumption in the process of manufacturing of aMBx is 6.83 kWh/kg.

11.4.2.3 Modified aMBx Bitumen Production (aMBx Binder)

It is estimated that the production of the aMBx-asphalt-cement using an Ultra Turrax T-50 mixer would require 0.004 kWh/kg of energy, and 0.32 L/kg of fuel (Ortíz Rodríguez, Ocampo Duque, & Duque Salazar, 2017).

11.4.2.4 Hot Mix Production (aMBxA and CA)

The energy consumption in the process of HMA production (mix of binder and aggregates) of CA was considered as 0.1 kWh/kg (Stripple, 2001), however, in the case of aMBxA, because of the higher working temperature, a greater energy is required for

production. In this study, the CA used a mixing temperature of 160oC while aMBxA 175^{o}C. A raise in 15^{o}C represents a 12% in the increment of the energy consumption (Padilha Thives & Ghisi, 2017). In this context, production of aMBxA would need 0.112 kWh/kg.

11.4.2.5 Use – Traffic Noise

Results of the Phase Angle from the Dynamic Modulus Test are presented in Table 11-5. For the estimation of noise emission, the average peak phase angle was chosen for each mixture type. Peak phase angles are 37.53^{o}C and 47.83^{o}C for CA and aMBxA respectively. Using the correlation between phase angle and the noise emission (refer figure 2) noise emission were estimated. Table 11-6 presents the estimated noise emission in decibels for both, CA and aMBxA pavements. Results showed that the amount of noise is 2.3dB less for aMBxA.

Table 11-5. Mixtures' Average Peak Phase Angle

Temp, ºC	Frequency Hz	Phase Angle (δ)	
		Control	20%aMBx_ WM
-10.0	25	6.6700	3.4000
	10	8.6900	4.1300
	5	9.0100	5.1000
	1	10.0600	5.3900
	0.5	10.5500	6.4300
	0.1	11.4900	8.0000
-4.4	25	8.6600	11.0800
	10	11.9700	16.1200
	5	13.4400	13.8900
	1	15.3100	16.3400
	0.5	17.0500	18.6900
	0.1	18.0700	22.7100
21.1	25	16.4900	19.9700
	10	20.1500	22.5300
	5	22.4900	24.8600
	1	29.0400	29.9500
	0.5	31.8700	31.7600
	0.1	35.8600	34.1300
38.8	25	25.3900	25.2600
	10	30.3900	31.9900
	5	32.8700	34.4000
	1	36.9000	39.1300
	0.5	36.3700	40.9300
	0.1	31.6100	39.6800
54.4	25	36.8300	39.8300
	10	37.3800	40.2600
	5	37.5300	41.8300
	1	33.8400	33.5100
	0.5	30.8200	34.4800
	0.1	25.1300	29.1300

Table 11-6. Estimated Noise level base on phase angle correlations.

Number of Axes	Conventional (CA) (dB)	Modified (aMBxA) (dB)
70	101.3	99

Level of noise for this study were estimated consistent with a FHWA study, in which the level of traffic noise perceived for an urban area in day-time situations considering conventional conditions could be about 75dBA (Corbisier, 2003), then, for aMBxA may be 73.3dBA.

11.4.2.6 Maintenance and Rehabilitation

For the milling process prior to the laying of the overlays in the maintenance and rehabilitation process, it was estimated the fuel consumption of 0.13 L/kg of fuel (Bartolozzi, Antunes, & Rizzi, 2013). The processes of crack sealing and surface treatments demands 0.01 kWh/m2 and 0.14 kWh/m2 respectively (Gangaram, 2014).

11.4.2.7 End of life

Because the milling process along the maintenance and rehabilitation phase, transportation from the site to the landfill for inert material disposal is needed. The distance between the project site and the inert material landfill is considered as 50km for both CA ad aMBxA. The excavated materials are included in the process.

Table 11-7. Transportation Distances for CA and aMBxA alternatives.

Life Cycle Assessment Phase	Type of transport means (HP, kW, weight)	Transport for each Process	Type of Asphalt Pavement	Distance min-max (km)	Origin - Destitination
(1) Raw Materials Production	Truck 30 tons	Natural Aggregates Extraction	CA & aMBxA	50	Aggregates Plant – Mixing Plant
		Asphalt Cement Production	CA & aMBxA	100	Refinery - Mixing plant
		Production of aMBx	aMBxA	30	Many locations - Mixing Plant
(2) Asphalt pavement mix design/production		Producction of The Asphalt Concrete	CA aMBxA	50	Mixing Plant - Road
(5) Maintenance and Rehabilitation		Crack Sealing, Surface Treatments, Milling	CA & aMBxA	50	Plant - Road
(6) End of life		Usage of Ladfill	CA & aMBxA	50	Road - Landfill

Table 11-8. LCI data considered in the case study.

Life Cycle Assessment Phase	Process Name	Type of Asphalt Pavement	Data Source	Data Type	Item	Value	Unit
(1) Raw Materials Production	Natural Aggregates Extraction	CA & aMBxA	Gravel, crushed {RoW}| production | Alloc Def, U' – Ecoinvent v.3 database	Secondary	Energy	0.01	kWh/kg
	Asphalt Cement Production	CA & aMBxA	'Bitumen, at refinery/kg/US' – USLCI database	Secondary	Gas	1.36	kWh/kg
	Production of aMBx	aMBxA	Calculated	Primary	Energy	6.83	kWh/kg
(2) Asphalt pavement mix design/production	aMBx Asphalt Cement	aMBxA	Ultra Turrax T-50 Mixer (Ortíz Rodríguez, et al., 2017)	Secondary	Energy	0.004	kWh/kg
				Secondary	Fuel	0.32	L/kg
	Producction of the Asphalt Concrete	CA	Stripple, 2001	Secondary	Energy	0.10	kWh/kg
		aMBxA	Estimated	Secondary	Energy	0.11	kWh/kg
(4) Use	Traffic Noise Generated	CA	Estimated	Secondary	Noise	75.00	dBA
		aMBxA		Secondary	Noise	73.30	dBA
(5) Maintenance and Rehabilitation	Crack Sealing	CA & aMBxA	Gangaram, 2014	Secondary	Energy	0.01	kWh/m2
	Surface treatments			Secondary	Energy	0.14	kWh/m2
	Milling		(Bartolozzi, et al., 2013)	Secondary	Fuel	0.13	L/kg
(6) End of life	Usage of Ladfill	CA aMBxA	Respective calcualted volumes when Maintenance and Rehabilitation occur				

11.5 Life Cycle Cost Analysis (LCCA)

A period of 55-years analysis was considered to include as many maintenance and rehabilitation activities as possible. These different interventions for each pavement were considered based on the expected performance presented in Table 11-2. All cost activities are presented in m2, except Crack Sealing (CS), which is in m. For simplicity, all calculations are based on 1 m2 of pavement, 7.5 cm (3") thick. Both, net present value (NPV) and the equivalent uniform annual costs (EUAC) methods are shown. The annual discount rate considered was 0.25%. The cost of aMBx per kilogram was estimate, as well as the cost of the modified mixture (aMBxA) per ton in two scenarios. The first one considering $20 per kilogram of aerogel, which is the cost of raw aerogel when this is imported from South Korea. The second calculation considers the possibility of manufacture our own aerogel. As a second scenario, assuming the minimum cost of raw material to manufacture aerogel, it was estimated that a kilogram of aMBx could cost $9.

The percentage of aMBx considered in this study was 20% based on the asphalt binder. Then, for 5.27% of binder (aggregates based), 9.8 kilograms of aMBx are need per ton of asphalt mixture. Additional raw material used to manufacture aMBx is asphalt binder. A ton of this material is currently $405. Also, 30% of production and administration fees, and 5% of transport for each kilogram of aMBx produced were considered.

The LCCA is carried out per m2, considering a pavement of 7.5cm thick for a period of 55 years. The Current Annual Discount Rate adopted was 0.25%. Salvage was assumed as 15% of the initial construction cost. Based on Table 11-2 it was done a maintenance interventions projection listed in Table 11-3. Cost of each intervention correspond to activities carried out in Phoenix, Arizona (Grupa, 2020) (Maricopa Association of Gobernments & KimleyHorn, 2019) for CA. Based on the costs for CA, aMBxA's costs were calculated when needed. To address Table 11-3, costs of the different items are presented below:

- Conventional Asphalt Mixture: $87 ton
- Crack Sealing: $0.95 ml
- Surface Treatment: $0.86 m2
- Mill and Fill (2.5cm) CA: 10.19 m2
- Conventional Pavement of 7.5cm: $6.63 m2
- Delivery and installation of pavements: $30 m2

11.6 Results and Discussion

The global endpoint ReCiPe 2016 method which are capable of quantifying life cycle impacts on human health, ecosystem services, and natural resources was used for the assessment to show the potential environmental impacts, the influence on human beings and the consumption of water, energy, and resources. Table 11-9 presents the characterization and damage assessments outputs using SimaPro 9.1.1 software. It is possible to observe that over the whole life cycle of the pavement, the CA pavement generates much more negative impact, in some impacts approximately twice as much as the aMBxA pavement does.

Table 11-9. Characterization and Damage Outputs of ReCiPe Endpoint Method.

Impact Category	*Unit*	*TOTAL CA*	*TOTAL aMBxA*	*TOTAL*	*% CA*	*% aMBxA*
Global warming, Human health	DALY	**1.62E-01**	**1.02E-01**	2.64E-01	61%	39%
Global warming, Terrestrial ecosystems	species.yr	**4.88E-04**	**3.08E-04**	7.95E-04	61%	39%
Global warming, Freshwater ecosystems	species.yr	**1.33E-08**	**8.42E-09**	2.17E-08	61%	39%
Stratospheric ozone depletion	DALY	**2.97E-05**	**1.62E-05**	4.60E-05	65%	35%
Ionizing radiation	DALY	**3.91E-05**	**1.19E-05**	5.09E-05	77%	23%
Ozone formation, Human health	DALY	**5.23E-04**	**1.92E-04**	7.15E-04	73%	27%
Fine particulate matter formation	DALY	**7.60E-02**	**2.86E-02**	1.05E-01	73%	27%
Ozone formation, Terrestrial ecosystems	species.yr	**7.61E-05**	**2.80E-05**	1.04E-04	73%	27%
Terrestrial acidification	species.yr	**6.52E-05**	**2.48E-05**	9.00E-05	72%	28%
Freshwater eutrophication	species.yr	**7.52E-06**	**2.71E-06**	1.02E-05	74%	26%
Marine eutrophication	species.yr	**6.19E-10**	**3.22E-10**	9.41E-10	66%	34%
Terrestrial ecotoxicity	species.yr	**1.19E-06**	**4.89E-07**	1.68E-06	71%	29%
Freshwater ecotoxicity	species.yr	**6.06E-07**	**2.67E-07**	8.73E-07	69%	31%
Marine ecotoxicity	species.yr	**1.36E-07**	**5.81E-08**	1.94E-07	70%	30%
Human carcinogenic toxicity	DALY	**8.70E-03**	**3.65E-03**	1.24E-02	70%	30%
Human non-carcinogenic toxicity	DALY	**9.60E-03**	**3.31E-03**	1.29E-02	74%	26%
Land use	species.yr	**1.56E-05**	**7.90E-06**	2.35E-05	66%	34%
Mineral resource scarcity	USD2013	**9.36E+01**	**3.11E+01**	1.25E+02	75%	25%
Fossil resource scarcity	USD2013	**2.55E+04**	**1.63E+04**	4.18E+04	61%	39%
Water consumption, Human Health	DALY	**1.79E-01**	**5.09E-02**	2.29E-01	78%	22%
Water consumption, Terrestrial ecosystems	species.yr	**1.09E-03**	**3.11E-04**	1.40E-03	78%	22%
Water consumption, Aquatic ecosystems	species.yr	**4.89E-08**	**1.42E-08**	6.31E-08	78%	22%
Damage Category	*Unit*	*TOTAL CA*	*TOTAL aMBxA*	*TOTAL*	*% CA*	*% aMBxA*
Human health	DALY	**4.35E-01**	**1.89E-01**	6.23E-01	70%	30%
Ecosystems	species.yr	**1.74E-03**	**6.84E-04**	2.43E-03	72%	28%
Resourses	USD2013	**2.55E+04**	**1.63E+04**	4.18E+04	61%	39%

11.6.1 Impact Assessment

The impact assessment method used was the ReCiPe Endpoint (H). Hierarchist (H) methods are the default model, and it stands for a medium time horizon (e.g., 100-year GWP). The system boundary includes the following LCA phases: raw materials production (phase 1), asphalt pavement mix design/production (phase 2), use (phase 4), maintenance and rehabilitation (phase 5), and end of life (phase 6). This analysis does not take into consideration the vehicle emissions associated to factors such as friction between tires and vehicles into use (phase 4), but it does include the assessing of noise implementing Doka's method. Noise assessment is included only in the EndPoint damage category "Impact in Human Life" because the similarity between the concepts and outputs' units

Figure 11-6 shows the environmental impacts determined by the Endpoint impact category. The superior environmental performance of the wearing course containing aMBxA material are confirmed. The impacts categories evaluated show that phase 1 (Materials production), and phase 2 (Asphalt pavement mix design/production) are the major contributors to environmental impacts in both cases CA and aMBxA. Overall, aMBxA pavement, impacts 27% less that CA.

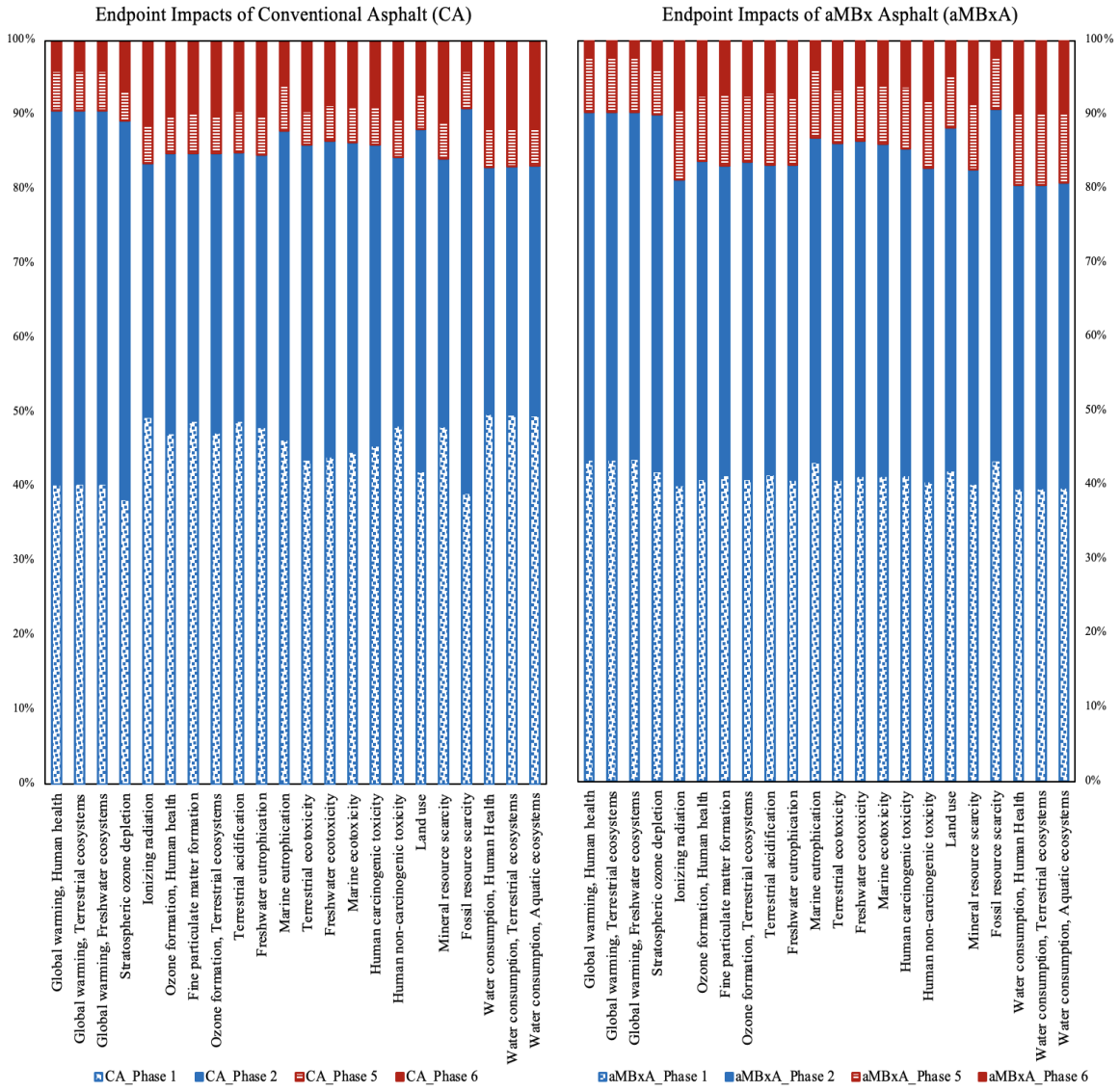

Figure 11-6. Phase Contribution to the Impact Categories of CA and aMBxA – Endpoint Approach.

11.6.2 Damage Assessment

Figure 11-7 shows a comparison of impact in Human Life of CA and aMBxA including all phases. This result is presented in units of DALY. The disability-adjusted life year (DALY) is a measure that represents the number of lost years of "healthy" life due to an illness, disability, or early death (World Health Organization, 2014). As it was

explained previously, use phase was analyzed separately following Doka's method and after added to the others phase's impact. Results of this implementation are shown below in Table 11-10.

Table 11-10. Damage Assessment for Use (phase 4) Considering Traffic Noise.

Type of Technology	Lp (dB)	EPL - Damage (DALY/vkm) by journey	Number of journeys for the study time	DALY for the study time	Life Days Less for the study time
CA	75	2.214E-06	9125	0.02020	7.4
aMBxA	73.3	1.496E-06	9125	0.01365	5.0

Overall, CA pavement has 0.435 DALY, while aMBxA pavement 0.250 DALY, which means that CA impacts 27% more in Human Life than aMBxA. Regarding to traffic noise assessment, results present that aMBxA has about 19% less impact in human life in DALY compared with CA. Traffic noise impact in both, CA and aMBxA cases, represents a contribution in the total human life impact of about 0.0006%, however, considering the study period (25 years), a reduction of 1.7dB in noise emission due to the implementation of aMBxA could represent 2.4 days of longer life for an individual.

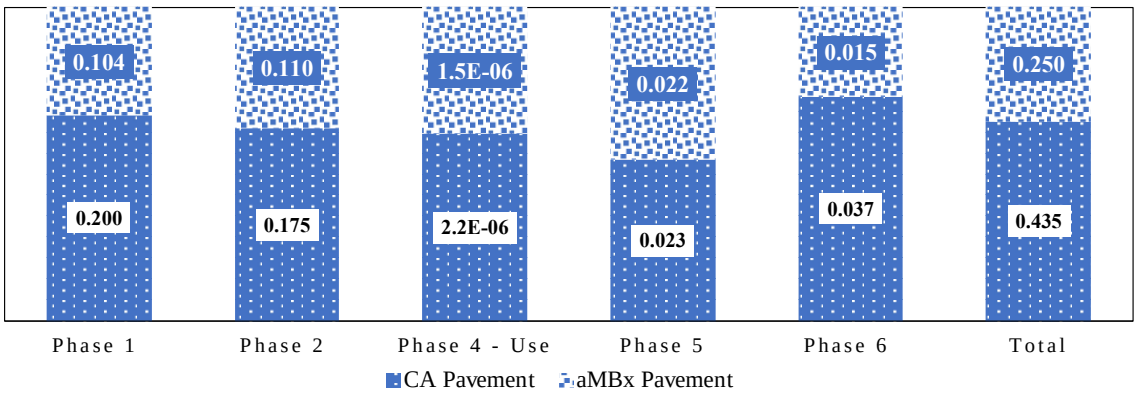

Figure 11-7. Comparison of Impact in Human Life between CA and aMBxA.

Figure 11-8 shows a comparison of impact in Ecosystems of CA and aMBxA pavements. This result is presented in units of species-years. It measures the extinction rate of species. “There is approximately one extinction estimated per million species-years” (Annenberg Foundation, 2016). The stacked bars present the system phases side-by-side and the total impact in Ecosystems. Phases 1 and 2 of both CA and aMBxA cause the major impact in Ecosystems. The results show that CA has 29% more impacts in the extinction rate of species than aMBxA. The comparison of impact in Resources of CA and aMBxA pavements is also shown in units of USD2013, which means a US Dollar for the value of the currency in 2013. In total, CA cause 17% more impact in resources than aMBxA. Phases 1 and 2 of CA aMBxA represent the highest impacts. Phase 5 (M&R) of both alternatives presents very similar impacts. The most typical intervention in Phase 5 is crack sealing, then this activity in terms of damage is not very representative.

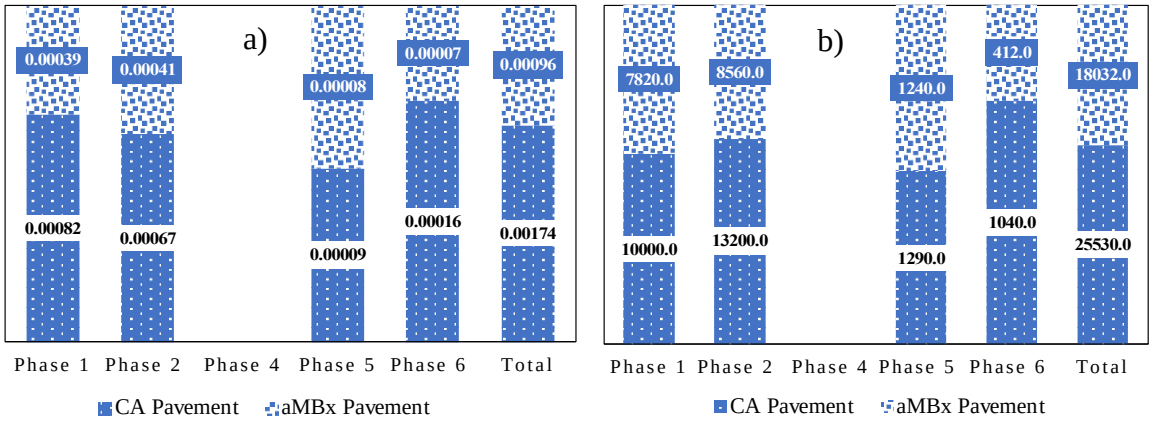

Figure 11-8. a) Comparison of Impact in Ecosystems, b) Comparison of Impacts.

In general, results show that the major difference in impacts between CA and aMBxA is represented in phase 1, 2 and 6. aMBxA has much better performance and less landfill requirements. These results show the aMBxA pavement is more environmentally friendly compared with the CA pavement material. This is a positive signal, aMBxA shows to be a more sustainable material in the transportation industry.

11.6.3 Single Score

Figure 11-9 shows the Endpoint evaluation after having normalized and weighted Human Health (30%), Ecosystems (40%), and Resources (30%).

It is possible to confirm that phases 1 and 2 are the phases with the highest impact. CA requires much more raw material and mix production because of the lower durability response.

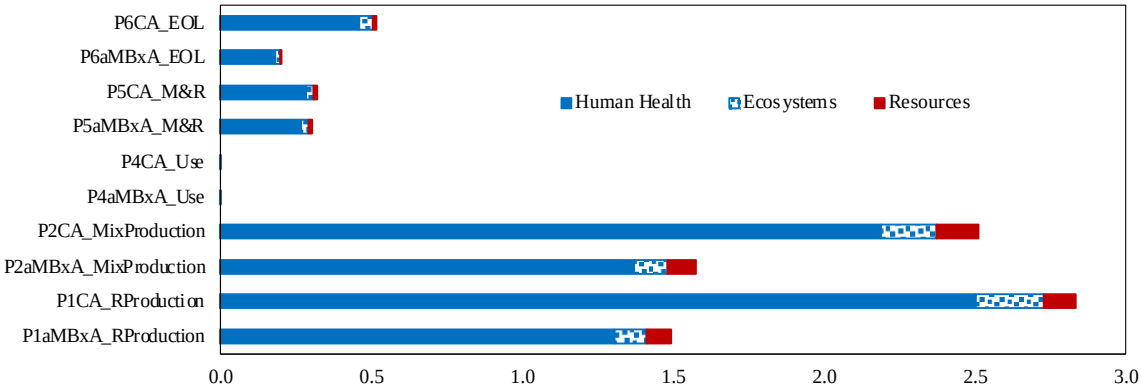

Figure 11-9. Endpoint (Single Score).

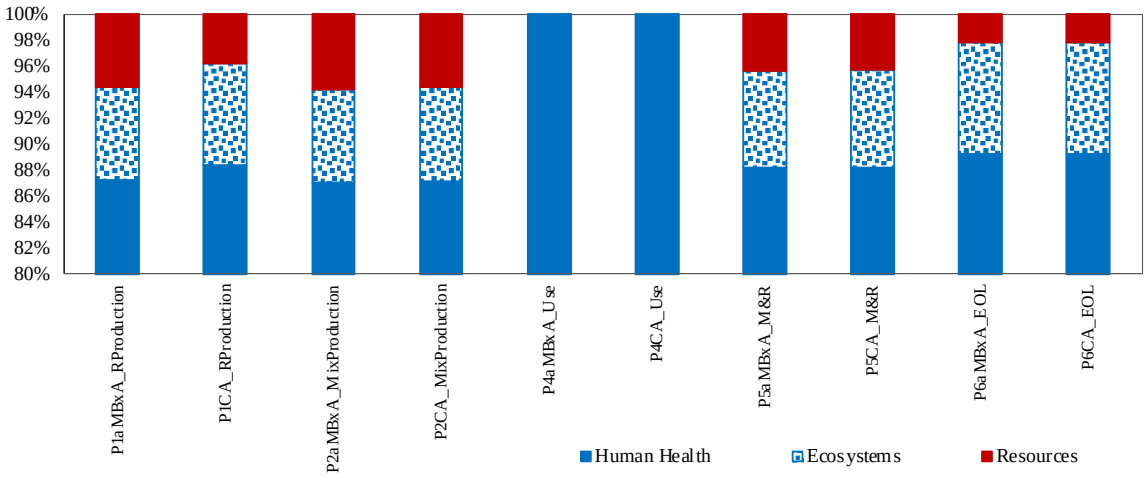

Figure 11-10. Endpoint (single score) impacts for each phase in percentages.

Since the impact of some phases in Figure 11-9 is not easy to see, Figure 11-10 shows the impact of each category assessment by phases. The major impact of the CA and aMBxA alternatives happens on Human Health, after Ecosystems and finally Resources.

11.6.4 Consequential Life Cycle Assessment (CLCA)

Figure 11-11 shows a Consequential analysis along 25 years using the Global Endpoint (H) method. Impacts were normalized, weighted, and distributed along the analysis period. As a result of the implementation of aMBx to produce the aMBxA, additional impacts in the environmental flows are created (i.e., production of aerogel, less need of materials because the better aMBxA durability), however, the avoided impacts are much lower. The overall exercise of aMBx represents around 25% less environmental damage than the Conventional technology.

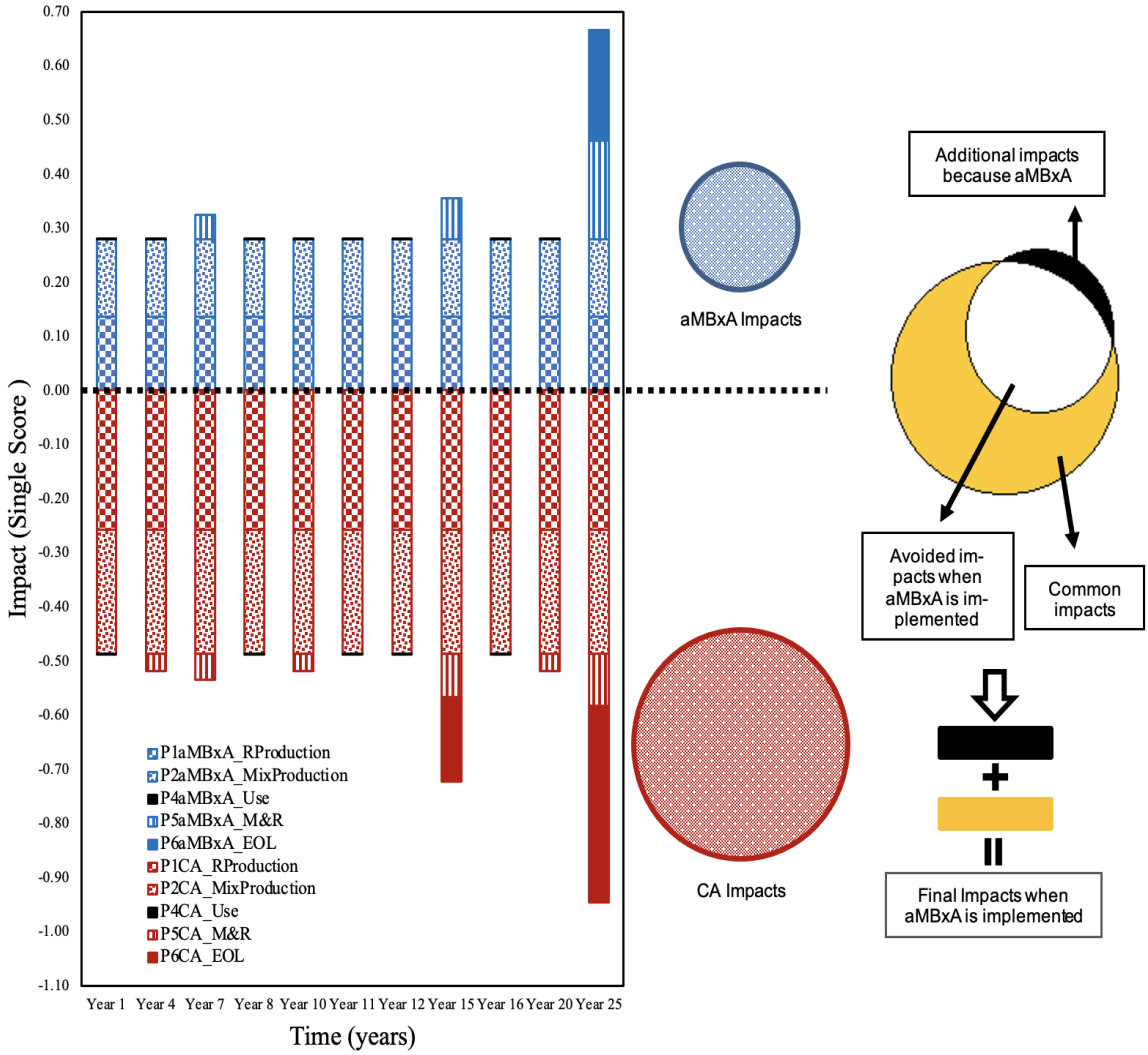

Figure 11-11. Life Cycle for each phase Along 25 Years – CLCA, Normalized and Weighted Emissions.

Despite aMBx's initial costs may be higher than CA's, the fact that there are difficulties related to the construction process, and the lack on normative to control and standardize all processes, utilizing aMBxA instead of CA is good in terms of performance and environmental impacts. As the major outcomes, the implementation of aMBxA in a 25-years analysis window, reduces the consumption of raw aggregates in around 43%, which represent a reduction in terms of Global Warming Potential (GWP) in about 1.178

kg-Co2eq for each Ton of asphalt produced (Park, et al., 2019). Binder use is reduced in about 51% representing a reduction of the GWP in around 7.5 kg-Co2eq for each Ton of asphalt supplied (Yang, et al., 2015). The implementation of aMBx in asphalt pavements not only generates better in-field pavement performance (less maintenance and rehabilitation interventions), less material to divert in the landfills, the reduction of raw aggregates as a long-term consequence, but also the reduction in noise emissions.

According to scientific studies environmental noise is associated to an elevated risk for high blood pressure, and in areas near airports, residents have a higher risk of heart attack and stroke. Noise contamination likewise impacts kids' learning development and growth (Matthews K. , 2018). In this framework, this study found that after a period of 25 years, residents exposed to a traffic noise coming from a CA source could experience a reduction in human life of around 7.4 days. When aMBxA is implemented, this value decreases to 5 days (19% less).

Since aMBxA represents a suitable alternative to use less raw materials, production processes, and less waste materials, the usage of aMBx into the road infrastructure is an approach in contrast to the traditional linear economy, which has a "take, make, dispose" concept of production. The implementation of aMBx fits in the circular economy concept where products, materials, equipment, and infrastructure are used for longer, improving the efficiency of these resources (Ministry of Ecological Transition, 2020). Based on the results of this study, the implementation of aMBxA enables societies and economies to become more sustainable, autonomous and in tune with the environment protection. Involving aMBx in the construction of pavements can provide solutions for the reduction of greenhouse gases emissions.

11.6.5 Life Cycle Cost Analysis (LCCA)

The service life for a conventional asphalt pavement varies depending on the materials quality, construction process and maintenance; generally, the service life can be in the range of 15 to 20 years before a major rehabilitation is needed. Based on the AASHTOWare Pavement ME simulation, parameters such Permanent Deformation, Fatigue, Thermal Cracking and Roughness in terms or International Roughness Index (IRI), the 20% aMBx using a wet method for the incorporation of the aMBx in the mixture showed better service life than the conventional pavement's life. Therefore, it is reasonable to assume that the aMBx pavement would provide at least last 50% longer service life than conventional pavement. First scenario is shown in Table 11-11 and Table 11-12.

Table 11-11. aMBx ($20 kg) and aMBxA (7.5cm) cost estimations.

Item	Cost US$
Raw Aerogel (kg)	20.0
Shiping and Transport (kg)	1.0
Importation Fees (kg)	1.0
Total Cost Raw Aerogel (kg)	**22.0**

Mixture Type	Cost US$ per Ton
Conventional Asphalt Mixture	87.0
20% aMBxA	220.8

Type of mixture	Asphalt Material (m2)	Asphalt Material + Delivery and Installation (m2)
CA	6.63	36.63
aMBxA	16.82	46.82

Binder Cost	Cost US$
Asphalt Binder (ton)	405.0

aMBx (kg)	Amount	Cost US$
Asphalt Binder (kg)	0.55	0.22
Aerogel (kg)	0.45	9.90
Production, Administration (30%)		3.04
Transport (5%)		0.51
Total Cost (kg)		**13.67**

20% aMBxA Quatities	kg	Cost US$
Kg Aggregates per Ton	941.27	
Kg Binder per Ton	48.95	
Kg aMBx per Ton	9.79	133.8
Kg Total	1000.0	

Table 11-12. LCCA considering $20 per kilogram of Aerogel, aMBx cost per kilogram $13.67.

P/F	Years	Conventional	Present Future Cost	Present Value	aMBx	Present Future Cost	Present Value
1.000	0	Initial Construction	36.63	36.63	Initial Construction	46.82	46.82
0.993	3	Crack Sealing (m)	0.95	0.94	No Action	0.00	0.00
0.983	7	CS + Surface Treatment	1.81	1.78	Crack Sealing (m)	0.95	0.93
0.975	10	Crack Sealing (m)	0.95	0.93	No Action		
0.966	14	2.5 cm mill and fill	10.19	9.84	Surface Treatment	0.86	0.84
0.951	20	Crack Sealing (m)	0.95	0.91	Crack Sealing (m)	0.95	0.91
0.939	25	Reconstruction	40.29	37.85	2.5 cm mill and fill	20.39	19.15
0.939	**25**	Salvage	-5.49	-5.16			
		Total Net Present Value (NPV)		**83.72**	**Total Net Present Value (NPV)**		**68.66**
		Equivalent Uniform Annual Costs (EUAC)		**3.46**	**Equivalent Uniform Annual Costs (EUAC)**		**2.84**
0.932	28	Crack Sealing (m)	0.95	0.89			
0.923	32	CS + Surface Treatment	1.81	1.67	Crack Sealing (m)	0.95	0.88
0.916	35	Crack Sealing (m)	0.95	0.87	No Action		
0.905	40	2.5 cm mill and fill	10.19	9.22	Surface Treatment	0.86	0.78
0.883	50	Crack Sealing (m)	0.95	0.84	Reconstruction	50.10	44.22
0.883	50			0.00	Salvage	-4.01	-3.54
0.872	55	Reconstruction	40.29	35.12	Crack Sealing (m)	0.95	0.83
0.872	**55**	Salvage	-5.49	-4.79			
		Total Net Present Value (NPV)		**127.55**	**Total Net Present Value (NPV)**		**111.83**
		Equivalent Uniform Annual Costs (EUAC)		**2.49**	**Equivalent Uniform Annual Costs (EUAC)**		**2.18**

Table 11-13 and 11-14 present the costs of aMBx per kilogram, and aMBxA pavement in m2 when the cost of raw aerogel is $9 kilogram.

Table 11-13. aMBx ($9 kg) and aMBxA (7.5cm) cost estimations.

Item	Cost US$
Raw Aerogel (kg)	9.0
Shiping and Transport (kg)	
Importation Fees (kg)	
Total Cost Raw Aerogel (kg)	**9.0**

Mixture Type	Cost US$ per Ton
Conventional Asphalt Mixture	87.0
20% aMBxA	143.5

Type of mixture	Asphalt Material (m2)	Asphalt Material + Delivery and Installation (m2)
CA	6.63	36.63
aMBxA	10.93	40.93

Binder Cost	Cost US$
Asphalt Binder (ton)	405.0

aMBx (kg)	Amount	Cost US$
Asphalt Binder (kg)	0.55	0.22
Aerogel (kg)	0.45	4.05
Production, Administration (30%)		1.28
Transport (5%)		0.21
Total Cost (kg)		**5.77**

20% aMBxA Quatities	kg	Cost US$
Kg Aggregates per Ton	941.27	
Kg Binder per Ton	48.95	
Kg aMBx per Ton	9.79	56.5
Kg Total	1000.0	

Table 11-14. LCCA considering $9 per kilogram of Aerogel, aMBx cost per kilogram $5.77.

P/F	Years	Conventional	Present Future Cost	Present Value	aMBx	Present Future Cost	Present Value
1.000	0	Initial Construction	36.63	36.63	Initial Construction	40.93	40.93
0.993	3	Crack Sealing (m)	0.95	0.94	No Action	0.00	0.00
0.983	7	CS + Surface Treatment	1.81	1.78	Crack Sealing (m)	0.95	0.93
0.975	10	Crack Sealing (m)	0.95	0.93	No Action		
0.966	14	2.5 cm mill and fill	10.19	9.84	Surface Treatment	0.86	0.84
0.951	20	Crack Sealing (m)	0.95	0.91	Crack Sealing (m)	0.95	0.91
0.939	25	Reconstruction	40.29	37.85	2.5 cm mill and fill	14.50	13.62
0.939	**25**	Salvage	-5.49	-5.16			
		Total Net Present Value (NPV)		**83.72**	**Total Net Present Value (NPV)**		**57.23**
		Equivalent Uniform Annual Costs (EUAC)		**3.46**	**Equivalent Uniform Annual Costs (EUAC)**		**2.36**
0.932	28	Crack Sealing (m)	0.95	0.89			
0.923	32	CS + Surface Treatment	1.81	1.67	Crack Sealing (m)	0.95	0.88
0.916	35	Crack Sealing (m)	0.95	0.87	No Action		
0.905	40	2.5 cm mill and fill	10.19	9.22	Surface Treatment	0.86	0.78
0.883	50	Crack Sealing (m)	0.95	0.84	Reconstruction	43.80	38.66
0.883	50			0.00	Salvage	-3.50	-3.09
0.872	55	Reconstruction	40.29	35.12	Crack Sealing (m)	0.95	0.83
0.872	**55**	Salvage	-5.49	-4.79			
		Total Net Present Value (NPV)		**127.55**	**Total Net Present Value (NPV)**		**95.28**
		Equivalent Uniform Annual Costs (EUAC)		**2.49**	**Equivalent Uniform Annual Costs (EUAC)**		**1.86**

Based on this LCCA, the aMBxA modified pavement would have a life cycle cost 10% lower than the conventional one in the first scenario. In the second scenario, aMBxA is around 17% more cost effective than CA. In both scenarios ($20 kilogram and $9 kilogram of aerogel), even only after a period of 14 years, the aMBxA alternative is more cost effective than CA in about 2%.

It is important to note that this analysis did not take into consideration the users costs associated to the number of maintenance interventions during the analysis period, and the cost related to the environmental impacts, which are significantly higher for the conventional alternative.

11.7 Conclusions

This study shows that the adoption of aMBx asphalt as a standardized paving process will produce a reduction in the impacts for a "cradle to grave" analysis. The impacts categories evaluated showed that phase 1. Materials production, and phase 2. Asphalt pavements mix design/production are the major contributors to environmental impacts in both cases, CA and aMBxA. Damage assessment using the Global Recipe Endpoint method showed that CA impacts 27% more in Human Life than aMBxA. Regarding traffic noise assessment, results presented that aMBxA has about 19% less impact in Human Life compared with CA, then, considering the study period (25 years), a reduction of 1.7dB in noise emission due to the implementation of aMBxA represents a positive impact in Human Life. The total impact in Ecosystems showed that CA has 29% more impact in the extinction rate of species than aMBxA, and in total, CA causes 17% more impact in Resources than aMBx. Consequential assessment showed that the implementation of the aMBx-Asphalt represents a 25% less environmental damage than the Conventional alternative. Despite that aMBx's initial costs are higher than CA', utilizing aMBxA instead of CA is not only good in terms of performance (longer lasting), but also in terms of environmental impacts. The most important factors to make aMBxA a more environmentally friendly alternative compared with CA, is the fact that aMBxA requires less raw material usage, and less mix production due to its better performance (less maintenance and rehabilitation interventions). Based on the LCCA, the aMBxA pavement would have a life cycle cost 10% lower than the conventional one in the first scenario. In the second scenario, aMBxA is around 17% more cost effective than CA. Therefore,

aMBxA represents a suitable alternative to help to build a sustainable society based on a circular model.

Future research should consider the potential effects of friction between vehicle's tires and pavements. Friction depends on various factors such as the characteristics of the pavement's surface, then, different types of pavements have distinct friction coefficients impacting on both fuel consumption and emissions.

CHAPTER 12

CONCLUSIONS

12.1 Summary

Emerging challenges related to environment protection, human development, and society, drive government agencies and the industry to consider new technologies to address these aspects. Currently, there are different modifiers in the asphalt industry to improve the response of the pavement materials. Each technology may be focused on addressing certain asphalt material's weakness, also with different levels of improvement. In this study, a new technology has been developed and tested. The proposed novel technology, called aMBx, is focused on addressing the thermal susceptibility of asphalt materials. The main improvement of this technology is in the bituminous materials' thermal expansion and contraction phenomenon; thus reducing the thermal cracking and providing longer lasting asphalt materials. With the implementation of aMBx, enhancements of permanent deformation, the urban heat island (UHI) phenomenon, and tire/pavement noise reduction have been identified. These improvements cater for longer lasting asphalt materials, with less maintenance interventions along the service life. These benefits have a direct impact in the saving of raw material exploitation, and therefore huge alleviation on environmental impacts, society, and human life. In addition, new test procedures and tools have been developed and tested. This included tests such the thermal conductivity for asphalt binders, the expansion-contraction of solid materials, and a computational tool such as the ACTS Calc, which estimates the pavement's thermal profile and stresses.

12.2 Innovations and Developments

12.2.1 Thermal Conductivity Test for Bituminous Materials

The determination of thermal conductivity of the asphalt binders is very important in the understanding and improvement of its thermal performance. There are very few test methods and equipment to measure thermal conductivity of asphalt binders. Some of those are expensive and require special equipment and instrumentation. In this study it was developed and validated a simplified alternative testing technique to measure thermal conductivity of asphalt binders. This method to estimate thermal conductivity of bitumen samples was found to provide an affordable alternative test procedure with good accuracy and precision. This test procedure was published in the Journal of Testing and Evaluation of the American Society for Testing and Materials (ASTM), DOI: 10.1520/JTE20210208, and currently with a patent application filed in the United States Patent and Trademark Office: serial number 63/146,987 filed on February 8, 2021.

12.2.2 Test Setup for the Thermal Expansion-contraction and the Estimation of the Respective Coefficients

This proposed laboratory test set-up intends to capture the strains that occurs due to the temperature variation along time, and then estimate the linear coefficients of expansion and contraction of asphalt mixture samples. The advantages of this procedure rely on the frictionless test set-up, on the sensibility of the features to accurately capture the data, and on the broad range of temperature to make a proper analysis. After the inducing of expansion and contraction in the asphalt mixtures, it was observed that certain deformation remains, which is the permanent thermal induced deformation (PTID). The

lower the PTID at the end of temperature cycle the more thermal resilient/less thermal susceptible the material

12.2.3 Computational Tool to Estimate the Pavement's Thermal Profile and Stresses

The Asphalt Concrete Thermal Stress Calculation (ACTS Calc) is a software involves and enhances previous research studies on the calculation of the thermal pavement profile using a 1-D semi-infinite thermal model. The pavement thermal profile model considers the heat transfer between the surroundings and the surface of the pavement including convection and radiation. The heat transfer in the pavement, as a semi-infite solid, considerers conduction. The estimation of the pavement's thermal stresses uses mechanical analogs concepts. This tool was done on Jupyter Notebook with a Python kernel, into a Graphical User Interface (GUI) developed with the DearPyGui library. The comparison between field temperature data and the simulated values gives an R^2 of 0.99 with a standard deviation and standard error of 1.5^{o}C and 1.09^{o}C respectively. The accuracy of the thermal profile estimation allows the estimation of a trustful thermal stresses pavement's profile.

12.2.4 Aerogel Modified Bituminous Materials (aMBx)

In this study it has been found that the usage of aerogel in asphalt binders has multiple benefits, however, the process of incorporation aerogel into these materials is not successful because it presents safety concerns as the aerogel particles by themselves, having a very low density, need careful grinding and handling procedures. They are considered hazardous; in the laboratory, they need a fume hood, blast shield, non-

flammable lab coat and specific gloves need to be worn by the user. These issues are magnified in field production at asphalt plants as the light-weight particles can cause dust clouds and ignite with the presence of the tiniest spark.

The concept of using aerogel in asphalt binders and mixtures safely was the focus of this study. It fits the general idea that asphalt binders and mixtures can be modified to reduce thermal cycling in pavements and other materials and increase their durability. The use of pre-treated aerogel composites solves the safety and handling concerns. This invention involved the design, development, and testing of an innovative ultralight product (aMBx) as a modifier in bituminous constituents to function as a high-performance material with unique thermal resistance properties and provide urban cooling benefits. The versatility of this product is such that it is possible to use aMBx in different infrastructure applications. This new technology has a patent application filed in the United States Patent and Trademark Office: serial number 63/210,891 filed on June 15, 2021.

12.3 aMBx-modified Pavement's Surface Temperature Towards Urban Cooling

The results showed that the modified mixtures with aMBx have lower heat transfer and higher heat storage. In Winter, aMBx pavement materials present lower surface temperatures than Control by ~0.3^{o}C during the day and night for thin scenarios, and similar values for thick scenarios. In Summer, results showed in contrast that surface temperatures of materials with aMBx are higher by ~0.26^{o}C compared to Control during the day for both, thin and thick scenarios. During the night, surface temperatures are lower than Control for thin structures by ~0.2^{o}C, and higher by ~0.2^{o}C for thick structures. Then,

the implementation of thin pavements structures (up to 7.5cm thick) modified with aMBx can collaborate the urban cooling during night-time.

Overall, managing pavement surface temperature is concluded to be addressed not only by changing the color of the surface (i.e., changing the Albedo), but also by varying the thermal properties of the pavement materials and overall thickness.

12.4. Thermal Cracking Potential Assessment

The expansion-contraction test showed that the level of strains for mixtures with lower thermal conductivity is also lower (i.e., aMBx pavements). This foretells lower thermal stresses so then lower thermal cracking. All mixtures modified with aMBx have lower α_e and α_c and vary depending on the temperature of the evaluation. The thermal resilience of the 20%aMBx_WM mixture is remarkably better than conventional ones.

Thermal stresses can be understood as tension and compression phenomena and are associated to the presence of heat.

Heat transfer in aMBx pavements, from hot to cold and vice versa, happens at slower pace than conventional pavements, making the aMBx modified mixtures less thermal susceptible. The change from cold to hot and vice versa happens in a smoother way, therefore, trauma associated with temperature changes is less.

The highest thermal stresses are found at the surface of the pavement, however, there is a critical thermal stress zone up to 7 cm below the pavement's surface. In this zone, the pavement is prone to suffer tension and contraction forces in the same day.

Since the thermal cracking can be promoted by the high daily gradient of temperature, a solution to mitigate the proliferation of thermal cracking is to consider mixtures more resilient to temperature change. The geographical regions where the freeze-thaw days per month is high, are the ones where the thermal cracking could flourish mostly if the proper mixture is not chosen. Therefore, the process of a mixture design not only has to consider mechanical aspects, but also the thermal properties of the mixture. To overcome or mitigate the proliferation of thermal cracking and then make longer lasting pavements, it must be considered in the mixture design, properties such as low thermal conductivity, high specific heat capacity and low thermal expansion and contraction coefficients. The estimation and analysis of thermal stresses can be catalogued as a good thermal cracking potential indicator.

12.5 aMBx Modified Asphalt Binders and Mixtures Durability Response

12.5.1 Binders Modified with Aerogel

The outcomes of this investigation are encouraging. The usage of Aerogel made possible to improve the thermal susceptibility of bitumen, which would be advantageous in terms of permanent deformation and thermal cracking, however, the mixing/working temperature of binders with aerogel may be increased to have better workability/fluidity. On the other hand, further investigation needs to be directed to meet the successfully implementation of aerogel in bituminous materials and other possible applications. Mixing procedures need further refining and research to be optimized and standardized. The procedures need to meet all the safety requirements and eliminate the dust formation and

electrostatic discharges. In addition, the homogeneity and right dispersion of the aerogel particles inside the binder must be evaluated and addressed.

The best BBS response for soft binders could be found around 7% of aerogel content, whereas in stiffer binders, the best response could be between 5% and 7% of aerogel content.

Results of thermal conductivity are encouraging. The lower thermal conductivity limits the heat transfer, so then it results into a less thermal susceptible and much more stable asphalt binder.

Results of BBR showed that the binder modified with aerogel becomes stiffer at subzero temperatures without losing the original flexible properties. Based on the results, contrary to the high temperature PG grading, the low temperature PG grading of binders modified with aerogel is not improved, however, it is slightly decreased in about 1.5^{o}C.

Cost is the aspect that stands out in the selection of aerogel. Thermal resistance properties and cost per kilogram of aerogel could determine the suitable aerogel product for further utilization.

12.5.2 Binders Modified with aMBx

Tests results showed that the benefits of using aerogel in asphalt binders (refer Chapter 4) are transferred when the aerogel-based composite, aMBx, is utilized. Important aspects to consider are that the aMBx binders has lower viscosity at high temperatures than the aerogel ones, it could help during the mixing process when working with asphalt mixtures and/or to make more workable modified binders with these modifiers. Low temperature PG grading is not affected respect to control when binders are modified with

aMBx, which represents an advantage in front of the aerogel modification. The usage of aMBx is replicating the aerogel effect in binders and can facilitate the blending with other bituminous materials.

All concerns related to health, security, and workability to make doable the implementation of the aerogel technology in bituminous materials is solved by the implementation of the aMBx composite, which constitutes the most important improvement of aMBx over the aerogel implementation. In other words, the aMBx technology brings the possibility of creating a new generation of bituminous materials with remarkable low thermal susceptibility to build longer lasting road applications.

12.5.3 Mixtures Modified with aMBx

Modified mixtures with aMBx have higher value of SHC, this means that it is needed more energy to heat this type of material but also, more heat storage capacity. The capability to transfer heat is lower for the modified mixtures because the TC is lower when the aMBx is present. Cracking tests such as SCB and fatigue, showed that mixtures modified with aMBx using the wet method (WM) would have similar performance at low temperatures (-10^{o}C) and moderate low temperatures (10^{o}C) than control. Results exposed that the higher the aMBx content in the mixture it behaves stiffer and should perform better than control as the temperature increase. Cracking potential estimation using the indirect tensile strength test considering the moisture effect and freeze-and-thaw process, showed that the addition of aMBx up to 30% do not affect the mixture's response. Analysis based on the E*, G*, and FN suggested that all modified mixtures with aMBx expose better rutting resistance (high temperature response) than control. All results indicated that the

responses of the 20%aMBx_WM mixture is remarkable better than the other considered mixtures. This confirmed that the WM would be the best mechanism to incorporate the aMBx in the mixtures. However, based on the results of HW and SCB analysis, aMBx contents above 20% are not recommended because the possible aMBx's interference in the binder-aggregates bonding mechanism. Looking at the *AASHTOWare Pavement ME* analysis for the two different climates considered (cold and hot), pavements modified with aMBx would perform better than control in distresses related to IRI, permanent deformation, and thermal cracking. 20%aMBx_WM pavements may have 0.15, 0.9, and 8 times better performance than control in IRI, AC permanent deformation and thermal cracking respectively.

12.6 The Interaction of aMBx with Bituminous Materials

Because the physical characteristics of the main constituent of aMBx, aerogel, the heat transfer phenomenon is well reduced. The high stability of bituminous materials (lower deformation and flow) modified with aMBx lies on the lower thermal susceptibly due to the porous/reticulated structure. This concept explains the high response at medium and high temperatures. Also, the aMBx-bitumen reticulated structure provides damping characteristics so then it absorbs better the loading providing higher recovery (less permanent deformation) as shown in Chapter 4. Finally, this porous structure allows a good load distribution when it exits externally (traffic).

12.7 Feasibility Assessment

12.1. Life Cycle Assessment (LCA)

This study shows that the adoption of aMBx asphalt as a standardized paving process will produce a reduction in the impacts for a “cradle to grave” analysis. Damage assessment using the Global Recipe Endpoint method showed that CA impacts 27% more in Human Life than aMBxA. Regarding traffic noise assessment, results presented that aMBxA has about 19% less impact in Human Life compared with CA, then, considering the study period (25 years), a reduction of 1.7dB in noise emission due to the implementation of aMBxA represents a positive impact in Human Life. Consequential assessment showed that the implementation of the aMBx-Asphalt represents a 25% less environmental damage than the Conventional alternative. Despite that aMBx’s initial costs are higher than CA’, utilizing aMBxA instead of CA is not only good in terms of performance (longer lasting), but also in terms of environmental impacts. The most important factors to make aMBxA a more environmentally friendly alternative compared with CA, is the fact that aMBxA requires less raw material usage, and less mix production due to its better performance (less maintenance and rehabilitation interventions).

12.2. Life Cycle Cost Analysis (LCCA)

Based on the LCCA, the aMBxA pavement would have a life cycle cost between 10% and 17% lower than the conventional one. Therefore, aMBxA represents a suitable alternative to help to build a sustainable society based on a circular model.

Future research should consider the potential effects of friction between vehicle’s tires and pavements. Friction depends on various factors such as the characteristics of the

pavement's surface, then, different types of pavements have distinct friction coefficients impacting on both fuel consumption and emissions.

12.8. Future Research

Although a comprehensive study on the development and implementation of the new technology, aMBx, was done in this dissertation, there are opportunities for supplementary studies and improvements.

Additional studies can investigate in details other coatings (as per the patent pending and identified in this study) to manufacture aMBx (i.e., implementation of other types of encapsulators). In this framework, future studies should confirm benefits in terms of field performance of the modified mixtures, costs and environmental impacts.

In addition, a large production effort of aMBx for industrial implementation, and the application of an in-depth LCCA to help promote this new material would be very important to investigate further. Below is an expanded explanation of these future research actions.

- Manufacture aMBx-like material using other type of encapsulators: as described in the patent, the usage of bio-oils and lignin-based products is promising, and preliminary success was achieved by the ASU research group although not reported in this study. The implementation of this alternative materials to manufacture aMBx could decrease the production cost, energy consumption during manufacturing, and

further improve environmental benefits. In this way, aMBx could be totally engrossed in a circular-economy model.

- Fabrication and testing of aMBx manufactured with additional aerogel sources. There are additional available aerogel sources that deserve to be explored further like testing protocols followed in this study.

- Optimize the different methods explored in this study to incorporate the aMBx in the paving mixtures: the optimization of the methods to incorporate the aMBx in asphalt mixtures is an important opportunity. Processes related to the wet and dry methods should be evaluated further, standardized and documented.

- Scale up the production of aMBx: production of aMBx for this study was done at a small laboratory scale. To successfully implement this new technology at an industrial level, scale up machinery is needed to increase the production rate but also ensuring the quality of the final product at the same time. Determining the right equipment and processes for the implementation of aMBx in pavements is crucial to the successful implementation of aMBx. As an example, it may be necessary to implement special production facilities within asphalt plants to better produce and incorporate aMBx into the final asphalt mixtures.

- LCCA: it is recommended to carry out further LCCA based on the additional recommended product manufacturing and field implementation. These additional economic studies will help to determinate the cost-effectiveness of the different scenarios in implementing aMBx in asphalt mixtures. Additional factors related to the users' costs such as the number of maintenance interventions during the analysis period, and the cost related to the environmental impacts, may need to be considered.

REFERENCES

Acharya, A., Joshi, D., & Gokhale, V. (2013). AEROGEL – A Promising Building Material for Sustainable Buildings. *Chemical and Process Engineering Research, 19*.

Adamczak, S., & Bochnia, J. (2016). Estimating the Approximation Uncertainty for Digital Materials Subjected to stress Relaxation Tests. *Metrology and Measurement Systems, 23*(4), 545-553.

ADOT. (2017, May 11). *ADOT's use of rubberized asphalt gives new life to recycled tires*. Retrieved from https://www.azdot.gov/mobile/media/news/2017/05/11/adot-s-use-of-rubberized-asphalt-gives-new-life-to-recycled-tires

Aerogel Technologies. (2004). *What are Aergels?* Retrieved March 8, 2021, from http://www.aerogeltechnologies.com/what-are-aerogels/

Aerogel.org. (2008). *Silica Aerogel*. Retrieved April 3, 2021, from http://web.archive.org/web/20210403170919/https://googleads.g.doubleclick.net/pagead/html/r20210331/r20190131/zrt_lookup.html

Alavi, M., Hajj, E., & Sebaaly, P. (2017). A comprehensive model for predicting thermal cracking events in asphalt pavements. *InternatIonal Journal of Pavement engIneerIng, 8*(9), 871-885.

Altieb, Z., Aziz, M., Bin Kassim, K., & Jibrin, H. (2016). A Short Review on Using Crumb Rubber as Modification of Bitumen Binder. *Jurnal Teknologi - Sciences & Engineering, 78*(7-3), 29-36.

Annenberg Foundation. (2016). Retrieved June 25, 2019, from https://annenberg.org/initiatives/education/annenberg-learner/

Asphalt Institute. (2022). *Individual Asphalt Binder Tests*. Retrieved from Asphalt Institute: https://www.asphaltinstitute.org/laboratory/testing-services/individual-asphalt-binder-tests/

AzariJafari, H., Yahia, A., & Amor, B. (2019). Removing Shadows from Consequential LCA through a TimeDependent Modeling Approach: Policy-Making in the Road. *Environ. Sci. Technol., 53*, 1087−1097. doi:10.1021/acs.est.8b02865

Babashamsi, P., Md Yusoff, N., Ceylan, H., & Md Nor, N. (2016). Evaluation of Pavement Life Cycle Cost Analysis: Review and Analysis. *International Journal of Pavement Research and Technology*, 31.

Baetens, R., Jelle, B., & Gustavsen, A. (2011). Aerogel insulation for building applications: A state-of-the-art review. *Energy and Buildings, 43*, 761–769.

Bartolozzi, I., Antunes, I., & Rizzi, F. (2013, January). Life Cycle Assessment of a Rubberized Asphalt Road in Lamia, Greece. *Fresenius Environmental Bulletin, 22*(7), 2104-2110.

Biligiri, K. (2008). *Asphalt mixtures' properties indicative of tire/pavement noise.* Tempe, AZ: Arizona State University.

Biligiri, K., & Kaloush, K. (2008). Influence of Paving Material Properties on Tire / Pavement Noise. *Annual Meeting of the Transportation Research Board*.

Bruton, E. (2020). *Rubberized Asphalt Benefits and History*. Retrieved June 20, 2021, from https://asphaltplus.com/rubberized-asphalt-history/

Cabot Corporation. (2013). *Enova Aerogel, Brochure.* Billerica, USA.

Carlson, J., Bhardwaj, R., Phelan, P., Kaloush, K., & Golden, J. (2010). Determining Thermal Conductivity of Paving Materials Using Cylindrical Sample Geometry. *ASCE Journal of Materials in Civil Engineering, 22*(2), 186-195.

Chadbourn, B. A. et al., 1999. The Effect of Voids in Mineral Aggregate (VMA) on Hot- Mix Asphalt Pavements, Minneapolis: Minesota Departament of Transportation.

Chehovits, J., & Galehouse, L. (2010). Energy Usage and Greenhouse Gas Emissions of Pavement Preservation Processes for Asphalt Concrete Pavements. *First International Conference on Pavement Preservation*, (pp. 27-42). Newport Beach CA, United States.

Chen, J., Wang, H., & Zhu, H. (2017). Analytical approach for evaluating temperature field of thermal modified asphalt pavement and urban heat island effect. *Applied Thermal Engineering, 113*, 739-748.

Collins, J., Bouldin, M., Gelles, R., & Berker, A. (1991). mproved performance of paving bitumens by polymer modification. *Journal of the Association of Asphalt Paving Technologists, 60*, 43-79.

Corbisier, C. (2003, August). *Living With Noise.* Retrieved November 2020, from https://www.fhwa.dot.gov/publications/publicroads/03jul/06.cfm

Corté, J.-F. (2020). Mastering bitumen for better roads and innovative applications. (Courcera, Ed.) France: Coursera.

Côté, J., Grosjean, V., & Konrad, J.-M. (2013). Thermal conductivity of bitumen concrete. *Canadian Journal of Civil Engineering, 40*, 172-180.

Czichos , H., Saito, T., & Smith, L. (Eds.). (2006). *Springer Handbook of Materials Measurement Method.* New York: Springer Science & Business Media.

Dave, E., & Hoplin, C. (2015, January 23). Flexible pavement thermal cracking performance sensitivity to fracture energy variation of asphalt mixtures. *Road Materials and Pavement Design, 16,* 423-441.

DeCarlo, C., Mo, W., Dave, E., & Locore, J. (2017). Sustainable pavement rehabilitation strategy using consequential life cycle assessment: An example of interstate 95. *The 10th International Conference on the Bearing Capacity of Roads, Railways and Airfields (BCRRA 2017).* doi:10.1201/9781315100333-311

DeDene, C., Gorman, J., Marasteanu, M., & Sparrow, E. (2016). Thermal conductivity of reclaimed asphalt pavement (RAP) and its constituents. *International Journal of Pavement Engineering, 17*(5), 435-439.

Doka, G. (2003). Ergaenzung der Gewichtungsmethode für Oekobilanzen Umweltbelastungspunkte' 97 zu Mobilitaets - UBP'97, Doka LCA. Zurich, Switzerland. Retrieved November 10, 2020, from https://www.doka.ch/mubp/AstraMUBP97DOKAv2.pdf

Dowson ,, M., Harrison, D., Craig, S., & Gill, Z. (2011). Improving the thermal performance of single-glazed windows using translucent granular aerogel. *International Journal of Sustainable Engineering , 4*(3), 266-280.

Ekvall, T. (2019). Attributional and Consequential Life Cycle Assessment. In *Sustainability Assessment at the 21st Century*.

Element. (2022). *Scanning Electron Microscopy (SEM) with EDX Analysis*. Retrieved February 2022, from https://www.element.com/materials-testing-services/scanning-electron-microscopy-sem

Engineering ToolBox. (2003). *Specific Heat of Solids*. Retrieved February 20, 2021, from http://web.archive.org/web/20210330044802/https://www.engineeringtoolbox.com/specific-heat-solids-d_154.html

Engineering ToolBox. (2003). *Thermal Conductivity of selected Materials and Gases*. Retrieved December 7, 2019, from http://web.archive.org/web/20210330045112/https://www.engineeringtoolbox.com/thermal-conductivity-d_429.html

Engineering ToolBox. (2011). *Plastics - Thermal Conductivity Coefficients*. Retrieved November 20, 2019, from

http://web.archive.org/web/20210330050557/https://www.engineeringtoolbox.com/thermal-conductivity-plastics-d_1786.html

EPA. (2018). *Inventory of U.S. Greenhouse Gas Emissions and Sinks: 1990-2016*. Retrieved July 15, 2019, from https://www.epa.gov/ghgemissions/inventory-us-greenhouse-gas-emissions-and-sinks-1990-2016

Farina, A., Zanetti, M., Santagata, E., & Blengini, G. (2017). Life cycle assessment applied to bituminous mixtures containing recycled materials: Crumb rubber and reclaimed asphalt pavement. *Resources, Conservation and Recycling , 117*, 204-212.

FHWA. (2001, February). Mix Design. *Superpave Mixture Design Guide*. Washington, DC: U.S. Department of Transportation.

FHWA. (2011). *Reclaimed Asphalt Pavement in Asphalt Mixtures: State of the Practice.* McLean, VA.

FHWA. (2014). *The Use of Recycled Tire Rubber to Modify Asphalt Binder and Mixtures - FHWA-HIF-14-015.* U.S: U.S Department of Transportation.

FHWA. (2017). *Superpave Fundamentals, Reference Manual.* U.S. Department of Transportation, NHI Course #131053.

Finnveden, G., Hauschild, M., Ekvall, T., Guinée, J., Heijungs, R., & Hellweg, S. (2009). Recent developments in life cycle assessment. *Journal of Environmental Management, 91*(1), 1-21. doi:: 10.1016/j.jenvman.2009.06.018

Gangaram, R. (2014). Eenrgy and Emssion Impact Quantification of Pavement Preservation Using Life Cycle Assessment. New Brunswick, New Jersey: Rutgers, The State University of New Jersey.

Garraín, D., Franco, V., Vidal, R., Moliner, E., & Casanva , S. (2008). The noise impact category in Life Cycle Assessment. Zaragoza: 12th International Congress on Project Engineering.

Ghose, A., Pizzol, M., & McLarenab, S. (2017). Consequential LCA modelling of building refurbishment in New Zealand- an evaluation of resource and waste management scenarios. *Journal of Cleaner Production, 165*, 119-133. doi:doi.org/10.1016/j.jclepro.2017.07.099

Goodfellow. (2019). *"Polymethylmethacrylate - online catalogue source - supplier of research materials in small quantities*. Retrieved November 20, 2019, from http://web.archive.org/web/20210330050225/https://www.google-analytics.com/ga.js

Gordon , D. (2002). heological evaluation of ethylene vinyl acetate polymer modified Bitumens. *Construction and Building Materials, 16,* 473-487.

Grupa, T. (2020, December 17). *How much does asphalt cost?* Retrieved February 2022, from HomeGuide: https://homeguide.com/costs/asphalt-prices

Gui, J., Phelan, P., Kaloush, K., & Golden, J. (2007). Immpact of Pavement Thermophysical Properties on Surface Temperatures. *Journal od Materials in Civil Engineering. ASCE, 19*(8), 683-690.

Happold, B. (2020, September 15). *Designing Buildings Wiki*. Retrieved April 2021, from Aerogel Isulation for Buildings: http://web.archive.org/web/20210410225715/https://www.designingbuildings.co.uk/wiki/Aerogel_insulation_for_buildings

Hardman, H. F., Hughes, E., & Franklin , V. (1956). *U.S, Lyndhurst, Ohio Patent No. 2,759,842.*

Harvey, J., Meijer, J., Ozer, H., Al-Qad, I., Saboori, A., & Kendall, A. (2016). *Pavement Life-Cycle Assessment Framework.* Federal Highway Administration.

Haselbach, L. (2009). Pervious Concrete and Mitigation of the Urban Heat Island Effect. *Proceedings; Transportation Research Board Annual Meeting.* Washington DC: Transportation Research Board of the National Academies.

Haslett, K., Dave, E., & Mo, W. (2019). Consequential Life Cycle Assessment-based Pavement . Waterloo.

Heijungs, R., & Cucurachi, S. (2017). Life Cycle Assessment of Noise Emissions: Comment on a Recent Publication. *Environ Model Assess, 22,* 183-184.

Hinislioglu, S. (2011). Optimization of the temperature susceptibility of bitumen modified with waste tire rubber by Taguchi method. *Journal of Science and Technology, 4*(1), 99-110.

Hinterhoelzl, R., & Schapery, R. (2004, March). FEM Implementation of a Three-Dimensional Viscoelastic Constitutive Model for Particulate Composites with Damage Growth. *Mechanics of Time-Dependent Materials, 8*(1), 65-94.

Holman, J. (2010). *Heat Transfer* (Tenth Edition ed.). New York: McGraw-Hill.

Islam, M., & Tarefder, R. (2015). Coefficients of Thermal Contractio and Expansion of Asphalt Concrete in the Laboratory. *Journal of Materials in Civil Engineering*, 1-6.

Islam, R., & Tarefder, R. (2014). Determining Coefficients of Thermal Contraction and Expansion of Asphalt Concrete Using Horizontal Asphalt Strain Gage. *ASTM - Advances in Civil Engineering Materials, 3*(1), 203-219.

Kotlarewski, N., Ozarska, B., & Gusamo, B. (2014). Thermal Conductivity of Papua New Guinea Balsa Wood Measured using the Needle Probe Procedure. *BioResources, 9*(4), 5784-5793.

Kua, H., & Lu, Y. (2016). Environmental impacts of substituting tempered glass with. *Journal of Cleaner Production, 137*, 910-921. doi:doi.org/10.1016/j.jclepro.2016.07.171
Kuennen, T. (2004). *Asphalt Rubber Makes a Quiet Comeback.* Better Roads Magazine.

Liao, J.-j., Gao, P.-z., Xu, L., & Feng, J. (2018). A study of morphological properties of SiO2 aerogels obtained at different temperatures. *Journal of Advanced Ceramics, 7*(4), 307-316.

Lienhard IV, J., & Lienhard V., J. (2003). *A Heat Transfer Texbook.* Cambridge, Massachusetts, U.S.A.: Phlogiston Press. Retrieved November 2019, from http://coolcosmos.ipac.caltech.edu/cosmic_classroom/light_lessons/thermal/transfer.html

Ling, M., Chen, Y., Hu, S., Luo, X., & Lytton, R. (2019, February 15). Enhanced model for thermally induced transverse cracking of asphaltpavements. *Construction and Building Materials, 206*, 130-139.

Mallick, R., & El-Korchi, T. (2018). *Pavement Engineering, Principles and Practice* (Third ed.). Taylor & Francis Group.

Mamlouk, M., Witczak, M., Kaloush, K., & Hasan, N. (2005, March). Determination of Thermal Properties of Asphalt Mixtures. *Journal of Testing and Evaluation, 33*(2), 15.
Marathon Petroleum. (2018). *Asphalt, Emultions and Roofing*. Retrieved June 10, 2021, from http://web.archive.org/web/20210612023356/https://www.mpcasphalt.com/Products/

Maricopa Association of Gobernments & KimleyHorn. (2019). *ADOT Roadway Maintenance Costs.* Tempe.

Matthews, H., & Hendrickson, C. (2001). Economic and Environmental Implications of Online Retailing in the United States.

Matthews, K. (2018). *Why We Need to Reduce Noise Levels in Cities*. Retrieved August 30, 2021, from Planetizen: https://www.planetizen.com/blogs/96881-why-we-need-reduce-noise-levels-cities

Mills, A. (1999). *Heat Transfer* (Second Edition ed.). New Jersey: Prentice-Hall.

Ministry of Ecological Transition. (2020, November 4). *Circular economy*. Retrieved August 30, 2021, from https://www.ecologie.gouv.fr/leconomie-circulaire

Minnesota Asphalt Pavement Association. (2008, 12 30). *Comprehensive Guide to PG Asphalt Binder Selection in Minnesota.* Retrieved January 2022, from https://cdn.ymaws.com/www.asphaltisbest.com/resource/resmgr/resources-economics/articles_and_flyers/guide_pg_binder_selection_mn.pdf

Mohesnin, N. (Ed.). (1980). *ThermalPropertiesofFoodAndAgriculturalMaterials* (1 ed.). New York: Gordon and Breach Science Publishers.

Mukherjee, A. (2016). *Life Cycle Assessment of Asphalt Mixtures in Support of an Environmental Product Declaration.* Houghton.

NASA. (2017). *Aerogels: Thinner, Lighter, Stronger*. Retrieved April 2021, from http://web.archive.org/web/20210403171735/https://www.nasa.gov/topics/technology/features/aerogels.html

Nuclear Power. (2022). *Aerogel - Thermal Isulation*. Retrieved February 2022, from https://www.nuclear-power.com/nuclear-engineering/heat-transfer/heat-losses/insulation-materials/aerogel/

Obando, C., & Kaloush, K. (2021). Estimating the Thermal Conductivity of Asphalt Binders. *Journal of Testing and Evaluation (ASTM), 50*(2), 13.

Obando, C., Kaloush, K., & Ozer, H. (2021). Asphalt Concrete Thermal Stress Calculation (ACTS Calc) Software . Tempe: 18th Arizona Pavement and Materials Conference.

Obando, C., Karam, J., Castro, S., Medina, J., & Kaloush, K. (2021). *Portrayal and Durability Assessment of Novel Silica-Based Modified Asphalt Pavements.* Tempe.

Obando, C., Karam, J., Medina, J., & Kaloush, K. (2022). *Analysis of the Temperature Profile of Modified Pavements* . Arizona State University (ASU), Tempe.

Ohanian, H., & Markert, J. (2007). *Physics For Engineers and Scientists* (Third Edition ed.). New York, USA: W.W Norton & Company.

Olidid, C., & Hein, D. (2004). *Guide for the Mechanistic-Empirical Design of New and Rehabilitated Pavement Structures.* Transportation Association of Canada (TAC).

Ortíz Rodríguez, O., Ocampo Duque, W., & Duque Salazar, L. (2017, December 13). Environmental Impact of End-of-Life Tires: Life Cycle Assessment Comparison of Three Scenarios from a Case Study in Valle Del Cauca, Colombia. *Energies, 10*, 1-13.

Osterkamp , T., & Baker, G. (1986). Measurments of the Linear Thermal Expansion Coefficients of Asphalt Pavement at Low Temperatures. *Cold Regions Science and Technology, 12*, 299-301.

Ozer, H. (2014). 3-D Generalization and Pseudo Variables.

Ozer, H. (2020). Part 1: Viscoelasticity L02: Integral Operators and Standard Excitations.

Ozer, H. (2020). Viscoelastic Material Model (Based on Abaqus Viscoelasticity Documentation and Hinterhoelzl and Schapery).

Padilha Thives, L., & Ghisi, E. (2017). Asphalt mixtures emission and energy consumption: A review. *Renewable and Sustainable Energy Reviews, 72*, 473–484.

Park, S. & Kim, Y., 1999. Interconversion between Relaxation Modulus and Creep Compliance for Viscoelastic Solids. Journal of Materials, February, 11(1), pp. 76-82.

Pavement Interactive, 2021. Theoretical Maximun Specific Gravity. [Online] Available at: https://pavementinteractive.org/reference-desk/testing/asphalt-tests/theoretical-maximum-specific-gravity/

Pekala, R. (1989, September). Organic aerogels from the polycondensation of resorcinol with formaldehyde. *Journal of Materials Science, 24*, 3221–3227.

Prasada, R., Rangaraju, S., & Guven, Z. (2008). *Life Cycle Cost Analysis Pavement Type Selection.* Final Report, Report No.FHWA-SC-08-01, SCDOT.

Purdue University. (2019). *Scanning Electron Microscope*. Retrieved February 2022, from https://www.purdue.edu/ehps/rem/laboratory/equipment%20safety/Research%20Equipment/sem.html

Roberts, F., Kandhal, P., Brown, E., Lee, D.-Y., & Kennedy, T. (1996). *Hot Mix Asphalt Materials, Mixture Design and Construction. Second Edition.* Lanham, MD , United States: NAPA Education Foundation.

Roylance, D. (2001). Engineering Viscoelasticity. Massachusetts Institute of Technology.
Santero, N., Masanet, E., & Horvath, A. (2010). *Life Cycle Assessment of Pavements: A Critical Review of Existing Literature and Research.* Department of Energy.

Schapery, R. (1975, February). A theory of crack initiation and growth in viscoelastic media. *Int J Fract, 11*(1), 141-159.

Schapery, R. (1975, June). A theory of crack initiation and growth in viscoelastic media II. Approximate methods of analysis. *Int J Fract, 11*(3), 369-388.

Schapery, R. (1984, July). ‘Correspondence principles and a generalizedJ integral for large deformation and fracture analysis of viscoelastic. *Int J Fract, 25*(3), 195-223. doi:10.1007/BF01140837

Schapery, R. (1999, April). Nonlinear viscoelastic and viscoplastic constitutive equations with growing damage. *International Journal of Fracture, 97*(1), 33-66. doi:10.1023/A:1018695329398.

Sen, S. (2015). Impact of Pavements on The Urban Heat Island. Urbana, Illinois, USA: University of Illinois at Urbana-Champaign.

ShengYue, W., QiYang, Z., YingNa, D., & PeiDong, S. (2013). Unidirectional heat-transfer asphalt pavement for mitigating the urban heat island effect. *Journal of Materials in Civil Engineering*.

SimScale. (2017). *Initial Boundary Value Problem (IBVP)*. Retrieved 2020, from https://www.simscale.com/forum/t/initial-boundary-value-problem-ibvp/66562

Speight, J. (2017). *Rules of Thumb for Petroleum Engineers.* John Wiley & Sons.

Stempihar, J., Pourshams-Manzouri, T., Kaloush, K., & Rodezno, M. (2012). Porous Asphalt Pavement Temperature Effects on Overall Urban Heat Island. *Proceeding of the 91st Annual Meeting of the Transportation Research Board.* Washington DC.: Transportation Research Board of National Academies.

Stokstad, E. (2020, September 3). *It’s not just cars that make pollution. It’s the roads they drive on, too*. Retrieved November 2020, from Science: https://www.sciencemag.org/news/2020/09/it-s-not-just-cars-make-pollution-it-s-roads-they-drive-too

Stripple, H. (2001). *Life Cycle Assessment of Road, A Pilot Study for Inventory Analysis* (Second Revised Edition ed.). Gothenburg, Sweden: IVL Swedish National Road Administration.

The Engineering ToolBox. (2003). *Electrical Equipment typical Power Consumption*. Retrieved February 2, 2022, from https://www.engineeringtoolbox.com/electrical-equipment-power-consumption-d_119.html

Thomas. (2019, December 19). *These 5 Innovative Materials Are Changing the World*. Retrieved April 3, 2021, from http://web.archive.org/web/20210403164844/https://www.thomasnet.com/insights/these-5-innovative-materials-are-changing-the-world/

Thomas, G. (2012, August 22). *What is Aerogel? Theory, Properties and Applications*. (AZO Materials) Retrieved March 2021, from https://www.azom.com/article.aspx?ArticleID=6499

Tomas, G. (2012, August 22). *What is Aerogel? Theory, Properties and Applications*. Retrieved 2019, from AZO Materials: https://www.azom.com/article.aspx?ArticleID=6499

U.S Department of Transportation. (2016). *Pavement Life Cycle Assessment Framework.* Washington D.C.

U.S. Department of transportation. (2019, March 5). *LTPP InfoPave*. Retrieved from https://infopave.fhwa.dot.gov/Media/AdvancedVisualization#
Vimmrová, A., & Výborný, J. (2002). *Building Materials 10: Materials and Testing Methods.* Vydavatelství ČVUT.

Vinson, T., & Janoo, V. (1989). SHRP-A-306 "Low Temperature and Thermal Fatigue Cracking. *Transportation Research Board*.

Virginia Asphalt Association. (2020). *The History of Asphalt*. Retrieved January 2020, from http://web.archive.org/web/20210409052653/https://vaasphalt.org/the-history-of-asphalt/

Wagle, R. (2020, Ausgust 24). Production of AP8b (C. Obando, Interviewer)

Walker, D. (2021). *The benefits of modified asphalts*. (Asphalt Institute) Retrieved February 2022, from Asphalt, The Magazine of The Asphalt Institute: http://asphaltmagazine.com/the-benefits-of-modified-asphalts/

Walls, J., & Smith, M. (1998). *Report No. FHWA-SA-98-079, Life-Cycle Cost Analysis in Pavement Design- Interim Technical Bulletin.* Washington, DC: Federal Highway Administration.

Welty, J., Wilson, R., & Wicks, C. (1997). *Fundamentals of Momentum, Heat, and Mass Transfer.* (Limusa, Ed.)

Witczak, M., Roque, R., Hiltunen, D., & Buttlar, W. (2000). *Modification and Re-Calibration of SUPERPAVE Thermal Cracking Model. NCHRP 9-19.* Arizona State University, Tempe.

Witczak, W. (2004). *Development of a Master Curve (E*) Database for Lime Modified Asphalt Mixtures.* Tempe, AZ: Arizona State University.

World Health Organization. (2014). World Halth Statistics 2014.

Ye, J., Zhang, Z., & Chu, Y. (2011). Strength behavior and collapse of spatial-reticulated structures under multi-support excitation. *Sci China Tech Sci, 54*(6), 1624-1638.

Yoder, E., & Witczak, M. (1975). *Principles of Pavement Design.* John Wiley & Sons, Inc.

Yuksel N. (2016). The Review of Some Commonly Used Methods and Techniques to Measure the Thermal Conductivity of Insulation Materials. In *Insulation Materials in Context of Sustainability.*

Yuksel, Avci, Kilic. (2012). The effective thermal conductivity of insulation materials reinforced with aluminium foil at low temperatures. *Heat and Mass Tranfer*, 1569-1574.

Yuksel, N. (2010). *The investigation of structure and operating parameters effect on the heat transfer coefficient in porous structures.* Bursa: Uludag University.

Zhu, J., Birgisson, B., & Kringos, N. (2014). Polymer Modification of Bitumen: Advances and Challenges. *European Polymer Journal, 54*, 18-38.

APPENDIX A

ASPHALT CONCRETE THERMAL STRESS CALCULATION (ACTS CALC) SOFTWARE – MANUAL

Documentation and Tutorial

This software is the result of the application and optimization of earlier studies about pavement's temperature profile and pavement's thermal-stresses calculation. This tool was realized on "Jupyter" using a "python kernel" into a Graphical User Interface (GUI) developed with the "DearPyGui" library (https://github.com/hoffstadt/DearPyGui). The goal is to estimate the thermal stresses due to the environment's temperature oscillation.

In this "pre-release" version, the pavement thermal profile is calculated using a complex model, which includes the effect of (Gui J. , Phelan, Kaloush, & Golden, Impact of Pavement Thermophysical Properties on Surface Temperatures, 2007):

- Radiation: incoming solar energy and outcoming infrared radiation (albedo)
- Convection: heat exchanges with air, considering wind velocity and the occurrence of turbulence (if needed)
- Conduction: heat transfer into the ground (semi-infinite solid)

The implied model allows the obtention of an accurate thermal profile because the implementation of the different physical phenomena accounting for heat exchanges between the asphalt and its surroundings (Gui J. , Phelan, Kaloush, & Golden, Impact of Pavement Thermophysical Properties on Surface Temperatures, 2007). Thus, the thermal stresses results configure a better approximation than an eventual one based on a simplified thermal model.

In the beginning, the software presents a "start page", on this, the "readme" and "about" sections are available on top of the screen. In the bottom of the page, the user can select a full calculation of thermal profile + thermal stresses or only the study of the thermal

profile. To start the analysis, the user must pick in the start button. Figure A-1 presents the start page of the software.

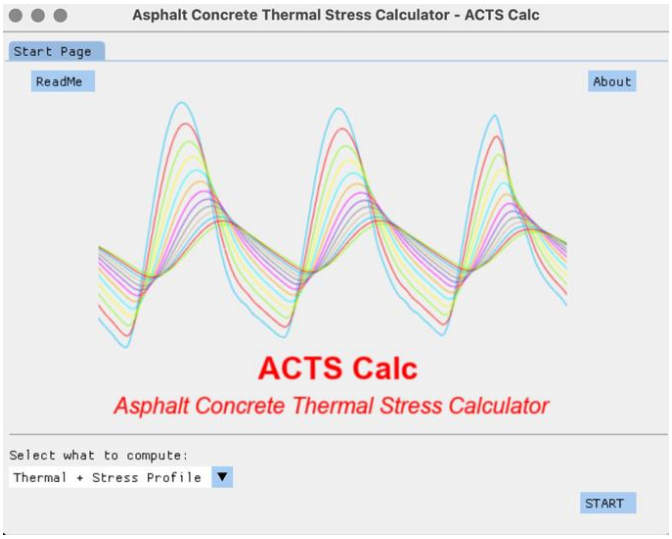

Figure A-1. Start Page

The different steps necessary to obtain the asphalt-pavement's stress profile are described below, alongside all mathematical equations and scientific background utilized.

I. Thermal Model

a. Thermal Model Inputs

To properly run the physical thermal model, various inputs are needed. First, the user is asked to fill an Excel table called "weather.xlsx" with weather data. This table needs meteorological measurements between 1 to 3 days (refer Figure A-2). Each day must be filled in a separated tab of the file. The required data are:

- The measured time stamp [h]
- The atmospheric temperature [ºC]

- The dew point temperature [ºF]
- The solar irradiance [W/m²]
- The wind velocity [mph]

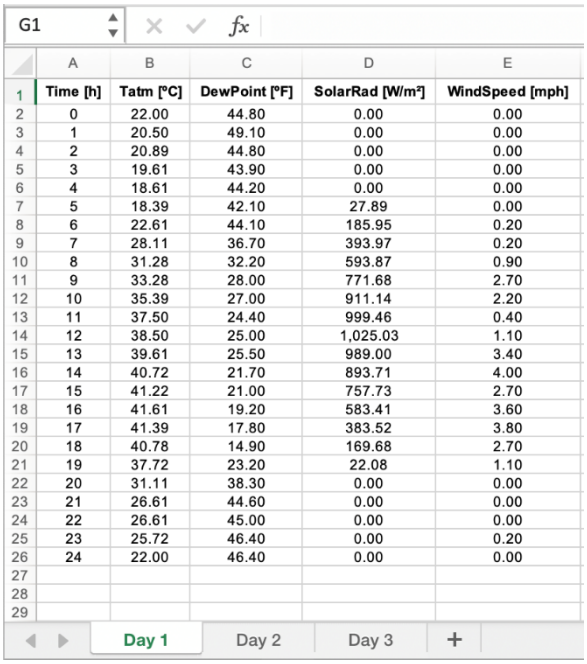

	A	B	C	D	E
1	Time [h]	Tatm [ºC]	DewPoint [ºF]	SolarRad [W/m²]	WindSpeed [mph]
2	0	22.00	44.80	0.00	0.00
3	1	20.50	49.10	0.00	0.00
4	2	20.89	44.80	0.00	0.00
5	3	19.61	43.90	0.00	0.00
6	4	18.61	44.20	0.00	0.00
7	5	18.39	42.10	27.89	0.00
8	6	22.61	44.10	185.95	0.20
9	7	28.11	36.70	393.97	0.20
10	8	31.28	32.20	593.87	0.90
11	9	33.28	28.00	771.68	2.70
12	10	35.39	27.00	911.14	2.20
13	11	37.50	24.40	999.46	0.40
14	12	38.50	25.00	1,025.03	1.10
15	13	39.61	25.50	989.00	3.40
16	14	40.72	21.70	893.71	4.00
17	15	41.22	21.00	757.73	2.70
18	16	41.61	19.20	583.41	3.60
19	17	41.39	17.80	383.52	3.80
20	18	40.78	14.90	169.68	2.70
21	19	37.72	23.20	22.08	1.10
22	20	31.11	38.30	0.00	0.00
23	21	26.61	44.60	0.00	0.00
24	22	26.61	45.00	0.00	0.00
25	23	25.72	46.40	0.00	0.20
26	24	22.00	46.40	0.00	0.00
27					
28					
29					

Figure A-2. Meteorological inputs in Excel

The user can validate if the information was uploaded correctly in the software (refer Figure A-3).

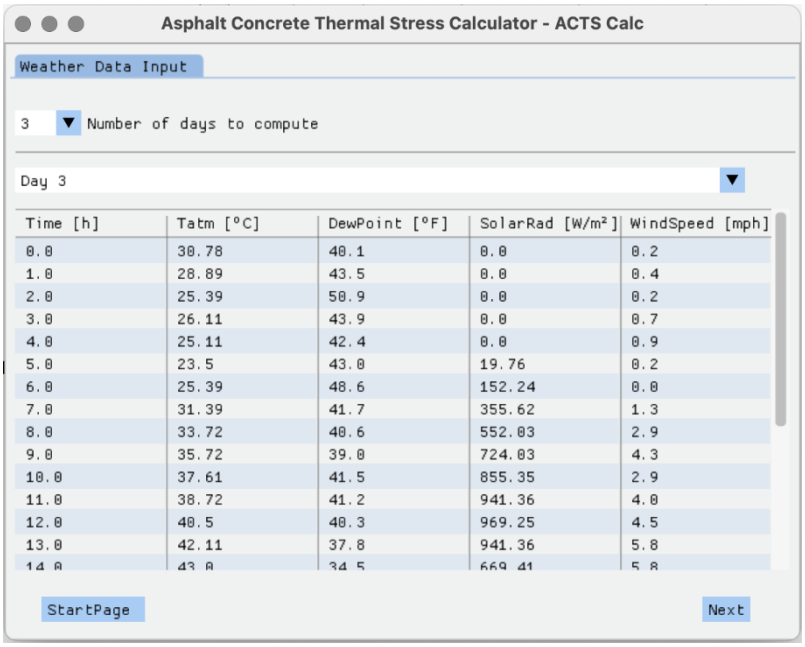

Figure A-3. Uploaded meteorological inputs in the software

By clicking the “Next” button, the user validates the importation, and a verification process is realized onto the imported weather data to prepare it for future use in the thermal model. Initially, an approximation of the wind velocity data is done. A cubic polynomial fit is applied to the measured data to smooth it without losing relevant information. The results of the fitting process are displayed graphically (refer Figure A-4), the acquired parameters as well as the R^2 error are shown for each of the 3 days.

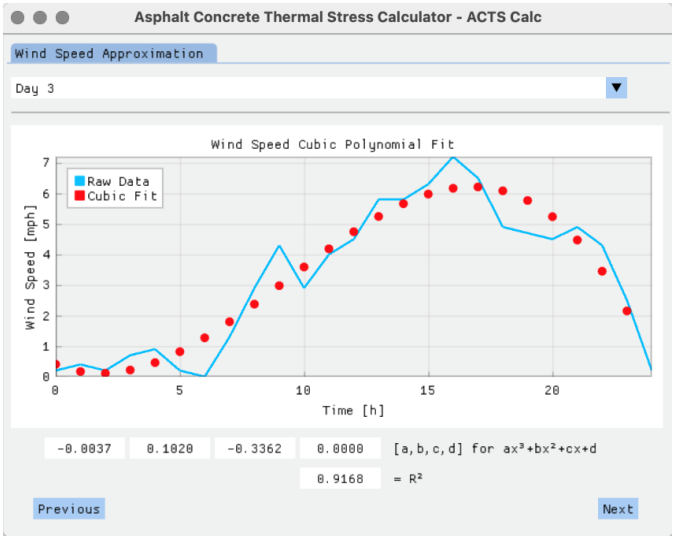

Figure A-4. Graphical fitting process

Depending on the number of days to compute, a "stitching process" could be needed between the day-by-day data (refer Figure A-5). This process is automatically done, and the results shown. In this time, the wind speed used is the one obtained after the cubic polynomial fit.

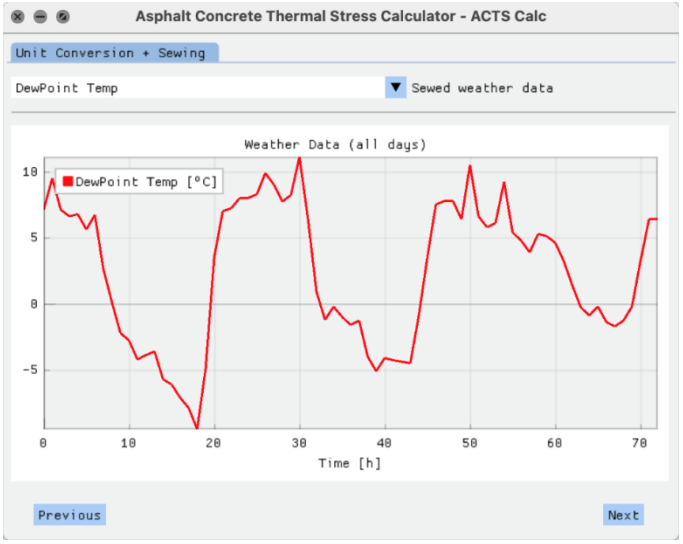

Figure A-5. Sewed weather data

In the next step, the user needs to enter the calculation parameters to perform the thermal profile estimation (refer Figure A-6). These are:

- The discrete time-step [s]
- The discrete spatial-step [m]
- The number of layers in the model [2-5]: There are at least two layers, the Hot Mix Asphalt (HMA) layer and the ground layer. However, the user can choose to include 3 more layers in-between those two (these could be old-HMA layers or other relevant soil information). The drop-down menu automatically updates the next windows, so the user can input material properties data for each of the layers
- The surface material and characteristic properties, including:

  - surface albedo (0-1)

  - surface emissivity (0-1)

  - sky view-factor (0-1)

  - solar view-factor (0-1)

  - characteristic length (for convection modelling) [m]
- The deep-ground properties, namely:

  - Deep-ground temperature [ºC]

  - Maximum ground depth [m]

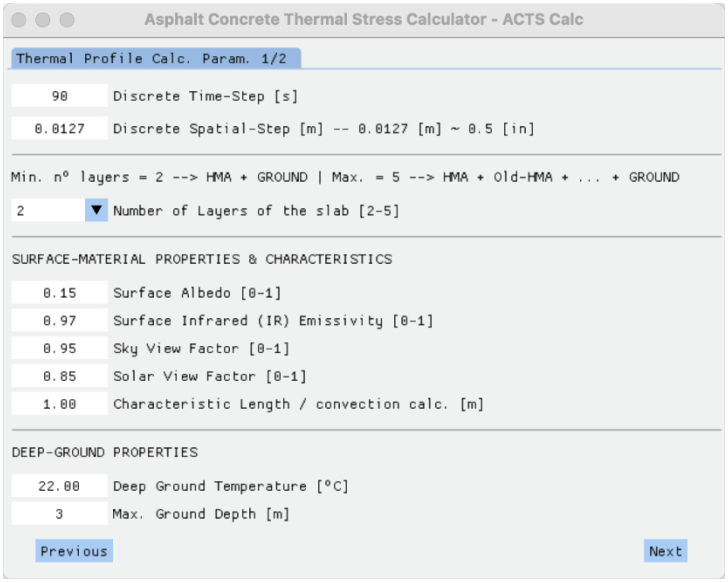

Figure A-6. Thermal Calculation Parameters

As previously said, depending on the number of layers defined, a dynamic table appears to input the layer properties (refer Figure A-7). The columns are organized left to right, from the surface layer to the subgrade. For all layers, the following properties are needed:

- Density [kg/m^3]
- Specific heat capacity [J/kg^{o}K]
- Thermal conductivity [W/m^{o}K]

For non-ground layers, two more properties are need:

- The layer thickness [m]
- The thermal contact resistance between this layer and the adjacent one (0-1). The thermal contact resistance corresponds to the resistance between asphalt and subgrade.

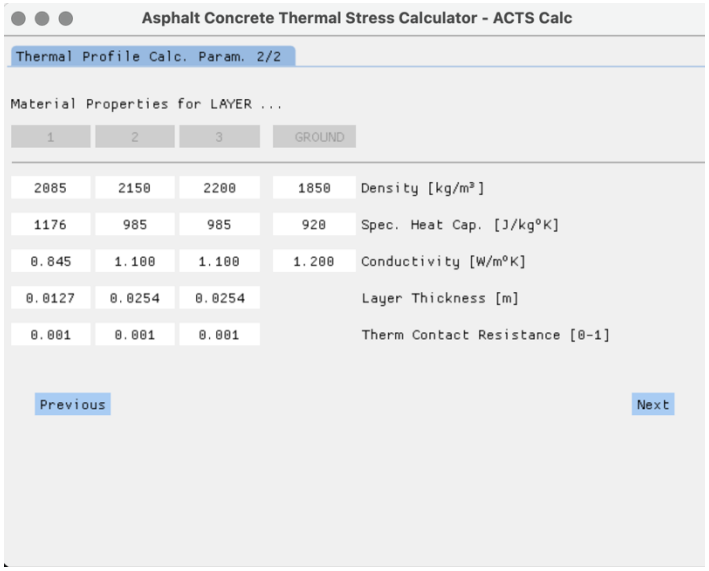

Figure A-7. Layer Properties

b. Thermal Model - Calculation Process & Results

Once validated the model parameters and material properties, the calculation begins. The physical model is solved using a "*Forward-Time Centered-Space Finite Difference*" method. The system of equation used induces recurring terms, it means that some equations use temperature results calculated at the same time-step, which themselves depend on these equations. The thermal profile will converge to the definitive solution at each step. Thus, an iterative process is needed to solve the problem. Figure A-8 shows how the calculation ongoing, and convergence is visualized numerically in the program, along with some "important event" notifications.

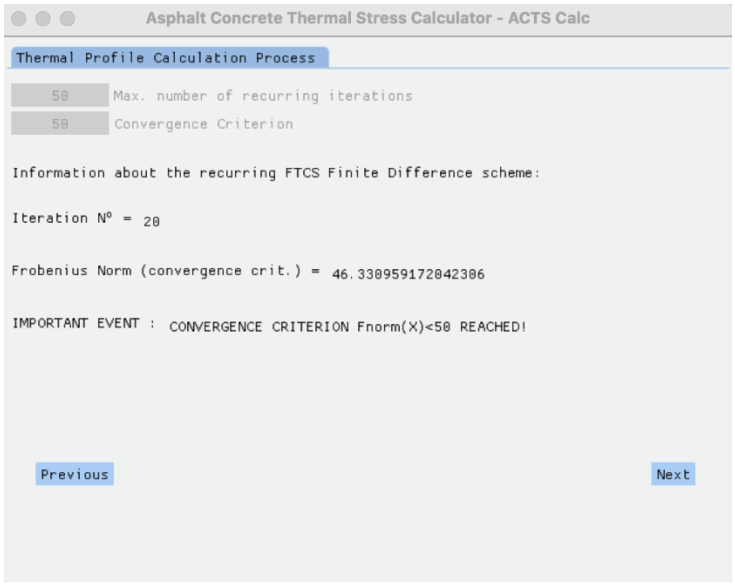

Figure A-8. Visualization of the ongoing calculation and convergence

The mentioned “important events” can refer to the following:

- The occurrence of turbulent flow in the calculation process
- The end of the calculation without reaching the convergence criterion
- The convergence of the iterative algorithm (information on the calculation convergence is given in the “recurring_iterations_log.xlsx” file)
- The occurrence of a numerical instability and the cancellation of the calculation. In this case, the user is asked to change the value of the time- and/or space-step, to ensure the CFL-criterion validation, which will be explained later in this document

If the calculation is done without a problem (“convergence reached”), the user can visualize the obtained thermal profile with respect to time. Even if the calculation is realized on the whole profile, down to the maximum ground depth, only non-ground results

are shown (refer Figure A-9). This is realized to optimize the visualization and obtain faster graphical results. However, a “temp_profile.csv” file, which contains the full data, and a more workable file called “temp_profile_subsample.xlsx”, are available to the user in the directory “Results”. The temperature values are expressed in [^{o}C]. In this table, the rows are related to the time step [s] whereas the columns refer to the depth-step [m] (refer Figure 9).

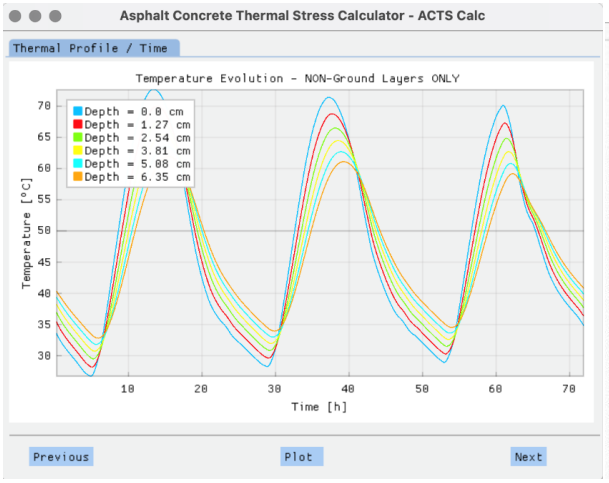

Figure A-9. Thermal calculation results, plot, and Excel file.

The library used to plot the graphs is highly dynamical. It allows to change the position of the legend, toggle on/off some curves, etc., by entering the plot menu (right click > settings > legend). In this way, cleaner curves can be obtained, as shown in Figure A-10.

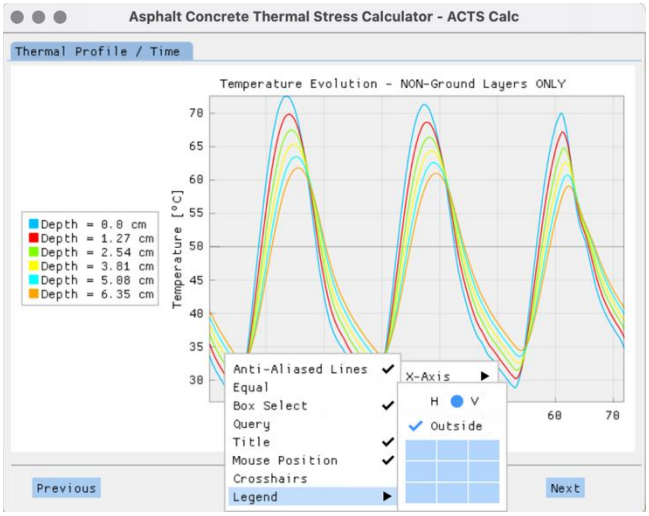

Figure A-10. Optimized view of the thermal calculation results

Next, the user can select a given time-step and visualize thermal profile with respect to the pavement depth. As previously, the graph can be rework (rectangle-zoom, by clicking and sliding) to enhance the visualization quality. An export of the thermal profile to an Excel file is also possible (refer Figure A-11).

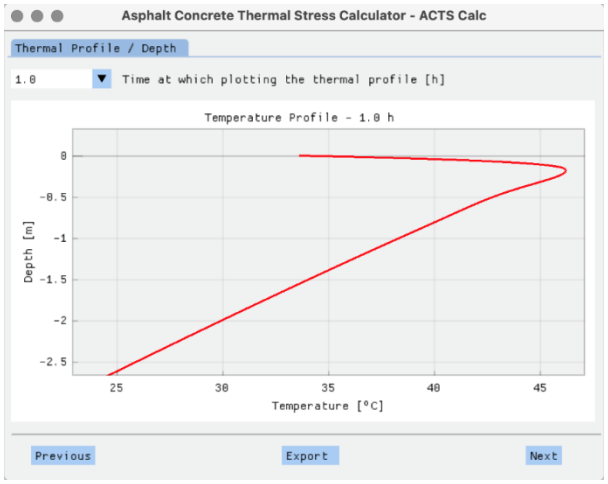

Figure A-11. Thermal calculation results at a specific time

II. Stresses Model

The stress calculation is realized only on the 1st pavement layer. Thus, only this part of the thermal profile previously calculated is considered in the following. This approach was chosen since the thermal cracking phenomenon mostly affect the top part of the pavement structure.

The stress profile within the surface layer is enough to estimate the pavement's cracking potential. Reducing the calculation to this sole portion of the pavement allows to decrease the computational burden of the calculation. Focusing the calculation of stresses in the first layer avoids the stress-discontinuity at the layers' interface due to the different thermal contraction coefficients.

It should be noted that the time-step use in the following is 10x higher than the one employed in the thermal calculation. Indeed, if a small time-step was needed in order to ensure the stability of the "explicit scheme", it is not the case anymore. The use of a bigger time-step allows a faster software responsiveness while maintaining a good accuracy.

a. Stresses Model Inputs

- Coefficient of Thermal Contraction

In this part of the software, the user can choose between 3 solutions (refer Figure A-12).

1. The user knows the linear Coefficient of Thermal Contraction of the asphalt concrete mixture and directly enters it: CTC_{mix} $[\frac{1}{°C}]$
2. The user only partially knows the mixture properties. CTC_{mix} thus, needs to be computed using the following user-inputs:

- CTC_{binder} = Linear coefficient of thermal contraction of the binder [$\frac{1}{°C}$]

- CTC_{agg} = Linear coefficient of thermal contraction of the aggregates [$\frac{1}{°C}$]

- VMA = Voids in Mineral Aggregate [%]

- V_{agg} = Aggregate volume in mixture [%]

CTC_{mix} calculation is performed using Equation (A-1) (Lytton, et al., 1993).

$$CTC_{mix} = \frac{VMA \times CTC_{binder} + V_{agg} \times CTC_{agg}}{3 \times V_{total}} \quad \text{(A-1)}$$

Where:

$$3 \times V_{total} = 3 \times 100[\%] = 300 \quad \text{(A-2)}$$

3. The user does not know any of the mixture properties. He then must enter the following information:

- CTC_{binder} = Linear coefficient of thermal contraction of the binder [$\frac{1}{°C}$]

- CTC_{agg} = Linear coefficient of thermal contraction of the aggregates [$\frac{1}{°C}$]

- Gsb = Aggregate bulk specific gravity []

- Gb = Binder specific gravity []

- Gmm = Asphalt mixture maximum specific gravity []

- AV = Air volume [%]

- BC = Binder content [%]

The software automatically calculates $VMA\ and\ V_{agg}$.

$$VMA = 100 - Gmb \cdot \frac{100-BC}{Gsb} \quad \text{(A-3)}$$

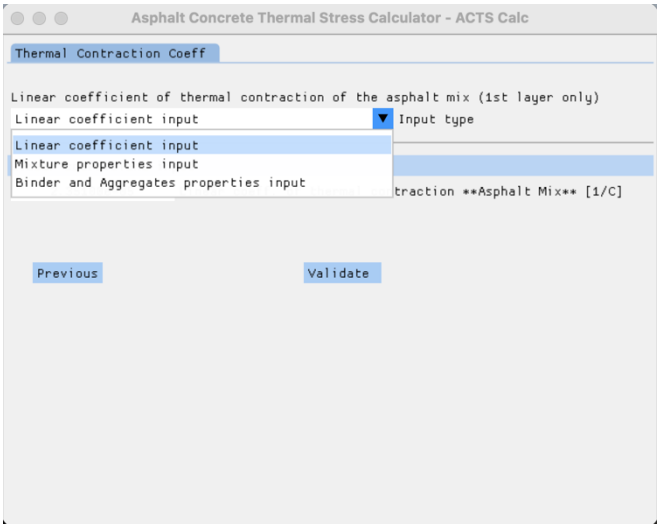

Figure A-12. CTC Input alternatives

Once the user "validates" (see button in figures above) the chosen method, the calculation(s) is (are) realized, and the results for CTC_{mix} actualized and shown in the shaded-out case "Coefficient used for calculation".

b. Mechanical Properties

The last step before performing the stress calculation consists in entering the mechanical properties of the material, and numerically manipulating them to obtain the Relaxation Modulus Master Curve (ErelMC).

To do so, the user has the choice between entering the “Creep Compliance” (CC) data obtained experimentally at different temperatures, or to inform the “Relaxation Modulus” (Erel) data for various testing temps. The data is imported from Excel tables that can be found in the “DATA” directory under the name of "creep_compliance.xlsx" and "relax_modulus.xlsx", respectively. Both tables are made up of 3 columns:

1. Testing temperature [ºC];
2. Testing time [s] or frequency [Hz];
3. Mechanical property value [1/GPa] or [GPa] respectively.

Through a drop-down menu, the user can choose to read one or another of the Excel files. Depending on the chosen option, 2 different scenarios emerge.

Creep Compliance Properties Entry Alternative:

- Material Input

If the user chose to enter CC measurements, the software will show the related data on the screen. This way, the user can verify that the importation process took place in a good manner (refer Figure A-13).

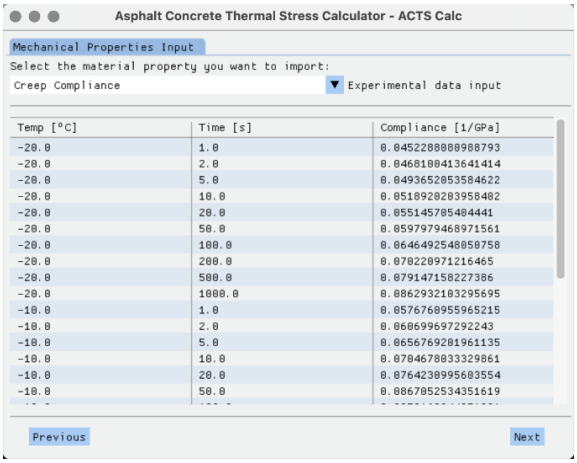

Figure A-13. Uploaded Creep Compliance data from the lab

Once the user validates the data, the software will plot the raw data, and the user can choose to observe the data on a log-log scale. Figure A-14 shows a second order polynomial function, which has been fitted to each log-log creep compliance curve (resulting in a polynomial for each testing temperature). The parameters of those functions can be exported in a text file clicking on “Export” and found in the “Result” directory under the name "polymial_optim_material.txt".

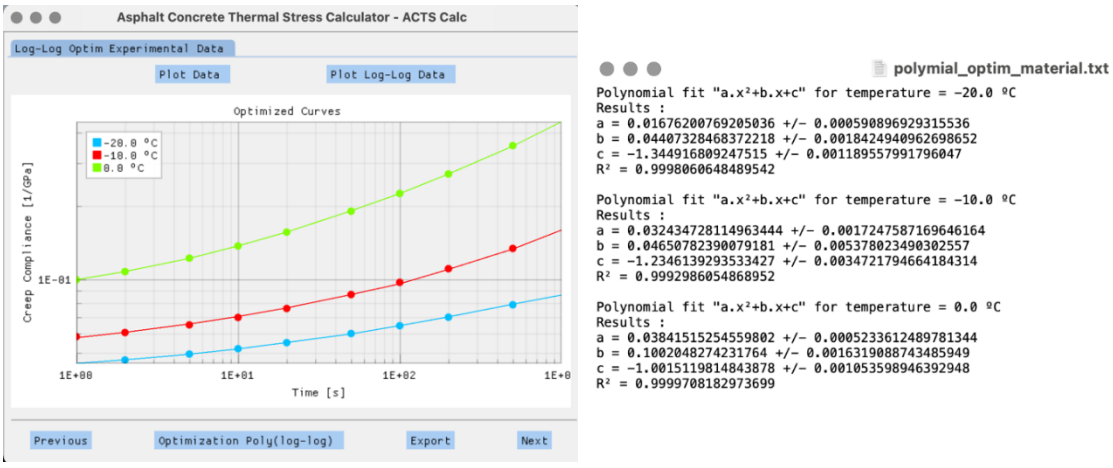

Figure A-14. Creep Compliance Plot and Fitted Polynomial Parameters

CCMC Construction

With this information, the Creep Compliance Master Curve (CCMC) can then be built. The Master Curve is obtained thanks to the application of the time-temperature superposition principle (TTSP) that stands for thermo-rheologically simple materials. In short, this principle states that the behavior of a material at low temperature is equivalent to its response to short time (or high frequency) excitations. Conversely, the material behavior at high temperature is assimilated to its response to long time (low frequency) excitations (Roylance, 2001). Thus, it is possible to calculate a shift-factor a_T for each testing temperature, to estimate a "reduced time" $\xi = \frac{t}{a_T}$ corresponding to their equivalent long- or short-time excitations at a constant temperature (Olsen, et al., 2001).

Here, the construction of the Master Curve is realized following a technique developed by Witczak, that allows an automatic horizontal shifting of the non-reference curves (Witczak, et al., 2000). It consists in calculating discrete shift-factor $\log(a_T)$ using the polynomial functions previously optimized. This process is closed to another method, called "equivalent slope", that shows significantly better results that traditional shifting techniques (Saboo & Kumar, 2018).

To obtain the CCMC of its material, the user just needs to choose a reference temperature. Depending on this choice, results might be accurate. Thus, the user is invited to test different reference temperature to find the most adequate (refer Figure A-15).

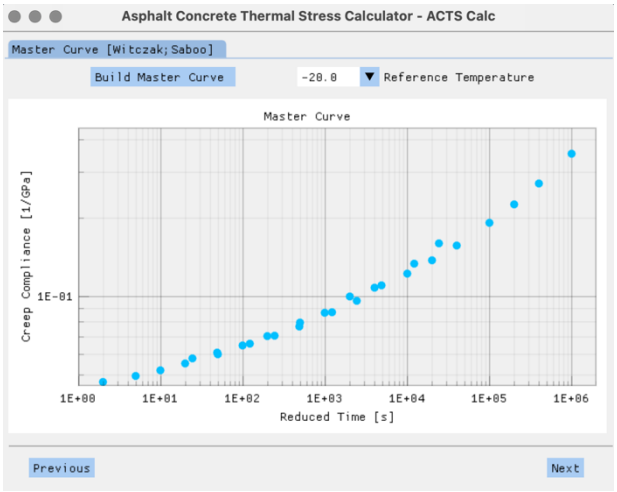

Figure A-15. CCMC with a specific reference temperature

The discrete shift-factors $\log(a_T)$ found during the construction of the master curve are accessible to the user. Those can be found under the "Results/discrete-shift.xlsx" file.

Continuous Shift-Factor

Once the CCMC and the associated discrete shift-factors are obtained, the user can choose between the *William-Landel-Ferry (WLF)* and the *Arrhenius law* to obtain a continuous evolution of the shift-factor with the temperature. The user is invited to take a close look to the obtained data, since the WLF law was initially developed in a semi-empirical fashion for plastic materials (amorphous polymers), considering α-transitions as the main relaxation mechanism. Those transitions occur when the material is slightly above the glass transition temperature ~ $[T_g; T_g + 100ºC]$. On the contrary, the Arrhenius law considers β-transformations, that are more common when the study temperature is well below T_g (Roylance, 2001).

Results obtained for the same set of discrete shift-factors with both methods are shown in Figure A-16.

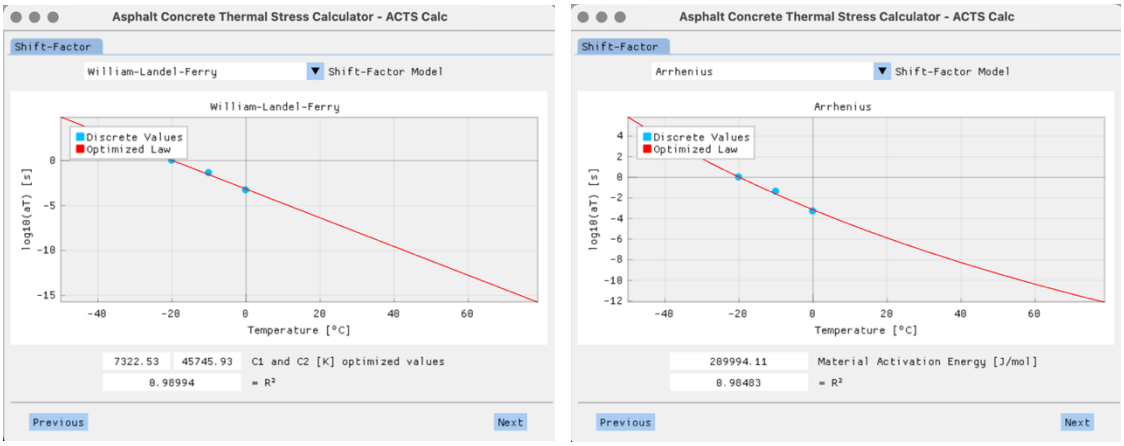

Figure A-16. WLF Optimized Law and Arrhenius Optimized Law respectively

Optimized parameters for one or another of the models are accessible to the user in the “Results” directory, in the Excel files named “optim-wlf.xlsx" or "optim-arrhenius.xlsx". They are also directly visible on the software screen, along with the R^2 resulting from the optimization process.

The user can choose the number of "branches" of the Power Serie, and to directly visualize the results of the optimization for the selection (refer Figure A-17).

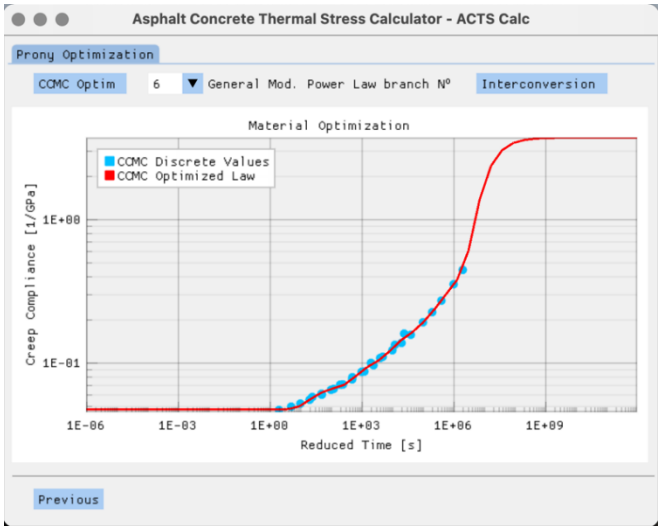

Figure A-17. CCMC - G-MPower Optimization

The optimized parameters can, once again, be found in the "*Results/optim-GenModPower_CCMC.xlsx" file (refer Figure A-18).

	A	B	C	D	E
1		**0**			
2	**D_0**	0.047352			
3	**D_1**	1697.634			
4	**tau_1**	0.068528			
5	**D_2**	7.681806			
6	**tau_2**	3.207072			
7	**D_3**	5378.967			
8	**tau_3**	0.040187			
9	**D_4**	0.477004			
10	**tau_4**	0.022448			
11	**D_5**	0.012505			
12	**tau_5**	0.194324			
13	**D_6**	596.8267			
14	**tau_6**	0.122907			
15	**k**	107.1704			

Figure A-18. CCMC - G-M Power Optimization Coefficients

CCMC Interconversion to ErelMC

To calculate the thermal stress resulting from the temperature profile previously defined, the known as Relaxation Modulus Master Curve is needed. In this case, it can be obtained through a process called “interconversion”, since the relaxation modulus $Erel$ is the conjugate of the creep compliance (Alavi, 2014) (Alavi, Hajj, & Sebaaly, A comprehensive model for predicting thermal cracking events in asphalt pavements, 2017).

The CCMC being modelled with a Power Serie, it is not possible to use an analytical development of the interconversion process, as shown in (Park & Kim, 1999). Thus, a general “discretized” approach of the interconversion is implemented on the simulated points obtained in the previous step. Figure A-19 shows the results for the ErelMC.

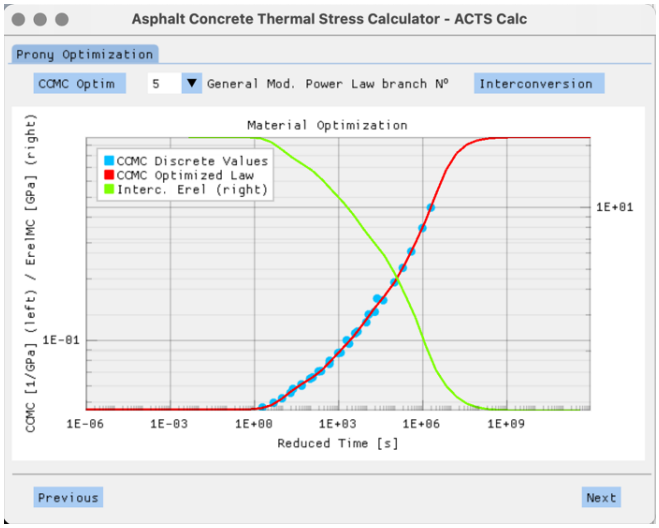

Figure A-19. CCMC Interconversion to ErelMC

- Prony Serie Optimization on ErelMC

Once the interconverted ErelMC is obtained, a new Prony Serie is optimized onto it. This time, the Prony function is adapted to a Generalized Maxwell Model (GMM), also known as Wiechert Model. The associated mechanistic scheme is shown in Figure A-20 (Adamczak & Bochnia, 2016).

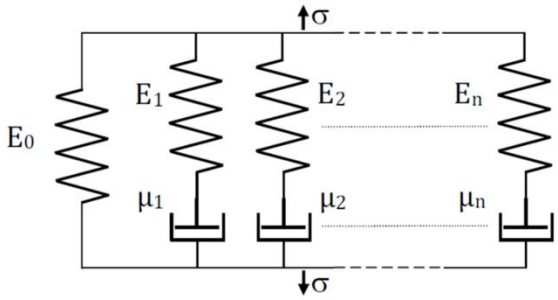

Figure A-20. Generalized Maxwell Model for Relaxation Modulus

Once more, the user can choose the number of "branches" of the GMM, and to directly visualize the results of the optimization for the selection (refer Figure A-21).

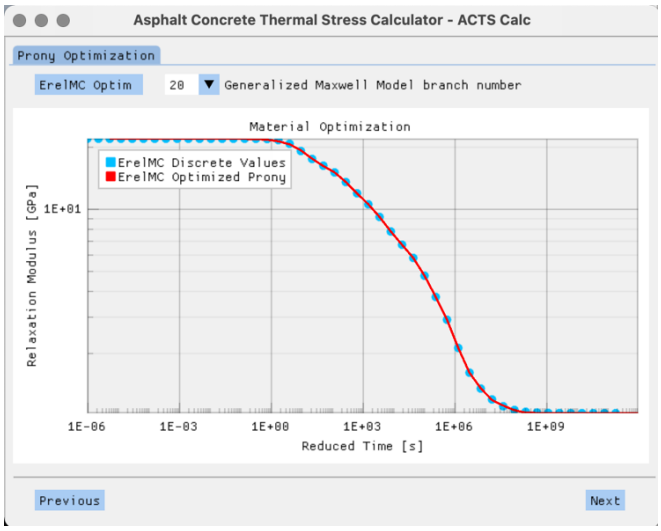

Figure A-21. ErelMC - Prony Optimization

The optimized parameters can be found in the "Results/optim-prony_ErelMC.xlsx" file (refer Figure A-22).

	A	B	C	D	E
1		0			
2	E_0	21.887714			
3	E_1	0.7369317			
4	log(tau_1)	2.3448441			
5	E_2	0.4015705			
6	log(tau_2)	1.1384852			
7	E_3	0.6416397			
8	log(tau_3)	1.1384857			
9	E_4	1.3813758			
10	log(tau_4)	2.3448428			
11	E_5	0.6807771			
12	log(tau_5)	6.6945394			
13	E_6	0.7917301			
14	log(tau_6)	2.3448436			
15	E_7	0.3990238			
16	log(tau_7)	1.1384857			

Figure A-22. ErelMC - Prony Optimization Coefficients

Despite the higher number of steps and the complexity behind the "presmoothing" process, the obtained results are of greater value compared to a dual application of Prony Series.

Relaxation Modulus Properties Entry Alternative:

As explained earlier, the second scenario consists in directly entering the relaxation modulus data for different testing temperatures. After selecting the input type, the user can verify that the importation process worked as expected.

In this case, there is no need to optimize a Prony Serie on a CCMC, or to realize an interconversion process, since we can directly obtain the ErelMC. To do so, a process like the one presented above is employed (Witczak, et al., 2000). However, the polynomial

functions used in this case to fit the experimental data are of first order. This was decided due to the linear behavior of the log-log plot. The parameters of the linear functions can be exported in a text file and found in the “Result” directory under the name "polymial_optim_material.txt" (refer Figure A-23).

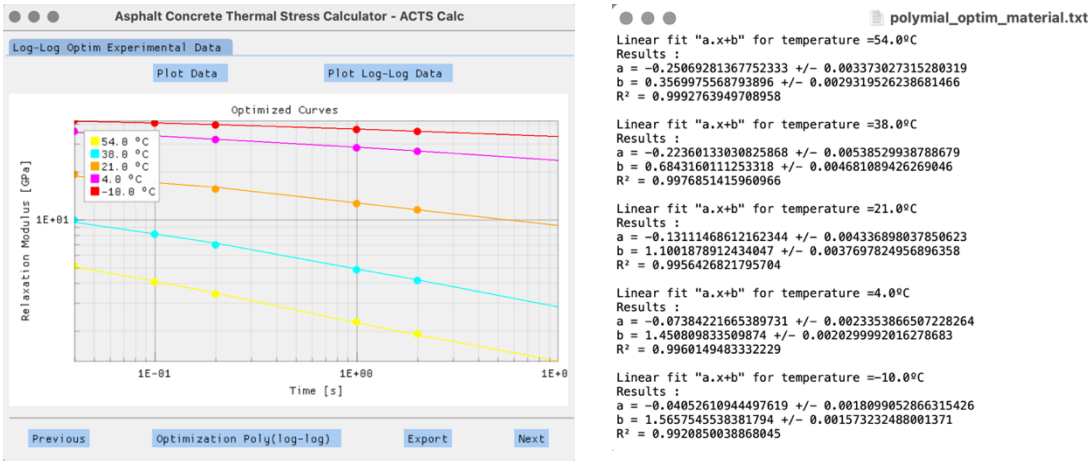

Figure A-23. Relaxation Modulus Optimization Plot and Fitted Polynomial Parameters

After this step, the Erel Master Curve is constructed, and a shift-factor model (*in this case is recordable to use Arrhenius*) selected.

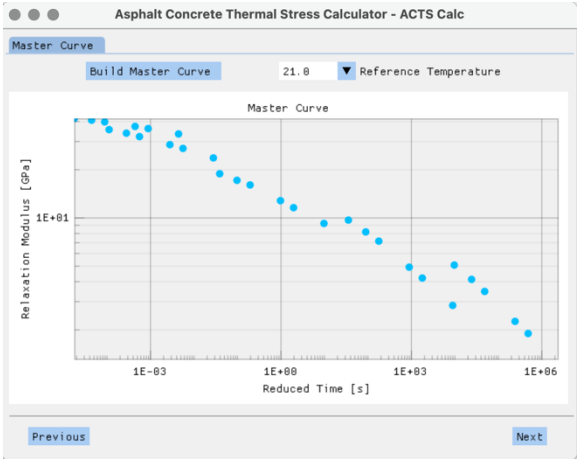

Figure A-24. ErelMC with a Specific Reference Temperature

Finally, a Prony Serie is optimized onto a Generalized Maxwell Model to obtain a continuous evolution of the Relaxation Modulus in function of the reduced time.

It should be noted that a higher number of Prony branches are needed in this case to obtain a smooth behavior at high reduced times. This leads to a higher computational resource and time demand. The optimized parameters are accessible to the user in the "Results" directory as "Results/optim-prony_ErelMC.xlsx" Excel file. Figure A-25 shows the result of the Prony optimization.

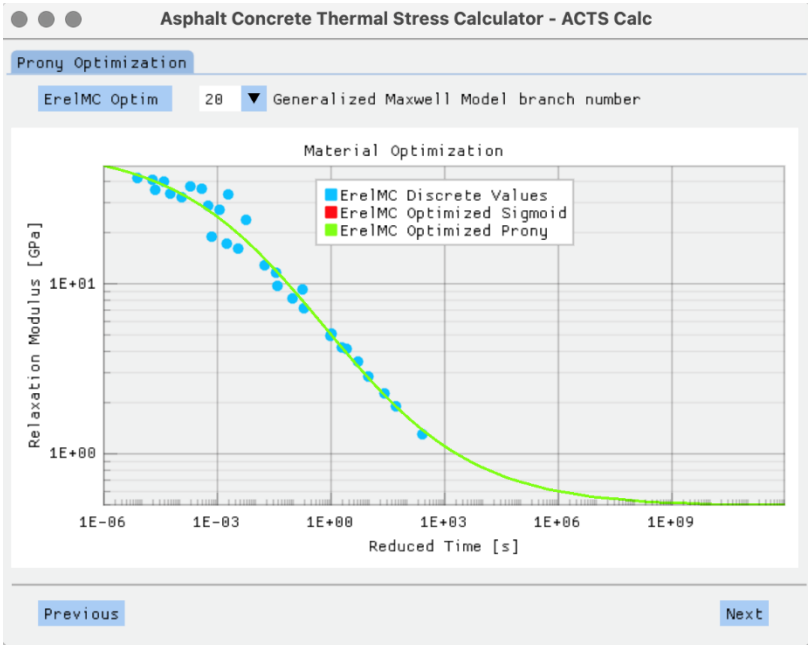

Figure A-25. Result of the Prony optimization

c. Thermal Stress Calculation

Various techniques allow solving the ordinary differential equation (ODE) that arise from the Generalized Maxwell Model. In the next paragraphs, we will describe two of them since both have been implemented and tested in the present software.

Despite the simplicity of such process and its easy numerical implementation, it could be observed a strong dependence of the results on tiny fluctuations of $E(\xi)$. Indeed, and as shown in previous figures, the optimization of a Prony Serie on the interconverted or experimental-shifted values of ErelMC induces a more or less pronounce waviness of $E(\xi)$, which in turn generates strong fluctuations in the calculation of σ^t at certain steps.

To solve this problem, the time-step Δt was artificially decreased to a small reasonable value using a linear interpolation scheme on the thermal profile. Nevertheless, this adjustment does not allow the complete correction of the observed phenomenon, as seen below in Figure A-26.

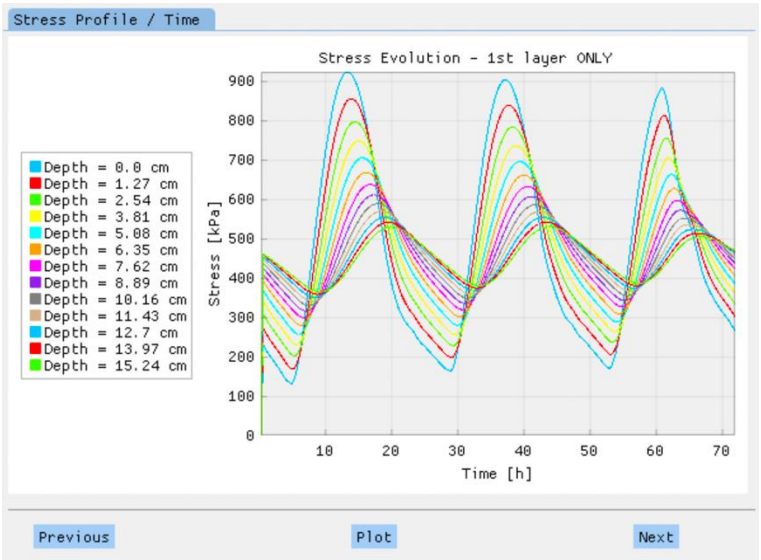

Figure A-26. Plot of the Stress Calculation Using Finite Difference Method (FDM)

Another calculation scheme, relying on a more stable implementation, was thus implemented, and tested.

Boltzman Superposition Integral:

Indeed, integrals consist in continuously summing operations, and it is thus possible to express the material viscoelasticity at a given time as the continuous sum (integral) of the responses to excitations imposed at all previous times. Therefore, such type of integral is also known as “hereditary integral”.

In short, the pseudo-variables method states that stresses in an elastic and viscoelastic body are the same, and thus, that it is possible to solve a viscoelastic problem.

A numerical implementation for isotropic material proposed by Hinterhoelzl and Schapery has been employed to integrate the equation discreetly in time, through the calculation of pseudo-variables increments (Hinterhoelzl & Schapery, 2004) (Ozer, 2020) (Ozer, 2014) (Ozer, 2020). This method showed better stability regardless of the time increment, as much as a high reliability. This technique is thus the one employed to compute all thermal stress calculations presented below.

- Stress vs. Time at all depth plot

Once the user validates the obtained Prony Serie for $E(\xi)$, the stress calculation is automatically realized, and the user is invited to “Plot” the results. The results are here shown “only for the 1st layer”, since the stress calculation is realized solely for this part of the pavement (refer Figure A-27).

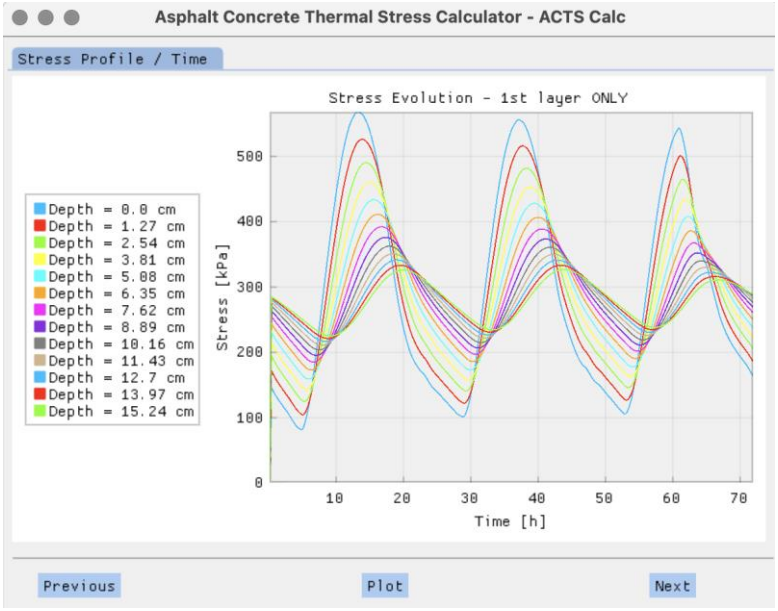

Figure A-27. Stress Profile Plot for the full pavement depth

As for the thermal profile plot, the preceding one is highly interactive: the legend can be shown or hidden in few steps (right click on the plot); the stress evolution at a given depth can be hidden by clicking on it in the legend; figure and/or axes can be zoomed in and out.

As the plot is showed, the program produces an Excel table containing all the results shown in the original plot (i.e., including all depths), with the stress values expressed in [GPa]. In this table, the rows are related to the time step [s] whereas the columns refer to the depth-step [cm] (refer Figure A-28).

	A	B	C	D	E	F	G	H	I	J	K	L	M	N
1		0	1.27	2.54	3.81	5.08	6.35	7.62	8.89	10.16	11.43	12.7	13.97	15.24
2														
3	900	0	0	0	0	0	0	0	0	0	0	0	0	0
4	1800	0.000145	0.000171	0.000194	0.000213	0.000229	0.000242	0.000253	0.000263	0.00027	0.000276	0.00028	0.000282	0.000284
5	2700	0.00014	0.000166	0.000189	0.000208	0.000225	0.000239	0.00025	0.00026	0.000267	0.000273	0.000278	0.000281	0.000282
6	3600	0.000135	0.000161	0.000184	0.000204	0.000221	0.000235	0.000247	0.000257	0.000265	0.000271	0.000275	0.000279	0.000281
7	4500	0.000131	0.000156	0.000179	0.000199	0.000217	0.000231	0.000244	0.000254	0.000262	0.000268	0.000273	0.000277	0.000279
8	5400	0.000127	0.000152	0.000175	0.000195	0.000213	0.000228	0.00024	0.000251	0.000259	0.000266	0.000271	0.000275	0.000277
9	6300	0.000123	0.000148	0.000171	0.000191	0.000209	0.000224	0.000237	0.000248	0.000257	0.000264	0.000269	0.000273	0.000275
10	7200	0.00012	0.000145	0.000167	0.000188	0.000205	0.000221	0.000234	0.000245	0.000254	0.000261	0.000267	0.000271	0.000274
11	8100	0.000116	0.000141	0.000164	0.000184	0.000202	0.000217	0.000231	0.000242	0.000251	0.000259	0.000264	0.000269	0.000272
12	9000	0.000113	0.000137	0.00016	0.00018	0.000198	0.000214	0.000227	0.000239	0.000248	0.000256	0.000262	0.000267	0.00027
13	9900	0.000109	0.000134	0.000156	0.000177	0.000195	0.000211	0.000224	0.000236	0.000246	0.000254	0.00026	0.000265	0.000268
14	10800	0.000105	0.00013	0.000153	0.000173	0.000191	0.000207	0.000221	0.000233	0.000243	0.000251	0.000257	0.000262	0.000266
15	11700	0.000101	0.000127	0.000149	0.00017	0.000188	0.000204	0.000218	0.00023	0.00024	0.000248	0.000255	0.00026	0.000264
16	12600	9.68E-05	0.000123	0.000146	0.000166	0.000185	0.000201	0.000215	0.000227	0.000237	0.000246	0.000253	0.000258	0.000262
17	13500	9.28E-05	0.000119	0.000142	0.000163	0.000181	0.000198	0.000212	0.000224	0.000235	0.000243	0.00025	0.000256	0.00026
18	14400	8.88E-05	0.000115	0.000138	0.000159	0.000178	0.000195	0.000209	0.000222	0.000232	0.000241	0.000248	0.000254	0.000258
19	15300	8.57E-05	0.000111	0.000135	0.000156	0.000175	0.000191	0.000206	0.000219	0.000229	0.000238	0.000246	0.000252	0.000256
20	16200	8.34E-05	0.000108	0.000131	0.000152	0.000171	0.000188	0.000203	0.000216	0.000227	0.000236	0.000243	0.000249	0.000254
21	17100	8.16E-05	0.000106	0.000128	0.000149	0.000168	0.000185	0.0002	0.000213	0.000224	0.000233	0.000241	0.000247	0.000252
22	18000	8.01E-05	0.000104	0.000126	0.000146	0.000165	0.000182	0.000197	0.00021	0.000221	0.000231	0.000239	0.000245	0.00025
23	18900	8.41E-05	0.000103	0.000124	0.000144	0.000162	0.000179	0.000194	0.000207	0.000219	0.000228	0.000236	0.000243	0.000248
24	19800	9.22E-05	0.000107	0.000124	0.000142	0.00016	0.000177	0.000191	0.000205	0.000216	0.000226	0.000234	0.000241	0.000246
25	20700	0.000103	0.000112	0.000126	0.000142	0.000159	0.000174	0.000189	0.000202	0.000214	0.000223	0.000232	0.000238	0.000244
26	21600	0.000115	0.00012	0.00013	0.000143	0.000158	0.000173	0.000187	0.0002	0.000211	0.000221	0.000229	0.000236	0.000242
27	22500	0.00013	0.000129	0.000136	0.000146	0.000159	0.000172	0.000185	0.000198	0.000209	0.000219	0.000227	0.000234	0.00024
28	23400	0.000148	0.000141	0.000143	0.00015	0.00016	0.000172	0.000184	0.000196	0.000207	0.000217	0.000225	0.000232	0.000238
29	24300	0.000167	0.000155	0.000152	0.000155	0.000163	0.000173	0.000184	0.000195	0.000205	0.000215	0.000223	0.00023	0.000236
30	25200	0.000187	0.00017	0.000162	0.000162	0.000167	0.000175	0.000184	0.000194	0.000204	0.000213	0.000221	0.000228	0.000234
31	26100	0.000208	0.000186	0.000174	0.00017	0.000172	0.000178	0.000186	0.000194	0.000203	0.000212	0.00022	0.000226	0.000232
32	27000	0.000229	0.000202	0.000187	0.000179	0.000178	0.000181	0.000187	0.000195	0.000203	0.000211	0.000218	0.000225	0.00023
33	27900	0.000251	0.00022	0.0002	0.000189	0.000185	0.000186	0.00019	0.000196	0.000203	0.00021	0.000217	0.000223	0.000229
34	28800	0.000273	0.000237	0.000214	0.0002	0.000193	0.000191	0.000193	0.000198	0.000204	0.00021	0.000216	0.000222	0.000227
35	29700	0.000294	0.000256	0.000228	0.000211	0.000201	0.000197	0.000197	0.0002	0.000205	0.00021	0.000216	0.000221	0.000226
36	30600	0.000315	0.000273	0.000243	0.000223	0.00021	0.000204	0.000202	0.000203	0.000206	0.000211	0.000216	0.000221	0.000225
37	31500	0.000337	0.000292	0.000258	0.000235	0.00022	0.000211	0.000207	0.000206	0.000208	0.000212	0.000216	0.00022	0.000225
38	32400	0.000358	0.00031	0.000274	0.000247	0.00023	0.000218	0.000212	0.00021	0.000211	0.000213	0.000216	0.00022	0.000224
39	33300	0.000378	0.000328	0.000289	0.00026	0.00024	0.000227	0.000218	0.000215	0.000214	0.000215	0.000217	0.000221	0.000224
40	34200	0.000397	0.000345	0.000304	0.000273	0.000251	0.000235	0.000225	0.000219	0.000217	0.000217	0.000219	0.000221	0.000224
41	35100	0.000417	0.000362	0.000319	0.000286	0.000261	0.000244	0.000232	0.000225	0.000221	0.00022	0.00022	0.000222	0.000225
42	36000	0.000436	0.000379	0.000334	0.000299	0.000272	0.000253	0.000239	0.00023	0.000225	0.000223	0.000222	0.000223	0.000225
43	36900	0.000453	0.000396	0.000349	0.000312	0.000283	0.000262	0.000246	0.000236	0.000229	0.000226	0.000224	0.000225	0.000226
44	37800	0.000469	0.000411	0.000364	0.000325	0.000294	0.000271	0.000254	0.000242	0.000234	0.000229	0.000227	0.000226	0.000227
45	38700	0.000485	0.000426	0.000377	0.000337	0.000305	0.00028	0.000262	0.000248	0.000239	0.000233	0.00023	0.000229	0.000229
46	39600	0.0005	0.000441	0.000391	0.00035	0.000316	0.00029	0.00027	0.000255	0.000244	0.000237	0.000233	0.000231	0.00023
47	40500	0.000513	0.000454	0.000404	0.000362	0.000327	0.000299	0.000278	0.000262	0.00025	0.000242	0.000236	0.000233	0.000232
48	41400	0.000524	0.000466	0.000416	0.000373	0.000337	0.000309	0.000286	0.000268	0.000255	0.000246	0.00024	0.000236	0.000234
49	42300	0.000534	0.000477	0.000427	0.000384	0.000348	0.000318	0.000294	0.000275	0.000261	0.000251	0.000244	0.000239	0.000237

Figure A-28. Stress Profile Table (GPa) vs. Time

The table can be found in the “Results” directory, under the name "calculated_stress_GPa.xlsx".

- Depth vs. Temperature at a given time plot

The "Next" tab allows observing the stress profile of the pavement at a given time-step. To do so, the user is invited to select the desired time to plot the stress profile through a drop-down menu. Once a time is selected, the plot automatically is actualized, and the user is given the option to "Export" the data. The user also can choose another time to visualize and export. The results are here shown only for the 1st layer since the stress

calculation is realized solely for this part of the pavement (refer Figure A-29). The depth is thus adjusted accordingly.

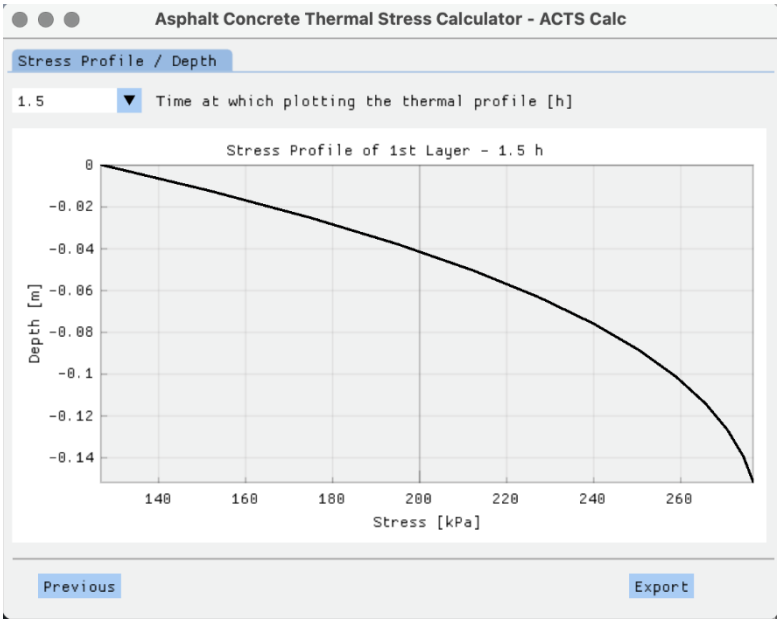

Figure A-29. Stress Profile Plot at a specific time.

If the "Export" button is clicked, a new Excel file is generated by the program. In this document, the rows represent the discrete depth-step of the slab, whereas the single column is related to the time of the stress profile. All stress values are expressed in GPa. The table can be found in the “Results” directory, under the name "depthVSstress_GPa_*xx*h.xlsx".